

ALMA MATER STUDIORUM - UNIVERSITÀ DI BOLOGNA
DIPARTIMENTO DI INGEGNERIA INDUSTRIALE

DOTTORATO IN INGEGNERIA ENERGETICA, NUCLEARE E DEL CONTROLLO
AMBIENTALE

CICLO XXVIII

SETTORE CONCORSUALE DI AFFERENZA 09/C2
SETTORE SCIENTIFICO DISCIPLINARE ING-IND/18

COVARIANCE EVALUATION
FOR NUCLEAR DATA OF INTEREST
TO THE REACTIVITY LOSS ESTIMATION OF THE
JULES HOROWITZ MATERIAL TESTING REACTOR

Presentata da:
Nicholas Terranova

Relatore:
Prof. Marco Sumini

Correlatori:
Dr. Olivier Serot (CEA)
Dr. Pascal Archier (CEA)

Coordinatore Dottorato:
Prof. Vincenzo Parenti Castelli

Esame Finale Anno 2016

Abstract

IN modern nuclear technology, integral reactor parameter uncertainty evaluation plays a crucial role for both economic and safety purposes. Target accuracies for operating and future nuclear facilities can be obtained only if the available simulation tools, such that computational platforms and nuclear data, are precise enough to produce reduced biases and uncertainties on target reactor parameters. Over the last decades, the interest on nuclear data grew robustly after having been latent for many years, making nuclear data improvement one of the modern main tasks for future and operating nuclear system development and optimization. The worldwide nuclear scientific community has recognized the importance of nuclear data, and their validation still is one of the major concerns. The quality of any engineering parameter uncertainty quantification analysis strongly depends on the reliability related to the covariance information contained in evaluated libraries. To propagate properly nuclear data uncertainty on nuclear reactor parameters, science-based variance-covariance matrices are then indispensable. The present work is devoted to nuclear data covariance matrices generation for reactivity loss uncertainty estimations regarding the Jules Horowitz Reactor (JHR), a material testing facility under construction at CEA-Cadarache (France). During depletion, in fact, various fission products appear and the related nuclear data are often barely known. In particular, the strenuous and worldwide recognized problem of generating fission product yields covariances has been mainly considered. Present nuclear data libraries such as JEFF or ENDF/B do not have complete uncertainty information on fission yields, which is limited to only variances. The main goal of this work is to generate science-based and physically consistent fission yields covariances to be associated to the existing European library JEFF-3.1.1. Variance-covariance matrices have been evaluated using CONRAD (COde for Nuclear Reaction Analysis and Data assimilation, developed at CEA-Cadarache) for the most significant fissioning systems. Uncertainty information on thermal neutron-induced fission of ^{235}U , ^{239}Pu , ^{241}Pu and on fast neutron-induced fission of ^{238}U have been tested on genuine reactor applications and on the JHR, to assess their impact on integral reactor parameters, such as decay heat and reactivity. The results obtained using CONRAD have demonstrated the possibility to reproduce consistently both JEFF-3.1.1 evaluated data and experimental fission observables, providing correlations that include effects from experimental measurements, theoretical model parameter fitting, physical conservation laws and statistical analyses.

Acknowledgements

THE present PhD work has been possible thanks to a collaboration between the University of Bologna and the CEA (*Commissariat à l'énergie atomique et aux énergies alternatives*) of Cadarache (France). There are many people I would like to thank for their help and encouragement, unfortunately I can mention only some of them and I apologize if someone is missing.

First of all I would like to thank my advisor Prof. Marco Sumini of the University of Bologna. He has been an extraordinary guidance during this PhD work, always being there for his students, in Bologna and abroad, allowing me to discover such a wonderful world of scientific research. His help will not be forgotten.

I am greatly indebted to my supervisors at CEA-Cadarache, Olivier Serot and Pascal Archier, for their constant support, encouragement, supervision and friendship. I really loved working with them for more than 2 years. They made all this work possible, teaching to me not only science but also important lessons of real life.

Special thanks go to Cyrille De Saint Jean, head of the Physical Studies Laboratory of the Reactor and Fuel Cycle Physics Section of CEA-Cadarache. Thanks to him I really felt *part of the family* in Cadarache. We had great discussions together, helping me a lot during this work.

I would like to thank those who contributed to the realization of this scientific collaboration, among them the direction of the Reactor and Fuel Cycle Physics Section of CEA-Cadarache, Frédéric Varaine and Philippe Darde, the JHR User Facility Interface Manager Gilles Bignan, my Nuclear Project Laboratory contact Claire Vaglio-Gaudard and the direction of the Doctoral School in Industrial Engineering of the University of Bologna.

I will be always grateful to the referees in charge of my Doctor Europaeus evaluation, Dr. Grégoire Kessedjian (LPSC-Grenoble), Prof. Janne Wallenius (KTH) and Prof. Elsa Merle-Lucotte (LPSC-Grenoble) who carefully have read my PhD dissertation.

I would like to thank also Prof. Barry Ganapol, Prof. Domiziano Mostacci, Prof. Mario Marengo and Ing. Alberto Previti who participated in the past to my professional education but they are always available for fruitful discussions and suggestions.

This thesis will not be done without my colleagues, PhD candidates and confirmed scientists, of the Reactor and Fuel Cycle Physics Section, always available for discussions

and fruitful talks, being patient at the beginning when French was still for me a mysterious language. Among the PhD students who will be always all dear to me, I would like to thank in particular Edwin and David, who shared with me not only the office where I worked for 2 years but also many good and bad times, tolerating my Italian exclamations.

All this great but also difficult experience abroad could not be possible without the famous *Italians of Cadarache*. Among them I cannot forget to mention Luca, Paolo, Salvatore, Davide and Chiara, who are still there, and those who already left after completing their studies such as Matteo, Christian, Francesco and Michele.

Special thanks go to my all-time Italian friends in Bologna and abroad (Brisbane, Chemintz, Lisbon and Minsk), always there for me in the difficult times and when I was back home from France. In these years they showed me that distance could be insignificant when true friendship exists, as did Simone who flew from Lisbon many times just to share a *magret de canard* and a glass of *Bordeaux* with his old friend, or Andrea who waited for me many hours in the night just to say me hello after a long trip from Aix.

Finally, I would like to thank my family, my parents Rosa and Domenico, my brother Francesco and his wife Francesca, they have always been my anchor during my whole life.

Nicholas Terranova

Contents

Introduction	1
Objectives and Outline of the Thesis	2
The Jules Horowitz Reactor	5
I Covariance Generation	9
1 Covariance Estimation Methodologies and Theory	11
1.1 Introduction	12
1.1.1 The Nature of Data Uncertainties	14
1.2 The Importance of Covariances	14
1.2.1 Covariance Definition	17
1.2.2 Error Propagation	19
1.3 Probability Theory for Data Evaluation	21
1.3.1 The Bayes Theorem and the Learning Process	21
1.3.2 Prior and Likelihood Distributions: The Maximum Entropy Theorem	22
1.3.3 Parameter Estimators	24
1.4 Parameter and Covariance Matrix Estimation	25
1.4.1 The Least-Square Methods	26
1.4.1.1 The Case of a Linear or Linearizable Theoretical Model .	26
1.4.1.2 Strongly Non-Linear Theoretical Model: The Iterative	
Process	30
1.4.2 Filtered Monte Carlo	31
1.4.3 Bayesian Monte Carlo	32
1.4.4 Hybrid Methods	33
1.5 The Problem of Systematic Uncertainties	34
1.5.1 The Marginalization Technique	35
1.5.1.1 Analytical Marginalization	36
1.5.1.2 Standard Monte Carlo Marginalization	37
1.5.1.3 Bayesian Monte Carlo Marginalization	38
1.6 A Few words on the Model Defect Problem	39
1.7 Conclusions	39
2 Fission Yields Semi-Empirical Models	43
2.1 The Main Features of the Fission Process	43
2.1.1 Hands on the Fission Process	44
2.1.2 Characteristics of the Fragments	45
2.1.3 Prompt Particles Emission	47
2.2 Models for Fission Yield Evaluation	48

2.2.1	Fission Yields Definitions	49
2.2.2	Modeling Mass Fission Product Yields	50
2.2.3	The Wahl Model for Isotopic Fission Yields	59
2.2.4	Isomeric Repartition: The Madland England Model	64
2.3	Conclusions	67
3	Nuclear Data Measurements and Evaluation	69
3.1	The Process of Nuclear Data Evaluation	69
3.1.1	Steps in Nuclear Data Preparation	70
3.1.2	The Nuclear Data Cycle	71
3.2	Fission Yields Measurements	73
3.2.1	Radiochemical Measurements	73
3.2.2	Inverse Kinematics	74
3.2.3	2-E and 2-v Methods	74
3.2.4	The Lohengrin Spectrometer	75
3.3	Features Added in the CONRAD Code	76
3.3.1	Code Presentation	77
3.3.2	Fission Yields Capabilities	78
3.3.2.1	Handling FY and Miscellaneous Fission Observables	78
3.3.2.2	Independent Fission Yields	81
3.3.2.3	Miscellaneous Fission Quantities	82
3.3.2.4	Cumulative Fission Yields: The Q-Matrix	83
3.3.2.5	The APOLLO2 Chains	86
3.4	Conclusions	89
4	Fission Yields Covariance Evaluation	91
4.1	The JEFF-3.1.1 FY Library	92
4.2	Covariance Generation General Procedure	93
4.2.1	The GLS Phase	93
4.2.2	The Retroactive Analysis	96
4.2.3	The Analytical Marginalization	97
4.2.4	Uncertainty Propagation for Independent and Cumulative FY	97
4.3	U-235 Thermal Fission	98
4.4	Pu-239 Thermal Fission	117
4.5	Pu-241 Thermal Fission	124
4.6	U-238 Fast Fission	130
4.7	Conclusions and Final Remarks	134
II	Uncertainty Propagation	137
5	Uncertainty Propagation Methodologies	139
5.1	Introduction	140
5.2	Deterministic Sensitivity Estimation	142
5.2.1	Local Sensitivity Analysis: First Derivative Based Methods	143
5.2.2	Few Words on Global Sensitivity Analysis	144
5.2.2.1	Elementary Effects	144
5.2.2.2	Variance Decomposition	145
5.3	Monte Carlo Uncertainty Propagation	146

5.3.1	General Features	147
5.3.2	Nuclear Data Monte Carlo Sampling	148
5.3.3	The Latin Hypercube Sampling	149
5.3.4	The Sample Size Determination	150
5.4	The URANIE-APOLLO-MENDEL Coupling	156
5.4.1	The URANIE Platform	156
5.4.2	Reactivity and Decay Heat Uncertainty Propagation	157
5.5	Conclusions	159
6	Uncertainty Quantification on Nuclear Reactor Applications	161
6.1	Reactor Applications Description	162
6.1.1	The PWR Pin-Cells	162
6.1.2	JHR Calculations in Reference Configuration	165
6.2	Sensitivity Coefficients Validation	166
6.3	FY Covariance Matrices Testing	171
6.3.1	U-235 Thermal Fission	171
6.3.2	Pu-239 Thermal Fission	184
6.3.3	Pu-241 Thermal Fission	189
6.3.4	U-238 Fast Fission	192
6.4	Conclusions	193
 Conclusions and Perspectives		 195
 A Least-Square Solution Schemes		 199
A.1	The $(\mathbf{I} + \mathbf{Q})$ -formulation	199
A.2	The $(\mathbf{C}_y + \mathbf{N})$ -formulation	200
 B The ENDF Format		 201
B.1	ENDF General Features	201
B.2	The Fission Product Yields File	202
 C CONRAD Main Functionalities		 205
C.1	Microscopic Data Assimilation	205
C.2	Integral Data Assimilation	207
 D Elementary Fission Decay Heat Calculations		 209
 E Complementary Results on FY Covariances		 211
E.1	Pu-239 Fast Fission	211
E.2	Pu-240 Fast Fission	217
 F Perturbation Theory		 223
F.1	Introduction	223
F.1.1	Basic Mathematical Concepts	224
F.1.2	Applications of the Perturbation Theory	224
F.2	Neutronic Applications	225
F.2.1	The Standard Perturbation Theory	225
F.2.2	The Generalized Perturbation Theory	226

Contents

F.2.3	Equivalent Generalized Perturbation Theory	227
F.3	Nuclide Concentration Applications	228
	Bibliography	243

Introduction

NUCLEAR power plants, which produce low-carbon electricity, are both a relevant part of the solution to global warming and an important mean for supplying energy to emerging and developed countries. 27%¹ of the European electricity has got nuclear origin. In 2014 the total nuclear energy generation amount was of 833.6 TWh, coming from 130 operating reactors, corresponding to an installed power of 120 GWe. As source of carbon-free electricity, nuclear power will play a crucial role in the next decades and new reactor concepts are under design to meet severe requirements on safety, sustainability, waste minimization, economic competitiveness, reliability, proliferation resistance and physical protection.

The optimization needed to comply to those new prescriptions requires focusing on research and development in any related fields, reactor physics included. Target accuracies for operating and future nuclear facilities can be obtained only if the available simulation tools, such that computational platforms and nuclear data, are precise enough to produce reduced biases and uncertainties on target reactor parameters.

A rigorous activity of Verification, Validation and Uncertainty Quantification (V&V and UQ) is therefore necessary in nuclear industry, as in other fields of science. Nuclear data, in this field, carry an extremely important role. The reliability of any calculated outcome strictly depends on the quality of the input data we provide to the simulation code. Over the last decades, the continuous development of more powerful computers has allowed an extraordinary improvement of analytical tools and reduced the approximation amount needed to solve numerically the Boltzmann neutron transport equation. The major source of uncertainty in the assessment of neutron balance in a nuclear reactor was then identified in nuclear data, and made nuclear data improvement in terms of accuracy and reliability one of current tasks for future nuclear system development.

The definition of target accuracies for integral reactor parameters is strictly related to the assessment of prior uncertainties for operating systems and future designs. Preliminary uncertainty studies can be performed once reference configurations, which are representative of the examined technology, are made available, and when realistic compilations of nuclear data uncertainties and correlations (so-called variance-covariance matrices) has been defined. In order to achieve this goal, tools designed for sensitivity and uncertainty analyses are therefore necessary to perform preliminary studies on the impact of nuclear data uncertainties on performance parameters (criticality, reactivity coefficients, irradiated fuel isotopic composition, external source effectiveness, decay heat etc.) [Aliberti et al., 2006] and have been developed in the last decades [Salvatores, 1988]. Several analyses

¹Source: World Nuclear Association.

have been carried on to understand the level of knowledge and reliability we can have on present and future technology design parameters (examples are given in Refs. [Salvatores and Palmiotti, 1985, Aliberti et al., 2006, Salvatores et al., 2007, Archier et al., 2012] among many others). Such studies demonstrated the importance to reduce the uncertainty due to nuclear data, that must be significantly decreased to get full benefit from modern advanced modeling and simulation tools [Salvatores et al., 2008].

To provide quantitative recommendations on possible improvements of the evaluated nuclear data files and to reduce at the same time the uncertainty associated to crucial reactor parameters, integral experiments and sensitivity analyses should be combined with model-based covariance data [Palmiotti et al., 2014]. The quality of any uncertainty quantification analysis strongly depends on the accuracy of nuclear data and then on the reliability related to the uncertainty information we retrieve from the evaluated nuclear data libraries.

Unfortunately, current inventory of such nuclear data uncertainty information is rather scarce in some cases, especially when measured against evolving requirements [Smith, 2004], such as the development of new generation reactors, minor actinides transmutation systems and high flux experimental facilities. Consequently, the necessity to generate more comprehensive and reliable uncertainty information persists and becomes still more critical for those data which have not yet been fully implemented in the design phase.

Objectives and Outline of the Thesis

To endorse the constant growing improvement and life extension of both Generation II and III reactors performance and safety, and to provide fundamental experimental data for Generation IV power plants design, the *Commissariat à l'énergie atomique et aux énergies alternatives* (French Atomic Energy Commission, CEA) has decided to initiate the design and subsequently build, on the site of Cadarache (south of France), a new international facility, named Jules Horowitz Material Testing high flux Reactor² (JHR). In its commissioning phase, a fundamental intense activity on uncertainty analysis and bias determination for safety and exploitation parameters is ongoing. In particular, safety target parameters uncertainty margins need to satisfy specific limits, imposed by the French nuclear regulation authority, in order to accomplish what is demanded regarding safety.

As for any other modern nuclear facility, design and safety analyses for JHR require validated simulation tools and nuclear data. Numerical validation demands evaluation of biases introduced by the calculation scheme (modeling approximations and simulation strategy), recurring for instance to reference 3D Monte Carlo detailed core modeling. Experimental validation requires, on the other hand, to determine the biases due to nuclear data, to perform a quantitative evaluation of how far we are from representing the real physical problem.

The simulation platform (neutron transport codes and nuclear data), dedicated to JHR, is called HORUS3D/N³ (HORowitz Reactor simulation Unified System [Döderlein et al., 2008]) and it has been developed in the last decade by CEA-Cadarache. Even if the JHR is a light-water reactor concept, this is a unique machine with peculiar characteristics which

²The first criticality is currently scheduled in 2020.

³N stands for Neutronics.

do not allow to use experimental results and simulation tools thought for commercial light water reactors or shipboard propulsion systems. Related validation procedure has been carried at CEA laboratories, to find the right optimization for HORUS3D/N calculation scheme and to satisfy safety and exploitation prerequisites.

For nuclear data validation, the first step is the determination of prior uncertainties due to nuclear data for safety-related parameters such as reactivity. To achieve that, once a reference reactor model is made available, nuclear data covariance matrices containing uncertainties and correlations need to be collected and combined with sensitivities to target reactor parameters. This step is the starting point for nuclear data uncertainty propagation. Prior investigations for the JHR Beginning Of Life (BOL) reference configuration were performed by Leray (see Refs. [Leray, 2012, Leray et al., 2012b]). The prior BOL reactivity uncertainty due to nuclear data, for the JHR reference configuration⁴ with a 19.75% enriched U_3Si_2Al fuel, was 637 pcm (1σ). Integral experiments were set up to validate experimentally nuclear data for JHR fuel materials. In particular, the VALMONT (*Validation du combustible ALuminium MOlybdène pour la NeuTronique* [Leray et al., 2012a]) experiment allowed some feedbacks on fuel material data, with the main goal of reducing uncertainties. A global JHR-oriented integral experiment, called AMMON [Klein et al., 2009], was designed to reach high level of representation for the JHR expected configurations, in order to control and reduce uncertainties and biases on integral reactor parameters, mapping AMMON results on the JHR geometry. A prior uncertainty propagation study for the AMMON reference configuration was performed [Vaglio-Gaudard et al., 2012], providing a 1σ -671 pcm uncertainty on reactivity, and has shown encouraging consistency with JHR estimations. Experimental assessments were collected [Vaglio-Gaudard et al., 2014] leading to the final estimated posterior reactor bias of 268 pcm associated to ± 349 pcm uncertainty at 1σ on JHR.

To optimize safety and exploitation, uncertainty quantification studies should be carried on also during the machine operation fuel cycle. During the evolution of the system, the nuclear fuel inventory evolves significantly. New materials appear and nuclear data associated to fission product nuclei are often barely known. In addition to the lack of nuclear data information, the difficulty to estimate reliable sensitivity coefficients during depletion aggravates considerably the problem of accurate uncertainty quantification. Present neutronics softwares do not have, in fact, available sensitivity tools to estimate reliable coefficients for the time-dependent neutron balance coupled to the inventory evolution problem.

The main task of the present thesis work is to support the JHR reactivity loss uncertainty quantification during depletion; generating, verifying and testing covariance data which are missing in present nuclear data libraries.

Several nuclear data needs were identified, involving especially a lack of fission products, structural and reflector material covariances. In particular, the strenuous and worldwide recognized problem of determining fission yield covariances has been mainly considered.

Current fission yield files in modern nuclear libraries (ENDF, JEFF, JENDL etc.), as many other kinds of scientific evaluated data, are based on the combination of experiments, theory and semi-empirical models [Mills, 1995]. Over these last decades, the birth of new

⁴As explained after in the text, the JHR is a really flexible machine, capable to perform simultaneously different irradiation experiments.

nuclear reactor concepts (Generation IV fast spectrum reactors and high flux experimental facilities) as well as the assessment of safety-related parameter target accuracies have drawn attention to the limits of the current fission yield files. These new applications requirements for fission product yields demand improved accuracy and covariance data, in order to allow proper uncertainty quantification of relevant engineering parameters. Fission yield uncertainty information, indeed, are incomplete in present nuclear data libraries and are restricted to only variances, without providing any correlations, which certainly do exist⁵. To meet recent needs on fission yields data, the NEA⁶ Working Party on International Nuclear Data Evaluation Co-operation⁷ (WPEC) opened an international collaboration sub-group (SG-37) for *Improved Fission Product Yields Evaluation Methodologies* [Mills, 2012]. The main goal of this working sub-group is the development of new fission yields evaluation methodologies, which are also capable to produce covariance data including effects from experimental measurements, model parameter fitting and statistical analyses.

The present thesis work has been divided in two parts. In the former, we recommend a fission yield covariance evaluation methodology, demonstrating the actual possibility to generate realistic and consistent covariance matrices to be associated to the existing European JEFF-3.1.1 library. Such methodology is based on deterministic Bayesian procedures which allow to take into account correlations due to experiment, models and statistical analyses.

In Chapter 1 of the first part, the main covariance statistical methodologies are reviewed. In particular the Generalized Least Square Method (GLSM), which has been used throughout the thesis, is described with more details. The statistical foundations of the method are provided, showing advantages and drawbacks compared to stochastic procedures.

In Chapter 2, fission yields semi-empirical models are described. To perform nuclear data evaluations, theoretical models are required. For fission yields, we adopted mostly those employed in present evaluations such as ENDF/B-VII and JEFF-3.1.1. We used the CONRAD code (COde for Nuclear Reaction Analysis and Data assimilation [Archier et al., 2014a]) as computational framework to evaluate covariances. The presentation of the code, the experimental techniques, the nuclear data evaluation process and the implementation of fission yield models are described in Chapter 3.

Finally, in Chapter 4, results on covariances, obtained during this thesis, are provided for those fissioning systems which are more significant for nuclear applications, such as the thermal neutron-induced fission of ${}_{92}^{235}\text{U}$, ${}_{94}^{239}\text{Pu}$ and ${}_{94}^{241}\text{Pu}$; or the fast neutron-induced fission of ${}_{92}^{238}\text{U}$.

The second part of the thesis is devoted to the uncertainty propagation for reactor applications. Fission yield covariances have been verified and tested on real application problems, to measure the impact of uncertainties and correlations on target reactor parameters.

As mentioned so far, determining reliable sensitivity coefficients in depletion calculations is

⁵Charge and particle conservation laws characterize, for instance, the fission process, introducing strong correlations between yield data.

⁶Nuclear Energy Agency.

⁷The working party was established to facilitate the exchange of information on nuclear data evaluations and provide a framework of co-operation between the participating projects (ENDF, JEFF, JENDL, ROSFOND/BROND, CENDL). The main goal is to assess nuclear data needs and promote joint evaluation and measurement efforts.

not straightforward because of a few available methodologies that are not yet implemented in present reactor analysis codes. The best compromise between accuracy and simplicity was chosen. Direct perturbation sensitivity coefficients were compared to a Monte Carlo uncertainty propagation method, described in Chapter 5. A statistical discussion was proposed to establish the sample size for Monte Carlo sampling, in order to estimate the level of confidence in our calculations. Both deterministic and the Monte Carlo approaches showed comparable results on simple test-case geometries, such as a PWR-pin-cell, and the JHR configuration.

In Chapter 6, the impact of fission yield covariances has been discussed performing decay heat and reactivity loss uncertainty calculations for simple applications, before treating whole reactor geometries. Results on the JHR showed the possibility to include this new covariance information in a more detailed uncertainty quantification study for safety and exploitation purposes.

The Jules Horowitz Reactor

Since the second half of the 20th century, reactors designed for studying structural and fuel materials behavior under irradiation conditions (better known as Material Testing Reactors or MTR) have tangibly contributed to make nuclear industry sustainable, safe and competitive. The coexistence of different interacting complex mechanisms, such as thermo-mechanical deformation, corrosion and fission product migration, occurring in intense irradiation conditions, makes simulation tools no longer sufficient to predict real material behaviors. An experimental activity is therefore necessary to support research and development for both the optimization of the existing power plant and the design of future facilities.



Figure 1: View of the Jules Horowitz Reactor.

The JHR (see Fig. 1) has been conceived to investigate structural materials and fuel properties for industrial and research needs, providing experimental information for a wide range of utilities, industries and regulators [Bignan and Estrade, 2012]. It is equipped with experimental loops designed to simulate PWR, BWR, CANDU and VVER configurations. The twofold neutron flux, fast in the core and thermal in the reflector, allows

indeed to perform irradiation ageing processes, delivering high in-core dpa⁸ rates for cladding and vessel component material testing. Experimental data can be then used in power plants life-extension programs, aiming at reducing the capital costs and enhancing competitiveness [Camprini, 2013]. The deployment of Generation III power plants will require experimental data to support structural material certification for power plant life management, safety demonstration and economic optimization. The role of JHR will be then crucial in supporting the incoming and ongoing nuclear reactor generation, providing fundamental data for R&D and licensing purposes.

Present and future fuel material performances can be tested in normal and accidental conditions. Fuel properties certification can be achieved and safety margins can be determined with the simulation of power transients ramps, such as those characterizing LOCA (Loss of Coolant Accident).

High neutron flux and elevated temperature loops have been designed to reproduce typical conditions for Generation IV reactors, supporting future system designs. The lack of experimental data for such new designs risks, in fact, to compromise their timely and effective development.

The JHR experimental facilities were not only designed to support nuclear industry but also to supply from 25% up to 50% of ⁹⁹Mo European demand for biomedical purposes. Biomedical radioactive nuclides for European hospitals are mainly produced by five experimental reactors: BR-2 (Belgium), HFR (Netherlands), OSIRIS (France, stopped in 2015), MARIA (Poland) and LVR-15 (Czech Republic). Most of these reactors are roughly 50 years old, and they are licensed to operate for only few more years.

Let us now describe briefly the layout and the main features of the JHR⁹.

The JHR is a pool-tank reactor which uses light water as coolant and moderator. The maximum thermal power designed for such reactor is 100 MW_{th}. The JHR has been conceived to provide high fluxes ($\sim 5 \times 10^{14}$ n cm⁻² s⁻¹ for the fast flux, $E \geq 0.907$ MeV, in the reactor core and $\sim 5.5 \times 10^{14}$ n cm⁻² s⁻¹ for the thermal flux, $E \leq 0.907$ MeV, in the reflector) to manage simultaneous in-core and in-reflector experimental campaigns.

The core is a $\sim \varnothing 60$ cm \times 60 cm aluminum rack characterized by 37 drilled holes ($\varnothing = 9.86$ cm) which can host 37 cylindrical fuel assemblies in the reference configuration or 34 assemblies plus 3 in-core large experimental devices. The cylindrical assemblies present a central cavity which can be filled by other in-core small experimental devices or by hafnium control rods. To achieve high flux performances, a 19.75% enriched UMoAl fuel has been designed in 8 concentric cylindrical fuel plates, able to supply 100 MW_{th} of nominal power. Unfortunately, such fuel assemblies did meet some certification thermo-mechanical problems under high irradiation environments (tested in OSIRIS), so an alternative U₃Si₂Al fuel has been conceived. To guarantee the same nominal power, an enrichment of 27% is necessary due to lower Uranium density (4.8 gU/cm³ for U₃Si₂Al, versus 8 gU/cm³ for UMoAl); otherwise, maintaining the same enrichment of 19.75% under proliferation guard, the nominal power decreases to 70 MW_{th}. The fuel cladding is made by a AlFeNiMg alloy (roughly 96%Aluminum, 1%Iron, 1%Nickel and 1% Magnesium). In the calculations fuel temperatures are set to 20 °C (cooled core after shut-down) and 100 °C (hot temperature during operation). The cooling is performed with slightly pres-

⁸Displacements per atom.

⁹A complete description of the reactor and its experimental capabilities would require an entire manuscript. The interested reader can look for more details in dedicated references, such as Ref. [Icrane, 2006, Icrane et al., 2008, Camprini, 2013, Leray, 2012, Vaglio-Gaudard et al., 2014].

surized low temperature light water (7 bars and 35 °C), circulating at 14.7 m s⁻¹ [Leray, 2012, Camprini, 2013, Vaglio-Gaudard et al., 2014].

A Beryllium reflector limits neutron radial leakage. It is made of different separated blocks which are cooled by water channels. They can be replaced in case of high poisoning levels¹⁰. Also the Beryllium reflector can host different experiments. Holes, that in normal conditions are filled with Be, can be occupied to install experimental devices and the removable blocks can be replaced by the largest measurement and positioning instrumentations.

The experimental capabilities of the JHR are tremendous. Several devices have been developed over the last years with several purposes. Some of them are conceived to be hosted in the JHR core such as CALIPSO (in-Core Advanced Loop for Irradiation in Potassium Sodium), MELODIE (MEchanical LOading Device for Irradiation Experiments) or CEDRIC (Creep Experimental Device for Research on Innovative Ceramic); some others are planned to be positioned in the reflector, such as MADISON (Multi-rod Adaptable Device for Irradiations of experimental fuel Samples Operating in Normal conditions) or LORELEI (Light water One-Rod Equipment for LOCA Experimental Investigations) [Camprini, 2012]. In the present work, we will simply refer to the bare core in nominal configuration, without any experimental device and with the all 37 fuel assemblies.

¹⁰Under strong irradiation, Be is affected by non-negligible helium build-up that causes swelling and changes in mechanical properties. Therefore, it has to be periodically replaced and so removable blocks are generally preferred in Be-reflected reactors. A second aspect, really significant for neutronics analysis, is the production of neutron absorbers such as ⁶Li and ³He that require investigation and estimation of reactivity effects due to Be depletion.

Part I

Covariance Generation

Chapter 1

Covariance Estimation Methodologies and Theory

Contents

1.1	Introduction	12
1.1.1	The Nature of Data Uncertainties	14
1.2	The Importance of Covariances	14
1.2.1	Covariance Definition	17
1.2.2	Error Propagation	19
1.3	Probability Theory for Data Evaluation	21
1.3.1	The Bayes Theorem and the Learning Process	21
1.3.2	Prior and Likelihood Distributions: The Maximum Entropy Theorem	22
1.3.3	Parameter Estimators	24
1.4	Parameter and Covariance Matrix Estimation	25
1.4.1	The Least-Square Methods	26
1.4.2	Filtered Monte Carlo	31
1.4.3	Bayesian Monte Carlo	32
1.4.4	Hybrid Methods	33
1.5	The Problem of Systematic Uncertainties	34
1.5.1	The Marginalization Technique	35
1.6	A Few words on the Model Defect Problem	39
1.7	Conclusions	39

NUCLEAR data improvement gained an outstanding importance in the scientific community in the last decades, becoming a prior need in advanced nuclear system design. Future innovative nuclear facilities are in fact imposing strict safety-by-design standards, requiring highly accurate engineering parameter uncertainty estimation. Several efforts have been spent in this direction for cross section uncertainty reduction, to improve the basic nuclear data knowledge to be applied in nuclear design calculation tools. It was in fact quickly recognized that the value and the credibility of any uncertainty analysis was strictly dependent on the scientific quality of variances and correlations [Palmiotti et al., 2014, Aliberti et al., 2006] associated to basic input data. Supplying complete covariance information gives in fact the opportunity to estimate realistically the interval of confidence on integral reactor parameters, providing reliable indications of the most significant sources of uncertainty. The main goal of this chapter is to provide an overview about uncertainty quantification and best estimates (mean values) evaluation, without

pretending to be exhaustive with many details, but giving the essentials for a straightforward comprehension of the whole manuscript.

Nuclear data follow a complex process of evaluation, correction and analysis to become useful in nuclear applications [Fröhner, 1997, Fröhner, 2000]. Measured raw data cannot be in fact directly applied. Transmission data, capture yields and fission rates are not the cross sections wanted for neutronic calculations, furthermore an interpolation-extrapolation process via nuclear model theories becomes necessary. In this dissertation we will often refer to neutron-induced reaction data, but the following principles of nuclear data evaluations have been used for several reaction cross sections and find wide applications also in other fields of science.

Modern methods for best estimates and covariances evaluation can be classified in three categories [Herman, 2011]:

- i) Deterministic, such as the Kalman filter and the Generalized Least Square Method (GLSM);
- ii) Stochastic, which use Monte Carlo sampling of model parameters;
- iii) Hybrid approaches, that combine deterministic and stochastic features.

Each method presents advantages and drawbacks. In the following sections we dedicate particular attention to the deterministic approach based on the Bayesian learning process, since it has been used throughout this work. However, a brief overview on modern Monte Carlo methods such as the Bayesian Monte Carlo (BMC) will also be discussed. The reader who is already familiar with data evaluation and covariance matrix generation methodologies is invited to proceed further and go to Chapter 2, where the semi-empirical models adopted here to generate covariance matrices for fission yields are presented.

1.1 Introduction

In the early 1970's, the growing computing power gave the possibility to carry on optimization studies capable to give economical benefits. Understanding our level of confidence on integral reactor parameters can have in fact a significant impact on nuclear reactor design and exploitation.

Especially after some severe nuclear accidents, mainly those at the Three Miles Island, Chernobyl and Fukushima nuclear power plants, a second concern that fed uncertainty analysis was safety. For the safety report, the uncertainty associated to target safety-related parameters, with precise margins assigned by nuclear regulation authorities, has to be determined.

The progress in science and technology is incredibly dependent on the synthesis we can make on quantities of interest from the combination of modeling, large-scale simulations and experiments. Uncertainty quantification plays an essential role in predictive science. The reliability of the estimation of quantities of interest, such as safety and control nuclear reactor parameters, is significantly affected by the confidence we have on the associated uncertainties which, in principle, should represent the effectiveness of our predictive potential. In a broad sense we can define the uncertainty quantification theory as the practice of identifying, quantifying and reducing the uncertainties associated with mathematical models,

numerical algorithms, experiment, input data and finally predicted outcomes [Smith, 2014].

In a broader activity of uncertainty quantification, a comprehensive process of *Verification and Validation* is therefore needed in nuclear technology to satisfy modern standards. Verification refers to the process of establishing the accuracy of the numerical algorithm implemented in the software we use to represent and to solve the mathematical problem. Validation, on the other hand, is in charge to describe how much our mathematical formulation is able to represent the physics of the problem we have in front of us. Designing a simulation tool, three sources of error are normally affecting calculations:

- i) Modeling Errors: The mathematical formulation of the physical problem can contain approximations which introduce unavoidable biases in our predictions. In neutronics such a source of error is not really significant. The Neutron Transport Theory is a fine description of neutron motion in matter, but if we think about the diffusion theory or the thermo-hydraulic empirical correlations, modeling errors can play a relevant role.
- ii) Numerical Error: The transport equation, for real cases, cannot be solved analytically. A numerical algorithm has to be designed and biases necessarily set in. An example is the multigroup approximation which is used to simplify the energy description of the neutron population.
- iii) Input data errors and uncertainties. Nuclear data are unavoidably containing errors and uncertainties which propagate through the simulation tool and affect the final results.

This latter source of error and uncertainty is often the most significant in neutronics calculation. Uncertainty propagation due to nuclear data is then a critical issue to be considered in our predictive models. Such validation activity demands to improve sensitive data according to the most updated model capabilities so generating reliable covariance matrices where missing. The present work can be then contextualized in this very last framework, providing missing covariance matrices and quantifying their impact on application calculations.

The mathematical foundation of modern nuclear data uncertainty analysis and evaluation lies mainly in the probability and statistical fields [Smith, 1990]. Nuclear data are in fact mainly deduced by measurements, which present dispersion in the observations. The statistical notions at the basis of the error analysis in physical measurements are still valid for nuclear data with some exceptions. Nuclear measurements can be, in fact, hardly repeated due to the cost of such measurements and often does not simply yield large data sets, but leads to complications in the interpretation and comparison of different results. Sometimes important nuclear reaction parameters cannot even be measured, so their knowledge is left only to models.

As it will be clearer in the following sections, the objective of the nuclear data evaluator is to deduce the best estimates and the most reliable associated uncertainties for input data of interest, merging experimental and theoretical knowledge in order to have a complete set of basic parameters to be used in application codes. Nuclear data is surely the most important source of uncertainty in reactor applications, and many efforts still have to be done to reach the high levels of accuracy required by next and present generation facilities.

1.1.1 The Nature of Data Uncertainties

As pointed out in the introduction we are focused on input data uncertainties and their impact on integral parameters of interest for nuclear reactor analysis and design. Before starting to enter deeply in covariance matrices generation and nuclear data evaluation, it can be useful to clarify the nature of data uncertainties.

Legitimate errors, which exclude erroneous procedure in measurements and evaluations introducing strong biases that are not considered in the present context, can be classified in *random* and *systematic*. The formers arise from the counting process we perform during the measurement procedure. If data acquisitions are independent and uncorrelated, the different measurements present a dispersion around a mean value that can be evaluated with classical moment estimators [Taylor, 1997]. If in principle we were able to perform an infinite number of such measurements, random uncertainties would be normally distributed. Random uncertainties can then be treated statistically and evaluated by data analysis techniques that give best estimates and associated variances in a quite straightforward way. In many books random uncertainties are also called *statistical* uncertainties, for their aleatory nature.

Systematic errors cannot be treated statistically. They introduce a bias in the measurements that are often hard to identify and quantify. For example if we are measuring a time and repeat the data acquisition thanks to the same stopwatch, our measurements will be statistically distributed around an average value that can be considered as the best estimate. If on the other hand our stopwatch runs *systematically* slowly, all our measurements will be necessarily underestimated, introducing a bias that cannot be detected by any measurement with the same stopwatch. So systematic errors correspond to those unavoidable deviations from the true values that cannot be assessed by the repetition of a particular procedure in the investigative process [Smith, 1990]. These kind of systematic deviations are fundamental in error propagation, as it will be clearer later on. They introduce biases which are generally greater than the usual statistical uncertainty, generating relevant *correlations* between data that must be taken into account¹.

Defective (non-legitimate) errors can arise in many ways, during the assessment, the analysis and the evaluation process. Bugs in the code, failings in the instrumentations, uncalibrated devices, errors in data corrections, etc. can introduce strange behavior in data values that should be detected and possibly rejected. Data consistency checks are then necessary and the identification of erroneous points has to be performed to guide data rejection or down-weighting.

1.2 The Importance of Covariances

Quantities of interest are functions of basic physical constants and their accuracy clearly depends on the knowledge on input data. In science one of the major objectives is to provide reliable uncertainties on physical quantities which play an important role in applied technology.

¹Actually even statistical uncertainties can produce correlations. The experimental set-up calibrations can correlate all the successive measurements. Statistical uncertainty on a reference assessment can introduce systematic effects on those measurements which use it as normalization.

According to what we mentioned before, our practical needs become a question of determining the moments of random variables which are themselves functions of other random variables whose principal moments are already known. Supposing for a sake of simplicity our quantity of interest q being a function of two input variables x and y , with uncertainties respectively δx and δy , what kind of uncertainty we expect on q ?

If q is simply the sum of the two input variables, calling x_{be} and y_{be} their best estimates, the highest and lowest probable values for $x + y$ are

$$x_{be} + y_{be} + \delta x + \delta y \quad (1.1)$$

and

$$x_{be} + y_{be} - \delta x - \delta y. \quad (1.2)$$

Therefore the best estimate for q is clearly given by $q_{be} = x_{be} + y_{be}$ and $\delta q \approx \delta x + \delta y$ is an estimation of the associated uncertainty.

If our quantity of interest is the product of the two input variables, we can still identify the probable highest and lowest values for our response. Let us write the physical quantities with the following notation:

$$x = x_{be} \left(1 \pm \frac{\delta x}{|x_{be}|} \right), \quad (1.3)$$

$$y = y_{be} \left(1 \pm \frac{\delta y}{|y_{be}|} \right). \quad (1.4)$$

The highest and lowest probable values for q are then given by

$$q_{max,min} = x_{be}y_{be} \left(1 \pm \frac{\delta x}{|x_{be}|} \right) \left(1 \pm \frac{\delta y}{|y_{be}|} \right). \quad (1.5)$$

Since

$$\left(1 \pm \frac{\delta x}{|x_{be}|} \right) \left(1 \pm \frac{\delta y}{|y_{be}|} \right) = 1 \pm \frac{\delta x}{|x_{be}|} \pm \frac{\delta y}{|y_{be}|} \pm \frac{\delta x}{|x_{be}|} \frac{\delta y}{|y_{be}|}, \quad (1.6)$$

if we have relatively small uncertainties we can omit the second order term obtaining:

$$q = x_{be}y_{be} \left[1 \pm \left(\frac{\delta x}{|x_{be}|} + \frac{\delta y}{|y_{be}|} \right) \right]. \quad (1.7)$$

We can repeat the same reasoning for the difference and the ratio of the input variables, finding again that for the difference we sum the absolute errors and for the ratio the relative ones.

To evaluate the uncertainty on the quantity of interest q , we supposed its range of variation considering the maximum and the minimum values according to the uncertainties associated to the input parameters x and y . To calculate the maximum values for $q = x + y$, we supposed in fact $q_{max} = x_{be} + y_{be} + \delta x + \delta y$. It is quite improbable, if our quantities are really statistically independent and so uncorrelated, that both x and y are underestimated

of their entire uncertainty. We can say, with a certain level of confidence, that $\delta x + \delta y$ represents an overestimation of our probable uncertainty for the quantity q . So what is the more realistic estimation of the uncertainty associated to q ? To answer to this question we need to do a brief discussion about a variable normally distributed.

When we measure physical quantities, if they are only affected by statistical uncertainties, they are normally distributed with a standard deviation σ that we assume as the associated uncertainty. In uncertainty propagation it is normal practice to use Gaussian distributions for the input parameters. If we suppose x and y distributed as uncorrelated normal functions:

$$x \propto \exp\left(-\frac{x^2}{2\sigma_x^2}\right), \quad (1.8)$$

$$y \propto \exp\left(-\frac{y^2}{2\sigma_y^2}\right). \quad (1.9)$$

If we are now back to the problem to evaluate $x + y$, and we consider independent variables, we can certainly say that the probability to have a specific value of x and of y follows the product rule:

$$P(x, y) \propto \exp\left[-\frac{1}{2}\left(\frac{x^2}{\sigma_x^2} + \frac{y^2}{\sigma_y^2}\right)\right]. \quad (1.10)$$

So, once we have the probability to get a given pair of values (x, y) , we can calculate the probability associated to the sum. To find the distribution for the quantity $q = x + y$ we need however to express our probability distribution as a function of $x + y$. To do so in this simple case it is sufficient to apply some algebra. Considering that

$$\frac{x^2}{\sigma_x^2} + \frac{y^2}{\sigma_y^2} = \frac{(x + y)^2}{\sigma_x^2 + \sigma_y^2} + \frac{(\sigma_y^2 x - \sigma_x^2 y)^2}{\sigma_x^2 \sigma_y^2 (\sigma_x^2 + \sigma_y^2)} = \frac{(x + y)^2}{\sigma_x^2 + \sigma_y^2} + z^2 \quad (1.11)$$

we can write the probability $P(x, y)$ as

$$P(x, y) \propto \exp\left[-\frac{(x + y)^2}{2(\sigma_x^2 + \sigma_y^2)} - \frac{z^2}{2}\right], \quad (1.12)$$

where we called z^2 the second addendum of the right-hand term. This last expression can be even written as

$$P(x + y, z) \propto \exp\left[-\frac{(x + y)^2}{2(\sigma_x^2 + \sigma_y^2)}\right] \exp\left[-\frac{z^2}{2}\right]. \quad (1.13)$$

Since we are interested in the probability to have a specific pair (x, y) , our results will not depend on the value of z , so this variable can be integrated giving a factor of $\sqrt{2\pi}$. We find therefore that the final expression for the probability associated to the sum $x + y$ is

$$P(x, y) \propto \exp\left[-\frac{(x + y)^2}{2(\sigma_x^2 + \sigma_y^2)}\right], \quad (1.14)$$

which shows that the sum q is normally distributed with a standard deviation of $\sqrt{\sigma_x^2 + \sigma_y^2}$.

This simple example shows as a more reliable estimation of the uncertainty associated to the quantity of interest q , sum of two input variables, can be given by the quadratic sum if the quantities are statistically independent and normally distributed. Let us now consider the case where q is simply a multiplication of the input variable x by a constant B . Supposing x normally distributed, the probability to obtain $q = Bx$ will be the same to have $x = q/B$. So according to the Gaussian formula we have

$$P(q) \propto \exp\left[-\frac{(q/B)^2}{2\sigma_x^2}\right] = \exp\left[-\frac{q^2}{2B^2\sigma_x^2}\right], \quad (1.15)$$

which says that q follows a Gaussian law with standard deviation $B\sigma_x$. Reasoning in the same way we can obtain for $q = x + A$

$$P(q) = P(x = q - A) \propto \exp\left[-\frac{(q - A)^2}{2\sigma_x^2}\right]. \quad (1.16)$$

These last simple examples, that can be easily extended to the case where x and y do not have the average equal to zero², allow us to extrapolate an important result for the uncertainty propagation of independent normally distributed variables to the general case, where q is a function of two entries $q(x, y)$.

Considering σ_x and σ_y relatively small compared to the averages \bar{x} and \bar{y} of two Gaussian distributed variables x and y , we can make the following assumption:

$$q(x, y) \approx q(\bar{x}, \bar{y}) + \left(\frac{\partial q}{\partial x}\right)(x - \bar{x}) + \left(\frac{\partial q}{\partial y}\right)(y - \bar{y}). \quad (1.17)$$

This expression tells us that q is given by the sum of a constant $q(\bar{x}, \bar{y})$ and two distributions centered in zero whose widths are respectively $\left(\frac{\partial q}{\partial x}\right)\sigma_x$ and $\left(\frac{\partial q}{\partial y}\right)\sigma_y$. Combining these terms and employing the results we just obtained for the simple examples we made so far, q will be normally distributed provided with a standard deviation given by

$$\sigma_q = \sqrt{\left(\frac{\partial q}{\partial x}\sigma_x\right)^2 + \left(\frac{\partial q}{\partial y}\sigma_y\right)^2}. \quad (1.18)$$

The quadratic sum is then giving us a general law to propagate uncertainties when the entries are independent and normally distributed, and when we identify their standard deviation with their associated uncertainties.

1.2.1 Covariance Definition

Let us now do a step forward considering input variables which depend from each other. The following paragraph will introduce the important concept of covariance and will give an idea of why it is so important in uncertainty quantification. The concept of covariance in fact arises naturally from the uncertainty quantification and it is an essential information to be given to perform correctly any error propagation [Taylor, 1997].

²In this case it is straightforward to demonstrate that for the sum. If we call \bar{x} and \bar{y} the averages, $\bar{q} = \bar{x} + \bar{y}$ and $\sigma_q = \sqrt{\sigma_x^2 + \sigma_y^2}$. For the multiplication by a factor B we obtain $\bar{q} = B\bar{x}$ and $\sigma_q = B\sigma_x$ and for the sum to a constant A we obtain $\bar{q} = \bar{x} + A$ and $\sigma_q = \sigma_x$.

We demonstrated so far that a function q of two independent normally distributed quantities is still normally distributed and its standard deviation is the quadratic summation in Eq. 1.18. To derive the definition of covariance³ let us consider two general quantities x and y that are measured N times and for which we do not know any other information than the measured values $(x_1, y_1), \dots, (x_N, y_N)$. Before proceeding we need to remember the definition of standard deviation

$$\sigma_x = \sqrt{\frac{1}{N} \sum_{i=1}^N (x_i - \bar{x})^2}, \quad (1.19)$$

if measurements are normally distributed, and so we are in the limit that N is large⁴, it can be shown that the uncertainty is coincident to the standard deviation appearing in the Gaussian formula. Whether or not the distribution is normal, the Eq. 1.19 gives a reasonable assessment of the random uncertainties in our measurements.

Once we have all the N measurements assimilated for x and y , we can compute for each pair our quantity of interest $q_i(x_i, y_i)$. If the uncertainties are relatively small we can perform a Taylor expansion truncated at the first order:

$$q_i \approx q(\bar{x}, \bar{y}) + \left. \frac{\partial q}{\partial x} \right|_{\bar{x}} (x_i - \bar{x}) + \left. \frac{\partial q}{\partial y} \right|_{\bar{y}} (y_i - \bar{y}). \quad (1.20)$$

Using this expression we can calculate the average value \bar{q} with the usual formula

$$\bar{q} = \frac{1}{N} \sum_{i=1}^N q_i = \frac{1}{N} \sum_{i=1}^N \left[q(\bar{x}, \bar{y}) + \left. \frac{\partial q}{\partial x} \right|_{\bar{x}} (x_i - \bar{x}) + \left. \frac{\partial q}{\partial y} \right|_{\bar{y}} (y_i - \bar{y}) \right]. \quad (1.21)$$

Since $\sum_{i=1}^N (x_i - \bar{x}) = 0$ and $\sum_{i=1}^N (y_i - \bar{y}) = 0$ we obtain

$$\bar{q} = q(\bar{x}, \bar{y}). \quad (1.22)$$

Let us now substitute the truncated Taylor expansion in our standard deviation estimator:

$$\begin{aligned} \sigma_q^2 &= \frac{1}{N} \sum \left[\left. \frac{\partial q}{\partial x} \right|_{\bar{x}} (x_i - \bar{x}) + \left. \frac{\partial q}{\partial y} \right|_{\bar{y}} (y_i - \bar{y}) \right]^2 = \\ &= \left(\left. \frac{\partial q}{\partial x} \right|_{\bar{x}} \right)^2 \frac{1}{N} \sum (x_i - \bar{x})^2 + \left(\left. \frac{\partial q}{\partial y} \right|_{\bar{y}} \right)^2 \frac{1}{N} \sum (y_i - \bar{y})^2 + \\ &\quad 2 \left. \frac{\partial q}{\partial x} \right|_{\bar{x}} \left. \frac{\partial q}{\partial y} \right|_{\bar{y}} \frac{1}{N} \sum (x_i - \bar{x})(y_i - \bar{y}), \end{aligned} \quad (1.23)$$

the last term is the *covariance* for x and y defined as

$$\sigma_{xy} = \frac{1}{N} \sum_{i=1}^N (x_i - \bar{x})(y_i - \bar{y}). \quad (1.24)$$

³An equivalent definition can be retrieved by classical statistics [Papoulis, 2002], which is the generalization of the variance for multivariate random distribution. By the way in this context we would like to see how the covariance definition comes out naturally from uncertainty propagation, to stress its important in any *Validation* activities.

⁴Thanks to the Central Limit Theorem.

The standard deviation for the quantity of interest q is finally given by

$$\sigma_q^2 = \left(\frac{\partial q}{\partial x} \right)^2 \sigma_x^2 + \left(\frac{\partial q}{\partial y} \right)^2 \sigma_y^2 + 2 \frac{\partial q}{\partial x} \frac{\partial q}{\partial y} \sigma_{xy}. \quad (1.25)$$

If the quantities x and y are actually independent, for large N the covariance should approach to zero, giving Eq. 1.18. This is due to the fact that, if the measurement or, more generally, the sample size⁵ is sufficiently large, positive values of $(x_i - \bar{x})$ must balance negative $(y_i - \bar{y})$ and vice-versa. Otherwise, if any correlation subtends between the x and y , positive $(x_i - \bar{x})$ can be accompanied by positive $(y_i - \bar{y})$, if they are positively correlated, or negative $(y_i - \bar{y})$, if they are negatively correlated (anti-correlated). This can give a positive or a negative contribution to the total uncertainty estimation that can have a significant role in proper error propagation.

1.2.2 Error Propagation

Before proceeding deeply in nuclear data evaluation techniques, we need to stress again on uncertainty propagation in the most general case, since it will be a fundamental knowledge for the following sections.

We call $\vec{x} = x_1, x_2 \cdots x_n$ a vector of random variables which have a multivariate distribution $p(\vec{x})$. Let us suppose to know the mean vector $\langle \vec{x} \rangle$, where $\langle \vec{x} \rangle = \int \vec{x} \cdot p(\vec{x}) d\vec{x}$ ($p(\vec{x})$ is the probability density for \vec{x}), and the covariance matrix $\mathbf{C}_x = \langle \delta x_i \delta x_j \rangle$. If we define $\delta x_i = (x_i - \langle x_i \rangle)$, the second moments of the multivariate distributions can be expressed as

$$\langle (\delta x_i)^2 \rangle = \text{var}(x_i^2) = \langle x_i^2 \rangle - \langle x_i \rangle^2, \quad (1.26)$$

$$\langle \delta x_i \delta x_j \rangle = \text{cov}(x_i, x_j) = \langle x_i x_j \rangle. \quad (1.27)$$

Identifying as usual with $q = q(\vec{x})$ our response, function of the random variables vector \vec{x} , we can define its different moments:

$$\langle q \rangle = \int p(\vec{x}) q(\vec{x}) d\vec{x}, \quad (1.28)$$

$$\langle q^2 \rangle = \int p(\vec{x}) q^2(\vec{x}) d\vec{x}, \quad (1.29)$$

$$\langle (\delta q)^2 \rangle = \text{var}(q) = \int p(\vec{x}) (q(\vec{x}) - \langle q \rangle)^2 d\vec{x} = \langle q^2 \rangle - \langle q \rangle^2. \quad (1.30)$$

These formulas are just the direct application of moment definition. In principle, if we had complete knowledge of the multivariate probability distribution $p(\vec{x})$ and of the function $q(\vec{x})$, which in our case can be really complicated such as the transport or fission operator, we would be able to perform those integrals and find the average and the variance of our quantity of interest q .

For a sake of simplicity let us suppose now that the response function is linear, such that $q(\vec{x}) = \sum_{i=1}^n s_i x_i$ with s_i constant coefficients. If we apply directly the definitions given so far, we obtain the following expressions

⁵We will see further in this manuscript that a convenient way to propagate uncertainties for complex models provided with many possibly correlated entries is the sampling method, followed by a statistical post-processing.

$$\langle q \rangle = \sum_{i=1}^n s_i \langle x_i \rangle, \quad (1.31)$$

$$\langle q^2 \rangle = \sum_{i=1}^n \sum_{j=1}^n s_i s_j \langle x_i x_j \rangle, \quad (1.32)$$

$$\langle (\delta q)^2 \rangle = \text{var}(y) = \sum_{i=1}^n \sum_{j=1}^n s_i s_j \langle \delta x_i \delta x_j \rangle. \quad (1.33)$$

Since the models involved in large-scale simulation are rarely linear, we can employ the last result as approximation to find a simple and practical law for uncertainty propagation, widely used in applications. Before starting let us assume some hypothesis [Smith, 1990]:

- i) The probability distribution $p(\vec{x})$ is quite localized around $\langle \vec{x} \rangle$;
- ii) The function q varies smoothly without any dramatic changes or fluctuations;
- iii) $q(\vec{x})$ is differentiable in $\langle \vec{x} \rangle$.

We can therefore perform a Taylor expansion centered in $\langle \vec{x} \rangle$ and truncate it at the first order to obtain a linearized model response:

$$q \approx q(\langle \vec{x} \rangle) + \sum_{i=1}^n \left(\frac{\partial q}{\partial x_i} \right) \Big|_{\langle x_i \rangle} \delta x_i, \quad (1.34)$$

calling $s_i = \left(\frac{\partial q}{\partial x_i} \right) \Big|_{\langle x_i \rangle}$, we can apply directly the equations seen before.

Keeping in mind the assumptions we made neglecting high order terms, we can extend the procedure to multi-variable responses. Supposing to have a vectorial function $\vec{q} = \vec{q}(\vec{x})$, each k -th of m component q_k is given by a different functions of the input parameters $q_k = q_k(\vec{x})$. In this case, for each component, we can perform the same procedure just seen, linearizing through Taylor expansion:

$$q_k \approx q_k(\langle \vec{x} \rangle) + \sum_{i=1}^n s_{i,k} \delta x_i, \quad (1.35)$$

$$\langle q_k \rangle = q_k(\langle \vec{x} \rangle), \quad (1.36)$$

$$\delta q_k = (q_k - \langle q_k \rangle) = \sum_{i=1}^n s_{i,k} \delta x_i, \quad (1.37)$$

$$\langle \delta q_k \delta q_r \rangle = \sum_{i=1}^n \sum_{j=1}^n s_{i,k} s_{j,r} \langle \delta x_i \delta x_j \rangle = \sum_{i=1}^n \sum_{j=1}^n s_{i,k} s_{j,r} \text{cov}(x_i, x_j), \quad (1.38)$$

$$\text{var}(q_k) = \langle (\delta q_k)^2 \rangle = \sum_{i=1}^n \sum_{j=1}^n s_{i,k} s_{j,k} \text{cov}(x_i, x_j), \quad (1.39)$$

$$\text{cov}(q_k, q_r) = \sum_{i=1}^n \sum_{j=1}^n s_{i,k} s_{j,r} \text{cov}(x_i, x_j). \quad (1.40)$$

The m arrays of dimension m ($\langle \delta q_k \delta q_r \rangle$) form the covariance matrix \mathbf{C}_q for \vec{q} . The parameters $s_{i,k}$ form the $n \times m$ -dimensional *sensitivity matrix*, that we will call \mathbf{S} . In a matrix form we can then write

$$\mathbf{C}_q = \mathbf{S}^\dagger \mathbf{C}_x \mathbf{S}$$

which is called *law of error propagation* or even *sandwich formula* by researchers of the field.

At this stage, the problem has been shifted to the calculation of the sensitivity matrix to perform uncertainty propagation. As it will be clearer once specific applications will be considered, the calculation of sensitivity coefficients cannot be always possible or at least feasible. In nuclear reactor analysis it is a common and diffuse practice employing the *adjoint* solution to the transport problem (i.e. the *importance*) to calculate sensitivities [Salvatores, 1988]. Nevertheless, when non-linear effects have a significant impact in response calculation, these methods are no longer applicable and Monte Carlo approaches are desirable to perform a proper uncertainty propagation. Further in the dissertation such Monte Carlo samplings followed by response post-processing will be discussed in the case of burn-up calculations.

1.3 Probability Theory for Data Evaluation

The nuclear data evaluation methodologies presented in this dissertation are all Bayesian techniques. Before embarking on a complete description of such methods, recalling the basic notions of the Bayesian theory could be useful for the interested reader not belonging to the field. In the following sections the Bayes theorem is recalled and some further useful tools will be presented.

1.3.1 The Bayes Theorem and the Learning Process

Experimental cross sections can be seen as outputs of theoretical models, that in principle should be capable to describe nature. Since in nuclear physics we rarely have predictive capabilities, theoretical models are based on parameters which are adjusted once new experimental information are available. The Bayes theorem provides the formalism at the basis of this learning process. In its simplest form,

$$P(A|BC) = \frac{P(B|AC)P(A|C)}{P(B|C)}, \quad (1.41)$$

Bayes theorem derives naturally from the product rule used to find the probability associated to the intersection of two events A and B :

$$P(A \cap B|C) = P(B|C)P(A|BC) = P(A|C)P(B|AC). \quad (1.42)$$

In our case the event B is the new experimental data which depend on the value of an unknown physical quantity A , under circumstances C . If we have a statistical model, able to tell us how likely is to obtain observables B under circumstances C if the model parameters A are given, and if also a prior probability $P(A|C)$ is available, the updated posterior probability is proportional to $P(B|AC)P(A|C)$. The generalization to n mutually exclusive events A_j is given by [Fröhner, 1997]

$$P(A_j|BC) = \frac{P(B|A_jC)P(A_j|C)}{\sum_{j=1}^n P(B|A_jC)P(A_j|C)}. \quad (1.43)$$

The application of the Bayes theorem is a cornerstone of the nuclear data evaluation. It shows as the *prior* knowledge of the parameters of a given model can be updated by new experimental evidence. The posterior probability is proportional to the prior one, which does not consider the new data, and a likelihood function which yields the probability to obtain the experimental data for given model parameters values:

$$posterior \propto prior \cdot likelihood. \quad (1.44)$$

In its continuous form, the Bayesian theorem can be written as

$$p_{post}(\vec{x} | \vec{y}U)d\vec{x} = \frac{p_{prior}(\vec{x} | U)\mathcal{L}(\vec{y} | \vec{x}U)d\vec{x}}{\int p_{prior}(\vec{x} | U)\mathcal{L}(\vec{y} | \vec{x}U)d\vec{x}}. \quad (1.45)$$

The *posterior* probability distribution $p_{post}(\vec{x} | \vec{y}U)$ on the model parameters \vec{x} is proportional to the *prior* distribution multiplied by the likelihood function that express the probability to obtain the observed data \vec{y} , given the prior parameters values. With U we indicated a prior assumption that we make in the adjustment procedure. Such assumption generally can be identified with the physical model we use to calculate the observables \vec{y} . The denominator is just a normalization constant.

The Bayesian theorem simply formulates the mathematical problem which translates our natural learning process. This theorem is just telling us in a formal way that, once new observations are available, we need to revise our prior knowledge. In technology applications we are just interested in the average and the variance of the parameters we are measuring. In principle we can apply moment definitions to get the information we are looking for. In this sense Bayesian techniques have been developed to infer the first and the second moments of the posterior probability distribution, avoiding the direct resolution of integrals that can require great efforts, especially for large number of parameters.

It needs to be emphasized that Bayesian adjustment procedures for model parameters are rigorous if theoretical models are validated. Model defects can in fact destroy the effectiveness of the learning process, introducing non negligible systematic errors that we do not take into account. Nevertheless, as previously explained, providing accurate and realistic theoretical models is not always expected in nuclear data evaluation and evaluators are forced to generate covariances and best estimates using empirical models that fit quite well the quantities we observe experimentally.

1.3.2 Prior and Likelihood Distributions: The Maximum Entropy Theorem

Thanks to the Bayes theorem we know that our posterior distribution will be proportional to the product of the prior times the likelihood. But what kind of probability distributions should we take? As mentioned so far, we identify with \vec{y} the collection of experimental values that represent the observations we need to consider to possibly improve our knowledge. Furthermore let us suppose to have available the associated experimental covariance matrix \mathbf{C}_y . We call with $\vec{t} = \vec{t}(\vec{x})$ the theoretical model which represents the physics of the problem. It is a vectorial function of the model parameters \vec{x} such that each observable y_i has an equivalent calculated $t_i(\vec{x})$. In this way we have observed experimental values \vec{y} and the corresponding calculated ones $\vec{t}(\vec{x})$ through a theoretical model.

Applying the *Theorem of Maximum Entropy*⁶ to statistical inference, the likelihood

⁶The *Theorem of Maximum Entropy* states that if we are seeking a probability density function obeying to precise constraints (such as mean and standard deviation for the random variable we are considering), we should use the one which

distribution can be expressed by a multi-variate Gaussian⁷:

$$\mathcal{L}(\vec{y}|\vec{x}) \propto \exp\left\{-\frac{1}{2}[\vec{y} - \vec{t}(\vec{x})]^\dagger \mathbf{C}_y^{-1} [\vec{y} - \vec{t}(\vec{x})]\right\}. \quad (1.47)$$

If nothing else than the mean and the standard deviation for a continuous random variable is given, the associated probability distribution that maximizes information entropy without introducing any spurious information is the Gaussian [Fröhner, 2000, Shannon, 1948]. If only experimental points are available without any information concerning their uncertainties, the Gaussian distribution will not be applicable anymore. It has to be emphasized that the distribution is not a Gaussian function on the model parameters \vec{x} , this happens only if the theoretical model $\vec{t}(\vec{x})$ is linear.

What is missing now is to determine the appropriate distribution for the priors. The assumption we make on the prior probability will determine if we proceed via the *Simple Least-Square Method* or the *Generalized Least-Square Method* [Smith, 1993]. The simple least-square method is suitable when we do not have any information about prior parameters. In fact, it comes out when we employ a non-informative prior probability function, i.e. a constant independent from the parameters \vec{x} . Imposing an unitary prior $p(\vec{x}) = 1$, the posterior distribution assumes the following form:

$$p(\vec{x}|\vec{y}) \propto \exp\left\{-\frac{1}{2}[\vec{y} - \vec{t}(\vec{x})]^\dagger \mathbf{C}_y^{-1} [\vec{y} - \vec{t}(\vec{x})]\right\}. \quad (1.48)$$

In this case we do have information about the prior, such as averages and associated uncertainties, we fall again in the case where we do not know anything else than some constraints on the distribution moments that should be respected. The most general distribution that maximizes information entropy is again the Gaussian, as seen for the likelihood function. So the posterior in this case takes the form

$$p(\vec{x}|\vec{y}) \propto \exp\left\{-\frac{1}{2}(\vec{x} - \vec{\theta})^\dagger \mathbf{C}_\theta^{-1} (\vec{x} - \vec{\theta}) - \frac{1}{2}[\vec{y} - \vec{t}(\vec{x})]^\dagger \mathbf{C}_y^{-1} [\vec{y} - \vec{t}(\vec{x})]\right\}, \quad (1.49)$$

where we called $\vec{\theta}$ the vector of prior parameters. As it will be clearer in the following sections, this last assumption will drive us to the formulation of the Generalized Least Square Method (GLSM), which constitutes the engine of any adjustment throughout the whole dissertation.

maximizes information entropy which is defined by [Shannon, 1948]

$$S = - \int dx p(x) \ln(p(x)). \quad (1.46)$$

The just defined information entropy is the unique measure of missing information. In order to avoid adding any other artificial information we are required to satisfying the constraints given to our problem and simultaneously maximizing entropy to infer the most general probability distribution describing the random variable under investigation. This definition of entropy is quite similar to what we find in thermodynamics. A thermodynamic system is expected to evolve into states with higher entropies. In a probabilistic sense S is the function that is measuring the information carried by $p(x)$, higher entropy means more lack of information [Conrad, 2000]. It can be shown that, applying Lagrange multipliers, since for the likelihood we know best estimates (i.e. the observables \vec{y}) and the standard deviations (i.e. the experimental covariance matrix \mathbf{C}_y), the entropy maximization is obtained with a Gaussian distribution centered in \vec{y} , with \mathbf{C}_y as covariance matrix. The beauty of the *Maximum Entropy Theorem* is that, unlike the *Central Limit Theorem*, it allows us to handle Gaussian distributions even when covariances are involved and without pretending uncorrelated random variables.

⁷The covariance matrix \mathbf{C}_y has to be symmetric with non-negative eigenvalues, since we need to obtain positive values $\vec{x}^\dagger \mathbf{C}_y \vec{x}$ whatever the vector \vec{x} is.

1.3.3 Parameter Estimators

As already said so far, we need to find the best estimates and the associated covariances for the model parameters. Statistics deals with the estimation of underlying features of probability functions, once we have collected a set of observations. Let us initially start with classical *parameter estimators*, and so with a *frequentist* formulation of statistical tools. Let us suppose we want to assign a value to a parameter x of a probability distribution governing a set of sampled data⁸ y_1, \dots, y_n . What we need is an *estimator* of the *true value* x_0 that is our unknown. Classical statistics offers us some *estimation rules* which can provide precise estimations of x , once a set of sampled data is delivered.

Let us assume we look for a single parameter x_0 to be estimated, on the basis of a set of sampled data y_1, \dots, y_n , knowing the form of the probability function but ignoring its parametrization⁹. If we presume a particular value x for the parameter we can in principle calculate the probability to find the sampled data with that assigned parametrization:

$$\mathcal{L}(y_1, \dots, y_n | x) = \prod_{i=1}^n p(y_i | x), \quad (1.50)$$

where $p(y_i | x)$ is the probability to find the sampled point y_i for a value x of the parameter sought. The method of the *Maximum Likelihood Estimator* consists essentially in recommending the parameter which maximizes the likelihood probability $\mathcal{L}(\vec{y}|x)$ for a set of sampled values \vec{y} .

The best known and widely used parameter estimator in classical statistics is the *method of least square*. The first formulation was given by K. Gauss when he was still a schoolboy. If we want to provide a single parameter x estimation for a given set of observations y_1, \dots, y_n with an associated uncertainty $\sigma_1, \dots, \sigma_n$, the least-square estimate for x_0 is that value x that satisfies:

$$\chi^2 = \sum_{i=1}^n \left[\frac{(y_i - x)^2}{\sigma_i^2} \right] = \min. \quad (1.51)$$

This methodology can be generalized and made more useful for nuclear applications. Suppose that we cannot measure directly the parameters we are seeking, but instead we have a mathematical model which relates the observables \vec{y} to the parameters \vec{x} through a function $\vec{t}(\vec{x})$. Once experimentation provides a set of experimental values \vec{y} and the associated covariance matrix \mathbf{C}_y , an estimator of the parameters \vec{x}_0 can be given by that vector \vec{x} that satisfies the matrix formulation of the previous equation:

$$\chi^2 = [\vec{y} - \vec{t}(\vec{x})]^\dagger \mathbf{C}_y^{-1} [\vec{y} - \vec{t}(\vec{x})] = \min, \quad (1.52)$$

which is called *conventional least-square* condition [Smith, 1990]. The method we just presented is nothing more than the generalization of the Gauss least-square method, when the observables are represented by functions of many parameters. Nevertheless Eq. 1.52 does not represent the most general least-square condition which could be considered. If we presume to have a prior knowledge on the parameters $\vec{\theta}$ with an associated covariance

⁸With sampled data we mean also observations which represent a sample of the entire population. We use the term *sample* to stress the finiteness of the information available from which we need to infer useful information.

⁹This is our case in fact, the *Theorem of Maximum Entropy* allowed us to give a Gaussian form to our probability distribution, even if we do not know the posterior parameters.

matrix \mathbf{C}_θ , the best estimator for the parameters is the vector \vec{x} which satisfies the new condition

$$\chi^2 = [\vec{x} - \vec{\theta}]^\dagger \mathbf{C}_\theta^{-1} [\vec{x} - \vec{\theta}] + [\vec{y} - \vec{t}(\vec{x})]^\dagger \mathbf{C}_y^{-1} [\vec{y} - \vec{t}(\vec{x})] = \min. \quad (1.53)$$

This procedure is called *generalized least-square method*, since it gives the possibility to include prior information in the least-squares.

Until now we have proposed two kinds of parameter estimators provided by classical statistics, which at the moment give the impression to be *ad hoc* postulates to find the best estimate of a set of model parameters. As it will be clearer hereinafter, there is a link between the Bayesian theory and the postulates of maximum likelihood and least-square just proposed.

Let us consider the sought parameters vector \vec{x} , whose true value can be called \vec{x}_0 . We know from Bayes theorem (see Sec. 1.3.1) that, once we deliver a set of new observables \vec{y} , the posterior probability distribution can be expressed as

$$p_{post}(\vec{x} | \vec{y}) \propto \mathcal{L}(\vec{y} | \vec{x}) p_{prior}(\vec{x}), \quad (1.54)$$

where the observables \vec{y} are related to the parameters \vec{x} through the theoretical model $\vec{t}(\vec{x})$. It can be demonstrated [Taylor, 1997] that the expected value and the square root of the variance, what we usually call standard deviation, can be suitable estimators respectively of the parameter value and uncertainty. This is the essence of Bayesian parameter estimation which applies directly the following formulas to estimate the parameter vector \vec{x} :

$$p(\vec{x} | \vec{y}) \propto \mathcal{L}(\vec{y} | \vec{x}) p_{prior}(\vec{x}), \quad (1.55)$$

$$\langle x_i \rangle = \int x_i p(\vec{x} | \vec{y}) d\vec{x}, \quad (1.56)$$

$$var(x_i) = \int (x_i - \langle x_i \rangle)^2 p(\vec{x} | \vec{y}) d\vec{x}, \quad (1.57)$$

$$cov(x_i, x_j) = \int (x_i - \langle x_i \rangle)(x_j - \langle x_j \rangle) p(\vec{x} | \vec{y}) d\vec{x}. \quad (1.58)$$

An important assumption behind this methodology is that prior and new experimental data are independent. Only in this case in fact the product of the two probability distributions is effectively proportional to the posterior one we are seeking. When high numbers of parameters are involved in the calculation, a rigorous Bayesian treatment could require formidable efforts in best estimates and covariance estimation. Multi-dimensional integrals and complex functional dependences between observations and parameters can burden the calculations. Therefore Monte Carlo methods or deterministic approximations are often used in nuclear applications to employ the Bayesian estimators. In the next section we describe the estimators and the approximations which have been used throughout the present work, clarifying the connection between Bayesian methods and the classical statistics.

1.4 Parameter and Covariance Matrix Estimation

In this section we will see the application of Bayesian theory for parameter and covariance estimation. We will not enter into the details of each method, but some essentials will be

provided to have the necessary background to understand how we proceeded in covariance generation for our purposes.

1.4.1 The Least-Square Methods

This section is devoted to the presentation of deterministic methods which, starting from the Bayesian formulation of the posterior probability density, proceed to parameter estimation through the minimization of a *cost function* of the same type of Eq. 1.52 and 1.53. We will explore two particular cases: firstly we will focus our attention on linear or at least linearizable theoretical models through Taylor expansion of the functional dependence \vec{t} . Afterwards, a more general approach will be presented, introducing the *iterative least-square fitting*, implemented in modern nuclear data evaluation and analysis codes.

1.4.1.1 The Case of a Linear or Linearizable Theoretical Model

The nature of the model which relates the data \vec{y} to the parameters \vec{x} determines whether the least-square condition, given as postulate in classical statistics, is instead perfectly coincident with a rigorous Bayesian approach. Let us then consider a theoretical model such that

$$\vec{t}(\vec{x}) = \vec{a} + \mathbf{G}\vec{x}, \quad (1.59)$$

where \mathbf{G} is frequently called *sensitivity* or *design matrix* and \vec{a} is a constant vector. In such case the observables can be expressed as a function that is explicitly linear in the parameters \vec{x} , for which we seek best estimates and covariances.

Starting from the case where we do not have any prior information, p_{prior} must be a non-informative function that we took previously as a constant. As mentioned before, the posterior probability in this case, once we have applied the *Theorem of Maximum Entropy* for the likelihood function, assumes the following form

$$p(\vec{x} | \vec{y}) \propto \exp \left\{ -\frac{1}{2} [\vec{y} - \vec{t}(\vec{x})] \mathbf{C}_y^{-1} [\vec{y} - \vec{t}(\vec{x})] \right\}. \quad (1.60)$$

Even if in general circumstances it is not the case, for a linear theoretical model Eq. 1.60 is a Gaussian distribution on the parameter \vec{x} . This allows us to directly apply the rigorous Bayesian analysis for parameter estimation. Finding the moments for the posterior probability is coincident to the minimization of the exponential of Eq. 1.60, which corresponds to the cost function χ^2 we introduced in Eq. 1.52, dealing with conventional least-square method. This reduces our problem to find those parameters such that

$$\chi^2 = [\vec{y} - \vec{t}(\vec{x})] \mathbf{C}_y^{-1} [\vec{y} - \vec{t}(\vec{x})] = [\vec{y} - \vec{a} - \mathbf{G}\vec{x}] \mathbf{C}_y^{-1} [\vec{y} - \vec{a} - \mathbf{G}\vec{x}] = \min. \quad (1.61)$$

It is amazing to find how in this case we have the convergence of the two statistical approaches. The Bayesian method and the classical statistics, based on a frequentist vision of nature, produce the same estimator through different reasonings. Furthermore, when we use non-informative prior distributions, this method is also corresponding to what we called the *Principle of Maximum Likelihood*.

Since we want to minimize the cost function χ^2 , we need to find a vector \vec{x} such that $d\chi^2 = \chi^2(\vec{x} + d\vec{x}) - \chi^2(\vec{x}) = 0$. Let us define [Smith, 1990]

$$\chi^2(\vec{x} + d\vec{x}) = [\vec{\eta} - \mathbf{G}(\vec{x} + d\vec{x})]^\dagger \mathbf{C}_y^{-1} [\vec{\eta} - \mathbf{G}(\vec{x} + d\vec{x})], \quad (1.62)$$

where we called $\vec{\eta}$ the vector $\vec{y} - \vec{a}$. We can simplify the notation using $\vec{z} = \vec{\eta} - \mathbf{G}\vec{x}$ [Smith, 1990], in such case we can write

$$\chi^2(\vec{x}) = \vec{z}^\dagger \mathbf{C}_y^{-1} \vec{z}, \quad (1.63)$$

$$\chi^2(\vec{x} + d\vec{x}) = (\vec{z} - \mathbf{G}d\vec{x})^\dagger \mathbf{C}_y^{-1} (\vec{z} - \mathbf{G}d\vec{x}). \quad (1.64)$$

Developing the matrix product we obtain

$$\chi^2(\vec{x} + d\vec{x}) = \vec{z}^\dagger \mathbf{C}_y^{-1} \vec{z} - [\vec{z}^\dagger \mathbf{C}_y^{-1} (\mathbf{G}d\vec{x}) + (\mathbf{G}d\vec{x})^\dagger \mathbf{C}_y^{-1} \vec{z}] + (\mathbf{G}d\vec{x})^\dagger \mathbf{C}_y^{-1} (\mathbf{G}d\vec{x}) \quad (1.65)$$

which allows us to write¹⁰

$$d\chi^2(\vec{x}) = \chi^2(\vec{x} + d\vec{x}) - \chi^2(\vec{x}) = -[(\vec{z}^\dagger \mathbf{C}_y^{-1}) (\mathbf{G}d\vec{x})] - [(\vec{z}^\dagger \mathbf{C}_y^{-1}) (\mathbf{G}d\vec{x})]^\dagger. \quad (1.67)$$

The two terms in Eq. 1.67 are two scalars. The transpose of a scalar quantity is the scalar itself. Therefore it is legitimate to express

$$d\chi^2(\vec{x}) = -2(\vec{z}^\dagger \mathbf{C}_y^{-1} \mathbf{G})d\vec{x}, \quad (1.68)$$

which leads us to have

$$\vec{z}^\dagger \mathbf{C}_y^{-1} \mathbf{G} = 0. \quad (1.69)$$

To find the parameters \vec{x} which satisfy Eq. 1.69, we still need to perform some algebraic operations. Employing the transpose of a matrix product rule we can write

$$\vec{z}^\dagger \mathbf{C}_y^{-1} \mathbf{G} = [(\mathbf{C}_y^{-1} \mathbf{G})^\dagger \vec{z}]^\dagger = [\mathbf{G}^\dagger \mathbf{C}_y^{-1} \vec{z}]^\dagger = 0, \quad (1.70)$$

and so

$$\mathbf{G}^\dagger \mathbf{C}_y^{-1} \vec{z} = 0. \quad (1.71)$$

If we substitute $\vec{z} = \vec{\eta} - \mathbf{G}\vec{x}$, we obtain

$$\vec{x} = (\mathbf{G}^\dagger \mathbf{C}_y^{-1} \mathbf{G})^{-1} \mathbf{G}^\dagger \mathbf{C}_y^{-1} \vec{\eta}, \quad (1.72)$$

which gives us the parameter vector satisfying the conventional least-square condition. We can also derive the associated covariance matrix applying the *law of error propagation*:

¹⁰In Eq. 1.65 the fourth addendum can be neglected since it is a second order term in the infinitesimal increment $d\vec{x}$ of the parameter space. Considering that covariance matrix \mathbf{C}_y is symmetric and non-singular, so $(\mathbf{C}_y^{-1})^\dagger = (\mathbf{C}_y^\dagger)^{-1} = \mathbf{C}_y^{-1}$, and remembering the rule of the transpose of a matrix product, $[\mathbf{A}\mathbf{B}]^\dagger = \mathbf{B}^\dagger \mathbf{A}^\dagger$, and that $(\mathbf{G}^\dagger)^\dagger = \mathbf{G}$ we can write

$$[(\mathbf{G}d\vec{x})^\dagger \mathbf{C}_y^{-1} \vec{z}] = [(\mathbf{C}_y^{-1} \vec{z})^\dagger (\mathbf{G}d\vec{x})]^\dagger = [(\vec{z}^\dagger \mathbf{C}_y^{-1}) (\mathbf{G}d\vec{x})]^\dagger. \quad (1.66)$$

$$\begin{aligned}
 \mathbf{C}_x &= [(\mathbf{G}^\dagger \mathbf{C}_y^{-1} \mathbf{G})^{-1} \mathbf{G}^\dagger \mathbf{C}_y^{-1}] \mathbf{C}_y [(\mathbf{G}^\dagger \mathbf{C}_y^{-1} \mathbf{G})^{-1} \mathbf{G}^\dagger \mathbf{C}_y^{-1}]^\dagger \\
 &= (\mathbf{G}^\dagger \mathbf{C}_y^{-1} \mathbf{G})^{-1} \mathbf{G}^\dagger (\mathbf{G}^\dagger \mathbf{C}_y^{-1})^\dagger [(\mathbf{G}^\dagger \mathbf{C}_y^{-1} \mathbf{G})^{-1}]^\dagger \\
 &= (\mathbf{G}^\dagger \mathbf{C}_y^{-1} \mathbf{G})^{-1} (\mathbf{G}^\dagger \mathbf{C}_y^{-1} \mathbf{G}) (\mathbf{G}^\dagger \mathbf{C}_y^{-1} \mathbf{G})^{-1} \\
 &= (\mathbf{G}^\dagger \mathbf{C}_y^{-1} \mathbf{G})^{-1}
 \end{aligned} \tag{1.73}$$

by considering that $(\mathbf{C}_y^{-1})^\dagger = \mathbf{C}_y^{-1}$ and $[(\mathbf{G}^\dagger \mathbf{C}_y^{-1} \mathbf{G})^{-1}]^\dagger = (\mathbf{G}^\dagger \mathbf{C}_y^{-1} \mathbf{G})^{-1}$.

Let us now deal with the case when we do have prior information on model parameters. As said before when we have information about the first and the second moment, the most general distribution which respects the *Theorem of Maximum Entropy* is a Gaussian, giving the following expression for the posterior probability distribution:

$$p(\vec{x}|\vec{y}) \propto \exp \left\{ -\frac{1}{2}(\vec{x} - \vec{\theta})^\dagger \mathbf{C}_\theta^{-1} (\vec{x} - \vec{\theta}) - \frac{1}{2}[\vec{y} - \vec{t}(\vec{x})]^\dagger \mathbf{C}_y^{-1} [\vec{y} - \vec{t}(\vec{x})] \right\}, \tag{1.74}$$

where $\vec{\theta}$ and \mathbf{C}_θ are respectively prior best estimates and the covariance matrix for the model parameters. Evoking again the case of linear theoretical model, we can apply the same procedure we have seen so far. Furthermore, since a prior knowledge is available, we can even think to use it to linearize non-linear problems through Taylor expansion of the functional dependence truncated at the first order¹¹, supposing that the theoretical model function can be well approximated by

$$\vec{t}(\vec{x}) \approx \vec{t}(\vec{\theta}) + \mathbf{G}\vec{x} = \vec{t}_\theta + \mathbf{G}(\vec{x} - \vec{\theta}) \tag{1.75}$$

where

$$G_{i,j} = \left. \frac{\partial t_i}{\partial x_j} \right|_{\vec{\theta}}. \tag{1.76}$$

Knowing that for linear models the following procedure is no longer an approximation, to find posterior best estimates and covariance matrix for the model parameters, we can proceed through classical statistics estimators minimizing the cost function

$$\chi^2(\vec{x}) = (\vec{x} - \vec{\theta})^\dagger \mathbf{C}_\theta^{-1} (\vec{x} - \vec{\theta}) + [\vec{y} - \vec{t}_\theta - \mathbf{G}(\vec{x} - \vec{\theta})]^\dagger \mathbf{C}_y^{-1} [\vec{y} - \vec{t}_\theta - \mathbf{G}(\vec{x} - \vec{\theta})]. \tag{1.77}$$

We leave to the last part of the paragraph the demonstration that, even in this case, if a linear theoretical model is available, the posterior distribution is still a multivariate Gaussian and therefore the classical least-square estimators are equivalent to a rigorous Bayesian treatment. Pursuing the same procedure seen above, let us call $\vec{s} = \vec{x} - \vec{\theta}$, $\vec{\eta} = \vec{y} - \vec{t}_\theta$ and $\vec{z} = \vec{\eta} - \mathbf{G}\vec{s}$, the cost function assumes then the following form

$$\chi^2(\vec{s}) = \vec{s}^\dagger \mathbf{C}_\theta^{-1} \vec{s} + \vec{z}^\dagger \mathbf{C}_y^{-1} \vec{z}. \tag{1.78}$$

Since we want to minimize χ^2 , we can find an expression for $\frac{d\chi^2(\vec{s})}{d\vec{s}}$ and put it equal to zero¹². Supposing an infinitesimal $d\vec{s}$ we can write

¹¹In principle we could use the Taylor expansion even in the previous case. Nevertheless, if a first guess is available for the Taylor series evaluation, that can be considered as prior information which might be employed in a entropy maximization process.

¹²As already mentioned before, we are supposing that the present procedure yields us to find an absolute minimum. This is true only if we have a prior knowledge of the parameters that is not so far from the pursued parameter values. The cost function in fact, if the theoretical model is truly representing the nature we are observing, has an absolute minimum around the true values of the model parameters.

$$\begin{aligned}
 \chi^2(\vec{s} + d\vec{s}) &= (\vec{s} + d\vec{s})^\dagger \mathbf{C}_\theta^{-1} (\vec{s} + d\vec{s}) + (\vec{z} - \mathbf{G}d\vec{s})^\dagger \mathbf{C}_y^{-1} (\vec{z} - \mathbf{G}d\vec{s}) \\
 &= \vec{s}^\dagger \mathbf{C}_\theta^{-1} \vec{s} + \vec{s}^\dagger \mathbf{C}_\theta^{-1} d\vec{s} + (d\vec{s})^\dagger \mathbf{C}_\theta^{-1} \vec{s} + (d\vec{s})^\dagger \mathbf{C}_\theta^{-1} d\vec{s} + \\
 &\quad + \vec{z}^\dagger \mathbf{C}_y^{-1} \vec{z} - \vec{z}^\dagger \mathbf{C}_y^{-1} \mathbf{G}d\vec{s} - (\mathbf{G}d\vec{s})^\dagger \mathbf{C}_y^{-1} \vec{z} + (\mathbf{G}d\vec{s})^\dagger \mathbf{C}_y^{-1} \mathbf{G}d\vec{s},
 \end{aligned} \tag{1.79}$$

which, neglecting the second order terms and subtracting $\chi^2(\vec{s})$, gives

$$d\chi^2 = \vec{s}^\dagger \mathbf{C}_\theta^{-1} d\vec{s} + (\vec{s}^\dagger \mathbf{C}_\theta^{-1} d\vec{s})^\dagger + \vec{z}^\dagger \mathbf{C}_y^{-1} \mathbf{G}d\vec{s} + (\vec{z}^\dagger \mathbf{C}_y^{-1} \mathbf{G}d\vec{s})^\dagger. \tag{1.80}$$

Reminding that the quantities $(\vec{s}^\dagger \mathbf{C}_\theta^{-1} d\vec{s})$ and $(\vec{z}^\dagger \mathbf{C}_y^{-1} \mathbf{G}d\vec{s})$ are two scalars, therefore, imposing $d\chi^2 = 0$, we obtain

$$\vec{s}^\dagger \mathbf{C}_\theta^{-1} - \vec{z}^\dagger \mathbf{C}_y^{-1} \mathbf{G} = 0. \tag{1.81}$$

Let us now do some algebra to find an explicit expression for the set of model parameters \vec{x} which maximize the cost function. We will call it \vec{x}_{BE} later on to highlight that they are the best estimates with the available information. Performing the transposition of Eq. 1.81, and expanding its terms we have

$$\mathbf{C}_\theta^{-1} \vec{s} - \mathbf{G}^\dagger \mathbf{C}_y^{-1} \vec{\eta} + \mathbf{G}^\dagger \mathbf{C}_y^{-1} \mathbf{G} \vec{s} = 0 \tag{1.82}$$

which gives

$$\vec{x}_{BE} = \vec{\theta} + (\mathbf{C}_\theta^{-1} + \mathbf{G}^\dagger \mathbf{C}_y^{-1} \mathbf{G})^{-1} \mathbf{G}^\dagger \mathbf{C}_y^{-1} \vec{\eta}. \tag{1.83}$$

We have find an expression for the model parameters obtained using the conventional generalized least square estimator from classical statistics. As we said before, we want now to show how this result can be obtained also performing the rigorous Bayesian analysis. Expanding the posterior probability equation (see Eq. 1.74), we obtain

$$\begin{aligned}
 \text{posterior} \propto \exp \left\{ -\frac{1}{2} \left[\vec{x}^\dagger \mathbf{C}_\theta^{-1} \vec{x} - \vec{x}^\dagger \mathbf{C}_\theta^{-1} \vec{\theta} - \vec{\theta}^\dagger \mathbf{C}_\theta^{-1} \vec{x} + \vec{\theta}^\dagger \mathbf{C}_\theta^{-1} \vec{\theta} + \right. \right. \\
 \left. \left. + \vec{\eta}^\dagger \mathbf{C}_y^{-1} \vec{\eta} - \vec{\eta}^\dagger \mathbf{C}_y^{-1} \mathbf{G} \vec{x} + \vec{\eta}^\dagger \mathbf{C}_y^{-1} \mathbf{G} \vec{\theta} - \vec{x}^\dagger \mathbf{G}^\dagger \mathbf{C}_y^{-1} \vec{\eta} + \vec{x}^\dagger \mathbf{G}^\dagger \mathbf{C}_y^{-1} \mathbf{G} \vec{x} + \right. \right. \\
 \left. \left. - \vec{x}^\dagger \mathbf{G}^\dagger \mathbf{C}_y^{-1} \mathbf{G} \vec{\theta} + \vec{\theta}^\dagger \mathbf{G}^\dagger \mathbf{C}_y^{-1} \vec{\eta} - \vec{\theta}^\dagger \mathbf{G}^\dagger \mathbf{C}_y^{-1} \mathbf{G} \vec{x} + \vec{\theta}^\dagger \mathbf{G}^\dagger \mathbf{C}_y^{-1} \mathbf{G} \vec{\theta} \right] \right\}
 \end{aligned} \tag{1.84}$$

which can be rewritten as

$$\begin{aligned}
 \text{posterior} \propto \exp \left\{ -\frac{1}{2} \left[(\vec{x} - \vec{\theta})^\dagger (\mathbf{C}_\theta^{-1} + \mathbf{G}^\dagger \mathbf{C}_y^{-1} \mathbf{G}) (\vec{x} - \vec{\theta}) + \vec{\eta}^\dagger \mathbf{C}_y^{-1} \vec{\eta} \right. \right. \\
 \left. \left. - \vec{\eta}^\dagger \mathbf{C}_y^{-1} \mathbf{G} \vec{x} + \vec{\eta}^\dagger \mathbf{C}_y^{-1} \mathbf{G} \vec{\theta} - \vec{x}^\dagger \mathbf{G}^\dagger \mathbf{C}_y^{-1} \vec{\eta} - \vec{\theta}^\dagger \mathbf{G}^\dagger \mathbf{C}_y^{-1} \vec{\eta} \right] \right\}.
 \end{aligned} \tag{1.85}$$

Since $(\vec{\eta}^\dagger \mathbf{C}_y^{-1} \vec{\eta})$ is a constant, we can write finally

$$\text{posterior} \propto \exp \left\{ -\frac{1}{2} \left[(\vec{x} - \vec{x}_{BE})^\dagger \mathbf{C}_x^{-1} (\vec{x} - \vec{x}_{BE}) \right] \right\}, \tag{1.86}$$

which is a multivariate Gaussian distribution for the model parameters provided with the covariance matrix¹³

¹³Supposing we do not have any prior information, an infinite prior covariance matrix leads to $\mathbf{C}_\theta^{-1} = 0$, which gives the same formula we found for the conventional least square.

$$\mathbf{C}_x = (\mathbf{C}_\theta^{-1} + \mathbf{G}^\dagger \mathbf{C}_y^{-1} \mathbf{G})^{-1}, \quad (1.87)$$

and the average values

$$\vec{x}_{BE} = \vec{\theta} + (\mathbf{C}_\theta^{-1} + \mathbf{G}^\dagger \mathbf{C}_y^{-1} \mathbf{G})^{-1} \mathbf{G}^\dagger \mathbf{C}_y^{-1} \vec{\eta}, \quad (1.88)$$

the same we found so far with classical estimators. In practical applications different ways to express the posterior covariance matrix exists [SAMMY, 2008]. Each has computational advantages and drawbacks, depending on the type of the application desired. For further details see App. A.

We have just shown how classical and Bayesian statistics lead us to the same results through different reasonings for linear theoretical models. In the next paragraph the iterative procedure for non-linear models, mostly used in nuclear data evaluation codes, is presented.

1.4.1.2 Strongly Non-Linear Theoretical Model: The Iterative Process

If the theoretical model representing the observables \vec{y} is non-linear, the least-square condition and the rigorous Bayesian treatment are equivalent only under approximated conditions. We need in fact to perform a Taylor expansion and a first-order truncation of the functional dependence between experimental data and model parameters to obtain a Gaussian posterior distribution. Having a posterior Gaussian distribution guarantees in fact to have the perfect correspondence between the minimization of the cost function and the evaluation of the distribution moments performing the integrals.

For strongly non-linear model a variant of what we saw so far is the application of iterative procedures to reduce the approximation introduced by the truncation at the first order. For each iteration, the Taylor expansion, instead of being performed around the prior parameter set $\vec{\theta}$, is evaluated around the intermediate value $\vec{x}^{(n)}$ associated to the n -th iteration. If we assume [SAMMY, 2008]

$$\vec{t}(\vec{x}) \approx \vec{t}(\vec{x}^{(n)}) + \mathbf{G}^{(n)}(\vec{x} - \vec{x}^{(n)}) = \vec{t}(\vec{x}^{(n)}) + \mathbf{G}^{(n)}(\vec{x} - \vec{\theta} + \vec{\theta} + \vec{x}^{(n)}), \quad (1.89)$$

where

$$G_{i,j}^{(n)} = \left. \frac{\partial t_i}{\partial x_j} \right|_{\vec{x}=\vec{x}^{(n)}}, \quad (1.90)$$

we can set up an iterative process starting with $\vec{x}^{(0)} = \vec{\theta}$. Replacing the expansion in the posterior distribution and following the same procedure shown above, we find

$$\vec{x}^{(n)} = \vec{\theta} + \mathbf{C}_x^{(n)} \left\{ \mathbf{G}^{(n-1)\dagger} \mathbf{C}_y^{-1} [\vec{y} - \vec{t}(\vec{x}^{(n-1)})] + \mathbf{G}^{(n-1)\dagger} \mathbf{C}_y^{-1} \mathbf{G}^{(n-1)} [\vec{x}^{(n-1)} - \vec{\theta}] \right\}, \quad (1.91)$$

where

$$\mathbf{C}_x^{(n)} = \left(\mathbf{C}_\theta^{-1} + \mathbf{G}^{(n-1)\dagger} \mathbf{C}_y^{-1} \mathbf{G}^{(n-1)} \right)^{-1}. \quad (1.92)$$

These last results are completely equivalent¹⁴ to

¹⁴It is straightforward to verify that

$$\vec{\theta} + \mathbf{C}_x^{(n)} \mathbf{G}^{(n-1)\dagger} \mathbf{C}_y^{-1} \mathbf{G}^{(n-1)} (\vec{x}^{(n-1)} - \vec{\theta}) = \vec{x}^{(n-1)} - \mathbf{C}_x^{(n)} \mathbf{C}_\theta^{-1} (\vec{x}^{(n-1)} - \vec{\theta}) \quad (1.93)$$

$$\vec{x}^{(n)} = \vec{x}^{(n-1)} + \mathbf{C}_x^{(n)} \left\{ \mathbf{G}^{(n-1)\dagger} \mathbf{C}_y^{-1} [\vec{y} - \vec{t}(\vec{x}^{(n-1)})] - \mathbf{C}_\theta^{-1} [\vec{x}^{(n-1)} - \vec{\theta}] \right\}, \quad (1.94)$$

which is an analogous expression for the model parameters deriving from the direct application of the Newton-Raphson method to the gradient of the cost function $\chi^2(\vec{x})$ (See Refs. [Fröhner, 1997, Fröhner, 2000, De Saint Jean et al., 2010a, Archier et al., 2014a]). Finding numerically the zero for the gradient of the cost function χ^2 corresponds to replace the posterior distribution with a multivariate Gaussian centered around the maximum of $p(\vec{x})$, with the same curvature. If the theoretical model is not excessively non-linear, through this method, we can well represent the posterior distribution at least in the domain which mostly contributes to integral calculations, when we evaluate moments. This kind of approximation is also called *Laplace approximation* or *saddle point integration*. The *generalized least square method* is no more than the Bayesian parameter estimation in *Laplace approximation*, when only averages and uncertainties are available, such that Gaussian distributions must be assumed to respect the principle of *Maximum Entropy* [Fröhner, 2000].

Deterministic methods present some issues when theoretical models are significantly distant from linearity, even if they work quite well in practical situations. In the next paragraphs other parameter adjustment techniques will be introduced just for the sake of completeness, such as Monte Carlo methods, which can solve efficiently the non-linearity problem, despite they have their own drawbacks.

1.4.2 Filtered Monte Carlo

The method considers mainly uncertainties coming from model parameters. It is basically a Monte Carlo uncertainty propagation, then equivalent to the sandwich rule. The main goal is to reproduce, as much faithfully as possible, experimental uncertainties [Smith, 2004, Herman, 2011]. The first step is to determine *central values* for the model parameters \vec{x} . Then the evaluator needs to choose suitable central parameters \vec{x}_0 , namely the best possible fit guided by experimental data and his own experience. Central parameter uncertainties have to be successively imposed, such that margins produced by their propagation can include the available scattered experimental data. So should ensure that the parameter-produced-uncertainty band will contain the experimental one. In that way a mechanism based on a binomial accepted-rejected process can be actuated as follows.

Model parameters \vec{x} are randomly sampled using normal distributions. Supposing we are about to perform a cross section evaluation according to the model $\vec{\sigma} = \vec{f}(\vec{x})$, we can calculate cross sections $\vec{\sigma}^{(k)}$ for each sampled parameter set $\vec{x}^{(k)}$. As previously mentioned, parameter normal central values are guessed according to experimental data available following the evaluator experience. In the optimization process, only those sampled parameter sets whose calculated cross sections fall inside the experimentally-determined uncertainty band are accepted. Successively the average covariance matrix for cross sections is given by

$$(\mathbf{C}_\sigma)_{i,j} = \frac{1}{K} \sum_{k=1}^K (\sigma_i^{(k)} - \sigma_i^{(0)}) (\sigma_j^{(k)} - \sigma_j^{(0)}) \quad (1.95)$$

where K is the accepted sample size and $\vec{\sigma}^{(0)}$ are the cross sections calculated using the central parameter set \vec{x}_0 . Through this method off-diagonal correlations should appear,

since only specific combinations of parameters would be accepted¹⁵. Furthermore experimental uncertainties should be respected. If no accepted/rejected experimental threshold has been adopted, such method is equivalent to a simple propagation of model parameter uncertainties. A certain number of calculations are necessary to reach a satisfactory statistics. An advantage of such methodology is that no linear assumption has been made, so the non-linearity of the theoretical model is fully preserved. However, the method presents some own drawbacks. As Monte Carlo method, computational time is substantially increasing if compared to the deterministic approach. Moreover, a comprehensive treatment of eventual experimental covariance matrices is not possible.

1.4.3 Bayesian Monte Carlo

In this paragraph we are going to describe what it is commonly called *Unified Monte Carlo* (UMC) [Smith, 2008] or *Bayesian Monte Carlo* (BMC) [Koning, 2015, Privas, 2015], since it is still based on a Bayesian formulation of the data evaluation problem. It is, in fact, a simple application of the Monte Carlo method to find averages and covariances of posterior model parameters, whose probability distribution is provided by the Bayes theorem. In the filtered Monte Carlo methodology we have seen, as one of the major drawbacks, the impossibility to include properly experimental covariance matrices. Thanks to the BMC, such an issue can be overcome, even if common Monte Carlo drawbacks remain. Experimental correlations are, in fact, included in the likelihood function of the Bayesian adjustment procedure.

Then, reminding the Bayes theorem, we have seen that the posterior probability is given by

$$p_{post}(\vec{x} | \vec{y}U) d\vec{x} = \frac{p_{prior}(\vec{x} | U) \mathcal{L}(\vec{y} | \vec{x}U) d\vec{x}}{\int p_{prior}(\vec{x} | U) \mathcal{L}(\vec{y} | \vec{x}U) d\vec{x}}. \quad (1.96)$$

The basic idea of the BMC is to evaluate the first and the second moments of the posterior distribution just given by Monte Carlo integration techniques. As already mentioned, in probability theory, the best estimate for a random variable turns out to be coincident with its expectation value. Therefore, what is needed to be evaluated is nothing else than

$$\langle x_i \rangle = \int x_i p_{post}(\vec{x}) d\vec{x}. \quad (1.97)$$

The same reasoning can be applied to find the covariance matrix $\mathbf{C}_{\mathbf{x}}$:

$$cov(x_i, x_j) = (\mathbf{C}_{\mathbf{x}})_{i,j} = \langle x_i x_j \rangle - \langle x_i \rangle \langle x_j \rangle. \quad (1.98)$$

From Sec. 1.3.2 we saw that the Principle of Maximum Entropy provided us the possibility to rigorously assign Gaussian distributions to the prior and likelihood probabilities. Therefore, performing a Monte Carlo sampling on model parameters, we can evaluate best estimates and covariances by simply relations [Capote and Smith, 2008, Smith, 2008]

$$\langle x_i \rangle_K = \frac{\sum_{k=1}^K x_{i,k} p_{post}(\vec{x}_k)}{\sum_{k=1}^K p_{post}(\vec{x}_k)} \quad (1.99)$$

¹⁵Such method is at the basis of the TENDL nuclear data bank generation [Sublet et al., 2014] and of the Total Monte Carlo uncertainty propagation method [Koning and Rochman, 2008]. The latter will be better described in a dedicated paragraph in Part II of present dissertation.

and

$$\text{cov}(x_i, x_j)_K = [(\mathbf{C}_x)_{i,j}]_K = \langle x_i x_j \rangle_K - \langle x_i \rangle \langle x_j \rangle_K, \quad (1.100)$$

where

$$\langle x_i x_j \rangle_K = \frac{\sum_{k=1}^K x_{i,k} x_{j,k} p_{\text{post}}(\vec{x}_k)}{\sum_{k=1, K} p_{\text{post}}(\vec{x}_k)}. \quad (1.101)$$

The K-dimensional sample on the model parameters can be built in different ways [Capote and Smith, 2008, Capote et al., 2010]. Without entering into the details, we will just provide essentials about common methods employed in BMC nuclear data evaluation.

In the CONRAD-code (COde for Nuclear Reaction and Data assimilation), developed at CEA Cadarache, model parameters are sampled according to the prior distribution. Consistently with the Maximum Entropy Principle, we can assume a Gaussian prior probability and best estimates and covariances can be obtained through [Privas, 2015]

$$\langle x_i \rangle_K = \frac{\sum_{k=1}^K x_{i,k} \mathcal{L}(\vec{y} | \vec{x}_k)}{\sum_{k=1, K} \mathcal{L}(\vec{y} | \vec{x}_k)}, \quad (1.102)$$

$$\langle x_i x_j \rangle_K = \frac{\sum_{k=1}^K x_{i,k} x_{j,k} \mathcal{L}(\vec{y} | \vec{x}_k)}{\sum_{k=1, K} \mathcal{L}(\vec{y} | \vec{x}_k)}. \quad (1.103)$$

The Brute Force sampling (BF) [Smith, 2008, Capote and Smith, 2008] is based on a uniform model parameter sampling on an interval range given by

$$\theta_i - \psi [(\mathbf{C}_\theta)_{i,i}]^{1/2} \leq x_{i,k} \leq \theta_i + \psi [(\mathbf{C}_\theta)_{i,i}]^{1/2}, \quad (1.104)$$

where the parameter ψ is a positive constant. If it is taken equal to one, it means that we allow a range of validity for parameter sampling included in one prior standard deviation. Therefore a sampled parameter value $x_{i,k}$ is then given by

$$x_{i,k} = \theta + (2\gamma - 1)\psi [(\mathbf{C}_\theta)_{i,i}]^{1/2}, \quad (1.105)$$

where γ is a random number between 0 and 1.

Other more sophisticated techniques are available such as the Metropolis-Hastings algorithm [Capote and Smith, 2008], the importance sampling [Koning, 2015, Privas, 2015] or the Markov chains Monte Carlo sampling [Smith, 2014]. Nevertheless we limit to their mentioning, since a full description goes far beyond the scope of this work.

1.4.4 Hybrid Methods

Hybrid methods combine Monte Carlo and deterministic analysis in order to overcome drawbacks which are peculiar for the methods employed in nuclear data evaluation just shown. A Monte Carlo approach is used to estimate uncertainties coming from the theoretical model. In this way the linear approximation at the basis of the deterministic GLSM is avoided, preserving all the non-linearities that can characterize models. To properly consider possible experimental covariance matrix a successive GLSM is then applied.

In the EMPIRE-code [Herman et al., 2007] for instance, a Monte Carlo method can be used in the fast neutron region to generate model covariances. A certain number of

model parameters, including fictitious scaling ones to take into account model defects (see Sec. 1.6), are sampled K times and an equal number of theoretical calculations are run. Applying conventional estimators, the first two moments can be calculated giving a covariance matrix which contains correlations due to the model behind the evaluation. Typically Gaussian distributions are used for sampling. The obtained covariance matrix can be successively used in a deterministic GLSM as prior covariance, in a full analysis that can rigorously take into account experimental uncertainties.

1.5 The Problem of Systematic Uncertainties

As already said, in nuclear data analysis and assimilation¹⁶ we can encounter different kinds of error. We classified uncertainties in *statistical* and *systematic*, giving their own definitions. In nuclear data evaluation it is fundamental to take into account all sources of error. Systematic uncertainties can for example affect measurements and they have to be properly included in the nuclear data evaluation process. Such uncertainties are not only responsible for data error enhancement, but they introduce also strong correlations between data.

One of the major challenge for physicists is to evaluate reliable uncertainties for nuclear data to be propagated in reactor physics studies [Aliberti et al., 2006]. Experimental values reported by experimentalists are rarely measured raw data. As it will be clearer in Ch. 3, raw data are normally subject to sophisticated processes of reduction and assimilation. Experimental parameters such as sample composition and temperature, energy resolution, normalization factors, background corrections, etc. affect significantly data uncertainties, introducing correlations. Nevertheless these parameters do not participate directly to the nuclear models employed in the evaluation process. For this reason, specialists of the field address to them as *nuisance* parameters [De Saint Jean et al., 2009, Habert, 2009, Habert et al., 2010, De Saint Jean et al., 2010b].

Treating systematic uncertainties is not straightforward at all. Often, experimental files are not provided with any covariance matrix but only variances are given, which cannot be easily parceled out in systematic and statistical. Furthermore diagonal experimental matrices are sometimes unrealistic, since systematic uncertainties are necessarily present, correlating all the assessments. For instance, normalizations are frequently affecting measurements, fully correlating all the experimental points since it is one of the major source of systematic error.

One solution to handle experimental nuisance parameters is to reinterpret experiments from raw data with a proper systematic uncertainty description [De Saint Jean et al., 2010b]. Such practice unfortunately can trigger a *Peelle's Pertinent Puzzle*¹⁷ (PPP) [Smith, 1990, Chiba and Smith, 1991]. It has been demonstrated that, in the case of a full correlation matrix due to a normalization factor which multiplies the theoretical model, the occurrence of unexpected mean values and uncertainties in statistical data analysis

¹⁶With data assimilation we indicate the updating of our knowledge integrating new experimental data. An example is the Bayesian learning process, which allows to adjust theoretical model parameters on new measurements.

¹⁷Peelle, in an informal memorandum of 1987 of the Oak Ridge National Laboratory, showed the possibility to obtain unexpected results for average parameters values and uncertainties when the adjustment procedure includes a fully correlated experimental covariance matrix. Such abnormal low results may induce to think that the GLS procedure fails in certain situations. Successively, in the present dissertation, the marginalization technique will be presented as a powerful method to introduce systematic uncertainties in the evaluation process.

of experimental points is not only due to the model non-linearity but also to improper estimation of the experimental covariance matrix [Neudecker et al., 2012].

For that reason Marginalization techniques have been developed to introduce an objective treatment of systematic uncertainties, able to avoid pathological behavior such as the PPP. In the following sections two methods will be presented, both developed at CEA-Cadarache [Habert, 2009] in the framework of the CONRAD project.

1.5.1 The Marginalization Technique

Let us suppose to have available a set of experimental data $\vec{y} = y_1, \dots, y_N$ which can be used as new experimental evidence in the Bayesian updating process of some model parameters \vec{x} . In Sec. 1.3.1 we have seen the Bayes theorem in its continuous formulation

$$p_{post}(\vec{x} | \vec{y}U) d\vec{x} = \frac{p_{prior}(\vec{x} | U) \mathcal{L}(\vec{y} | \vec{x}U) d\vec{x}}{\int p_{prior}(\vec{x} | U) \mathcal{L}(\vec{y} | \vec{x}U) d\vec{x}}, \quad (1.106)$$

where we supposed the existence of only experimental data \vec{y} , model parameters \vec{x} and some prior knowledge U . If we desire to propagate uncertainties related to some nuisance parameters \vec{v} during the fitting process of parameters \vec{x} , a possible strategy could be recurring to the Bayesian marginalization of the \vec{v} parameters [Leonard and Hsu, 1999]. \vec{v} can be considered in fact as vector of input parameters affected by uncertainties, which are added to the list of unknown random variables. In that case, we can suppose an extended probability density $p(\vec{x}, \vec{v} | \vec{y}, U)$ and derive a marginal distribution integrating over the nuisance parameters:

$$p_{\vec{v}}(\vec{x} | \vec{y}U) = \int d\vec{v} \cdot p(\vec{x} \vec{v} | \vec{y}U). \quad (1.107)$$

Thanks to the conditional probability theorem we can rewrite Eq. 1.107 as

$$p_{\vec{v}}(\vec{x} | \vec{y}U) = \int d\vec{v} \cdot p(\vec{x} | \vec{v} \vec{y}U) p(\vec{v} | \vec{y}U), \quad (1.108)$$

which, if \vec{v} does not depend on \vec{y} , is equivalent to

$$p_{\vec{v}}(\vec{x} | \vec{y}U) = \int d\vec{v} \cdot p(\vec{x} | \vec{v} \vec{y}U) p(\vec{v} | U). \quad (1.109)$$

We can now reformulate the Bayes theorem including some knowledge on nuisance parameters, which is effectively given by the experimental conditions. Let us then settle the following relation between posterior and prior density functions:

$$p(\vec{x} | \vec{y} \vec{v} U) = \frac{p_{prior}(\vec{x} | \vec{v} U) \mathcal{L}(\vec{y} | \vec{x} \vec{v} U) d\vec{x}}{\int p_{prior}(\vec{x} | \vec{v} U) \mathcal{L}(\vec{y} | \vec{x} \vec{v} U) d\vec{x}}, \quad (1.110)$$

where again U is the background information from which we assume prior knowledge (\vec{x}, \vec{v}) , supposed independent from \vec{y} . It is quite reasonable to presume that our prior knowledge on the parameters \vec{x} is independent from the nuisance vector \vec{v} ¹⁸. In such case we have

¹⁸This is true if, to deduce priors, completely independent experiments have been performed, using their own normalization and reduction procedure. This could be not the case when, for example, experimental values are normalized using *standard* quantities, well known data widely used in many applications.

$$p(\vec{x} | \vec{y} \vec{\nu} U) = \frac{p_{\text{prior}}(\vec{x} | U) \mathcal{L}(\vec{y} | \vec{x} \vec{\nu} U) d\vec{x}}{\int p_{\text{prior}}(\vec{x} | U) \mathcal{L}(\vec{y} | \vec{x} \vec{\nu} U) d\vec{x}}, \quad (1.111)$$

which, if substituted in Eq. 1.109, gives [De Saint Jean et al., 2009]

$$p_{\vec{\nu}}(\vec{x} | \vec{y} U) = \int d\vec{\nu} \cdot p(\vec{\nu} | U) \cdot \frac{p_{\text{prior}}(\vec{x} | U) \mathcal{L}(\vec{y} | \vec{x} \vec{\nu} U) d\vec{x}}{\int p_{\text{prior}}(\vec{x} | U) \mathcal{L}(\vec{y} | \vec{x} \vec{\nu} U) d\vec{x}}. \quad (1.112)$$

Our main goal is finally reduced to the estimation of the first two moments of this last probability distribution. Model parameter averages and covariance matrix, including nuisance parameters effects, can be then obtained. In the next paragraphs few methodologies to accomplish this task will be briefly presented.

1.5.1.1 Analytical Marginalization

In Sec. 1.4.1 we have seen the formulation of the Generalized Least Squares Method which is based on several ingredients, among which we find the Maximum Entropy theorem that allows us to treat prior and likelihood distributions as Gaussians. If we suppose that nuisance parameters $\vec{\nu}$ are normally distributed, once they are provided with an associated covariance matrix \mathbf{C}_{ν} , an analytical procedure can be set up to find the first two moments of distribution 1.112.

We can define an extended parameter vector \vec{X} as

$$\vec{X} = \begin{pmatrix} \vec{x} \\ \vec{\nu} \end{pmatrix}, \quad (1.113)$$

and the associated covariance matrix $\mathbf{C}_{\mathbf{X}}$

$$\mathbf{C}_{\mathbf{X}} = \begin{pmatrix} \mathbf{C}_{\mathbf{x}} & \mathbf{C}_{\mathbf{x},\nu} \\ \mathbf{C}_{\nu,\mathbf{x}} & \mathbf{C}_{\nu} \end{pmatrix}. \quad (1.114)$$

Let us suppose to have an experimental file which is affected by a certain uncertainty on the normalization. Such uncertainty correlates systematically all the experimental points $\vec{y} = (y_1, y_2, \dots, y_{k-1}, y_k)$, so we want to marginalize such error propagating it on the parameters which participate directly to the theoretical model $\vec{f}(\vec{x})$. The experimental data points are generally depending on one or more independent variables. If we are considering a cross section, for example, experimental values will be cross section values provided for specific energies. Otherwise, if fission yields are considered, they will be provided for a specific mass number, charge and isomeric state. Such experimental points define a specific grid (e.g. an energy grid) for which we can calculate corresponding theoretical values. To simplify notations, let us call $\vec{t} = (t_1, \dots, t_k)$ the theoretical values calculated in the same grid points in which experimental data are provided. The covariance matrix for the theoretical model \vec{t} can be obtained as follows:

$$\mathbf{C}_{\mathbf{t}} = \mathbf{G} \mathbf{C}_{\mathbf{X}} \mathbf{G}^{\dagger}, \quad (1.115)$$

where

$$\mathbf{G} = \begin{pmatrix} \mathbf{G}_{\mathbf{x}} & \mathbf{G}_{\nu} \end{pmatrix}, \quad (1.116)$$

$$\mathbf{G}_x = \begin{pmatrix} \frac{\partial t_1}{\partial x_1} & \cdots & \frac{\partial t_1}{\partial x_n} \\ \vdots & & \vdots \\ \frac{\partial t_k}{\partial x_1} & \cdots & \frac{\partial t_k}{\partial x_n} \end{pmatrix}, \quad (1.117)$$

and

$$\mathbf{G}_\nu = \begin{pmatrix} \frac{\partial t_1}{\partial \nu_1} & \cdots & \frac{\partial t_1}{\partial \nu_n} \\ \vdots & & \vdots \\ \frac{\partial t_k}{\partial \nu_1} & \cdots & \frac{\partial t_k}{\partial \nu_n} \end{pmatrix}. \quad (1.118)$$

At this stage, our final goal is to deduce a marginalized covariance matrix for the model parameters \mathbf{C}_x^μ able to duplicate the same \mathbf{C}_t we get applying the sandwich rule to the original matrix \mathbf{C}_x . A straightforward way to do that is to simply impose

$$\mathbf{G}_x \mathbf{C}_x^\mu \mathbf{G}_x^\dagger = \mathbf{G} \mathbf{C}_x \mathbf{G}^\dagger. \quad (1.119)$$

Just multiplying on the left by \mathbf{G}_x^\dagger and on the right \mathbf{G}_x we obtain

$$\mathbf{G}_x^\dagger \mathbf{G}_x \mathbf{C}_x^\mu \mathbf{G}_x^\dagger \mathbf{G}_x = \mathbf{G}_x^\dagger \mathbf{G} \mathbf{C}_x \mathbf{G}^\dagger \mathbf{G}_x. \quad (1.120)$$

$\mathbf{G}_x^\dagger \mathbf{G}_x$ is a n -dimensional square matrix, where n is the number of model parameters. Such matrix can be inverted if \mathbf{G}_x has a rank equal to the number of model parameters. In other words the number of experimental points has to be greater than the number of parameters and the partial derivatives over the different parameters must be linearly independent. Once these conditions are verified we find [Habert et al., 2010]

$$\mathbf{C}_x^\mu = (\mathbf{G}_x^\dagger \mathbf{G}_x)^{-1} \mathbf{G}_x^\dagger \mathbf{G} \mathbf{C}_x \mathbf{G}^\dagger \mathbf{G}_x (\mathbf{G}_x^\dagger \mathbf{G}_x)^{-1}. \quad (1.121)$$

Once the adjustment procedure has been completed, such formula can be applied allowing us to find the *marginalized* covariance matrix for the model parameters \mathbf{C}_x^μ . The experimental covariance matrix needs to contain only statistical uncertainties, presenting therefore zero off-diagonal values to not take into account twice the same source of error. Systematic uncertainties are then retained by nuisance parameters and are absorbed by the nuclear reaction model ones. The final covariance matrix \mathbf{C}_x might be then seen as

$$\mathbf{C}_x = \mathbf{C}_x^{\text{stat}} + \mathbf{C}_x^\mu, \quad (1.122)$$

where $\mathbf{C}_x^{\text{stat}}$ is provided by statistical uncertainties only.

Such technique have been widely adopted to introduce systematic uncertainties and so correlations among FY model parameters. In the next paragraph the Monte Carlo procedure will be shown for a sake of completeness, even if not really used in present dissertation.

1.5.1.2 Standard Monte Carlo Marginalization

As already said the first goal in marginalization techniques is to find the first two moments of distribution $p_{\vec{v}}(\vec{x} | \vec{y} U)$ in Eq. 1.112. Performing Monte Carlo sampling using the $p(\vec{v} | U)$ distribution, we can provide a set of $\vec{v}^{(k)}$ ($k = 1, \dots, K$) values which allow us to solve the problem in a stochastic way. For each sampled vector $\vec{v}^{(k)}$, in fact, we can fit the parameter vector \vec{x} using the GLSM and so minimizing a cost function for [De Saint Jean et al., 2009]

$$p_{\vec{\nu}=\vec{\nu}^{(k)}}(\vec{x} | \vec{y}U) \propto p(\vec{x} | U) \cdot \mathcal{L}(\vec{y} | \vec{x} \vec{\nu} = \vec{\nu}^{(k)}), \quad (1.123)$$

where $p_{\vec{\nu}=\vec{\nu}^{(k)}}(\vec{x} | \vec{y}U)$ is still the posterior probability seen in Sec. 1.4.1, but now with given nuisance parameters $\vec{\nu}^{(k)}$. Therefore, performing the GLS procedure K times, an equal number of $\vec{x}^{(k)}$ parameter vectors are available, knowing that, even in this case, the assumptions made for GLS are still needed. Also K covariance matrices $\mathbf{C}_x^{(k)}$ are similarly produced by the method.

Vectors $\vec{x}^{(k)}$ can be seen as best estimators of the model parameter averages, once their posterior probability distribution is given by the Bayes theorem. In formulas we can write

$$\vec{x}^{(k)} = \mathbb{E}(\vec{x} | \vec{\nu} = \vec{\nu}^{(k)}). \quad (1.124)$$

Thanks to the theorem of total expectation¹⁹, we can write

$$\mathbb{E}(\vec{x}^{(k)}) = \mathbb{E}(\vec{x}). \quad (1.126)$$

Therefore model parameter best estimates can be found averaging $\vec{x}^{(k)}$ vectors. A similar operation can be achieved even for the covariance matrices produced applying the GLSM multiple times, once the different set of nuisance parameters are sampled. K covariance matrices can be hence generated and we call

$$(\mathbf{C}_x^{(k)})_{i,j} = cov(x_i, x_j | \vec{\nu} = \vec{\nu}^{(k)}) \quad (1.127)$$

the covariance matrix associated to the k -th sampling. Invoking the total covariance theorem²⁰, we obtain [De Saint Jean et al., 2009]

$$cov(x_i, x_j) = cov[\mathbb{E}(x_i | \vec{\nu} = \vec{\nu}^{(k)}), \mathbb{E}(x_j | \vec{\nu} = \vec{\nu}^{(k)})] + \mathbb{E}[cov(x_i, x_j | \vec{\nu} = \vec{\nu}^{(k)})] \quad (1.129)$$

or in other words

$$cov(x_i, x_j) = cov(x_i^{(k)}, x_j^{(k)}) + \mathbb{E}[(\mathbf{C}_x^{(k)})_{i,j}]. \quad (1.130)$$

The estimation of the final marginalized covariance matrix is thus obtained by the sum of two matrices: the former is generated applying the standard covariance estimator to the parameter samplings and the latter is given by the average of all the K covariance matrices obtained applying the GLSM.

1.5.1.3 Bayesian Monte Carlo Marginalization

Similarly to what we saw for best estimates and covariances generation, we can perform a Monte Carlo marginalization using BMC. Without pretending to be exhaustive, new features have been added in CONRAD [Privas, 2015] to achieve marginalization of nuisance parameters $\vec{\nu}$ using BMC. The principle is basically the same, we perform K Monte Carlo

¹⁹Combining the Bayes and Fubini theorems (see Ref. [Roe, 2001]) it can be demonstrated that, if two random variables Z_1 and Z_2 are given, then

$$\mathbb{E}[\mathbb{E}(Z_1 | Z_2)] = \mathbb{E}(Z_1), \quad (1.125)$$

which is called theorem of total expectation.

²⁰If three random variables Z_1 , Z_2 and Z_3 are given, the total covariance theorem says that [De Saint Jean et al., 2009]

$$cov(Z_1, Z_2) = \mathbb{E}[cov(Z_1, Z_2 | Z_3)] + cov[\mathbb{E}(Z_1 | Z_3), \mathbb{E}(Z_2 | Z_3)]. \quad (1.128)$$

The full proof can be found in Ref. [Panjer, 1973].

samplings on the extended \vec{X} parameter vector, as defined in Eq. 1.113. Then, posterior parameters can be estimated by

$$\langle x_i \rangle_K = \frac{\sum_{k=1}^K x_{i,k} \mathcal{L}(\vec{y}_k | \vec{x}_k \vec{\nu}_k)}{\sum_{k=1}^K \mathcal{L}(\vec{y}_k | \vec{x}_k \vec{\nu}_k)}, \quad (1.131)$$

and the posterior covariance matrix is simply obtained by

$$(\mathbf{C}_x^\mu)_{i,j}^K = \text{cov}(x_i, x_j)_K = \langle x_i, x_j \rangle_K - \langle x_i \rangle_K \langle x_j \rangle_K, \quad (1.132)$$

where

$$\langle x_i, x_j \rangle_K = \frac{\sum_{k=1}^K x_{i,k} x_{j,k} \mathcal{L}(\vec{y}_k | \vec{x}_k \vec{\nu}_k)}{\sum_{k=1}^K \mathcal{L}(\vec{y}_k | \vec{x}_k \vec{\nu}_k)}. \quad (1.133)$$

1.6 A Few words on the Model Defect Problem

As it will be clearer in Ch. 4, one major issue in nuclear data evaluation is the unrealistic small uncertainties often obtained at the end of the adjustment procedure. Often, such underestimated uncertainties are partially justified by missing experimental correlations which would introduce systematic errors in nuclear data. For that reason marginalization techniques have been developed to rigorously and objectively propagate such uncertainties to model parameters.

Nevertheless, one of the major concerns challenging physicists is that Bayes theorem works properly and consistently if and only if our prior knowledge U (see Eq. 1.45) is actually *true*. Inside U we have tacitly included our knowledge about the theoretical model behind the nuclear data we are evaluating. Such models are often imperfect and they can derive from systematics or semi-empirical assumptions. We will see in Chapter 4 that the Bayesian theorem, and so all the methods which derive from it, are strongly guided by small uncertainty experimental data points. Such uncertainties can have an outstanding impact on covariance matrix evaluations. Since the theoretical model behind is actually considered true, accurate experimental points which can be well represented by model calculations cover a major role in the adjustment procedure, steering model best estimates and uncertainties. Including such model deficiencies can be then an important practice in enhancing data uncertainties, since we include in our evaluation the leak of knowledge coming from our ignorance on the physical process.

Such model defect uncertainties is by the way hard to be included in a mathematically rigorous way. The addition of extra uncertainty implies a certain degree of speculation and subjectivity in the evaluation. In the present dissertation no deep use of techniques including model deficiencies will be presented, we leave such topic to future developments of the work.

1.7 Conclusions

In this chapter the main features of data and covariance matrix evaluation methodologies have been presented, providing the theoretical background needed to accomplish the goals proposed in the present doctoral work.

In Sec. 1.1 we explored the context from a more general point of view, abstracting from the

strict nuclear application. We saw how this covariance matrix and uncertainty quantification work can be collocated, in a broaden sense, in code validation activities. Different kinds of uncertainty have been considered, highlighting the difference between statistical and systematic, which have been of primary importance in the development of the present work.

The importance of covariances in a proper uncertainty propagation and quantification exercise was highlighted in Sec. 1.2. The uncertainty propagation law, better known as sandwich rule, has been defined, since it is widely used in this and other similar activities. It was emphasized how the sandwich rule was actually obtained performing a first-term truncation of the Taylor expansion for the sought quantity of interest functional, $q(\vec{x})$. In this case sensitivity coefficients can be simply deduced from first-order derivatives, which is an acceptable approximation if $q(\vec{x})$ does not show strong non-linearities.

Sec. 1.3 was devoted to the probabilistic foundation of data evaluation methodologies. The Bayes and the Maximum Entropy theorems have been introduced. The former provides an updating procedure for the posterior model parameter probability distribution, once new experimental evidence is available. The latter gives us the possibility to use Gaussians for the prior and the likelihood distributions. It builds in fact the connection between the frequentist approach, on which classical statistics was born, and the Bayesian formulation, demonstrating the equivalence between the classical least square postulations and the Bayesian-derived GLSM.

In Sec. 1.2 different covariance evaluation methodologies have been explored, giving more space to the deterministic GLSM, since it has been preferred in present work covariance evaluations. Advantages and drawbacks have been enunciated for deterministic and Monte Carlo approaches. All these adjustment tools were already available in CONRAD and no further implementation work in this field was demanded.

In Sec. 1.5 the problem of systematic uncertainties was approached. The marginalization technique, developed at CEA-Cadarache, was described in its analytical and stochastic formulation. Such techniques provide powerful tools to an objective and comprehensive inclusion of systematic uncertainties associated to nuisance parameters, which are propagated to the nuclear reaction ones. The marginalization technique is extremely useful especially if no information is provided on systematic uncertainties in experimental data files, and it has been extensively used in the present work. Nevertheless, recent significant efforts [Kessedjian, 2015] have been made to develop methodologies capable to estimate experimental systematic uncertainties for fission yields, which are the nuclear data of principal interest treated here. Such experimental covariance matrices, which include systematic information, should be properly taken into account in a comprehensive evaluation process.

Finally the problem of model defects has been risen. The Bayes theorem is an extraordinary theoretical tool but it relies on prior theoretical information, which is considered indisputably true. We have anticipated that nuclear reaction and fission yield models might be approximated, or even deriving from empirical conclusions. Such model defects should be in principle taken into account, but rigorous and objective ways to proceed still need to be conceived.

The next chapter will be devoted to fission yield semi-empirical models. Based on

physical principles, they essentially rely on empirical assumptions since no effective predictive model exist for fission yields. They will contribute to the term $\vec{t}(\vec{x})$ in a GLS formalism, providing calculated values for those isomers whose experimental fission yield is available and employed in model parameter adjustment.

Chapter 2

Fission Yields Semi-Empirical Models

Contents

2.1	The Main Features of the Fission Process	43
2.1.1	Hands on the Fission Process	44
2.1.2	Characteristics of the Fragments	45
2.1.3	Prompt Particles Emission	47
2.2	Models for Fission Yield Evaluation	48
2.2.1	Fission Yields Definitions	49
2.2.2	Modeling Mass Fission Product Yields	50
2.2.3	The Wahl Model for Isotopic Fission Yields	59
2.2.4	Isomeric Repartition: The Madland England Model	64
2.3	Conclusions	67

FISSION product yields (FY) are fundamental nuclear data for burn-up and activation calculations, including those of decay heat, shielding, dosimetry, fuel handling, waste disposal and safety [Mills, 1995]. Nowadays full uncertainty information are not available in current data banks and the nuclear community expressed the need for reliable fission yield covariance matrices, taking into account complete uncertainty data and so correlations [Mills, 2012].

In this chapter some fission yield models to generate best estimates and associated uncertainties are discussed. Before starting describing the models we adopted in the adjustment procedure, some essentials of the neutron-induced fission process will be provided. The models implemented in CONRAD and so used in a GLS procedure will be deeply examined. In particular, once definitions for independent and cumulative fission yields are given, model descriptions for mass, charge and isomeric distributions will be provided together with the Q-matrix formalism at the basis of cumulative yield estimations. Such models will represent theoretical FY calculations in the Bayesian adjustment procedure, so they will play a role in Eq. 1.94 through the term $\bar{t}(\vec{x})$ described in the previous chapter.

2.1 The Main Features of the Fission Process

In this section some general features of the nuclear fission process will be presented, without pretending to be exhaustive and without providing a complete phenomenon description,

that can be found in dedicated references (e.g. [Wagemans, 1991]). The main objective of this brief presentation is to allow, who is not specialist of the field, to have a straightforward comprehension of the following paragraphs concerning fission yields models. Those who own already a deep knowledge about the fission process can directly skip to Sec. 2.2.2 and discover, without any waste of time, which models have been chosen in FY evaluation and covariance generation.

2.1.1 Hands on the Fission Process

Nowadays we associate the official discovery of the fission process to the paper published by O. Hahn and F. Strassmann in January 1939 [Hahn and Strassmann, 1939] in the *Naturwissenschaften* journal. The reaction which led the two scientists (and Lise Meitner) to find out that a nucleus can decay into two fragments was the neutron-induced fission of Uranium. Other fission-related events were observed before that day, such as the discovery of ^{99}Tc by Noddack in 1925, as Uranium fission product. Since then, many experiments have been carried on to understand such fascinating phenomenon and many fission theories have been proposed. However, many unexplained behaviors shown by fission observables as well are still challenging physicists and much more has to be done.

The nuclear fission at low excitation energy is a compound nucleus reaction in which a heavy nucleus splits in two fragments, whose masses are in general not identical. For induced fission, the first step is to supply a sufficient quantity of excitation energy which can overcome the fission barrier B_f ¹. Those nuclei which can achieve so thanks only to the binding energy of a thermal neutron are called *fissile*. Otherwise, if the neutron separation energy of the compound nucleus $S_n < B_f$, fission is a threshold reaction and only neutrons with enough kinetic energy to transmit an excitation larger than B_f can induce fission with a non-negligible probability. Such nuclei are called *fissionable* or *fertile*. An example of a fissile nucleus is ^{235}U , since ^{236}U , the compound nucleus, has $S_n = 6.5$ MeV which exceeds the fission barrier $B_f = 5.7$ MeV. On the other hand, ^{239}U has $S_n = 4.8$ MeV, so ^{238}U needs a neutron with a kinetic energy of at least 1.5 MeV to overcome the fission barrier of 6.45 MeV [Gönnenwein, 2014].

Once the compound nucleus is excited, it can return to the ground state by emission of γ rays or neutrons. Otherwise, it can find a configuration, which is called *saddle point*, unstable towards fission. At this stage, according to the present knowledge, the nucleus is already presenting a significant deformation, which consists in two spherical lobes connected by a thinner neck. The two fragments start then to separate, driven by the Coulombian force. The neck, becoming thinner, reaches the rupture point and two distinct fragments are generated, accelerating under Coulombian repulsion. As it is just described, we often talk about binary fission, where only two fragments are the result of the scission process. However, experimental evidence [Serot et al., 2007] showed the emission of a third light particle, such as scission neutrons or light nuclei (e.g. α particle).

After full acceleration, fission fragments still have some excitation energy so prompt neutrons and gammas are emitted. We commonly call *primary fragments* or simply *fission fragments* the nuclides being formed just after the nuclear scission. Generally, with *fission products*, reactor physicists allude to isotopes which have already emitted prompt neutrons

¹Actually, there is not a single fission barrier, hence we should consider the highest one.

and gamma [Wagemans, 1991]. Prompt neutron evaporation is a very fast process. All neutrons are expelled in 10^{-14} s, so experimental observations are referred necessarily to fission products. As it will be clearer hereinafter, this is an important issue, since light and heavy fission fragments evaporate a different average number of prompt neutrons. Therefore, the original double-humped pre-neutron evaporation distribution is no longer symmetric after prompt neutron emission.

Even after prompt neutron emission, fission products are still neutron rich and hence unstable. To reach the stability line in the nuclide chart, fission products typically undergo β^- decays. It can happen that such decays lead to excited states, above the S_n . Therefore delayed neutrons are then emitted, whose importance is well known in controlling nuclear reactors.

2.1.2 Characteristics of the Fragments

In this section the general features of nuclear fission characteristics and observables are described. The main goal is to analyze the most significant elements deduced by experimental observations, which can guide us during the Bayesian adjustment. Again, solely elementary aspects are treated hereinafter, for a complete and refined overview we leave the reader to specific references [Wagemans, 1991].

Neutron-induced fission has been studied mostly using actinides as target nuclei, hence elements whose atomic number goes from $Z=89$ (Actinium) to $Z=103$ (Lawrencium). Since the beginning, measurements of neutron-induced fissions showed remarkable asymmetry in the charge and mass repartition between the two fragments for isotopes included between ^{229}Th and ^{254}Es in the nuclide chart [Gönnenwein, 2014]. In Fig. 2.1 fission fragments evaluated mass distributions are presented to show asymmetric split. Fission reactions induced by thermal neutrons seem to have some significant features that should be taken into account during evaluations:

- i) The heavy peak remains almost in the same position, starting to rise around mass $A_H \approx 132$ amu. The corresponding magic numbers are $Z = 50$ and $N = 82$, due to shell effects.
- ii) The post-neutron mass yield distribution exhibits fluctuations due to prompt neutron emission that, in principle, should be taken into account during the evaluation process.

Experimental observations showed the coexistence of asymmetric and symmetric fission modes, with different fission barriers. Potential surface theoretical calculations [Möller et al., 2009] confirmed higher symmetric fission barriers for those actinides who presented a predominant asymmetry. With ^{258}Fm we find the transition between asymmetric and symmetric scission, which has been corroborated by theoretical fission models. According to experimental and so evaluated data, as it is also pictured by Fig. 2.1, there are two mass regions where fission products mass distributions seems to be anchored, if several fissioning systems are analyzed. In the super-asymmetric light region ($A \approx 75$ amu, that could be due to $Z=28$ and $N=50$), mass yields appear almost identical between different fissioning systems. Such behavior is roughly repeated in the asymmetric heavy region ($A \approx 132$ amu), where different systems fission yields assume quite similar values.

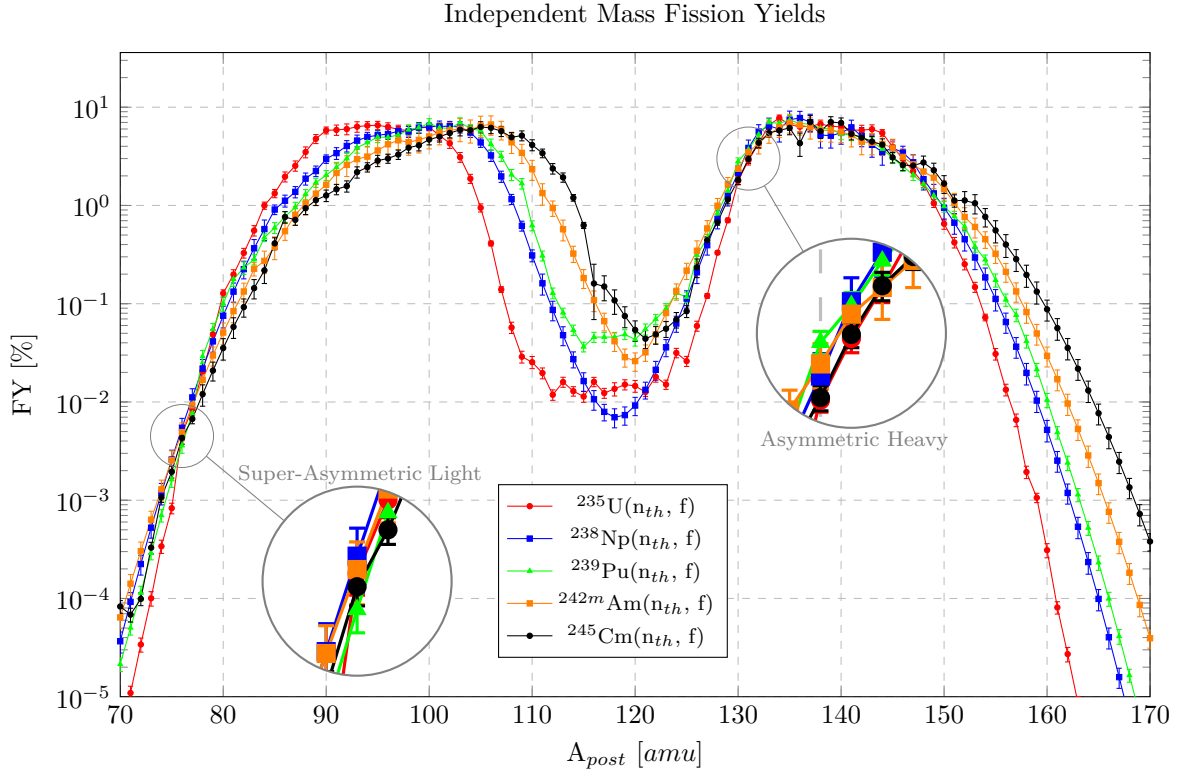


Figure 2.1: Independent mass fission yields for several thermal fissioning systems, data from JEFF-3.1.1 library.

The total available energy at the scission point in a neutron-induced fission is the Q -value:

$$Q = M_T + M_n + E_n - (M_L^{pre} + M_H^{pre}), \quad (2.1)$$

where M_T is the target nucleus mass, M_n and E_n are respectively neutron mass and energy, M_L^{pre} and M_H^{pre} are the masses of the light and the heavy fragments before prompt neutron emission. Such energy is shared between the total kinetic energy TKE and the total excitation energy TXE of the fission fragments:

$$Q = TKE + TXE, \quad (2.2)$$

the average value for the total kinetic energy for the thermal fission of ^{235}U is about 170 MeV. In the center of mass system, fragment momenta cancel out so we obtain

$$M_L^{pre} v_L^{pre} = M_H^{pre} v_H^{pre}, \quad (2.3)$$

$$\frac{M_L^{pre}}{M_H^{pre}} = \frac{E_H^{pre}}{E_L^{pre}}, \quad (2.4)$$

where E_L^{pre} and E_H^{pre} are kinetic energies of the heavy and light fragments. In Fig. 2.2 experimental values of the average kinetic energy as a function of the pre-neutron mass are provided for the thermal neutron induced fissions of ^{235}U and ^{239}Pu .

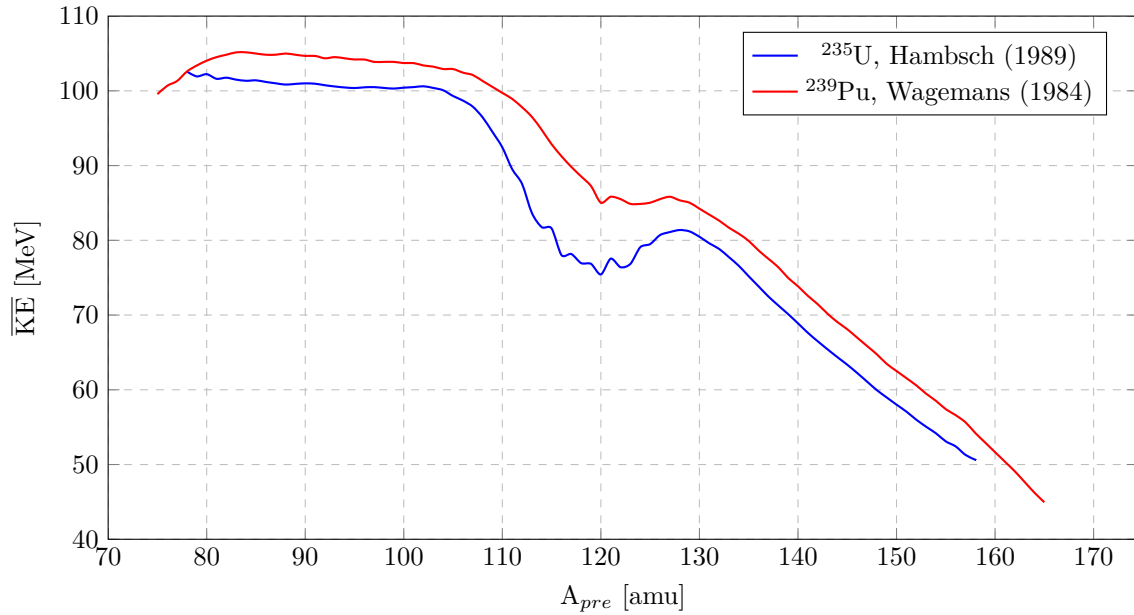


Figure 2.2: Average kinetic energy as a function of the pre-neutron mass for the thermal fission of ^{235}U [Hambusch et al., 1989] and ^{239}Pu [Wagemans et al., 1984].

Fragment energies and velocities are often used in experiments to determine masses in double-velocity and double-energy techniques (see Sec. 3.2). Nevertheless, prompt neutron evaporation is extremely fast and happens in 10^{-14} s. Such thin time window does not allow any pre-neutron fragment detections, then only post-neutron evaporation fission products can be measured. In this sense, to measure fragment mass yields, the double-velocity technique is preferable since the almost isotropic neutron emission does not induce any variation in fragment velocities.

2.1.3 Prompt Particles Emission

Most of the Q -value is transferred to the fission fragments as kinetic energy. However a significant fraction is shared by the fragments as excitation energy which has to be dissipated to reach lower energy states and so more stable levels. Since such nuclei are neutron rich, the first possible disexcitation way is through neutron evaporation. Prompt neutrons are normally emitted by the fission fragments between 10^{-18} s and 10^{-14} s, once fully accelerated. During such time interval, a neutron- γ emission competition sets in until the binding energy of the last neutron is reached. Successively, fission fragments cool down and get rid of the residual excitation energy by only γ emission. The mechanism of how the two fission fragments share available excitation energy is still obscure. A sure indicator of fragment excitation energy is the average number of prompt neutrons emitted. Heavy and light fragments evaporate prompt neutrons differently, the average number of prompt neutron emitted by a single fragment $\bar{\nu}$ depends in fact on the pre-neutron fragment mass A_{pre} . Experimental observations showed that, for many fissioning systems, $\bar{\nu}(A_{pre})$ is characterized by a saw-tooth shape. In Fig. 2.3 the saw-tooth for the thermal fission of ^{239}Pu is presented.

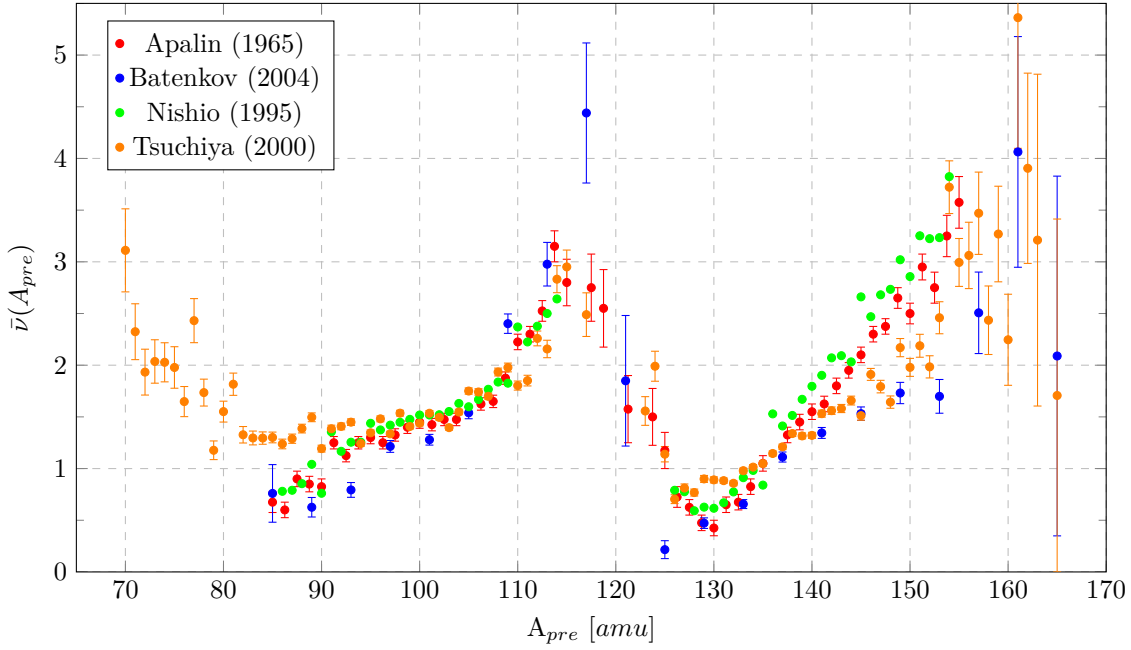


Figure 2.3: Average number of prompt neutrons emitted by a fission fragment of mass A_{pre} for the thermal neutron-induced fission of ^{239}Pu , from different experiments (Refs. [Apalin et al., 1965, Nishio et al., 1995, Tsuchiya et al., 2000, Batenkov et al., 2004]).

The average number of prompt neutrons emitted shows a minimum around $129 \div 132$ amu, which is probably correlated to magic numbers of ^{132}Sn . Such peculiarities in saw-tooth distributions induce asymmetries in the post-neutron mass yields. After scission, light and heavy fragments have complementary masses, such that their sum equals the compound nucleus mass A_f . Just after scission and before any prompt neutron emissions, yields are symmetric since complementary masses exhibit the same yields. After prompt neutrons emission, yields are not symmetric anymore, light fragments emit on average more neutrons than the heavy ones and the mass distribution strongly depends on the saw-tooth shape.

2.2 Models for Fission Yield Evaluation

The discussion of the main features of the fission process seen in the previous section gave a general overview of the fission process. In the following paragraphs the models we used for FY covariance generation are presented.

Several fission models exist in literature and are applied to understand better the fission process and the experimental data. They are mostly phenomenological, since no predictive theories exist at the moment able to describe the fission process. They can be classified in macroscopic models, which consider the global evolution of the nucleus during the fission event as would be, for instance, a liquid drop, and microscopic ones, which are based on more rigorous theoretical foundations treating nucleon-nucleon interactions. However, none of them is actually able to reproduce successfully exact quantitative results for a so difficult many-bodies problem as the fission reaction.

To generate covariances which could be consistent with existing JEFF-3.1.1 library, the FY models at the basis of such evaluation were mainly considered. The cornerstone of such evaluation is the application of the Brosa model [Brosa et al., 1990], which successfully

predicted the existence of different fission channels, resulting in different fission modes². Nevertheless, while the Brosa model has been used in JEFF-3.1.1 to fill gaps [Mills, 1995] in post-neutron mass yields distributions when experimental data were not available, here it has been consistently and physically applied to pre-neutron distributions, how it was meant to be. The prompt-neutron evaporation has been successively modeled with a Gaussian distribution.

Since no physical and predictive theories exist for isotopic and isomeric distributions, the Wahl and the Madland-England semi-empirical models have been used, as done in JEFF-3.1.1 in absence of experimental measurements.

2.2.1 Fission Yields Definitions

In the ENDF (Evaluated Nuclear Data Format) format (see App. B) we files two kinds of fission yields: *independent* and *cumulative*. Independent yields concern fission products after prompt neutron evaporation but before any radioactive decay. As already done in the previous sections, we will also refer to such yields as *post-neutron*. Therefore, primary fission fragments will be usually identified by *pre-neutron* distributions. Independent FY are crucial for decay and elementary fission heat calculations since they allow to determine the initial concentration of the fission fragments inventory that will release energy through the radioactive decay. As it will be better explained in the following sections, codes such as MENDEL³ can in fact solve the Bateman equation describing the evolution of nuclei concentrations in the nuclear reactor, once the neutron flux is provided. Most of the present work will be dedicated to generate application-oriented covariance matrices for independent FY, to be used in depletion calculations.

After the prompt neutron evaporation, the fission fragments are still neutron rich and β^- decays set in. Usually, fission products are located at about 3 charge units far from the β^- -decay stable line. For nuclei very far from the stability, the half-lives are reduced such that for a 6-units far isotope we find $T_{1/2} \leq 1$ s. To take into account radioactive decay cumulative FY are used. Cumulative FY are in fact the summation of all the contributions to a given isotope overall the entire decay time, since the fission process happened. In formulas given in Ref. [Mills, 1995], for the generic cumulative yield C_i we can write:

$$C_i = Y_i^{post} + \sum_j C_j b(j \rightarrow i), \quad (2.5)$$

where i indicates a generic triplet $(A, Z, M)_i$ and $b(j \rightarrow i)$ is the branching ratio which gives the probability that an isomer $(A, Z, M)_j$ decays into $(A, Z, M)_i$. Y_i^{post} is the corresponding independent yield for the isomer i . In matrix form the last equation can be written as

$$\vec{C} = \mathbf{Q}\vec{Y} \quad (2.6)$$

where

$$\mathbf{Q} = (\mathbf{I} - \mathbf{B})^{-1}, \quad (2.7)$$

²The fission process is a complex phenomenon. In the present work we left out any discussion on fission cross section, compound nucleus formation, and how the saddle point is reached. We are more focused on exit channels and fragment characteristics, at the basis of FY distributions. For more details on the fission process we leave the reader to dedicated references (e.g. [Wagemans, 1991]).

³MENDEL is an inventory/decay-heat calculation code developed at CEA which is capable to read APOLLO2 [Sanchez et al., 1988], APOLLO3 [Golfier et al., 2009] and TRIPOLI-4 [Brun et al., 2015] outputs to retrieve fluxes and self-shielded cross sections that are necessary to solve the Bateman equation.

with \mathbf{B} indicating the branching ratio matrix and with \vec{C} and \vec{Y} respectively the cumulative and the independent FY vectors.

In the ENDF format FY are given specifying mass, charge and isomeric state. So we usually talk about *isomeric* FY, which consider the isomeric repartition of the fission fragments if metastable states are possible.

In the present FY nuclear data library, such as JEFF-3.1.1, semi-empirical models are employed to calculate independent fission yields. Such models are used in a fitting procedure to interpolate-extrapolate missing data, especially for those fissioning systems which have few available experimental measurements. Independent isomeric fission yields can be written as the product of three functions

$$Y_{post}(A, Z, M) = Y_{post}(A)f(A, Z)R(A, Z, M) \quad (2.8)$$

where $Y_{post}(A)$ is the post-neutron mass distribution, $f(A, Z)$ is the charge distribution giving the fractional independent isotopic yield and $R(A, Z, M)$ is the isomeric ratio which gives how yields are subdivided between different metastable states. For each factor in Eq. 2.8 a model must be defined to calculate independent fission yields. Isotopic FY, denoted as $Y_{post}(A, Z)$, can be obtained summing over the available metastable states

$$Y_{post}(A, Z) = \sum_M Y_{post}(A, Z, M) = Y_{post}(A)f(A, Z), \quad (2.9)$$

$$\sum_M R(A, Z, M) = 1.0. \quad (2.10)$$

Post-neutron mass yields are similarly given by

$$Y_{post}(A) = \sum_{Z, M} Y_{post}(A, Z, M), \quad (2.11)$$

$$\sum_Z f(A, Z) = 1.0. \quad (2.12)$$

Since ternary fission is neglected in the present treatment, we have

$$\sum_A Y_{post}(A) = 2.0. \quad (2.13)$$

Independent mass yields $Y_{post}(A)$ differ of few percents by chain yields, $Ch(A)$. The latter are equal to the sum of all stable long-lived cumulative yields for a given mass chain [Mills, 1995]. The main reason is that unstable neutron-rich fission isomers mostly decay through β -particle emission, without any mass change. In the following sections the semi-empirical models we used to reproduce the JEFF-3.1.1 library and to generate covariances will be discussed.

2.2.2 Modeling Mass Fission Product Yields

JEFF-3.1.1 FY evaluated data are the result of weighted averages of experimental independent, cumulative and chain data obtained by different techniques and authors. In absence of any measurements, theoretical models have been used to fill gaps in the data, fitting model parameters. As better explained in Chapter 4, the Brosa model [Brosa et al., 1990] was chosen to be applied on mass FY. However, in JEFF evaluation, model parameters were fitted on post-neutron mass yields. To preserve consistency with JEFF data and respect the actual physical quantities that such model proposes to describe,

in the present work the Brosa fission modes are determined for pre-neutron FY distributions.

The Brosa model [Brosa et al., 1990, Brosa et al., 1999] gave a successful theoretical demonstration of the existence of different fission channels in spontaneous fission or low-energy induced fission, which have been observed from the pre-actinides to the heaviest nuclei⁴. It consists in a brilliant combination of multi-channels calculations, needed to determine the pre-scission shapes, and the random neck rupture theory. With the term scission we define the precise instant of the nucleus rupture, when the nucleus stretches beyond the pre-scission shapes. The pre-scission shape is the geometrical configuration of the nucleus thought as a liquid drop, with two lobes and a central thinner neck, just before the scission. Then rupture takes place, and Coulomb repulsion accelerates the fragments.

In the Brosa model, potential energies E_{def} of the deformed nucleus are calculated using the approach of Strutinsky [Strutinsky, 1968], where E_{def} has two origins. The former is macroscopic and derives from the *Liquid Drop Model* determination of the deformation potential. In the Brosa model the liquid drop geometrical configuration is similar to the classical 5-parameters Lawrence's description [Lawrence, 1965], with the additional feature of having globally a flat neck, which guarantees a random rupture (see Fig. 2.4). The second deformation potential component is due to shell effects, and is derived from microscopic quantum-mechanical calculations.

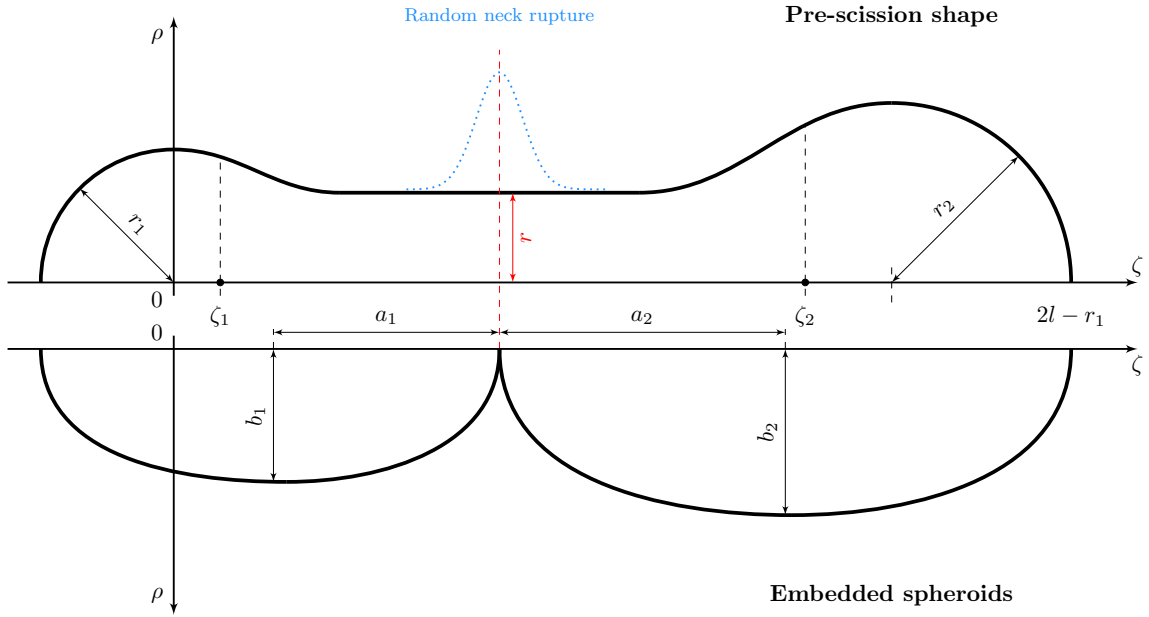


Figure 2.4: Representation of the pre-scission shape (figure reproduced from Ref. [Brosa et al., 1990]). The parameters in the figure are those used by Brosa modeling the geometrical description (see Ref. [Brosa et al., 1990] for details). ζ_1 and ζ_2 are the two centers of mass of the two lobes obtained after the compound nucleus stretching.

The calculation of deformation potentials performed by Brosa and his collaborators showed the presence of multiple minima, different valleys that suggested the possibility to

⁴In the present work no exhaustive details are provided on the physical basis of the Brosa model and calculations. The interested reader can refer to [Brosa et al., 1990], where the computational procedure is excellently described.

guide the nucleus evolution through different paths. The search of such paths performed by Brosa, following the steepest descend principle, showed the possibility for the evolving nucleus to face bifurcation points leading to different pre-scission shapes. This showed the existence of multiple fission channels leading to different fission modes, characterized by distinct pre-scission shapes. The pre-scission shapes and the associated energies are responsible for the fragments characteristics. Brosa's results allowed to explain finally the observed mass distributions (with the right asymmetric fission mode deviations from the half of the compound nucleus in the mass domain) and the kinetic energies as functions of the pre-neutron mass (see for instance Refs. [Hambusch et al., 1989, Dematté, 1996]). For low-energy spontaneous and induced fission Brosa identified three most significant fission modes, which have been called *Standard I*, *Standard II* and *Super Long*, able to cover more than 98% of the total fission events for different fissioning actinides.

Brosa describes the fission process as a sequences of instabilities during the evolution of the shape of the nucleus. Firstly the fission barriers have to be overcome. Afterwards the nucleus starts to stretch and a flat neck takes place. The nuclear material is described as a viscous fluid where two kinds of instabilities are possible, the shift instability and the capillarity or Rayleigh one. The shift instability is responsible for the random position of the future constriction, the capillarity instability deepens the dent where it is and accomplishes the separation of the two fragments. Once the pre-scission shape is assumed by the nucleus and the random neck position is determined by hydrodynamic instabilities, the mass of the two new-born fragments can be determined. The multi-channel calculations showed the right asymmetric position for the *Standard* modes and the right standard deviation thanks to the random neck rupture which give the proper dispersion around an average mass provided by pre-scission configurations. Longer necks are characterized by higher standard deviations and this is also the case for the results obtained in Chapter 4. The numerical results obtained by Brosa and his collaborators can be perfectly represented by Gaussian functions for low-energy spontaneous and induced fission. Therefore the modes mentioned so far can be represented by a central Gaussian, for the symmetric Super Long, and by heavy and light complementary Gaussian functions for the asymmetric Standard I and II modes.

The Brosa model provides a symmetric⁵ total mass distribution centered in the half of the compound nucleus mass. Only primary fragment mass distributions in fact can be considered symmetric respectively to $A_f/2$, if uniquely binary fissions are considered (see Fig. 2.5(a)). The prompt neutron emission follows in fact the saw-tooth curve distribution, that exhibits a different behavior between heavy and light fragments (see Fig 2.5(a) and also Fig. 2.3). This clearly destroys the original symmetry of the primary fragment mass yields, making the fission product mass distribution quite asymmetric with significant fluctuations (see Fig. 2.5(b)), such that it cannot be in principle described by symmetric models. To reproduce independent mass fission yields we propose to combine the Brosa model for primary fragment mass distribution and a simplified model to describe the prompt neutron emission probability.

⁵It is still double-humped, but symmetric around $A_f/2$.

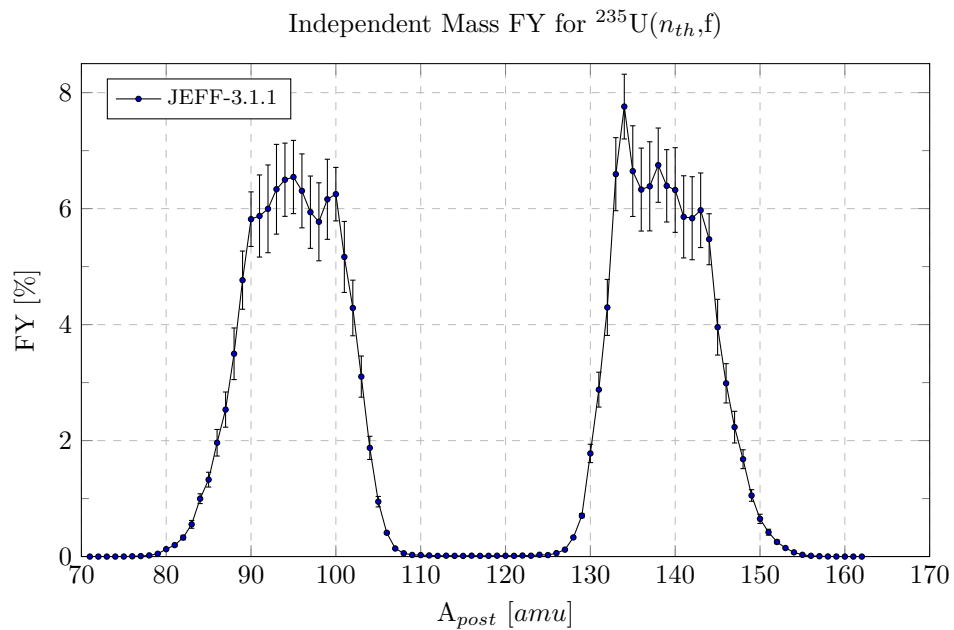
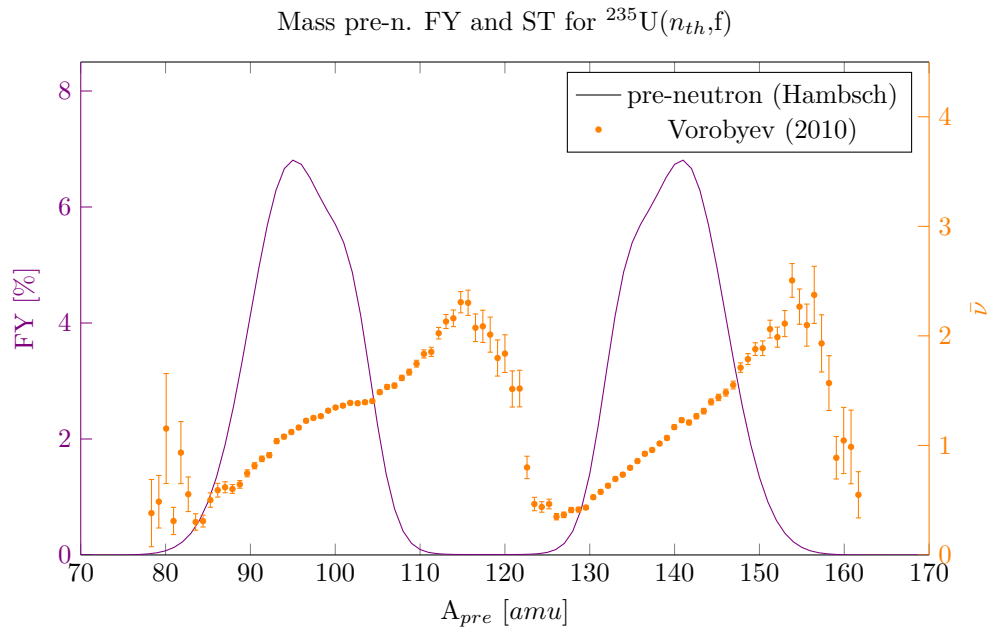


Figure 2.5: (a) Pre-neutron (from Zeynalov [Zeynalov et al., 2005]) distribution and average number of prompt neutrons emitted by a primary fragment (from Vorobyev’s experiment [Vorobyev et al., 2010]) for the thermal fission of ^{235}U . (b) Post-neutron mass distribution from JEFF-3.1.1 ^{235}U evaluation.

Therefore if we want for instance to calculate the post-neutron mass distribution for the mass 140 (see Fig. 2.6), this will be given by the following summation:

$$Y_{post}(140) = Y_{pre}(140) \cdot p_{140}(0) + Y_{pre}(141) \cdot p_{141}(1) + Y_{pre}(142) \cdot p_{142}(2) + \dots \quad (2.14)$$

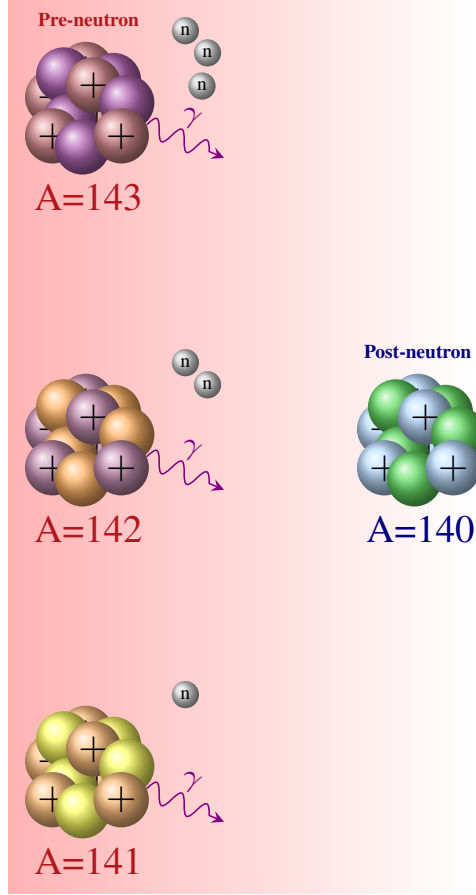


Figure 2.6: Example for the prompt neutron emission which gives a post-neutron fission product of mass 140.

So generalizing

$$Y_{post}(A) = \sum_{\nu_i=0}^{\infty} Y_{pre}(A + \nu_i) \cdot p_{A+\nu_i}(\nu_i), \quad (2.15)$$

where $Y_{pre}(A)$ is the pre-neutron distribution, while $p_{A+\nu_i}(\nu_i)$ is the probability for a primary fragment of mass $A + \nu_i$ to emit ν_i prompt neutrons. The Brosa model [Brosa et al., 1990] is used in this work through its multi-Gaussian representation for primary fragment yields. Considering only the three principal fission modes for low-energy fissions

$$Y_{pre}(A) = \sum_{i=St.I, St.II} \sum_{\Delta=\pm D_i} \frac{N_i}{\sqrt{2\pi}\sigma_i} \cdot e^{-\frac{(A-A_f/2-\Delta)^2}{2\sigma_i^2}} + \frac{2N_{SL}}{\sqrt{2\pi}\sigma_{SL}} \cdot e^{-\frac{(A-A_f/2)^2}{2\sigma_{SL}^2}}, \quad (2.16)$$

$$\sum_{i=St.I, St.II, SL} N_i = 1.0. \quad (2.17)$$

N_i are the weights of the several fission modes, σ_i the corresponding widths and D_i the deviations from the mass symmetry for the two asymmetric fission modes.

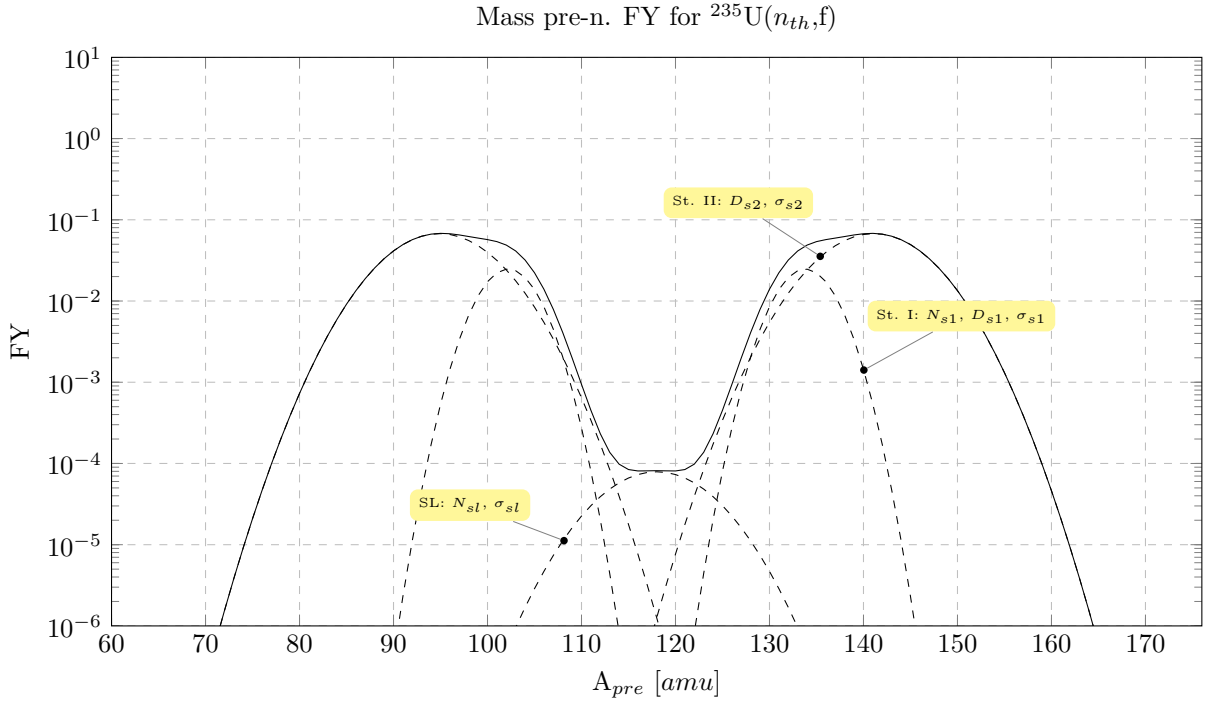


Figure 2.7: 5-Gaussian representation of the primary fragment distribution for the thermal fission of ^{235}U .

According to Brosa's notations [Brosa et al., 1990], we used the already mentioned fission modes called *Super Long* (SL) for symmetric fission, and *Standard I* (St.I) and *Standard II* (St.II) for asymmetric fission, corresponding to different neck elongations in the scission process. The SL describes in fact a purely symmetric subdivision of the compound nucleus, giving an average mass \bar{A} equal to half compound nucleus $A_f/2$ and therefore a single Gaussian distribution centered in the symmetric region. The St.I is related to slight asymmetric scissions, while the St.II is responsible of all the far wing yields in the very far asymmetric region of the mass domain. Since the SL is characterized by only one Gaussian in the center, we finally have 5-Gaussians (see Fig. 2.7).

To model the prompt neutron emission we supposed its probability distribution behaving as a Gaussian function. Different probability distributions were actually tested (e.g. Poisson, Log-Normal), but they provided worse comparisons to the experimental total prompt neutron probabilities (see Fig. 4.9 in Chapter 4). The average $\bar{\nu}(A)$ has been assumed depending on pre-neutron fragment masses, while we took a unique standard deviation σ . To represent discrete probabilities for a non-negative random variable such as the number of prompt neutrons evaporated, we renormalized to the positive axis and we performed a piece-wise integration (see Fig. 2.8). In formulas

$$p_A(\nu) = \int_{\nu-0.5 \text{ or } 0}^{\nu+0.5} \frac{N}{\sqrt{2\pi}\sigma} \exp\left(-\frac{(\nu - \bar{\nu}(A))^2}{2\sigma^2}\right) d\nu, \quad (2.18)$$

where N is a normalization factor which guarantees

$$\int_0^\infty \frac{N}{\sqrt{2\pi}\sigma} \exp\left(-\frac{(\nu - \bar{\nu}(A))^2}{2\sigma^2}\right) d\nu = 1. \quad (2.19)$$

Solving the integral, we get

$$N = \frac{2}{1 - \operatorname{erf}\left(-\frac{\bar{\nu}}{\sqrt{2}\sigma}\right)}. \quad (2.20)$$

The explicit formula for $p_A(\nu)$ can be easily obtained invoking the error function

$$p_A(\nu) = \frac{N}{2} \left[\operatorname{erf}\left(\frac{\nu + 0.5 - \bar{\nu}}{\sqrt{2}\sigma}\right) - \operatorname{erf}\left(\frac{\nu - 0.5 - \bar{\nu}}{\sqrt{2}\sigma}\right) \right], \quad (2.21)$$

which gives the missing definition in Eq. 2.15.

The Gaussian mean value $\bar{\nu}$ and variance σ^2 still have to be defined. In principle the most plausible value for $\bar{\nu}$ is the average number of prompt neutrons emitted. However, cutting the negative tail through renormalization, the average of the original Gaussian, defined on the whole real axis, is not preserved anymore, especially for small average numbers of prompt values. To build a discrete probability distribution provided with an average equal to the corresponding saw-tooth value, we solved iteratively for $\bar{\nu}$, included in $p_A(\nu)$, the following equation

$$\bar{\nu}_{ST}(A) = \sum_{\nu} p_A(\nu)\nu, \quad (2.22)$$

where we called $\bar{\nu}_{ST}(A)$ the average number of prompt neutrons emitted by a single pre-neutron fragment of mass A , given by the saw-tooth curve (ST). It is clear that for ST values far from zero, the normalization does not affect the original Gaussian, allowing $\bar{\nu}$ values very close to $\bar{\nu}_{ST}$. As already mentioned, for the variance σ^2 we did not suppose any dependence on the fragment mass.

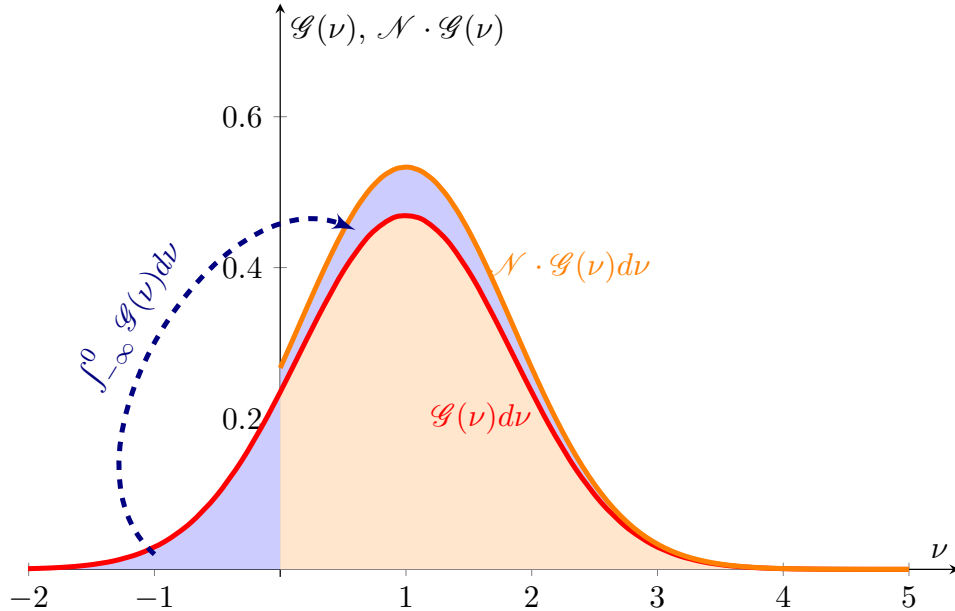


Figure 2.8: Renormalization of the Gaussian distribution to only positive values. A piece-wise integration allows us to obtain discrete probabilities.

This simplified model for prompt neutron emission probabilities was compared to FIFRELIN⁶ calculations [Litaize and Serot, 2010]. FIFRELIN is a Monte Carlo simulation

⁶Fission FRagment Evaporation Leading to an Investigation of Nuclear data.

tool for the fission fragments disexcitation process [Regnier, 2013]. The hyperspace of fission fragment states is reproduced by Monte Carlo sampling of experimental distributions for masses and kinetic energies. Once primary fragment states are available, neutron evaporation followed by γ emission are simulated to reproduce fragment disexcitation. A Hauser-Feschbach engine is conceived to simulate the prompt neutron- γ emission competition during primary fragments cooling down [Regnier, 2013]. We post-processed prompt neutron multiplicities for 10^5 histories, deducing prompt neutron emission probabilities for each pre-neutron fragment mass, $p_A(\nu)$. These were compared to CONRAD calculations, using the same input pre-neutron yield distribution and the same saw-tooth obtained from FIFRELIN.

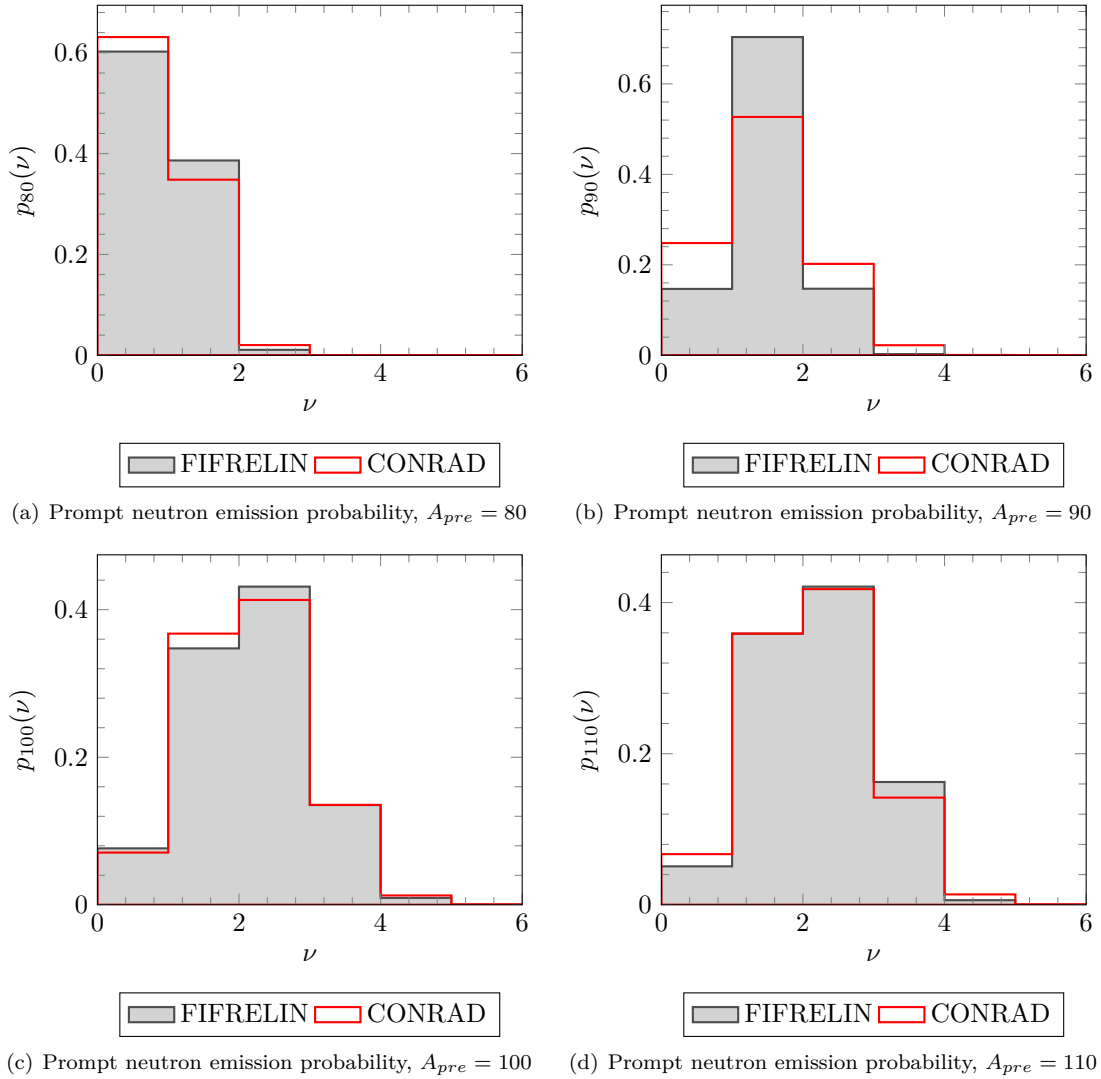


Figure 2.9: Prompt neutron emission probability comparison between FIFRELIN and CONRAD for different masses in the light peak of $^{235}\text{U}(n_{th}, f)$ mass distribution.

Results for $^{235}\text{U}(n_{th}, f)$, presented in Fig. 2.9 and Fig. 2.10, show, on average, satisfactory agreement, however non-negligible discrepancies emerged especially for those masses in the symmetry region (see $A_{pre} = 120$ amu in Fig. 2.10). The main objective of such comparison was to verify that the simplified prompt neutron emission probability model presented so far was actually capable to give reasonable results. The discrepancies observed between

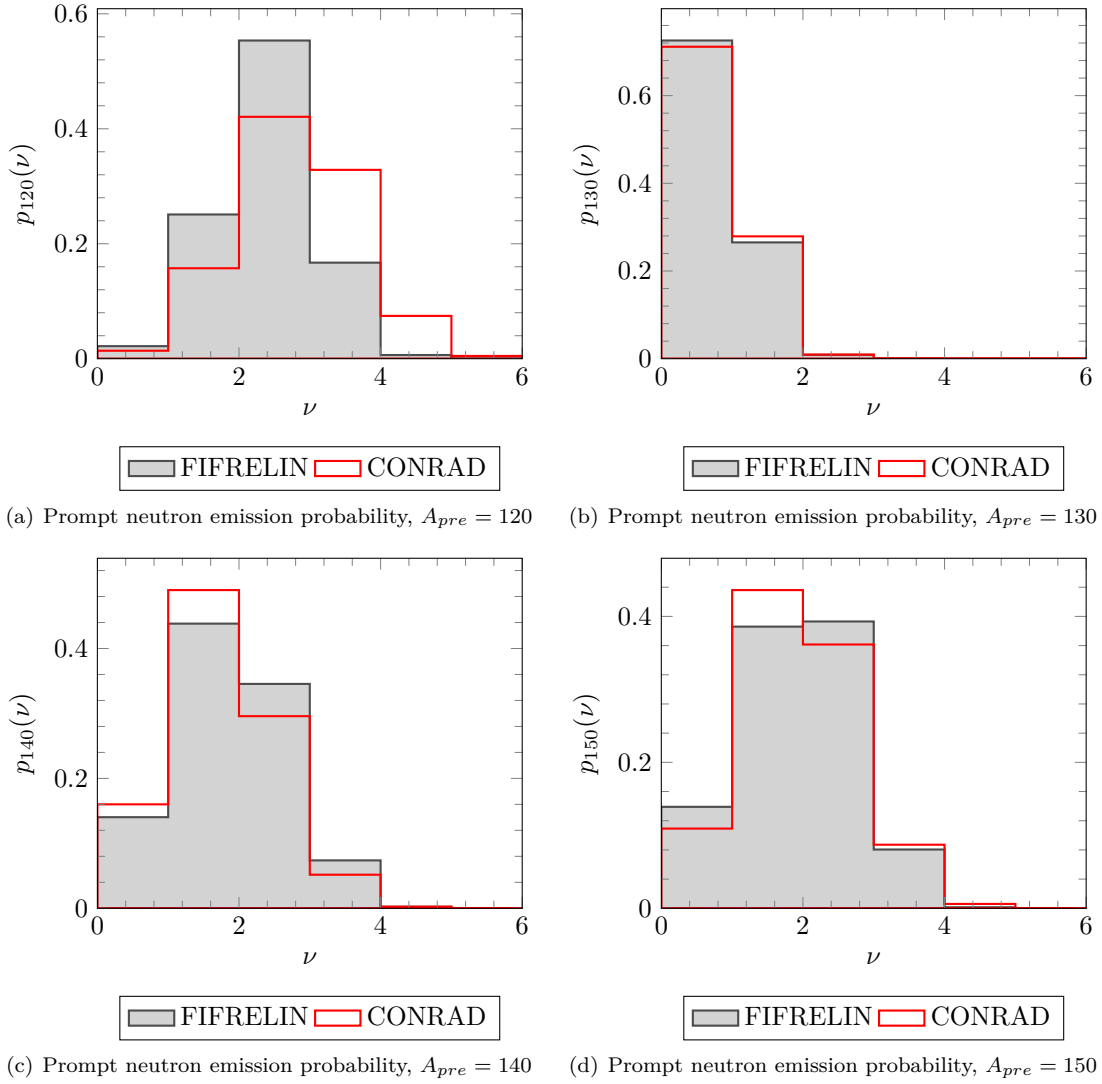


Figure 2.10: Prompt neutron emission probability comparison between FIFRELIN and CONRAD for different masses in the heavy peak of $^{235}\text{U}(n_{th}, f)$ mass distribution.

this straightforward analytical model and the Monte Carlo disexcitation might have hardly detectable different origins. The Monte Carlo disexcitation engine is surely a precise and powerful tool for prompt neutron and γ description. However, it does not describe perfectly the phenomena involved, hence it cannot be used as a comprehensive numerical reference for validation purposes. We decided finally that the simplified Gaussian formula was sufficiently efficient to satisfy our purposes of generating FY covariances taking into account prompt neutron emission.

To summarize, a mass FY model has been described as a convolution of the Brosa fission modes for the pre-neutron distribution with a simplified model based on a Gaussian distribution to calculate prompt neutron emission probabilities, with $\bar{\nu}(A_{pre})$ given by experimental data. These two models use two distinct groups of parameters which are:

- i) The means (\bar{A}_i), the standard deviations (σ_i) and the weights (N_i) of pre-neutron fission modes, with $i = St.I, St.II, SL$ (Standard I, Standard II and Super Long).
- ii) The averages $\bar{\nu}_{ST}$ of each distribution $p_A(\nu)$ (saw-tooth values) and the unique standard

deviation σ of all the Gaussians we integrate to get $p_A(\nu)$ probabilities.

Since the fission mode weights need to satisfy Eq. 2.16 and the average of the SL mode is half mass of the compound nucleus, the number of Brosa's parameters is reduced from 9 to 7. For the prompt neutron emission probabilities all the averages given by the saw-tooth curve have been taken as parameters in the calculation.

2.2.3 The Wahl Model for Isotopic Fission Yields

The nuclear charge distribution describes the isotopic yields of more a thousand of fission products of mass A and atomic number Z [Wahl, 2002]. Since only a small fraction of isotopic yields are experimentally available, a model to represent the whole inventory is necessary to develop libraries suitable to nuclear applications. Furthermore, the unavailability of theories able to effectively predict charge distributions induced scientists to develop semi-empirical models which, even if still based on physical assumptions, present *ad hoc* functions, fitting finely experimental results. In the following section the model we choose to calculate charge distributions and so isotopic fission yields is shown.

Isotopic fission yields can be expressed as

$$Y_{pre}(A, Z) = Y_{pre}(A) \cdot f(A, Z), \quad (2.23)$$

where $f(A, Z)$ is the charge distribution for a fission fragment of mass A . The Wahl Z_P -model [Wahl, 2002] is a semi-empirical model based upon the Unchanged Charge Density assumption (UCD). According to the UCD, the charge has not enough time to be re-distributed during the descent between the saddle and the scission points and the average charge for a fission fragment of mass A is $Z_P(A) = \frac{Z_f}{A_f} A$. In JEFF-3.1.1 the Wahl model has been employed to fill gaps when experimental data were not available. We decided to resort to such model in our calculations, but, as done for Brosa, applying it to pre-neutron mass distributions, as shown in Eq. 2.23. The original aim of Wahl model was instead to analyze post-neutron distributions with piece-wise functions depending on pre-neutron fragments masses, which are derived using an average prompt neutron number estimated by the modified Terrell method [Terrell, 1962]. Since the saw-tooth values participate directly to our mass FY model, we applied the Wahl systematics directly on pre-neutron FY.

In his Z_P -model, Wahl proposes a $Z_P(A)$ -centered Gaussian of width $\sigma_Z(A)$ to represent the charge distribution $f(A, Z)$, including polarization effects [Wahl, 1988] by adding a correction term $\Delta Z(A)$:

$$f(A, Z) = \int_{Z-0.5}^{Z+0.5} \frac{1}{\sqrt{2\pi\sigma^2}} \cdot e^{-0.5 \left(\frac{Z-Z_P(A)}{\sigma_Z(A)} \right)^2} dZ \quad (2.24)$$

with

$$Z_P(A_H) = A_H \left(\frac{Z_f}{A_f} \right) + \Delta Z(A_H) \quad (2.25)$$

$$Z_P(A_L) = A_L \left(\frac{Z_f}{A_f} \right) - \Delta Z(A_{H_c}) \quad (2.26)$$

$$(A_{H_c} = A_f - A_L), \quad (2.27)$$

where A_H and A_L indicate respectively heavy and light pre-neutron fission fragment masses (the subscript *pre* has been omitted for simplicity). Integrating 2.24 from $Z - 0.5$ to $Z + 0.5$, we obtain :

$$f(A, Z) = [0.5][F(A)][N][erf(V) - erf(W)], \quad (2.28)$$

where

$$V = \frac{Z - Z_P(A) + 0.5}{\sigma_Z(A)\sqrt{2}} \quad (2.29)$$

$$W = \frac{Z - Z_P(A) - 0.5}{\sigma_Z(A)\sqrt{2}}. \quad (2.30)$$

$F(A)$ is a term that includes odd-even effects given by

$$F(A) = \begin{cases} [F_Z(A)][F_N(A)] & \text{if } Z \text{ is even and } N \text{ is even,} \\ [F_Z(A)]/[F_N(A)] & \text{if } Z \text{ is even and } N \text{ is odd,} \\ [F_N(A)]/[F_Z(A)] & \text{if } Z \text{ is odd and } N \text{ is even,} \\ 1/[F_Z(A)][F_N(A)] & \text{if } Z \text{ is odd and } N \text{ is odd.} \end{cases} \quad (2.31)$$

and N is a normalization factor that yields $\sum_Z f(A, Z) = 1.0$.

The Wahl model formulation, as it is here presented, has been directly applied on pre-neutron fission fragments, with A indicating the fragment mass before the prompt neutron evaporation. Nevertheless, since prompt neutron emission is a phenomenon which happens in a time window included between 10^{-18} s and 10^{-14} s, pre-neutron experimental data are not directly retrievable, limiting FY evaluations exclusively on the analysis of post-neutron yields.

For this reason Wahl actually meant to calculate the fraction $f(A, Z)$ to be applied directly to the post-neutron mass distribution⁷, deducing the pre-neutron mass A from

$$A = A' + \nu_P(A') \quad (2.35)$$

where A' is the post-neutron mass and $\nu_P(A')$ is the number of prompt neutron emitted by a primary fragment as a function of the post-neutron mass⁸.

Therefore, a peculiarity of the Wahl model in its original formulation is the $\nu_P(A')$, which is *the average number of post-fission neutrons emitted to finally form a fission product of mass A'* [Wahl, 2002]. According to our nomenclature, the $\nu_P(A')$ in Wahl's formulation gives the average number of prompt neutrons emitted by a pre-neutron fragment which gives, after prompt neutron emission, a post-neutron isotope of mass A' . Since the saw-tooth curve conveys more physical sense, expressing the correlation between the mass

⁷The equations actually used in the Wahl model return the isotopic fraction to be convoluted with the post-neutron mass distribution $Y_{post}(A)$. They can be envisaged as follows:

$$Z_P(A'_H) = [A'_H + \nu_P(A'_H)]\left(\frac{Z_f}{A_f}\right) + \Delta Z(A_H) \quad (2.32)$$

$$Z_P(A'_L) = [A'_L + \nu_P(A'_L)]\left(\frac{Z_f}{A_f}\right) - \Delta Z(A_{Hc}) \quad (2.33)$$

$$(A_{Hc} = A_f - A'_L - \nu_P(A'_L)), \quad (2.34)$$

where A'_H and A'_L are post-neutron masses.

⁸This function is different from the saw-tooth which is a function of the pre-neutron fission fragment mass.

of a neutron-rich pre-neutron fragment and the emission of prompt neutrons, and since most of the Wahl formulas and systematics are expressed as pre-neutron-mass functions, we decided to apply directly the isotopic fraction to pre-neutron distributions, calculated using the Brosa fission modes. We obtain then

$$Y_{post}(A, Z) = \sum_{\nu_i=0}^{\infty} Y_{pre}(A + \nu_i) \cdot p_{A+\nu_i}(\nu_i) \cdot f(A + \nu_i, Z). \quad (2.36)$$

To complete the description of the Wahl model we need to define the quantities which compare in Eqs. 2.28, 2.29, 2.30 and 2.31. The values for $\Delta Z(A)$, $\sigma_Z(A)$, $F_Z(A)$ and $F_N(A)$ for low energy fissions can be represented by simple linear piece-wise functions of the pre-neutron mass that Wahl proposed to nicely fit experimental results. First of all, let us define boundaries in the mass domain:

Boundaries

$$\begin{aligned} B_1 &= 70 \\ B_2 &= 77 + 0.036 \cdot (A_f - 236) \\ B_3 &= A_f - B_4 \\ B_4 &= \frac{\Delta Z_{max} - \Delta Z(140) + A_{max} \cdot [SL50] + 140 \cdot [\partial \Delta Z / \partial A]}{SL50 + \partial \Delta Z / \partial A} \\ B_5 &= A_f - B_2 \\ B_6 &= A_f - B_1 \\ B_a &= A_f - A_{max} \\ B_b &= A_{max} \\ A_{max} &= F_1 \cdot AK_1 + F_2 \cdot AK_2 \\ F_1 &= \frac{(250.0 - A_f)}{14.0} \\ F_2 &= 1.0 - F_1 \\ AK_1 &= 50.0 \frac{A_f}{Z_f} - \frac{\Delta Z_{max}}{SL50} \\ AK_2 &= (50.0 - \Delta Z_{max}) \frac{A_f}{Z_f} \end{aligned}$$

The mass boundaries identify regions in the FY distribution where ΔZ , σ_Z , F_Z and F_N are differently defined by distinct piece-wise functions. Hereinafter, the several piece-wise functions are provided.

Peak Region ($B_2 \leq A \leq B_3$, $B_4 \leq A \leq B_5$)

$$\begin{aligned} \Delta Z(A) &= \Delta Z(140) + \frac{\partial \Delta Z}{\partial A}(A - 140) \\ \sigma_Z(A_H) &= \sigma_Z(140) + \frac{\partial \sigma_Z}{\partial A}(A_H - 140) \\ \sigma_Z(A_L) &= \sigma_Z(A_{H_c}) \quad (A_{H_c} = A_f - A_L) \end{aligned}$$

$$F_Z(A) = F_Z(140)$$

$$F_N(A) = F_N(140)$$

Near-Symmetry Region ($B_3 < A < B_4$)

$$F(A) = 1.0 \tag{2.37}$$

$B_3 < A \leq B_a$:

$$\Delta Z(A) = \Delta Z(B_3) - SL50 \cdot (A - B_3)$$

$$\sigma_Z(A) = \sigma_{50}$$

$B_a < A < B_b$:

$$\Delta Z(A) = \Delta Z(B_a) + \frac{(A - B_a)}{(B_a - B_b)} \cdot (\Delta Z(B_b) - \Delta Z(B_a))$$

$$\sigma_Z(A) = \sigma_Z(140) - \frac{\partial \sigma_Z}{\partial A} \cdot (140 - B_b)$$

$B_b \leq A < B_4$:

$$\Delta Z(A) = \Delta Z(B_4) + SL50 \cdot (B_4 - A)$$

$$\sigma_Z(A) = \sigma_{50}$$

Wing Region ($B_1 \leq A < B_2$, $B_5 < A \leq B_6$)

$$\Delta Z(A) = \Delta Z(B_5) + \Delta ZSLW \cdot (A - B_5)$$

$$\sigma_Z(A_L) = \sigma_Z(A_{H_C}), \quad (A_{H_C} = A_f - A_L)$$

$$\sigma_Z(A_H) = \sigma_Z(B_5) + \sigma_ZSLW \cdot (B_2 - A_L)$$

$$F_Z(A_L) = F_Z(140) + F_ZSLW \cdot (B_2 - A_L)$$

$$F_Z(A_H) = F_Z(140) + F_ZSLW \cdot (A_H - B_5)$$

$$F_N(A_L) = F_N(140) + F_NSLW \cdot (B_2 - A_L)$$

$$F_N(A_H) = F_N(140) + F_NSLW \cdot (A_H - B_5)$$

Far-Wing Region ($A < B_1$, $A > B_6$)

$$\Delta Z(A) = \Delta Z(B_5)$$

$$\sigma_Z(A) = \sigma(B_5)$$

$$F_Z(A) = F_Z(140)$$

$$F_N(A) = F_N(140)$$

In the formulas just written, when there were differences in function definitions between light and heavy fragments, we specified the fragment mass with notations A_H and A_L . Only ΔZ is not always split in two formulas for each region, since the function variation between light and heavy fragment mass domain is already included in Eq. 2.25. We highlighted in red the parameters which are actually used in the Wahl model, preserving their original notations. Such parameters will be addressed to CONRAD as adjustable

during the GLS procedure, as it will be clarified in Chapter 4. Plots of ΔZ , σ_Z , F_Z and F_N functions using Wahl's parameter values [Wahl, 2000] and calculated by CONRAD are shown in Fig. 2.11, 2.12 and 2.13.

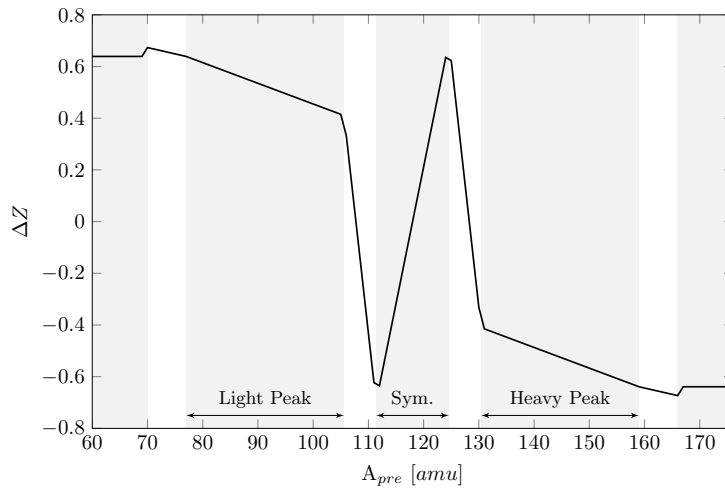


Figure 2.11: Piece-wise $\Delta Z(A)$ function using Wahl's values for the isotopic distribution parameters.

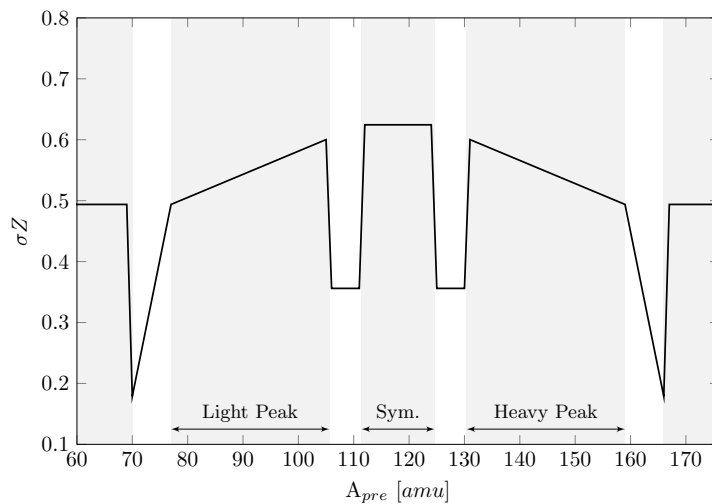


Figure 2.12: Piece-wise $\sigma Z(A)$ function using Wahl's values for the isotopic distribution parameters.

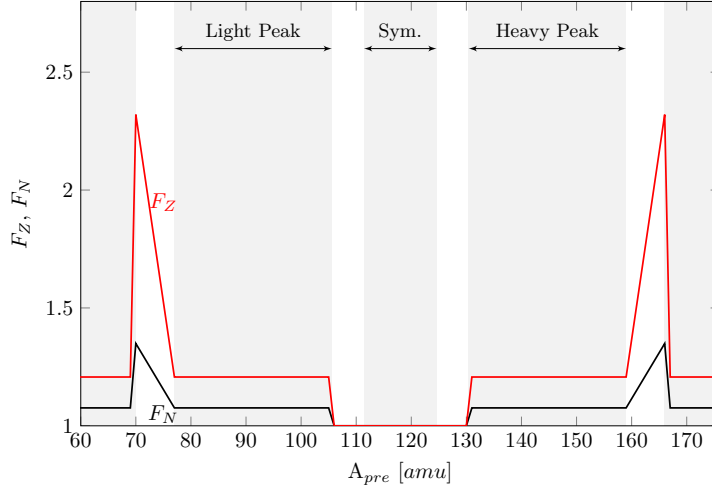


Figure 2.13: Piece-wise $F_Z(A)$ and $F_N(A)$ functions using Wahl's values for the isotopic distribution parameters.

2.2.4 Isomeric Repartition: The Madland England Model

In the previous section we have seen how to calculate independent isotopic fission yields using the Wahl model for the charge distribution. The Wahl model can be directly applied to the pre-neutron mass distribution, deduced using the Brosa fission modes, then post-neutron yields can be obtained using prompt neutron emission probabilities based on the saw-tooth averages. In formulas

$$Y_{post}(A, Z) = \sum_{\nu_i=0}^{\infty} Y_{pre}(A + \nu_i) \cdot p_{A+\nu_i}(\nu_i) \cdot f(A + \nu_i, Z). \quad (2.38)$$

Nuclear isomeric states are low-lying (excitation energy lower than 1 MeV) metastable states that occur when presenting significant angular momentum differences compared to the ground state, with a corresponding little energy gap. In this case electromagnetic transition probabilities and times are strongly reduced, giving long-lived (≥ 1 ms) states. The presence of different competing decay modes for metastable state transitions, such as internal conversion and beta decay, sees several lifetimes and the birth of various decay paths to the stability line. Thus the inventory of possible metastable states has to be necessarily determined in order to calculate the energy release in time of a collection of fission fragments.

Primary fission fragments are neutron-rich nuclides characterized by high excitation energy. Prompt neutron emission allows the transition to lower energies until the fragment reaches an energy level no longer sufficient to emit further neutrons. At this stage the excited nuclei undergo a cascade of prompt gamma decays towards the ground state. Nuclei can decay rapidly to the ground state or be *trapped* in states where transitions to lower states are characterized by low energy but with high momentum gap. Roughly 800 primary fission fragments are formed. Approximately 100 are stable while 700 are not, triggering a decay cascade. About 150 ($\sim 20\%$) have known isomeric states with half-lives ≥ 0.1 s.

To deduce yields for different isomers, a specific ratio which gives the repartition between two or more metastable states is needed. We can finally calculate isomeric fission yields

through the following expression

$$Y_{post}(A, Z, M) = \left[\sum_{\nu_i=0}^{\infty} Y_{pre}(A + \nu_i) \cdot p_{A+\nu_i}(\nu_i) \cdot f(A + \nu_i, Z) \right] \cdot R(A, Z, M). \quad (2.39)$$

In the following sections we will show a simple one-parameter model developed by Madland and England [Madland and England, 1977] to calculate the isomeric ratio $R(A, Z, M)$, which has been implemented in CONRAD and used in JEFF-3.1.1 FY evaluations when no experimental data were available.

Madland and England developed a simplified model to calculate branching isomeric ratio for FY prediction [Madland and England, 1977]. Even if a complete cascade calculation approach would provide a more rigorous answer, this requires a complete description of the fission fragments that is not certainly available with the present knowledge of the fission process. For this reason Madland and England proposed a one-parameter model able to directly provide the ratio $R(A, Z, M)$.

The Madland-England model is based on the following assumptions [Madland and England, 1977]:

- i) Fission fragments are formed with a total angular momentum J , which follows a density distribution, $P(J)$, given by

$$P(J) = P_0(2J + 1)e^{\left[\frac{-(J+\frac{1}{2})^2}{J_{rms}^2} \right]}, \quad (2.40)$$

which is predicted by the statistical model [Bethe, 1937]. Actually with the notation J_{rms} literature indicates the spin cut-off [Wagemans, 1991]. In this case the quantity at the denominator of Eq. 2.40 is not really the spin cut-off but something that is quite close to it.

- ii) J_{rms} is constant for all the fragment masses but varies with the incident neutron energy.
- iii) The branching mechanism is quite straightforward: fragments with J closer to the angular momentum of the isomeric state J_m decays to that isomeric state, fragments with J closer to the angular momentum of the ground state J_g decays to the ground state. Fragments with J exactly in the middle between J_m and J_g follows an equal repartition between both.

The branching ratio is obtained by integrating the distribution $P(J)$, therefore if $J_m > J_g$:

$$\frac{Y(A, Z, m)}{Y(A, Z, m) + Y(A, Z, g)} = \frac{\int_{J_c}^{\infty} P(J)dJ}{\int_{0 \text{ or } 1/2}^{\infty} P(J)dJ}, \quad (2.41)$$

and if $J_g > J_m$:

$$\frac{Y(A, Z, g)}{Y(A, Z, m) + Y(A, Z, g)} = \frac{\int_{J_c}^{\infty} P(J)dJ}{\int_{0 \text{ or } 1/2}^{\infty} P(J)dJ}, \quad (2.42)$$

where J_c is taken in order to respect assumption iii).

According to Ref. [Madland and England, 1977], to calculate $R(A, Z, M)$ we can distinguish 8 different cases depending on the mass number A of the fragment, if $|J_m - J_g|$ is even or odd and if $J_m > J_g$ (see Tab. 2.1). Let us suppose that $J_m > J_g$, Eq. 2.41 must

be used to calculate the ratio for the isomer in the metastable state. If A is even (odd) the lower limit of the integral in the denominator is 0 (1/2). Despite of A is even or odd, if $|J_m - J_g|$ is odd, then $J_c = \frac{1}{2}(J_m + J_g) + \frac{1}{2} = \frac{1}{2}(J_m + J_g + 1)$. If $|J_m - J_g|$ is even, then $J_c = \frac{1}{2}(J_m + J_g) + 1 = \frac{1}{2}(J_m + J_g + 2)$, but there is an additional term due to the contribution coming from $J = \frac{1}{2}(J_m + J_g)$ that is equal to

$$\frac{1}{2}(J_m + J_g + 1) \exp \left[\frac{-(J_m + J_g + 1)^2}{4J_{rms}^2} \right]. \quad (2.43)$$

Such contribution provides an equal repartition if J is perfectly in between J_g and J_m . Similar conclusions can be drawn for the case $J_m < J_g$. In such case the equation that must be used is Eq. 2.42.

Performing the integrations, the several isomeric ratios can be calculated through the functions F_i (see Tab. 2.1) defined as:

$$F_1 = \exp \left(\frac{1}{J_{rms}^2} \right) \left\{ \exp \left[- \left(\frac{1}{J_{rms}^2} \right) \left(\frac{J_m + J_g + 3}{2} \right)^2 \right] + \left(\frac{1}{J_{rms}^2} \right) \left(\frac{J_m + J_g + 1}{2} \right) \exp \left[- \left(\frac{1}{J_{rms}^2} \right) \left(\frac{J_m + J_g + 1}{2} \right)^2 \right] \right\}, \quad (2.44)$$

$$F_2 = \exp \left(\frac{1}{J_{rms}^2} \right) \left\{ \exp \left[- \left(\frac{1}{J_{rms}^2} \right) \left(\frac{J_m + J_g + 2}{2} \right)^2 \right] \right\}, \quad (2.45)$$

$$F_3 = \left\{ \exp \left[- \left(\frac{1}{J_{rms}^2} \right) \left(\frac{J_m + J_g + 2}{2} \right) \left(\frac{J_m + J_g + 4}{2} \right) \right] + \left(\frac{1}{J_{rms}^2} \right) \left(\frac{J_m + J_g + 1}{2} \right) \exp \left[- \left(\frac{1}{J_{rms}^2} \right) \left(\frac{J_m + J_g}{2} \right) \left(\frac{J_m + J_g + 2}{2} \right) \right] \right\}, \quad (2.46)$$

$$F_4 = \exp \left[- \left(\frac{1}{J_{rms}^2} \right) \left(\frac{J_m + J_g + 1}{2} \right) \left(\frac{J_m + J_g + 3}{2} \right) \right]. \quad (2.47)$$

	A	$ J_m - J_g $	$R(A, Z, m)$
$J_m > J_g$	odd	even	F_1
		odd	F_2
	even	even	F_3
		odd	F_4
$J_m < J_g$	odd	even	$1 - F_1$
		odd	$1 - F_2$
	even	even	$1 - F_3$
		odd	$1 - F_4$

Table 2.1: Isomeric ratios for different cases.

In JEFF-3.1.1 evaluated FY, for the thermal fission of ^{235}U , 14 nuclides have more than two isomeric states. To treat the case of three isomeric states we proceed applying the Madland-England model twice. Calling high, medium and low the three isomeric states we calculate $R_h = R(A, Z, \text{high})$ through the Madland-England model considering the

couple (high, medium) and $R_l = R(A, Z, \text{low})$ considering the couple (low, medium). The ratio for the medium isomeric state can be then calculated by

$$R_m = R(A, Z, \text{medium}) = 1 - R_l - R_h. \quad (2.48)$$

Sometimes the library (JEFF-3.1.1) we used to retrieve spin numbers to be employed in Madland-England model calculations, even if showing the existence of metastable states, does not provide spin numbers. In this cases, when spins are unknown, we adopted the straightforward strategy of equal ratios, giving $R_g = R_m = 0.5$ or $R_g = R_m = R_n = 0.33$ (the third metastable state is usually indicated by the letter n).

2.3 Conclusions

The Bayesian learning process allows the updating of theoretical model parameters once new and independent experimental data are available. To do so, a theoretical model based on adjustable parameters is then necessary.

In this chapter we presented and described the FY models we used to generate covariance matrices for FY. Our main goal is to generate covariances that can be consistently associated to the JEFF-3.1.1 evaluation. In such evaluated library (as in the American ENDF/B-VII) the Brosa model is used through its multi-Gaussians representation to fit post-neutron mass fission yields and fill the gaps, when experimental data are missing. Nevertheless, in the section we briefly presented the physical foundation of the Brosa model which can be consistently applied only to pre-neutron distributions, which are symmetric respectively to the half mass of the compound nucleus.

To represent the fine structure observed for post-neutron FY, the Brosa fission modes must be convoluted with prompt neutron emission probabilities, whose average is provided by the saw-tooth curve. A simplified model was then applied and compared to Monte Carlo calculations performed using FIFRELIN.

Since no predictive theories exist for FY isotopic and isomeric distributions, we adopted those used in JEFF-3.1.1 to extrapolate data in absence of experimental measurements. The Wahl and the Madland-England models were then adopted respectively for the isotopic distribution and the isomeric ratio. The general features of the models and the list of adjustable parameters have been provided.

The missing piece of the puzzle is the experimental dataset. In the next chapter the most important techniques for measuring FY are briefly described. A general overview of the nuclear data evaluation process is also provided for a sake of completeness.

All this theoretical models were missing in CONRAD, the computational tool we decided to use for our purposes. The next chapter will also provide a general description of the new features implemented in CONRAD during the present thesis work, completing the list of all the ingredients we needed to produce the covariance results presented in Chapter 4.

Chapter 3

Nuclear Data Measurements and Evaluation

Contents

3.1 The Process of Nuclear Data Evaluation	69
3.1.1 Steps in Nuclear Data Preparation	70
3.1.2 The Nuclear Data Cycle	71
3.2 Fission Yields Measurements	73
3.2.1 Radiochemical Measurements	73
3.2.2 Inverse Kinematics	74
3.2.3 2-E and 2-v Methods	74
3.2.4 The Lohengrin Spectrometer	75
3.3 Features Added in the CONRAD Code	76
3.3.1 Code Presentation	77
3.3.2 Fission Yields Capabilities	78
3.4 Conclusions	89

NUCLEAR data evaluation is the result of a sophisticated process of merging experimental values and theoretical models. In Chapter 1 we have seen the probability theory behind data evaluation and covariance matrix generation. We pointed out the techniques used in the present work to generate covariances through the Bayesian GLSM, once experimental data are provided. In Chapter 2 the FY semi-empirical models have been outlined. The following chapter is devoted to nuclear data generation for applications, focusing on microscopic experiments for fission yields. The CONRAD code is also presented. The general features of the code are enunciated to give an idea of its capabilities. In particular, we dedicate special attention to the new theoretical models implemented in CONRAD to perform calculations on fission yields and miscellaneous quantities, and how they are plugged-in to treat different types of observables. The specialized reader, who already knows fission yield measurement techniques and has a deep knowledge of the nuclear data cycle, can directly proceed further to the next chapter, where FY covariance results are provided.

3.1 The Process of Nuclear Data Evaluation

The quantities we can actually measure are not the final cross sections or the fission yields we seek, and some work is then needed to develop a complete nuclear data file.

Furthermore, nuclear experimental set-ups require technological advanced facilities, which are not always available for economical reasons. Complete and abundant data are then hardly produced, even if many efforts have been recently spent to provide auto-consistent experimental data with associated covariance matrices [Chebboubi, 2015, Kessedjian, 2015]. To generate continuous cross sections and thorough fission yields data, an evaluation process is therefore necessary. In this section we will present the several steps which roughly describe nuclear data preparation for applications and we will spend a few words on the nuclear data cycle, which plays an essential role in nuclear reactor design.

3.1.1 Steps in Nuclear Data Preparation

Nuclear data for technological applications are usually generated in several steps, each one performed by scientists of different nature. Just to offer a general grasp of what kind of activities lay behind nuclear data files for applications, let us take an example for neutron induced cross sections [Fröhner, 2000]. Such steps are

- i) **Measurement:** at this stage physicists collect experimental data points. The most straightforward quantity is the total cross section, which is “simply” deduced by transmission measurements. Partial cross sections are much more complicated to be determined. Usually, they are indirectly obtained by measuring miscellaneous quantities, observing capture yields to determine the (n, γ) cross section for instance. The yield is given by the fraction of the beam impinging the target which undergoes the reaction we are looking for. This can happen after multiple collisions, whose yield can be a very complicated functional in thick samples. The observed count rate is a convolution of the flux, the yield and the detector efficiency. Then normalization uncertainties correlate observables which in principle should be provided with full experimental covariance matrices.
- ii) **Raw data reduction:** at this point raw data need a cleaning operation to eliminate background, to include normalization and to correct data from sample contamination. Multi-collision contributions have to be taken into account in partial cross section measurements and other corrections, depending on the specific experiment, need to be adopted. At this stage the cross sections we sought are still not available and functionals are needed to transform the reaction yields or the transmissions in measured cross sections.
- iii) **Clean data analysis:** once experimental points are available the GLSM can be used to get final isotopic nuclear data. Whenever available, nuclear data are in fact parametrized by theoretical models which ensure completeness, through data interpolation and extrapolation, and physical consistency, including necessary constraints. Theoretical cross sections must be converted, through specific functionals, in calculated quantities of the same nature of the experimental observables, in order to allow comparisons.
- iv) **Nuclear data processing:** for energy-dependent quantities, used in deterministic transport code for reactor analysis calculations, for instance, group averages need to be determined. Doppler-broadened point-wise cross sections are therefore calculated for different temperatures, then averaged over energy to get group constants in a multigroup formulation of the transport problem. Data processing codes allow to evaluate infinite-dilution and self-shielded group cross sections. The latter are tabulated

at different temperatures and dilutions to be used in specified applications. This last step is in fact problem-dependent. The energy mesh boundaries and refinement are strictly problem-related, for this reason we often talk about special-purpose libraries. In the framework of nuclear data uncertainty reduction for reactor parameters of interest, such nuclear constants are adjusted through least-square fitting to integral parameter measurements performed on experimental test reactors or mock-up facilities [Fröhner, 2000].

3.1.2 The Nuclear Data Cycle

In the previous section we have seen the general steps which are necessary to generate nuclear data for applications. In this one we propose to outline, in a non-exhaustive way, the main features of the nuclear data evaluation cycle.

Modern nuclear facilities, to be safe and sustainable, are demanding more and more increased accuracies on safety-related reactor parameters. The validation of the nuclear data constants, provided as input to neutronics simulation tools, is then a crucial activity. Moreover, future reactor technologies cannot rely their own experimental data but are designed in the framework of a *virtual prototyping* philosophy supported by representative mock-up and integral experiment facilities, and on the available predictive power offered by reactor analysis computational tools. To fulfill the strict safety margins imposed by the regulation authority, nuclear data improvement, validation and qualification need to be set up in order to enhance our predictive power.

As already mentioned, in this context, the activities of sensitivity analysis and uncertainty quantification play an outstanding role to understand the major sources of uncertainty due to nuclear data and reactor modeling, providing scientifically based indications on how and where to operate.

In Fig. 3.1, a global approach based on sensitivity/uncertainty quantification methods, statistical data adjustment, integral experiment interpretation and the utilization of science-based cross-section covariance data is schematically shown [Palmiotti et al., 2009, Palmiotti et al., 2014]. The present work has been dedicated to the development of rigorous (i.e.: without *ad hoc* adjustments) model-based covariance matrices for nuclear applications, and specifically for the JHR. Such uncertainty determination and propagation activity can be envisaged as a part of the whole validation process of neutronics simulation packages (as already mentioned in Chapter 1).

This validation process includes the determination of the uncertainty impact due to nuclear data, which are subject to qualification and improvement to satisfy modern demands. Nuclear data evaluation and improvement can be seen as a cyclic process. Since, theoretical nuclear reaction model cannot predict accurately data, an intense experimental activity is needed together with the determination of reliable uncertainty information. Therefore microscopic and integral experiments are generally performed.

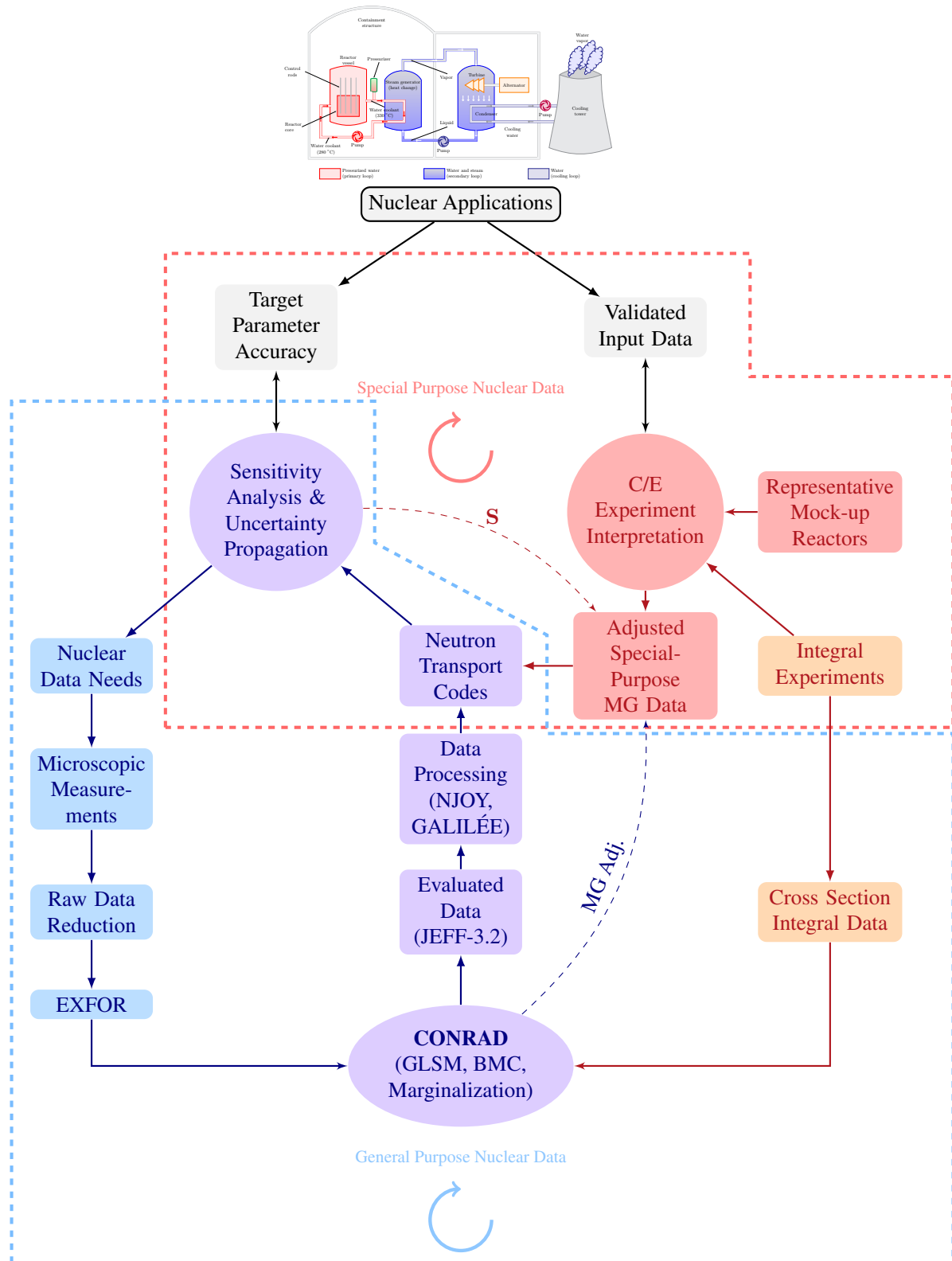


Figure 3.1: A synthetic flow-chart for the nuclear data evaluation cycle. Nuclear data improvement can be performed through statistical adjustment thanks to experimental data deriving from mock-up configurations of a particular reference facility, which leads to special-purpose nuclear data library for the specific application. Otherwise, integral experiments can be designed, which have as main goal to be clean and application-independent. These results can be included in the nuclear reaction parameter evaluation process, leading to general-purpose evaluated data.

Generally, two types of integral experiments have been used in the validation of neutronics simulation packages:

- i) Mock-up experiments: they provide *global* validation information since they are very close to the reference configuration. Experimental data on mock-up reactor parameters provide indications on how much the simulation tool and the input nuclear data are representing the real mock-up configuration. Biases and uncertainties can be then mapped to the reference facility by deterministic or Monte Carlo methods.
- ii) Clean integral experiments: mock-up reactor facility experiments can provide only information on special purpose applications, for which they are simulating the operational conditions. Many materials coexist, and compensation effects between different nuclear reactions can occur in integral parameter determination and measurement. Designing general purpose clean integral experiments, where only specific nuclear reactions or isotopes are taken into account, allow to perform general purpose nuclear data validation, applicable to a wider range of applications.

This last type of integral experiments participates to the general purpose nuclear data cycle, highlighted in blue in Fig. 3.1. Microscopic and clean integral experiments are in fact combined in a nuclear model parameter adjustment process (via CONRAD for instance) to improve knowledge on data and provide reliable uncertainties. Such uncertainties, in the form of covariance matrices, are used to estimate properly error margins on integral reactor parameters for safety and exploitation purposes. In this framework, sensitivities analyses play a very important role, since they identify nuclear data needs. According to sensitivity results (S in Fig. 3.1) provided by modern deterministic and Monte Carlo transport codes, microscopic and integral experiments can be then effectively designed.

Calculated biases, uncertainty margins and experimental measurements of representative mock-ups can be combined to determine posterior values that must be mapped on the target application. Special purpose libraries can be produced through the adjustment of multi-group constants (MG Adj.) according to the integral experiment data. The uncertainties we have on experimental configurations need to be mapped on the real reactor, which has similar characteristics and will be built successively in the near future. The final goal is, in fact, to produce estimated nominal values with reduced biases and uncertainties to be delivered to the regulation authority with a detailed safety report and to produce a validated simulation package (code and nuclear data) to be used for analysis and design.

3.2 Fission Yields Measurements

In this section a few words are devoted to those techniques usually adopted to perform microscopic measurements for FY. This part of the dissertation has been included just for a sake of completeness, to give a general outline on how experimental data are provided. As it will be clearer afterwards, FY experimental data will not be directly employed in the covariance generation proposed in the present work.

3.2.1 Radiochemical Measurements

Radiochemical methods consist in a chemical separation of irradiated sample constituents, coupled with a β - γ spectroscopy in order to achieve mass and charge identification of the

fission fragments [Poenaru and Greiner, 1997]. The needs of chemical separation depend on the identification capabilities available performing γ and β measurements. To accomplish such kind of measurement, a complete knowledge of isotope decay properties are necessary.

Recalling the fission process sequence of events, prompt neutrons are evaporated almost instantaneously after the scission process. Once prompt γ 's are emitted, fission products undergo radioactive decay. Chemical processes are usually time consuming, so what we measure are then cumulative yields. This happens because no chemical separation is sufficiently fast to take place before than any β -decay sets in. The longer we wait, the closer we are to the stability line in the nuclide chart. For this reason, to measure independent fission yields, physical methodologies have been developed during the years to perform fragment detection in less than few μs .

3.2.2 Inverse Kinematics

The general principle behind inverse kinematics measurements is to accelerate heavy actinides (such as ^{238}U) towards a light target, typically ^{12}C . This method was developed at the GSI in Darmstadt inducing Coulombian fission of relativistic ^{238}U projectile fragments to study fissioning systems ($A < 238$) which are not accessible in conventional fission experiments [Schmidt et al., 2000]. Relativistic secondary beams actinides and pre-actinides exiting the light target are selected by the Fragment Separator, and their fission is triggered by electromagnetic interactions in a set of adjacent lead foils. This technique achieves high Z resolutions. The highly accelerated fission fragments loose in fact all the electron shell, so the charge q corresponds to the atomic number. The drawback of such experimental configuration is the impossibility to investigate low energy fissioning systems, since excitation energies of about 11 MeV are induced, corresponding to neutron energies of about 5 MeV for the neutron induced fission of ^{235}U . Such energies are quite far from typical neutron spectra in nuclear reactors, even if fast facility conceptions are considered. Furthermore, only nuclear charge FY can measured.

Further extensions were made since the first experiment at GSI. To improve resolution and investigation capabilities, including the possibility to perform mass yield observations, the SOFIA (Study On FISSION with Aladin) experimental campaign has been planned, which employs the full-acceptance recoil-spectrometer ALADIN [Boutoux et al., 2013] (preliminary results from SOFIA experiment can be found in [Chatillon et al., 2015]). Parallel experimental set-ups took place at GANIL facility, where inelastic and multi-nucleon transfer reactions, induced by a ^{238}U beam impinging a ^{12}C target, were used to analyze neutron-rich fissioning systems from Uranium to Curium [Rodriguez-Tajes et al., 2014].

3.2.3 2-E and 2-v Methods

To determine mass yields, experiments purely based on momentum conservation law can be designed [Schmitt et al., 1966, Wagemans, 1991]. (2E) and (2v)-methods are powerful techniques which allow to study kinematics and energy-mass correlation for fission fragments.

The basic idea for (2E)-experiments is to use a twin back-to-back ionization chamber which can measure the kinetic energies of the two fission fragments traveling in opposite

directions after scission. Modern experimental set-ups are based on semi-conductors detectors to measure kinetic energies, but the physical principle behind such technique is essentially the same. Neglecting for a moment prompt neutron emission, in a non-relativistic framework, conservation laws can be written as follows:

$$m_L + m_H = A_f, \quad (3.1)$$

$$m_L v_L = m_H v_H, \quad (3.2)$$

$$\frac{E_L}{E_H} = \frac{m_H}{m_L}, \quad (3.3)$$

where m_i and E_i with $i = L, H$ are the masses and the energies of the light and heavy fragments, and A_f is as usual the mass of the fissioning compound nucleus. Therefore, once, for binary fission events, two complementary fragments are recorded, masses can be deduced applying momentum conservation law.

Such a technique works nicely if no prompt neutron evaporation is considered. However, fission fragments emit prompt neutrons once they are fully accelerated and what we measured are then post-neutron evaporation fission products. As already mentioned, prompt neutron multiplicities are characterized by probability distributions whose average depends on the fragment mass (see Fig. 2.3). This induces not only a shift in the averages of the measured mass values but also a broadening of the observations which are characterized by higher variances. This effect is less conspicuous for velocities which are less influenced by prompt neutron emission, allowing better resolutions. For this reason (2E)-experiments are often coupled with time of flight measurements to detect fission fragment velocities [Doré et al., 2014].

A significant drawback for such technique is that we measure post-neutron fission products, while conservation law are applicable only to pre-neutron fragments. Therefore the saw-tooth curve has to be known to relate measurements to pre-neutron quantities. Such values are unfortunately not well known, even for the most important fissioning systems.

3.2.4 The Lohengrin Spectrometer

Since it has been one of the most successful facilities to study fission yields, we decided to dedicate a specific section to the Lohengrin spectrometer. Situated in the Institut Laue-Langevin (ILL) in Grenoble, it allows a mass separation of unsloved fission products by using a magnetic field followed by an electric one.

A heavy water pool-type reactor guarantees high fluxes to be used as neutron source at ILL. A fissile target can be placed in the reactor and can be exposed to high fluxes of about $5.5 \times 10^{14} \text{ n cm}^{-2} \text{ s}^{-1}$. Lohengrin set-up has direct access to the reactor and unsloved fission products can be collimated through a 23 m-long channel [Faust and Geltenbort, 1981].

After scission, fission fragments fly in opposite directions and they access the Lohengrin through a solid angle window of about $3.2 \times 10^{-5} \text{ sr}$. They cover the 23 m of the spectrometer in roughly $2 \mu\text{s}$, so fission products emit prompt neutrons and γ 's but they do not have time to undergo radioactive decay, so post-neutron fission products can be measured.

During this path, fission products are deflected horizontally by a magnetic field \vec{B} and vertically by an electrical one \vec{V} . The two fields are orthogonal to the ion trajectories which are arcs characterized by a radius of the osculating circle of respectively ρ_B and ρ_V . The centripetal acceleration \vec{a}_c is given by

$$\vec{a}_c = \frac{q\vec{V}}{A} + \frac{q\vec{v} \times \vec{B}}{A}, \quad (3.4)$$

where

$$a_c = \frac{v^2}{\rho_{B,V}}. \quad (3.5)$$

Using some algebra, we can determine the ratios A/q and E/q for given magnetic and electric fields:

$$\frac{A}{q} = \frac{B^2 \rho_B^2}{V \rho_V}, \quad (3.6)$$

$$\frac{E}{q} = \frac{V \rho_V}{2}, \quad (3.7)$$

which allow a selection of fission products with a given mass A , kinetic energy E and ionic charge q . Thanks to such a set-up, the Lohengrin allows a fine selection of the fission products, even if some contamination issues can occur in the symmetry region when the related A/q and E/q ratios are close to those addressing some other products with higher fission yields [Martin, 2013, Chebboubi, 2015]. This facility accomplishes an outstanding comprehensive investigation of the fission process. The only drawback is the time required by the investigation. To get a single mass fission yield, in fact, complete scans in energy and charge are necessary to perform proper integration. Furthermore, since a one-shot measurement is not possible, several and frequent sample burn-up measurements are then necessary to provide the correct normalization. Nevertheless the Lohengrin facility still remain a powerful experimental set-up to measure fission yields for nuclear applications.

To measure isotopic fractions, the Lohengrin spectrometer is provided with a second magnet (Reduction of Energy Dispersion) which deflects and canalize fission fragments towards a magnetic band, surrounded by γ detectors. This magnetic band is used as support to deposit fission products and perform γ spectroscopy through 8 high-purity Ge-detectors. After prompt and γ emission, fission products undergo β decay, so a γ spectroscopy can be utilized to identify isotopes [Bail, 2009, Bail et al., 2011, Martin, 2013, Amouroux, 2014, Chebboubi, 2015].

Since 2007, in the framework of a collaboration between CEA, LPSC¹ and ILL, several fissioning systems ($^{233,235}\text{U}(n, f)$, $^{239,241}\text{Pu}(n, f)$ and $^{241}\text{Am}(2n, f)$) have been studied in the region of heavy masses through such γ -spectroscopy technique [Serot et al., 2014].

3.3 Features Added in the CONRAD Code

In this section we give a non-exhaustive insight of the CONRAD code for nuclear data evaluation and assimilation. After a brief presentation, the new features we added for fission yields data evaluation will be described, providing some elements of code verification.

¹Laboratoire de Physique Subatomique et Cosmologie, in Grenoble (France).

3.3.1 Code Presentation

The CONRAD project was born in 2005 in the heart of the Physics Studies Laboratory (LEPh), which belongs to the Service of Reactor and Fuel Cycle Physics (SPRC) of the CEA [De Saint Jean et al., 2007]. CONRAD is an object-oriented code developed in C++. Its architecture was thought to yield high implementation flexibility. A multi-version project management performed by the Subversion² (SVN) platform allows simultaneous and parallel developments which can be performed by different collaborators.

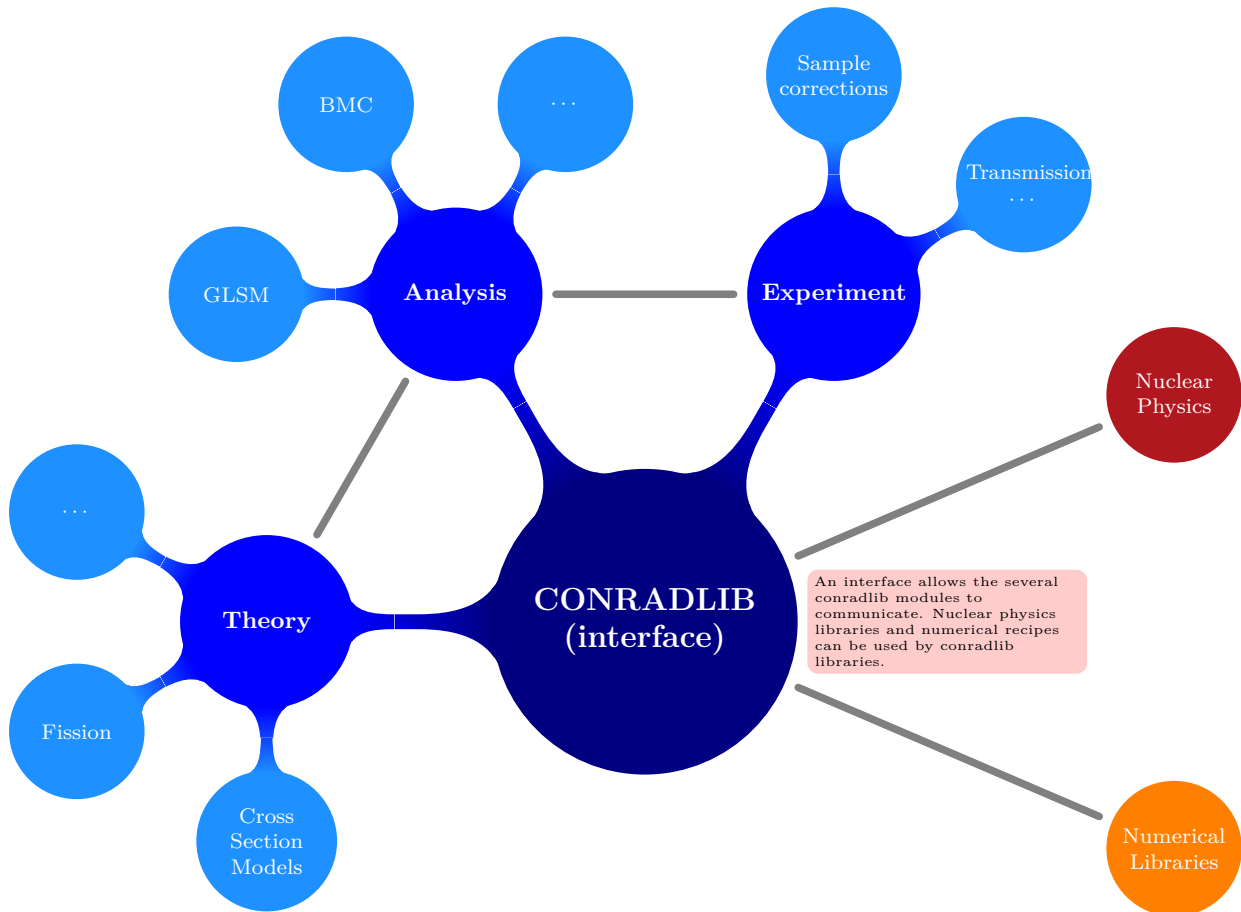


Figure 3.2: Conradlib dynamical libraries structure in the CONRAD project.

The heart of the CONRAD code is a dynamical library called *conradlib*. The executable file is called *conradtui*³ and allows the user to access to different functionalities made available by *conradlib*. As schematically shown in Fig. 3.2, *conradlib* is subdivided in several sub-libraries which perform different tasks in the nuclear data evaluation process [Archier, 2011]:

- i) Analysis classes which provide statistical tools such as Bayesian and marginalization techniques for data evaluation methodologies and covariance generation. Such features can rely on Monte Carlo or deterministic numerical methods.
- ii) Theoretical modules for nuclear reactions and fission models to treat cross sections and fission observables such as fission yields or prompt neutron fission spectra.

²<http://subversion.tigris.org>

³conradtui: CONRAD Text User Interface

- iii) Experimental classes to treat microscopic measurements and to assimilate integral information.
- iv) Interface classes allowing other *conradlib* classes to communicate, but also able to handle different output formats.

Different functionalities are implemented in the CONRAD code. Monte Carlo and deterministic evaluation methodologies are available and can be selected in the input data file for the `conradtui` executable. The architecture consists on a generic data model, which allows the development and the plug-in of new theoretical classes, based on a compound nucleus formation, quite intuitively [De Saint Jean et al., 2007]. The interface only needs to provide transition probabilities between two channels, characterized by different quantum numbers (e.g. angular momentum, parity etc.).

Several cross section models can be employed in the nuclear data evaluation in the whole [0, 20 MeV]-range, depending on the energy of the particles which induce the nuclear reactions and on target nuclei. CONRAD is not just a new R-matrix fitting code such as SAMMY [SAMMY, 2008] or REFIT [Moxon et al., 2010]. It allows modern and comprehensive cross section evaluation for the different energy regions of interest for nuclear applications (*theory* module), providing also the possibility to treat other kind of physical observables such as PFNS or FY [Terranova et al., 2015b, Berge, 2015]. For further details on the functionalities available in CONRAD, dedicated references and Appendix C can be consulted.

3.3.2 Fission Yields Capabilities

In this section some of the new features implemented in CONRAD to achieve the goals proposed in the framework of the present doctoral project will be explored and discussed. No exhaustive explanations will be provided here, but just some essential aspects will be presented just to give a grasp of the preliminary work needed to obtain the results shown in the following chapters.

Most of the coding was involved in the *theory* module of *conradlib* to add fission yields observables and semi-empirical models. Some side-work on other CONRAD domains resulted necessary to integrate this new kind of physical quantities, quite far from the cross section concept for which the code was designed and developed.

3.3.2.1 Handling FY and Miscellaneous Fission Observables

The CONRAD code was firstly designed to assimilate, analyze and evaluate cross section data. Cross sections are energy-dependent continuous quantities and, unless double differential cross sections are measured and analyzed, they are functions of only one variable. FY and other miscellaneous fission quantities, such as the average number of prompt neutron emitted or the total prompt neutron emission probability, on the contrary, can be functions of multiple variables. To assimilate fission yields in the CONRAD framework, a multi-grid class has been added and integrated in the experimental module.

In Fig. 3.3 a portion of an experimental file used to analyze independent isotopic and isomeric FY is shown. To identify the isomer we need to indicate the charge, the mass and the isomeric state. The ground state and the successive metastable states are indicated

by integers starting from zero to infinity. Normally no more than two metastable state are found in fission yield data. Such a multi-grid class has been conceived in a general way, to be used also in other kinds of experiments. An example is the assimilation of miscellaneous fission quantity experiments.

```

[/Analysis/]
  NormalizationFactor = 1.0
[/Experiment/]
  MeasurementType = "ISOMERIC_FISSION_YIELDS"
[/Experiment/Sample/Nucleus_0/]
  Name           = "U235"
  Abundance      = 1.0E+00
[/Spectrum/]
  GridStructure  = "Charge Mass State"
  Uncertainty    = 1
  Values = "
    32   82   0   1.2173E-03   2.4710E-04
    33   82   1   1.1215E-03   2.1243E-04
    33   83   0   2.7440E-03   5.0813E-04
    33   84   0   1.1335E-03   3.1525E-04
  
```

Figure 3.3: Portion of an experimental file used as input for CONRAD to analyze independent isotopic and isomeric FY. To identify the isomer we need the charge, the mass and the isomeric state.

In Figs. 3.4 and 3.5 the experiment files for the prompt neutron multiplicity $\bar{\nu}$ and for the total prompt neutron emission probability distribution are respectively shown. To represent for example prompt neutron emission probabilities we need to explicit just one coordinate, the number of prompt neutron emitted by the fissioning system. If no grid is necessary, a Null grid format can be asked to be included in the analysis by CONRAD using a fictitious zero abscissa.

```
[/Analysis/]
  NormalizationFactor = 1.0
[/Experiment/]
  MeasurementType = "FISSION_NEUTRON_MULTIPLICITY"
[/Experiment/Sample/Nucleus_0/]
  Name      = "U235"
  Abundance = 1.0E+00
[/Spectrum/]
  GridStructure = "Null"
  Uncertainty = 1
  Values = "0    2.42    0.01"
```

Figure 3.4: Portion of an experimental file used as input for CONRAD to analyze prompt neutron multiplicity.

```
[/Analysis/]
  NormalizationFactor = 1.0
[/Experiment/]
  MeasurementType = "PNU_TOT_CURVE"
[/Experiment/Sample/Nucleus_0/]
  Name      = "U235"
  Abundance = 1.0E+00
[/Spectrum/]
  GridStructure = "Nu"
  Uncertainty = 1
  Values = "
    0    0.0333    0.0005
    1    0.1745    0.001
    2    0.3349    0.002"
```

Figure 3.5: Portion of an experimental file used as input for CONRAD to analyze total prompt neutron emission probabilities.

3.3.2.2 Independent Fission Yields

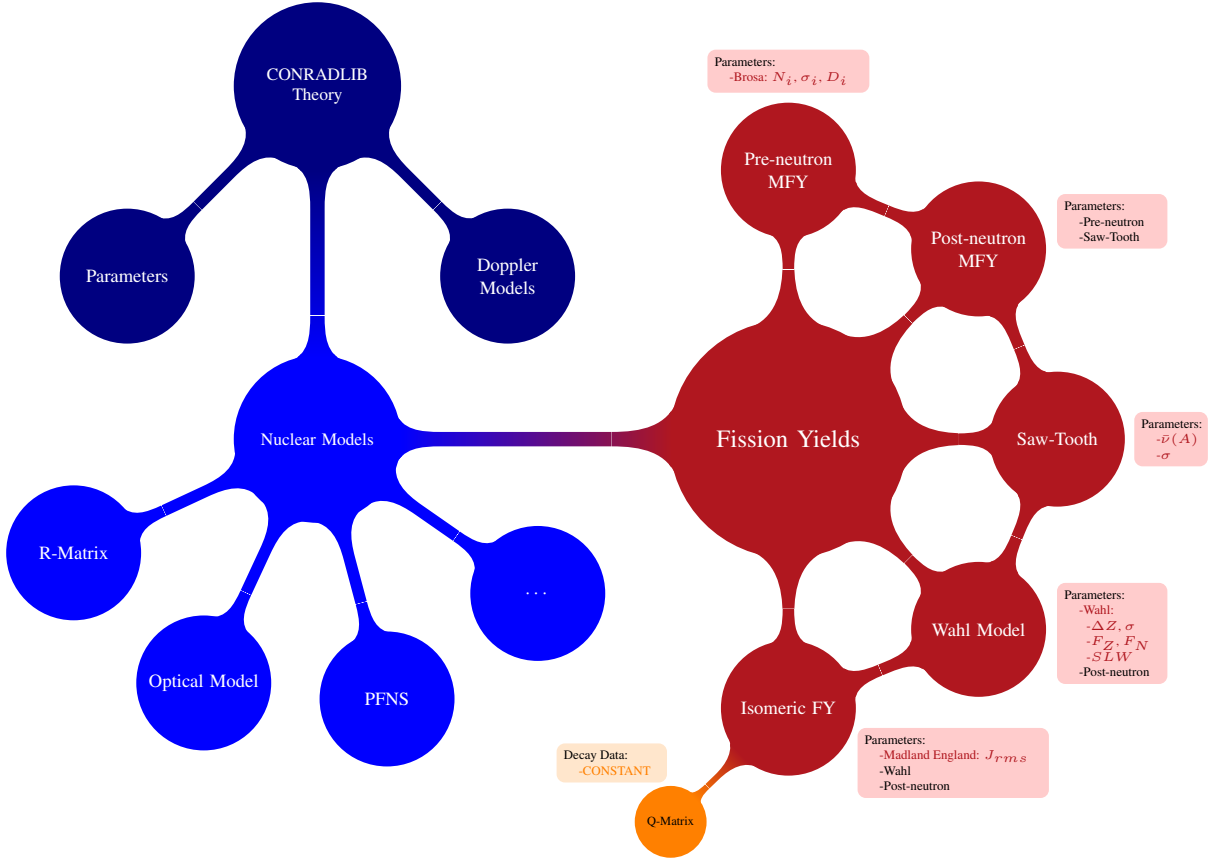


Figure 3.6: Schematic picture of what has been implemented in the theory module of *conradlib*.

Most of the implementation work concerned the fission yield semi-empirical models presented in Chapter 2. In Fig. 3.6 a schematic representation of what has been plugged in the theory module of *conradlib* is presented. Independent classes for mass, isotopic and isomeric FY have been included. Each class has its own model parameters (in red in the figure), but it can be allowed to have access to other class parameters in order to perform independently different kind of analysis according to the available observables.

The *pre-neutron* class is responsible for the Brosa model calculation for pre-neutron evaporation mass FY. It can be used independently allowing pre-neutron experimental data analysis and adjusting Brosa parameters for the weight, the width and the asymmetry of the fission modes. To treat prompt neutron emission the *saw-tooth* class has been added to calculate prompt fission emission probabilities for different pre-neutron fragments. Its own parameters are the all average numbers of prompt neutrons emitted by pre-neutron fragment and the unique width of the distribution, which is not considered dependent on the fragment mass. This class was not meant to be used in any experimental data analysis. Independent mass fission yields can be analyzed using the *post-neutron* model which has access to pre-neutron and saw-tooth parameters and objects to perform the Brosa- $p_A(\nu)$ convolution. Miscellaneous fission quantities have been considered in FY covariance evaluation. Emission probabilities and multiplicities can be included, for instance, during FY data analysis.

The *Wahl Model* class is devoted to the semi-empirical Z_P -model for isotopic FY distributions, as explained in Chapter 2. Wahl model parameters for the ΔZ and σ piece-wise functions can be adjusted. Odd-even effect factors F_Z and F_N , and parameters for the very asymmetric regions (SLW) are also adjustable, and they can be updated if wing FY are examined. Only boundary Wahl systematics has been taken as constant. Thanks to such a class, it is possible to perform post-neutron isotopic FY calculations, resorting to post-neutron objects and attributes.

Finally, isomeric FY can be treated using the *isomeric* class. The latter can perform independent and cumulative FY calculations depending on the experimental files. If only the ISOMERIC_FISSION_YIELDS observable is provided to CONRAD through the experimental input file, Wahl and post-neutron models are resorted and convoluted together with the Madland England ratio to get independent isomeric fission yields. To calculate isomeric ratios spin numbers are necessary. In the present work spin numbers were taken from the JEFF-3.1.1 data library.

If CUMULATIVE_FISSION_YIELDS are sought on the other hand, the Q-matrix is generated and employed to perform the calculation (see Sec. 3.3.2.4).

3.3.2.3 Miscellaneous Fission Quantities

To design safe and sustainable nuclear facilities, an accurate knowledge of the uncertainty margins on safety-related reactor parameters is necessary. In the last decade, many efforts have been spent to produce science-based covariance data to be employed in proper uncertainty propagations.

Even for FY, we attempted to produce covariance matrices with the highest physical content possible, with the currently available theoretical models. To do so, we included in FY analysis miscellaneous fission quantities whose values were measured in totally independent experiments.

Total prompt neutron emission probabilities experimental data were included in the GLSM when available. CONRAD can calculate such quantities by using the following formula

$$P(\nu_t) = \sum_{A_i > \frac{A_f}{2}}^{A_f} Y_{pre}(A_i) \sum_{\nu_j=0}^{\nu_t} p_{A_i}(\nu_j) p_{A_f-A_i}(\nu_t - \nu_j). \quad (3.8)$$

$Y_{pre}(A_i)$ gives the probability to have two scission pre-neutron fragments of mass A_i and $A_f - A_i$, where A_f is still the compound nucleus mass. The two fragments must evaporate a complementary number of prompt neutrons, whose sum has to be equal to ν_t . All the combinations are considered in the $\sum_{\nu_j=0}^{\nu_t} p_{A_i}(\nu_j) p_{A_f-A_i}(\nu_t - \nu_j)$ sum.

Similarly to the $P(\nu_t)$ distribution, prompt neutron multiplicities have been included in the analysis. The following formula have been implemented in CONRAD:

$$\bar{\nu}_T = \sum_{A=0}^{\infty} Y_{pre}(A) \bar{\nu}(A), \quad (3.9)$$

$$\bar{\nu}_L = \sum_{A=0}^{A_f/2} Y_{pre}(A) \bar{\nu}(A), \quad (3.10)$$

$$\bar{\nu}_H = \sum_{A=A_f/2}^{\infty} Y_{pre}(A) \bar{\nu}(A), \quad (3.11)$$

where $\bar{\nu}_L$ and $\bar{\nu}_H$ are the average number of prompt neutron emitted by the fissioning system considering only the light and the heavy fragments respectively, while $\bar{\nu}_T$ is the total prompt neutron multiplicity.

3.3.2.4 Cumulative Fission Yields: The Q-Matrix

In Sec. 2.2.1, cumulative fission yields have been defined as the summation of all contributions to a given isomer overall the entire decay time after a fission event. In formulas

$$C_i = Y_i^{post} + \sum_{j=0}^N C_j b(j \rightarrow i), \quad (3.12)$$

with the usual meaning of the symbols, and reminding that the $b(j \rightarrow i)$ is the branching ratio from an isomer j to an isomer i . We mentioned also the matrix formalism for cumulative FY, introducing what is normally called the Q-matrix [Mills, 1995]:

$$\vec{C} = \mathbf{Q} \vec{Y} \quad (3.13)$$

where

$$\mathbf{Q} = (\mathbf{I} - \mathbf{B})^{-1}, \quad (3.14)$$

with \mathbf{B} the branching ratio matrix.

To generate the Q-matrix in CONRAD, a separate C++ program was written to extract branching ratios from the ENDF format of the JEFF-3.1.1 decay data file. An ASCII readable format has been chosen for decay data in the input theory file for CONRAD (see Fig. 3.7). The numbers between brackets are the charge, the mass and the isomeric state (zero for the ground state) of the isomer we are considering. Even if post-neutron fission products mostly undergo β^- decay, we included almost all the available decay channels to provide the most accurate Q-matrix possible (see Tab. 3.1).

```
[/Theory/FissionYields/Cumulative]
Decay(26,46,0) = "B+subm=64 B+,p:18 B+,psubm:18"
Decay(26,47,0) = "B+=13 B+,p:87"
Decay(26,48,0) = "B+=96.4 B+,p:3.6"
Decay(26,49,0) = "B+=48 B+,p:52"
```

Figure 3.7: Example of Decay data input for CONRAD.

Decay mode	CONRAD
β^-	B-
β^+	B+
$2\beta^-$	2B-
$2\beta^+$	2B+
α	AL
Isomeric Transition	IT
(β^-, n)	B-, n
(β^+, p)	B+, p
$(\beta^-, 2n)$	B-, 2n
$(\beta^+, 2p)$	B+, 2p
(β^-, α)	B-, AL
(β^+, α)	B+, AL
n	n
$2n$	2n
p	p
$2p$	2p

Table 3.1: Decay modes considered to generate the Q-matrix used in CONRAD. Transitions to metastable states have been considered, just adding `subm` and `subn` for the first and the second metastable state respectively.

(a) R. Mills Q-Matrix

Qij	⁸⁵ Ge	⁸⁵ As	⁸⁶ Ga	⁸⁶ Ge	⁸⁶ As	⁸⁵ Se	⁸⁵ Br	^{85m} Kr	⁸⁵ Kr	⁸⁵ Rb
⁸⁵ Ge	1.00	0.85				0.67	0.67	0.67	0.14	0.67
⁸⁵ As		1.00				0.78	0.78	0.78	0.17	0.78
⁸⁶ Ga			1.00	1.00	1.00	0.33	0.33	0.33	0.07	0.33
⁸⁶ Ge				1.00	1.00	0.33	0.33	0.33	0.07	0.33
⁸⁶ As					1.00	0.33	0.33	0.33	0.07	0.33
⁸⁵ Se						1.00	1.00	1.00	0.22	1.00
⁸⁵ Br							1.00	1.00	0.22	1.00
^{85m} Kr								1.00	0.21	1.00
⁸⁵ Kr									1.00	1.00
⁸⁵ Kr										1.00

(b) CONRAD Q-Matrix

Qij	⁸⁵ Ge	⁸⁵ As	⁸⁶ Ga	⁸⁶ Ge	⁸⁶ As	⁸⁵ Se	⁸⁵ Br	^{85m} Kr	⁸⁵ Kr	⁸⁵ Rb
⁸⁵ Ge	1.00	0.86				0.67	0.67	0.67	0.14	0.67
⁸⁵ As		1.00				0.78	0.78	0.78	0.17	0.78
⁸⁶ Ga			1.00	1.00	1.00	0.33	0.33	0.33	0.07	0.33
⁸⁶ Ge				1.00	1.00	0.33	0.33	0.33	0.07	0.33
⁸⁶ As					1.00	0.33	0.33	0.33	0.07	0.33
⁸⁵ Se						1.00	1.00	1.00	0.22	1.00
⁸⁵ Br							1.00	1.00	0.22	1.00
^{85m} Kr								1.00	0.21	1.00
⁸⁵ Kr									1.00	1.00
⁸⁵ Kr										1.00

Table 3.2: Comparison between two Q-matrix portions, from R.Mills (see Ref. [Mills, 2014]) (top) and CONRAD (bottom).

We compared in Tab. 3.2 the CONRAD-generated Q-matrix to dedicated references [Mills, 2014], whose values have been employed in JEFF-3.1.1 FY data evaluation. The Q-matrix portion, reported in Ref. [Mills, 2014], is almost coincident to what can be reproduced by CONRAD (see Tab. 3.2).

Further verifications were performed comparing the cumulative FY generated by simply multiplication of the CONRAD-generated Q-matrix by the JEFF-3.1.1 independent yields to JEFF-3.1.1. In Fig. 3.8, the relative discrepancies between CONRAD and JEFF-3.1.1 cumulative yields are presented for the thermal fission of ^{235}U .

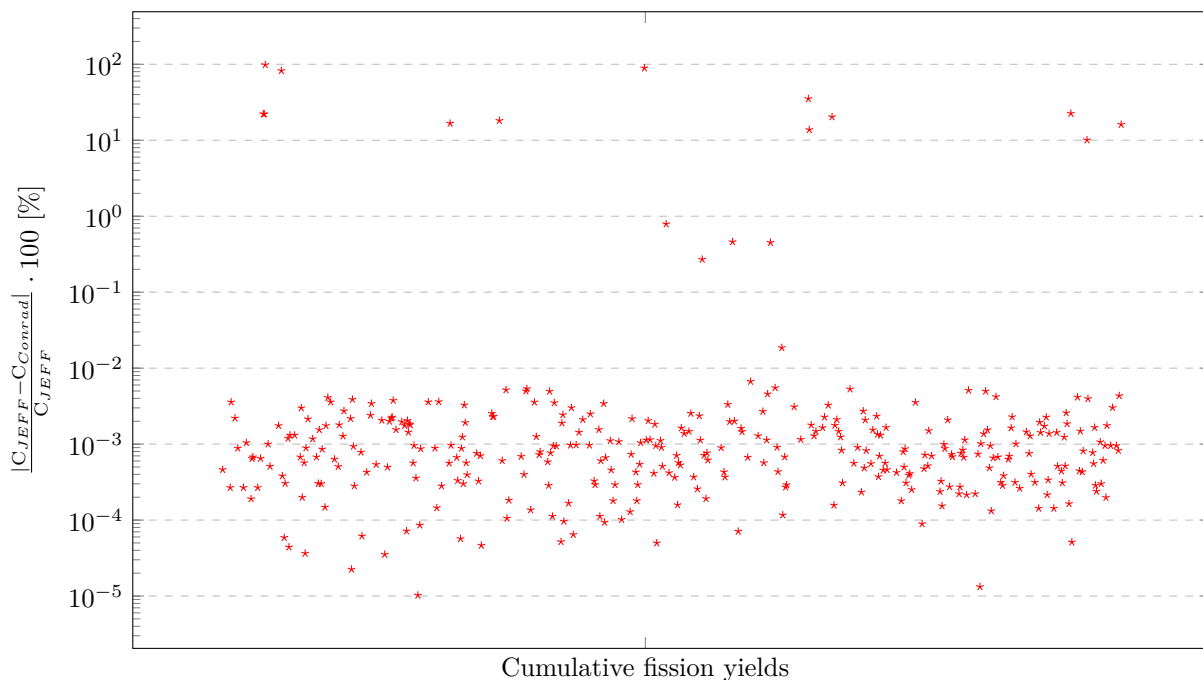


Figure 3.8: Comparison between cumulative yields generated using the CONRAD Q-matrix and the cumulative FY given in JEFF-3.1.1, for the thermal fission of ^{235}U . No significant differences have been found for almost the whole library, except for some fission products whose parents have long characteristic decay times.

The whole cumulative JEFF-3.1.1 library is globally well reproduced by CONRAD. However some computational discrepancies have been found showing possible differences in the Q-matrix calculated by CONRAD compared to the one used in JEFF evaluation. Most of these inconsistencies turned out to be due to long-lived nuclei, characterized by geological decay-times. Such nuclei, even if classified as unstable in JEFF decay heat library, can be considered actually stable for nuclear applications. An example is the cumulative yield of ^{99}Ru . The CONRAD value is 6.1318E-02, much greater than the JEFF-3.1.1 one, equal to 1.9979E-06. ^{99}Ru is mostly produced by the radioactive decay of ^{99}Tc in its ground state, a long-lived nuclide which has a half-life of about 2.14×10^5 y. In JEFF-3.1.1 cumulative FY library, ^{99}Tc is considered stable. This is confirmed by the comparison between JEFF-3.1.1 (6.1316E-02) and CONRAD (6.1316E-02⁴) ^{99}Tc cumulative yields, and even more by the comparison between ENDF-B/VII (6.1087E-02) and CONRAD (6.1318E-02⁴) ^{99}Ru cumulative yields.

⁴We recall that these values are obtained without using any independent yield modeling. These are just the simple multiplication of JEFF-3.1.1 independent yields by the CONRAD Q-matrix.

In the present work a decay time threshold was not considered. Since we propagate consistently the uncertainty related to independent FY, such cumulative FY discrepancies between CONRAD and JEFF do not affect any decay heat and neutronic calculation. Other few differences of small entity ($\sim 1\%$) have been found, probably due to the different decay modes considered in the branching ratio matrix construction.

It has to be emphasized that the Q-matrix has been considered as a constant in the present work. In principle, when cumulative FY are evaluated, branching ratio uncertainties should be taken into account. When different decay modes for one nucleus are possible, branching ratios are necessarily affected by uncertainties and they are correlated. Further developments of such methodology are expected to improve such aspect, including proper uncertainties for the Q-matrix.

3.3.2.5 The APOLLO2 Chains

As it will be shown in Chapter 6, to test FY covariances we propose to propagate CONRAD uncertainties in calculations for real applications. In particular, we evaluated the effects produced by CONRAD-generated covariance matrices on decay heat and reactivity calculations for a PWR pin-cell and for the JHR. For neutron transport calculations, we picked the APOLLO2 code [Sanchez et al., 1988], at the basis of the HORUS-3D/n platform, which performs JHR safety analysis. APOLLO2 works thanks to a specifically generated library called APOLIB. In the latter, a shortened list of fission product is edited. Such a list contains the most neutronics-sensitive isotopes which have the most significant impact on light water reactor physics, covering the 99% of reactivity effects. Furthermore, only nuclei whose cross sections are available can be included, since not all the nuclide chart is covered by present cross sections evaluations.

Such isotopes are provided with particular fission yields which must be evaluated according to the decay chain dependences specified in the neutronic code library. APOLLO2 FY include in fact both independents and cumulatives, but a non-negligible number of FY are not attributable to any FY value in JEFF-3.1.1. These FY can be classified as semi-cumulative, since they have values greater than their own independent FY but lower than the corresponding cumulative. The reason for this relies on how each depletion code, such as the APOLLO2 evolution module, works. Beside the fact that a specific list of FY has been designed to generate the APOLLO2 library, the selected fission products are also the only isotopes produced by any fission event during the reactor simulation. The reactor inventory evolves according to the time-scale adopted for the depletion calculation. Therefore APOLLO2 fission products will actually decay in the evolution part of the code, as expected from their own decay constant. To calculate APOLIB FY for each nuclide, we need to cumulate all FY contributions coming from fission products not included in the APOLIB list. The residual part will be taken into account during the depletion calculation, following the decay chains and dependencies.

Fig. 3.9 shows an example of APOLIB FY calculation. ^{135}I , ^{135}Xe and ^{135}Cs , in blue, are fission products in the APOLLO2 selection. Such isotopes will decay during the depletion calculation following its own decay constant. For this reason their decay modes must be ignored during FY calculations, to not take into account twice their contributions.

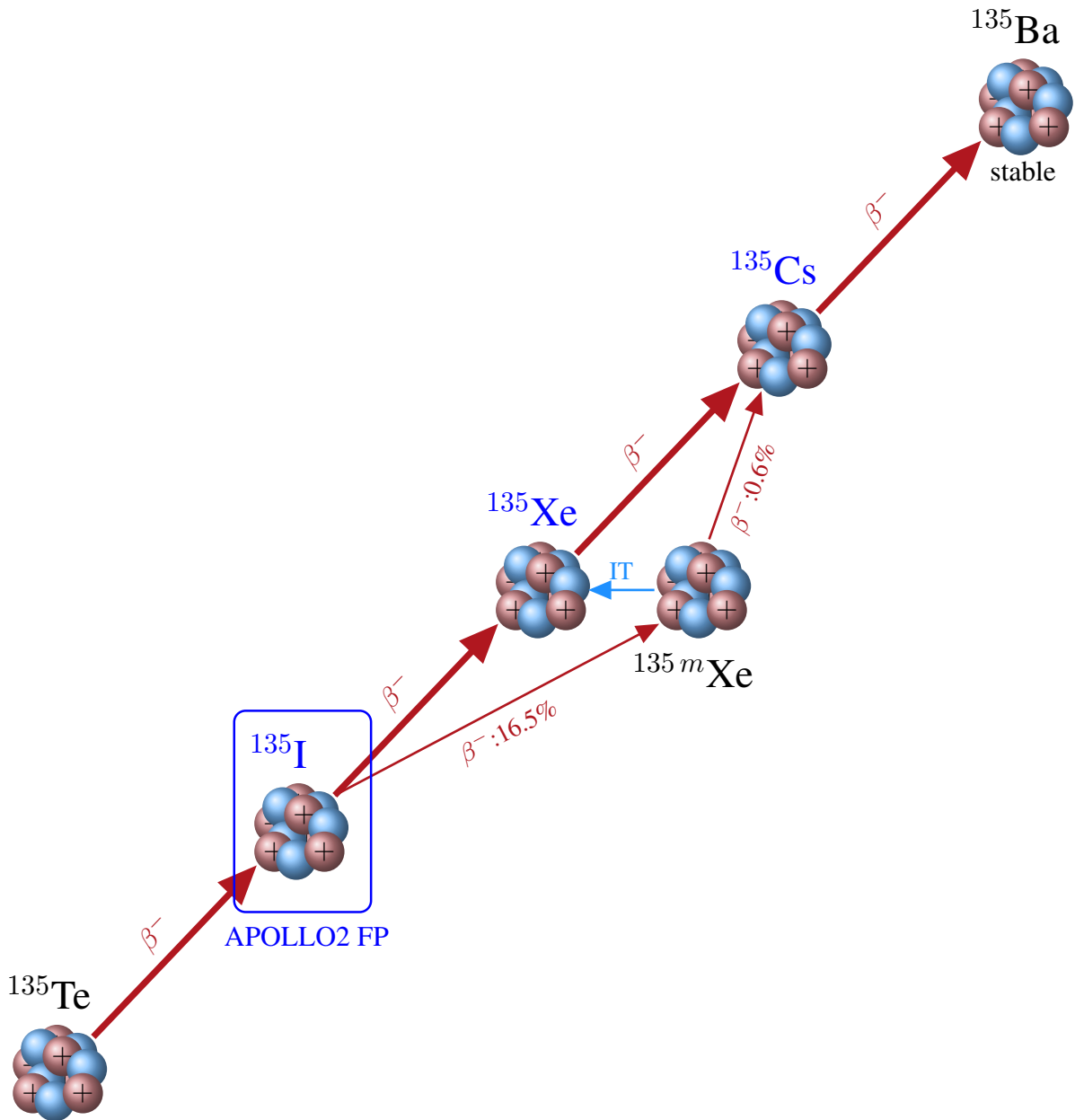


Figure 3.9: Overview of some fission product decays. APOLLO2 fission products have been highlighted in blue. Their decays are ignored calculating their cumulative FY for APOLLO2, since they will be already considered in the inventory calculations performed by the depletion module.

Therefore, in the APOLLO2 library:

- i) The ^{135}I APOLLO2 is given as FY cumulative fission yield, since no parent nuclei are included in the APOLLO2 list.
- ii) ^{135m}Xe does not belong to the list, so no FY is provided.
- iii) ^{135}Xe and ^{135}Cs are semi-cumulative FY. Their FY values are calculated according to the following formulas:

$$C_{AP}^{135\text{Xe}} = Y_{post}^{135\text{Xe}} + 0.994 \cdot C^{135m\text{Xe}}, \quad (3.15)$$

$$C_{AP}^{135\text{Cs}} = Y_{post}^{135\text{Cs}} + 0.006 \cdot C^{135m\text{Xe}} + C^{135m\text{Cs}}. \quad (3.16)$$

Cumulative fission yields contributions from ^{135}I and ^{135}Xe are normally needed to be included for $C_{135\text{Xe}}$ and $C_{135\text{Cs}}$ evaluated data, but, as already said, this is not the case for APOLLO2.

To evaluate APOLLO2 FY, CONRAD can calculate a Q-matrix specifically dedicated to APOLLO2 needs. A special branching ratio matrix \mathbf{B}_{AP} is obtained considering the nuclei in the APOLIB list as stable. In that way, APOLLO2 fission products decay modes are ignored in FY calculations and correct Q-matrix values can be obtained to evaluate the semi-cumulative yields delivered to the depletion module. This CONRAD capability is crucial in uncertainty propagations, especially performing FY Monte Carlo samplings.

As it will be clearer in Chapter 5, once a certain number of independent FY data sets are sampled, the APOLLO2 Q-matrix is indispensable to generate FY for depletion calculations. In Fig. 3.10 ratios between APOLLO2 yields calculated by CONRAD and the CEA2005-APOLIB library⁵ values, employed by HORUS3D, are shown. For almost the whole fission product inventory, we do not have any deviation from unity, meaning a quite impressive agreement between the decay dependencies calculated by CONRAD and those used to generate the CEA2005-APOLIB library.

However discrepancies have been found for some nuclides. For ^{235}U thermal fission, ^{88}Sr , ^{103}Rh , ^{121}Sb and ^{137}Cs CONRAD FY showed the most significant differences. Some of them are due to several independent FY values used in the CEA library which cause discrepancies in ^{88}Sr , ^{103}Rh and ^{137}Cs semi-cumulative yield calculations. Similar conclusions have been deduced analyzing ^{239}Pu thermal FY. ^{109}Ag and ^{142}Ce are different for analogous reasons; modifications in the JEFF-3.1.1 independent FY library have been introduced generating the CEA APOLIB.

For the ^{121}Sb yields we found differences since ^{121m}Sn is missing in APOLIB decay chains, provoking discrepancies for all fissioning systems.

⁵The CEA2005-APOLIB library of the APOLLO2.8/JEFF-3.1.1 package contains all the necessary data to perform APOLLO2 calculations. Different versions are available and all are based on JEFF-3.1.1 nuclear data library. The different libraries can benefit from several energies meshes optimized for light water reactor calculations [Leconte, 2009].

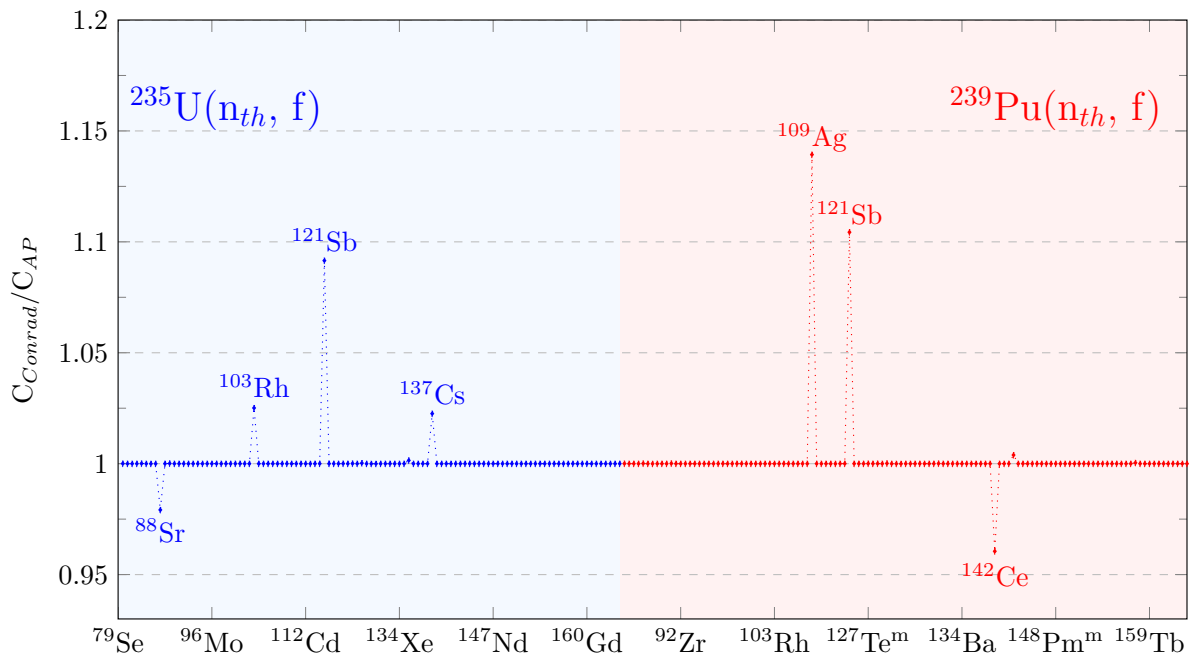


Figure 3.10: Ratios between the CONRAD calculated APOLLO2 FY and the CEA2005-APOLIB version based on JEFF-3.1.1 for the thermal fissions of ^{235}U and ^{239}Pu .

3.4 Conclusions

This chapter was devoted to nuclear data evaluation providing the missing pieces in the general puzzle introduced in Chapter 1 and 2. In Sec. 3.1 the general procedure at the basis of nuclear data evaluation for applications has been briefly presented, outlining the most important steps which have to be followed to generate a multi-group cross section library.

The nuclear data cycle has been described, highlighting the importance of science-based covariance matrix and new integral and fundamental experiments for modern nuclear facility design.

In Sec. 3.2 a few words have been spent to enumerate the most important techniques for FY experimental measurements. Special attention has been dedicated to Lohengrin spectrometer, whose measurements have been fundamental in recent FY evaluations.

The second half of the chapter was dedicated to the CONRAD code, the computational tool mainly used in the present PhD work. After a brief presentation of the main capabilities of CONRAD, the new features added to accomplish the goals proposed by this doctoral thesis have been described, giving some elements of the code verification pursued during the implementation.

CONRAD has now the capability to perform fission yields and miscellaneous quantity calculations, generating associated covariance matrices. Cumulative FY can be calculated thanks to the Q-matrix and specific APOLLO2 FY can be evaluated. APOLIB FY play a key role in uncertainty propagation issues, since evaluated independent FY are normally not used directly in neutron transport code. A selection of fission products is in fact

generally made and semi-cumulative FY must then be calculated. An important point has to be emphasized for future perspectives of the present doctoral work: the Q-matrix has been considered as a constant during the whole dissertation. In principle, branching ratio uncertainties and correlations need to be taken into account to perform a proper uncertainty propagation of FY parameter models.

In the next chapter we will see some applications of FY best estimates and covariance matrix evaluation using the CONRAD code. Some results of covariance matrix on the most important fissioning systems will be proposed as possible uncertainty information to be attached to the present JEFF FY evaluation and to test the FY impact on JHR reactivity loss uncertainty estimation.

Chapter 4

Fission Yields Covariance Evaluation

Contents

4.1	The JEFF-3.1.1 FY Library	92
4.2	Covariance Generation General Procedure	93
4.2.1	The GLS Phase	93
4.2.2	The Retroactive Analysis	96
4.2.3	The Analytical Marginalization	97
4.2.4	Uncertainty Propagation for Independent and Cumulative FY	97
4.3	U-235 Thermal Fission	98
4.4	Pu-239 Thermal Fission	117
4.5	Pu-241 Thermal Fission	124
4.6	U-238 Fast Fission	130
4.7	Conclusions and Final Remarks	134

FISSION yields are essential nuclear data used to analyze the evolution of the system in depletion calculations. Complete FY uncertainties must be taken into account to estimate properly the intervals of possible variation of integral reactor parameters with both safety and economic purposes. For a high flux material testing reactor, such as the JHR, FY can play a non-negligible role. The reactivity loss during depletion (and so the cycle length) is, in fact, surely affected by neutron absorber concentrations, whose calculated values are closely related to the precision we have on FY data.

As already mentioned before (see main objectives in the Introduction), present FY nuclear data libraries offer incomplete FY uncertainty information, limited to only variances. Diagonal covariance matrices are not enough for modern uncertainty propagation purposes anymore, and the nuclear community is expressing the need for physically consistent FY covariances (see WPEC/SG-37 proposals in Ref. [Mills, 2012]).

Important efforts have been spent to develop a methodology able to determine experimental covariances (e.g. using measurements at ILL [Kessedjian, 2015]) and several methodologies have been proposed by different organizations to generate covariances for evaluated FY data [Fiorito et al., 2014, Pigni et al., 2015, Fiorito et al., 2016]. Here, we propose our own procedure [Terranova et al., 2015c, Terranova et al., 2015a, Terranova et al., 2015b] to generate covariance matrices for existing evaluated FY provided in JEFF-3.1.1. The main goal is not in fact to propose a new evaluation but to reproduce the available European library JEFF-3.1.1, using the semi-empirical models seen so far, and add associated consistent covariance information.

After a general description of the analysis scheme we adopted using the CONRAD code,

the different sections will be devoted to the analysis of the most significant thermal and fast neutron induced fissioning systems. The covariance matrices obtained from CONRAD calculations will be successively used in uncertainty propagations for integral reactor parameters, to test the results obtained and see the impact of this kind of nuclear data on real applications.

4.1 The JEFF-3.1.1 FY Library

Before starting to describe the general procedure we decided to adopt in order to generate covariance matrices, let us spend some words on the JEFF-3.1.1 FY library which is the last release at present time¹.

In JEFF-3.1.1 several neutron induced fissioning systems are provided with FY data. As already mentioned in the introduction, best estimates and uncertainties are given for independent and cumulative isomeric FY, but correlations are totally missing.

According to Ref. [Kellett and Mills, 2009], JEFF-3.1.1 FY evaluation is adopted from the United Kingdom evaluation UKFY-3.6A which is based on Mills PhD work, extensively described in Ref. [Mills, 1995]. The UKFY-3.6A database contains 12109 absolute measurements, 1342 relative measurements and 1480 ratio to ratio measurements. Absolute experimental values are the most straightforward since they provide directly the FY. Relative measurements are normalized to a FY value that can be considered well-known. Ratio to ratio measurements assume that the yields for the fission product of interest and the monitor one are known for a reference fissioning system. The yield for the fission product of interest can be deduced for the fission reaction of interest once its monitor product yield is known.

The inverse variance weighting has been used to obtain FY averages [Mills, 1995], performing down-weighting of discrepant assessments based on χ^2 tests. Separate analyses have been performed for chain, independent and cumulative yields, whose averages and standard deviations have been used as inputs to semi-empirical model fitting to perform interpolations and extrapolations. Chain yields are nothing else than cumulative yields for stable nuclei, since they collect the whole contribution coming from the decay chain over an infinite time after the fission event. They generally differ of few per cent from the mass yields, since usually no mass changes take place due to the radioactive decay (mostly β^-).

In UKFY-3.6A independent yields are envisaged as

$$Y(A, Z, M) = Y(A)f(A, Z)R(A, Z, M), \quad (4.1)$$

where $Y(A)$ is the post-neutron mass yield, $f(A, Z)$ the isotopic fraction and $R(A, Z, M)$ the isomeric ratio. Mass yields are fitted by a set of Gaussians to fill the gaps and produce a complete data set. The theoretical justification provided in Ref. [Kellett and Mills, 2009] is based on the Brosa fission modes theory. However, as seen in Chapter 2, Brosa proposes a model for pre-neutron yields which is not applicable after prompt neutron emission and no models are provided for that.

The isotopic fractions have been fitted using the Wahl Z_P systematics, while the isomeric ratio has been provided using the Madland-England model, even if preference was given to directly measured ratios.

¹The publication of release 3.2 is now underway.

Ternary fission has been considered according to the results proposed by Serot (see Ref. [Serot et al., 2004b]), but it has not taken into account in the present work.

Cumulative FY can be obtained once the Q-matrix is built, as it was explained in Chapter 2. The Q-matrix for JEFF-3.1.1 was determined from JEFF-3.1 decay data, considering long-lived nuclei as stable. The uncertainties of cumulative yields δC_j were determined from the variances coming from both adjusted independent yields and experimental chain ones, given by the following approximation [Kellett and Mills, 2009]:

$$\delta C_j = \sqrt{\left[\left(1 - \frac{C_j}{Ch}\right) \sum_i Q_{i,j} \delta Y_j \right]^2 + \left(\frac{C_j}{Ch} \delta Ch \right)^2} \quad (4.2)$$

The JEFF-3.1.1 FY library provides only isotopic (and isomeric) independent and cumulative yields in a ENDF format. To retrieve other kind of FY (such as mass distributions) summations are needed. For this reason nuclear data visualization softwares, such as JANIS-4.0 [Soppera et al., 2014], can only perform quadratic summations to calculate mass yield uncertainties, and this has been a key point in the Bayesian adjustment procedure, as explained in the following sections². As shown also in Ref. [Fiorito et al., 2016], generating independently post-neutron evaporation and cumulative yields and attributing cumulative yield uncertainties through Eq. 4.2 produces discrepancies. If independent uncertainties are propagated through the Q-matrix relationship, JEFF cumulative yield error bars will not be reproduced and they will exhibit significantly smaller values. This behavior is explicable because independent measurements are clearly affected by higher uncertainties, while chain yields are known better. Further details on this topic will be provided in the next sections, talking about the cumulative yield uncertainty issue deriving from these discrepancies.

4.2 Covariance Generation General Procedure

This section is devoted to the description of the general procedure we adopted to generate covariance matrices for independent FY. Independent FY are in fact the most used data in applications, and nuclei concentration evolution is generally calculated solving the Bateman equation. In Fig. 4.1 the schematic flow-chart of the procedure we adopted to generate FY covariances is presented. Some of the methodologies described in Chapter 1 and implemented in CONRAD (see Chapter 3) have been used together with the semi-empirical models presented in Chapter 2 to generate physically consistent covariance matrices, to be associated to the European JEFF-3.1.1 library.

4.2.1 The GLS Phase

As first step we perform an iterative GLSM, which is exhaustively described in Chapter 1. The GLSM needs experimental data and FY theoretical models based on adjustable parameters to perform a Bayesian learning process and provide best estimates and covariances.

²Calculating the square root of the yield variances summation is equivalent to the sandwich rule on a diagonal variance matrix, since no correlations are provided between yields.

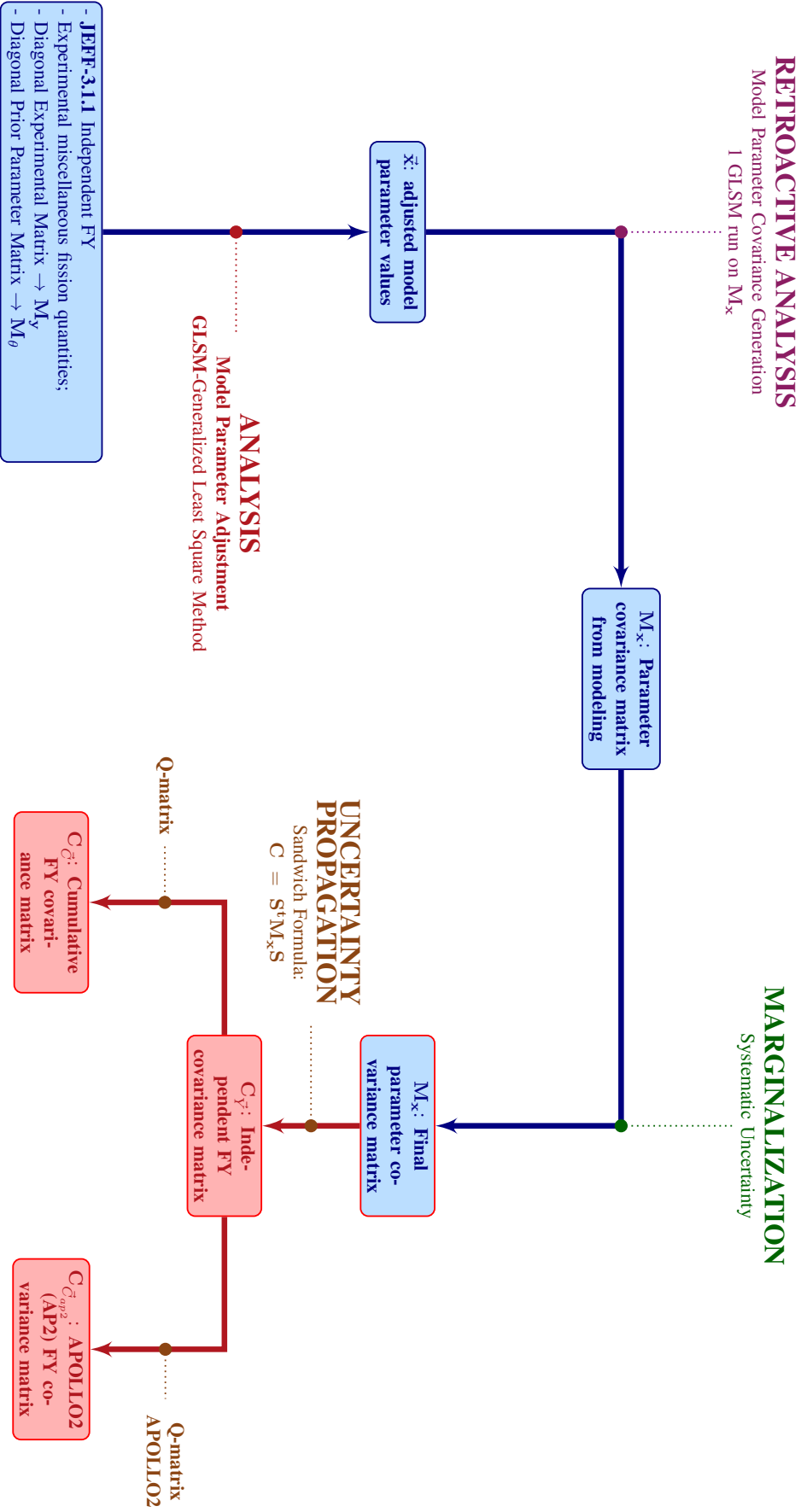


Figure 4.1: Schematic flow-chart of the procedure we adopted to generate FY covariance matrices.

In CONRAD the iterative GLS adjustment is available, allowing the reduction of possible non-linearity issues. The algorithm implemented in CONRAD is recalled in the following equations

$$\vec{x}^{(n)} = \vec{\theta} + \mathbf{C}_x^{(n)} \left\{ \mathbf{G}^{(n-1)\dagger} \mathbf{C}_y^{-1} [\vec{y} - \vec{t}(\vec{x}^{(n-1)})] + \mathbf{G}^{(n-1)\dagger} \mathbf{C}_y^{-1} \mathbf{G}^{(n-1)} [\vec{x}^{(n-1)} - \vec{\theta}] \right\}, \quad (4.3)$$

$$\mathbf{C}_x^{(n)} = \left(\mathbf{C}_\theta^{-1} + \mathbf{G}^{(n-1)\dagger} \mathbf{C}_y^{-1} \mathbf{G}^{(n-1)} \right)^{-1}, \quad (4.4)$$

whose meaning is explained in Sec. 1.4.1.2.

As pseudo-experimental data, we used JEFF-3.1.1 independent FY. The main goal of this work is in fact to reproduce the evaluated library, without performing any new evaluation, and to propose covariances. Isotopic, isomeric and mass yields have been provided to the CONRAD code as experimental files. One issue was to estimate uncertainties for mass yields. As already mentioned in the chapter, mass yields are not provided in the ENDF files and can be only obtained adding isotopic yields with the same mass number.

Since no correlations are given in the library, uncertainties for mass yields will be necessarily over-estimated if a direct uncertainty propagation is performed. To overcome this issue, we decided to assign error bars comparable to typical statistical experimental uncertainties to the calculated mass yield data derived from JEFF-3.1.1. In such way, more realistic uncertainty bounds were provided allowing a better representation of the mass yields, whose values are generally quite accurate³.

In Fig. 4.2 the comparison between the uncertainties obtained by simple error propagation of isotopic yields and those used in CONRAD experimental files is shown. Performing a quadratic summation of JEFF-3.1.1 isotopic independent yield uncertainties gives a homogeneous 10% overall the mass domain. As well known, neutron induced fission for the most important actinides produces asymmetric distributions, so peak fission yields should present lower uncertainties, since they are characterized by better statistics in the measurement process. What we attempted to build up is a more realistic mass yield uncertainty distribution, attributing higher values to the symmetry and the wing regions.

In the GLS procedure, parameters for Brosa fission modes, $p_A(\nu)$, Wahl isotopic fractions and Madland-England isomeric ratios (see Chapter 2) have been adjusted, producing simultaneously best estimates and covariance matrices. The Brosa model has been correctly applied to pre-neutron FY distribution, explained in Chapter 2 and the generic isomeric independent yield has been calculated using the following equation

$$Y_{post}(A, Z, M) = \left[\sum_{\nu_i=0}^{\infty} Y_{pre}(A + \nu_i) \cdot p_{A+\nu_i}(\nu_i) \cdot f(A + \nu_i, Z) \right] \cdot R(A, Z, M), \quad (4.5)$$

exhaustively described in Chapter 2. For the prompt neutron emission probability all the saw-tooth values (see Chapter 2) have been adjusted together with a unique standard deviation for all the fragment masses. Experimental files concerning miscellaneous fission quantities have been included in the Bayesian adjustment when available. For the most important fissioning systems for applications, such as the thermal fissions of ²³⁵U, ²³⁹Pu

³It is not rigorously correct to assume experimental uncertainties on JEFF-3.1.1 data, a full and comprehensive evaluation procedure should be in fact performed. However, for our purposes, such methodology allowed us to reach a satisfactory representation of the FY evaluated library, which is fundamental to reproduce consistent covariance matrices.

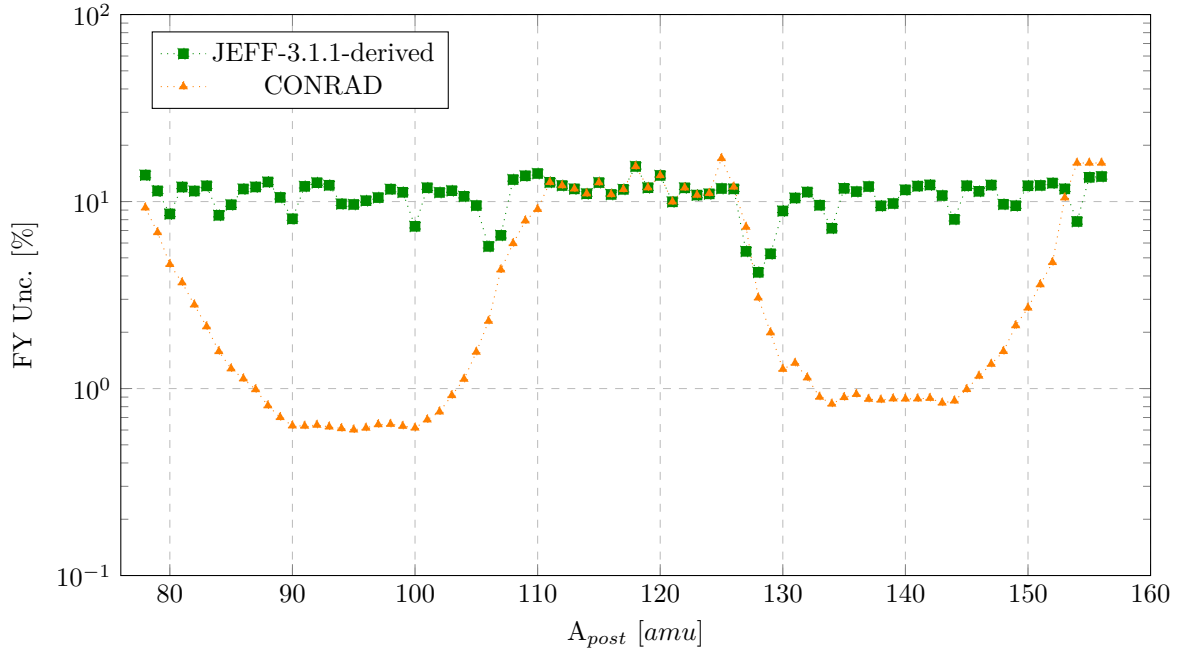


Figure 4.2: Comparison between the uncertainties derived by direct uncertainty propagation of JEFF-3.1.1 isotopic uncertainties without correlations and those used in the CONRAD adjustment phase, for the thermal fission of ^{235}U .

and ^{241}Pu , measurements on the total prompt neutron multiplicities and on the total prompt neutron emission probabilities are available in the EXFOR database, so they have been included in CONRAD calculations.

4.2.2 The Retroactive Analysis

Adjusting all the average numbers of prompt neutrons emitted, provided by the saw-tooth curve, allowed us to reproduce JEFF-3.1.1 data quite precisely, especially for FY in the peak regions. As it will be clearer in the following sections, where some results are presented, moderate modifications from prior experimental saw-tooth curves for the most important fissioning systems allowed a satisfactory representation of the evaluated JEFF-3.1.1 data using the models proposed in Chapter 2.

The asymmetric behaviors in the mass yield distributions can be actually reproduced only if the prompt neutron emission is taken into account. Nevertheless, no models are unfortunately available for the saw-tooth shape and to generate physically consistent correlations between data we decided to proceed with a retroactive analysis to retrieve more realistic parameter uncertainties.

The retroactive analysis step consists in maintaining the best estimates provided by the GLS procedure, reassigning prior uncertainties and calculating a new covariance matrix by only performing the covariance matrix update

$$\mathbf{C}_{\mathbf{x}}^{(n)} = \left(\mathbf{C}_{\theta}^{-1} + \mathbf{G}^{(n-1)\dagger} \mathbf{C}_{\mathbf{y}}^{-1} \mathbf{G}^{(n-1)} \right)^{-1}, \quad (4.6)$$

where $(n-1)$ values are those provided by the GLSM and the $\mathbf{C}_{\mathbf{x}}^{(n)}$ is the updated parameter covariance matrix. In this phase we did not consider the saw-tooth values

as parameters, which instead have been assumed as constant and equal to the adjusted values obtained at the first step. In that way only the Brosa parameters are called to represent experimental uncertainties for mass FY, and the obtained correlations are no longer influenced by the saw-tooth.

4.2.3 The Analytical Marginalization

Once the adjustment procedure is achieved, the analytical marginalization is performed. This phase turned out to be extremely important to have a better representation of JEFF-3.1.1 uncertainties.

The Bayes theorem, in fact, does not take into account model defects. The theoretical model is assumed as prior true information. Nuclear data which are well represented by the model and have small error bars significantly constrain the Bayesian learning process, inducing reduced parameter uncertainties. In our case most of the evaluated FY come directly from experimental measurements and, in many cases, their values can be quite well known. To overcome this last issue and introduce a systematic uncertainty component, we resorted to the analytical marginalization, presented in Chapter 1. A typical example is the measurement of isotopic FY. To obtain isotopic distributions, counting rates must be normalized by the corresponding mass or charge yield value that is obviously affected by a given uncertainty, which correlates data. In the following analyses, we marginalized uncertainties for JEFF-3.1.1 pseudo-experimental files related to Tellurium and Iodine FY⁴, since their isotopes presented the most sensitive FY to reactivity loss applications (see Chapter 6).

4.2.4 Uncertainty Propagation for Independent and Cumulative FY

Once the parameter covariance matrix is generated by CONRAD, independent and cumulative FY best estimates and covariances need to be evaluated. For the average values a simple theoretical calculation using the semi-empirical and the Q-matrix models described in Chapter 2 is sufficient. To generate a full FY covariance matrix the sandwich rule can be applied using the parameter covariance matrix. Since the theoretical models are mostly non linear, finite difference calculations are used in CONRAD to calculate derivatives and then sensitivities.

In the following sections some results for the most important thermal and fast fissioning systems are provided. All the analyses follow the guidelines just described, with very few variations depending on the fissioning system and on the availability of experimental data for the saw-tooth curve and the miscellaneous fission quantities. Some details on model parameter values are also provided that could give interesting indications on the physical aspects involved in the fission process.

⁴We chose Tellurium and Iodine as reference nuclei because the main goal of the present work is to generate covariances for reactivity uncertainty quantification, even if the results obtained could be applied for a wide range of problems. Using such isotopes was clearly a choice of the evaluator and underlines the non-uniqueness of any nuclear data evaluations and the clear orientation towards nuclear system applications.

4.3 U-235 Thermal Fission

Let us start with the description of the model parameters adjustment for the thermal fission of ^{235}U . The parameter average values used as priors for the Brosa fission modes have been taken from Hamsch and Zeynalov (see Ref. [Zeynalov et al., 2005]) and reported in Tab. 4.1. We took 5% of uncertainty on the Standard I and Standard II mass symmetry deviations, 20% on the weight of the Super Long and 10% on the other Brosa parameters⁵. In the same table also the values obtained after the adjustment procedure are given. We did not notice any significant variations, except for the weight of the Standard I, who passed from 16% to almost 23%.

Parameter	Prior BE	Prior Unc. [%]	Posterior BE	Posterior Unc. [%]
$D_{St.I}^*$	15.8	5	16.0	0.7
$D_{St.II}^*$	23.1	5	23.4	0.3
$\sigma_{St.I}^*$	2.60	10	2.10	3
$\sigma_{St.II}^*$	4.95	10	4.77	1.5
σ_{SL}^*	5.05	10	5.53	7
$N_{St.I}$	0.162	10	0.227	5.5
N_{SL}	0.002	20	0.002	6

* Expressed in [amu].

Table 4.1: Fission mode parameters best estimates (BE) and uncertainties before (prior) and after (posterior) the analysis using CONRAD for the thermal fission of ^{235}U .

In Tab. 4.2, the Wahl and Madland-England model parameters adjusted using the GLSM are provided. As prior average values, we picked those reported in Ref. [Wahl, 2000] and Ref. [Madland and England, 1977] for the thermal fission of ^{235}U . We took 20% uncertainty on Wahl parameters and 10% on the Madland-England spin cut-off.

Parameter	Prior BE	Prior Unc. [%]	Posterior BE	Posterior Unc. [%]
$\sigma_Z(140)$	0.566	20	0.424	21.2
$\Delta Z(140)$	-0.487	20	-0.510	6.3
σ_{50}	0.356	20	0.316	3.7
$F_N(140)$	1.076	20	1.04	23
$F_Z(140)$	1.207	20	1.35	16.3
$SL50$	0.191	20	0.327	10
ΔZ_{max}	0.699	20	0.559	2.2
$\sigma_Z SLW$	-0.045	20	0.143	5
$\Delta Z SLW$	0.0049	20	0.005	20
$F_Z SLW$	0.039	20	-0.006	20
$F_N SLW$	0.159	20	-0.010	20
J_{rms}^L	7.5	10	7.61	2
J_{rms}^H	7.5	10	7.54	1.3

Table 4.2: Wahl and Madland-England parameters best estimates (BE) and uncertainties before (prior) and after (posterior) the analysis using CONRAD.

⁵Prior uncertainties were another choice made by own personal sensibility. However, different values were tested leading to the same results in terms of model parameter best estimates. Slight modifications were observed for the associated variances, washed away in the successive analytical marginalization.

To obtain a better representation of JEFF-3.1.1 isomeric ratios, whose evaluated values were preferably taken from experiments (when available, see Ref. [Kellett and Mills, 2009]), two distinct parameters were adjusted for the light and heavy domain (J_{rms}^L and J_{rms}^H respectively) to increase the flexibility of the model. However, no significant differences between them were observed.

We attempted to adjust also the Wahl parameters which are related to very asymmetric regions (called *SLW* using Wahl's nomenclature). Since we are interested mostly in applications, our first goal is to reach a satisfactory representation of the most significant FY, namely $> 10^{-4}$. To do that we performed the adjustment in two steps. The first one involved JEFF-3.1.1 yields greater than 10^{-4} , where we looked for Brosa and Wahl parameter best estimates, assuming *SLW* ones as constant. Successively smaller yields have been considered, with a threshold at 10^{-7} to get *SLW* values.

Posterior uncertainties given in Tab. 4.1 and 4.2 are already those we obtained resorting to the analytical marginalization technique (see Sec. 1.5 and further in the present section). In Figs. 4.3 and 4.4 the comparison between JEFF-3.1.1 mass independent FY and what we obtained using the models implemented in CONRAD is presented in linear and logarithmic scales.

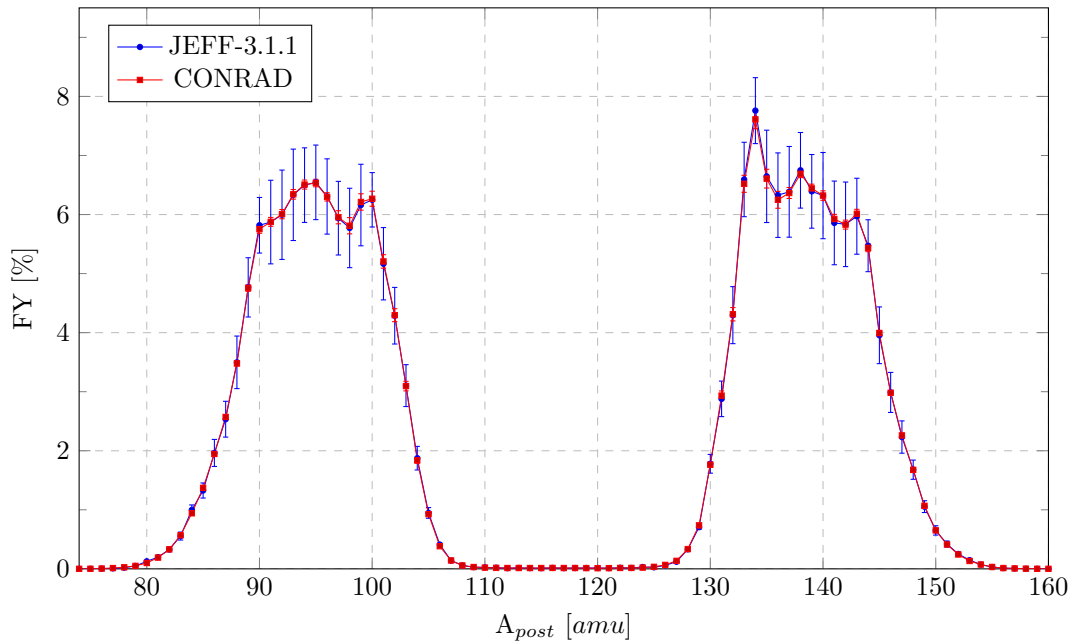


Figure 4.3: Comparison between JEFF-3.1.1 and CONRAD independent mass FY for the thermal fission of ^{235}U in linear scale. FY model parameters have been adjusted using CONRAD to reproduce the JEFF-3.1.1 evaluated library and generate covariances. The convolution between the pre-neutron model based on Brosa fission modes and the saw-tooth curve allows a satisfactory representation of the available FY data.

Thanks to the adjustment of the saw-tooth curve, JEFF-3.1.1 FY averages are quite well reproduced by the models, especially for those yields which are greater than 10^{-4} . This is also confirmed by the elementary fission decay heat calculations performed with the MENDEL code, used to solve the Bateman equation describing the fission products evolution. JEFF-3.1.1 FY data were substituted with CONRAD results for the fissioning systems analyzed during the present work. As shown in Appendix D, CONRAD FY allow to calculate elementary fission decay heat values which are in excellent agreement with those evaluated using JEFF. Such calculations demonstrated only globally the consistency between CONRAD and JEFF, but they showed how CONRAD does not provoke relevant discrepancies for this kind of applications in term of average values.

For the thermal fission of ^{235}U , acceptable results have been obtained even in the symmetry region of the mass domain. FY evaluation in the symmetry region is certainly a difficult task. Experimental data are not abundant at all, and they are affected by higher uncertainties due to the low statistics for thermal neutron induced fission of the actinides between ^{229}Th and ^{254}Es . For mass FY, JEFF-3.1.1 error bars in Figs. 4.3, 4.4, 4.5 and 4.6 are given by the quadratic summation of the isotopic FY uncertainties, so they are necessarily overestimated.

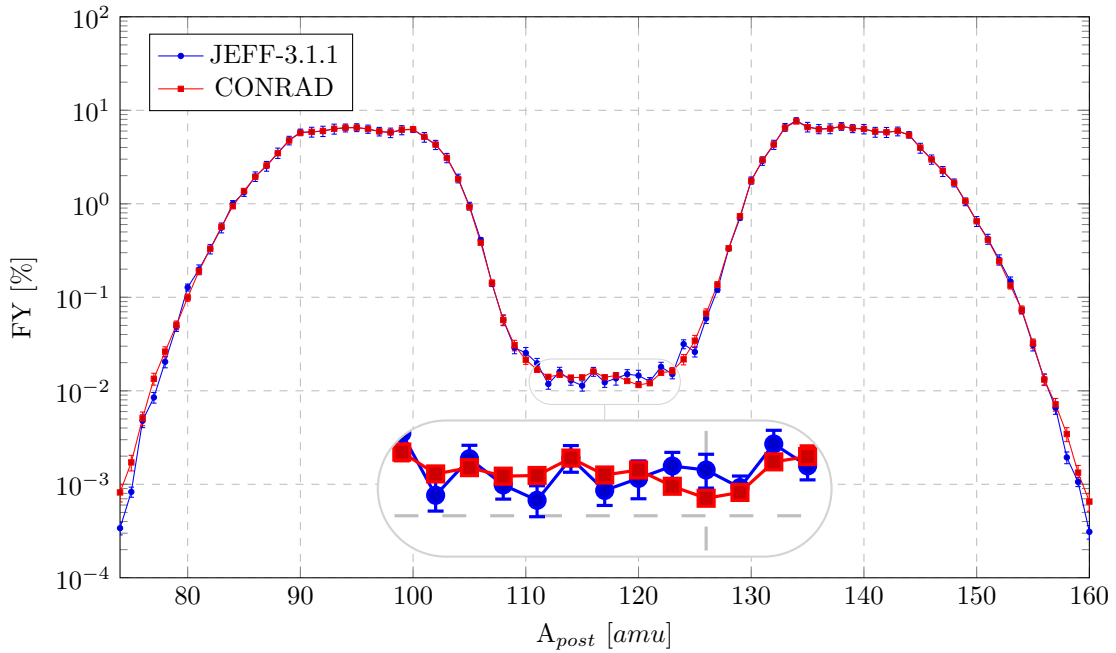


Figure 4.4: Comparison between JEFF-3.1.1 and CONRAD independent mass FY for the thermal fission of ^{235}U in logarithmic scale. FY model parameters have been adjusted using CONRAD to reproduce the JEFF-3.1.1 evaluated library and generate covariances. The convolution between the pre-neutron model based on Brosa fission modes and the saw-tooth curve allows a satisfactory representation of the available FY data even in the symmetry region.

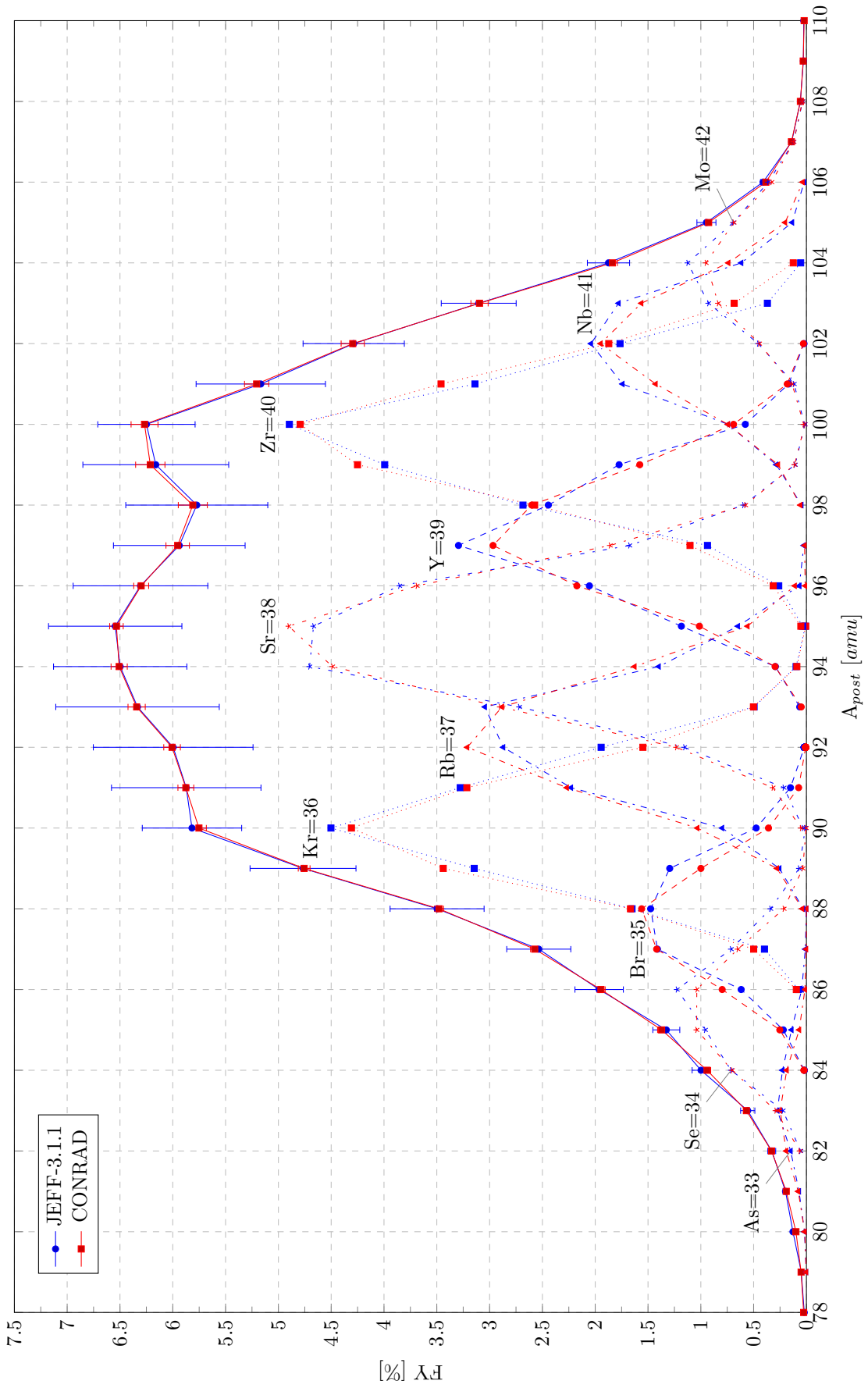


Figure 4.5: Light peak mass and isotopic FY for the thermal fission of ²³⁵U.

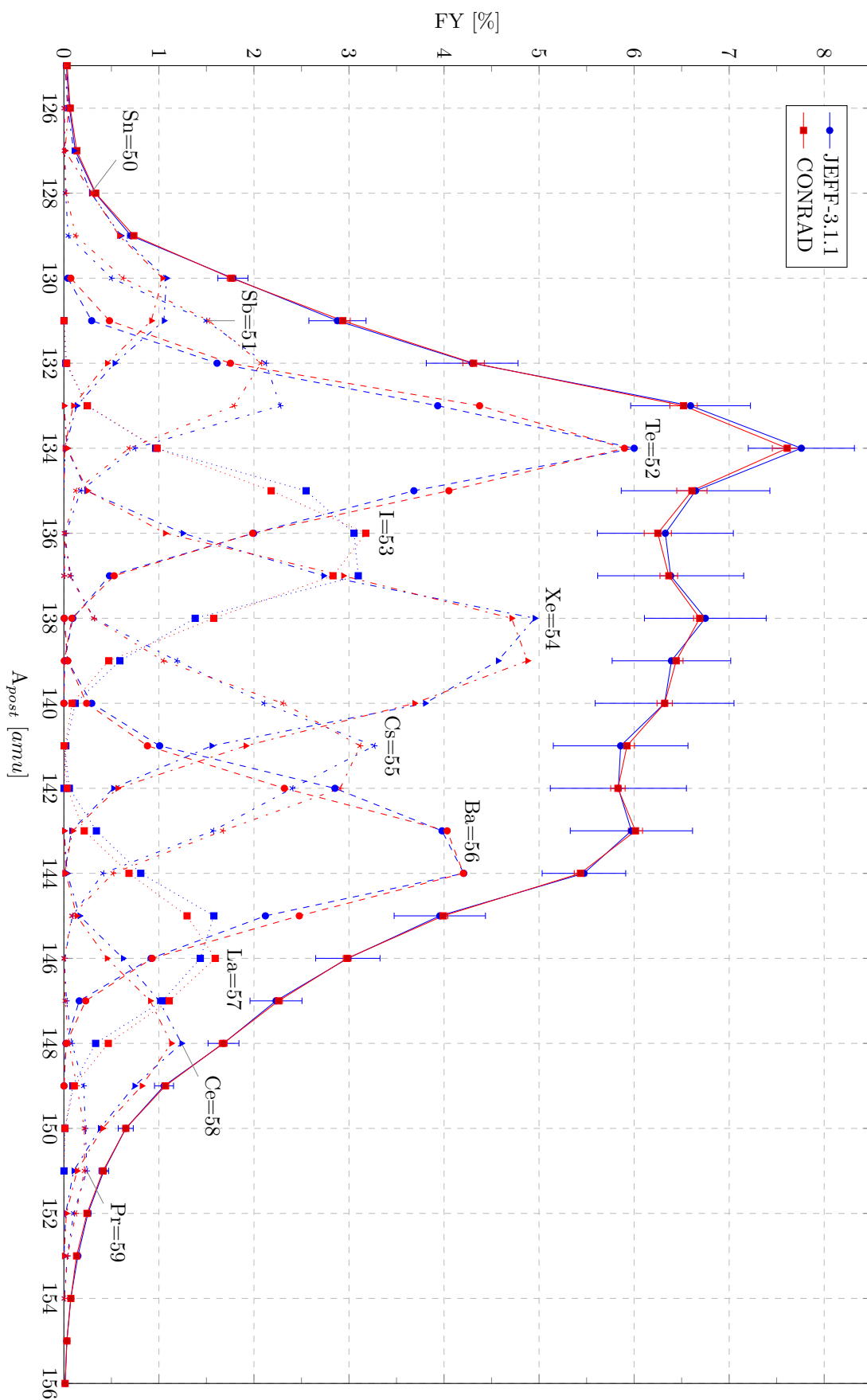


Figure 4.6: Heavy peak mass and isotopic FY for the thermal fission of ^{235}U .

In Fig. 4.7 the comparison between Vorobyev’s experiment⁶ and the adjusted CONRAD values is presented. Some deviations from the experiment values can be observed. These variations allowed us to represent the JEFF-3.1.1 library in details. It has to be emphasized that this kind of experiments are extremely hard to perform. The mass precision for this kind of data is around 2 or in some cases even 3 amu and double error bars should be taken into account, degrading the accuracy of this type of measurement⁷. For the prompt neutron emission probability standard deviation parameter σ , we finally obtained an adjusted value of 0.86 with a 1.5% of relative uncertainty (the prior was 0.5 with 10% of uncertainty).

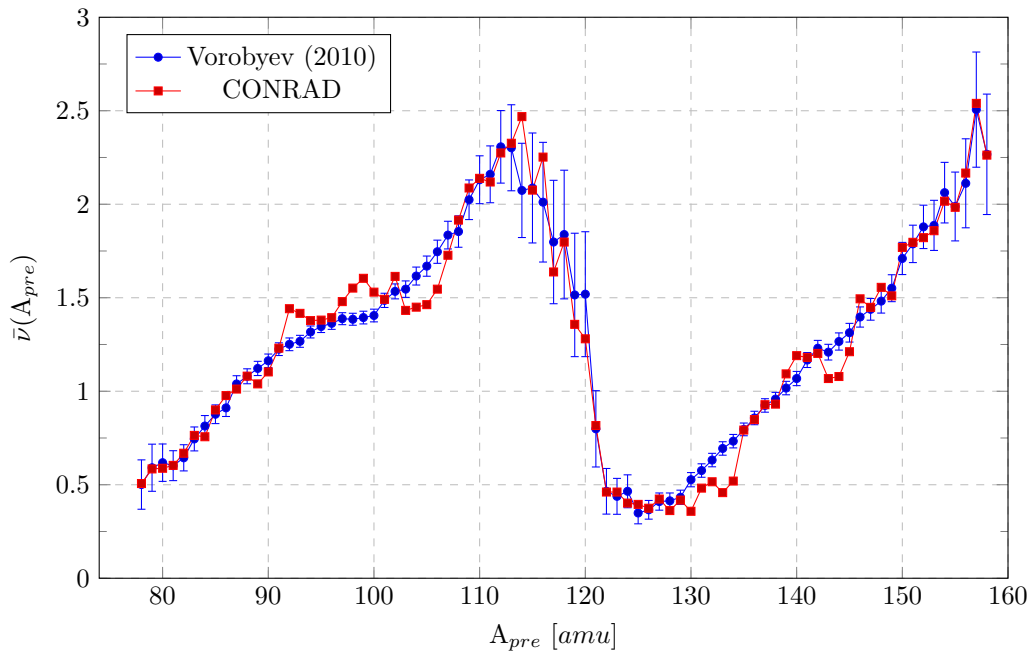


Figure 4.7: Comparison between experimental (from Vorobyev [Vorobyev et al., 2010]) and CONRAD-adjusted average number of prompt neutrons emitted as function of the pre-neutron fragment mass. Slight deviations from the experimental values allow an extraordinary representation of the evaluated FY data.

In Fig. 4.8 Boldeman’s experimental data are compared to CONRAD-calculated total prompt neutron emission probabilities, showing almost excellent agreement⁸. To calculate prompt neutron emission probabilities we relied on truncated Gaussian distributions. Fig. 4.9 shows how much the comparison can be worse if Poisson distributions are considered instead. Furthermore, using Poisson distributions creates some convergence issues in the iterative GLSM, and no satisfactory results can be obtained.

⁶Such experiment has been taken as prior in the GLS procedure.

⁷The reduced $\chi^2 = \frac{1}{(n-1)} \sum_{i=1}^n \frac{(\bar{\nu}_i^C - \bar{\nu}_i^{exp})^2}{(\sigma_i^{exp})^2}$ calculated using CONRAD theoretical values (C) compared to the experimental data provided by Vorobyev (exp) is equal to 4.8. The most significant contributions to the total χ^2 come of course from those masses which present highest deviations from the experimental data. However, it should be emphasized that the experimental data considered present a quite smoothed behavior characterized by probably only statistical uncertainty. To perform a rigorous χ^2 -test, full experimental uncertainty information should be included.

⁸The reduced χ^2 in this case is equal to 10.9. The uncertainties provided by Boldeman for the data which mostly contribute to the total χ^2 are of the order of 0.5%, which are probably underestimated and of only statistical nature.

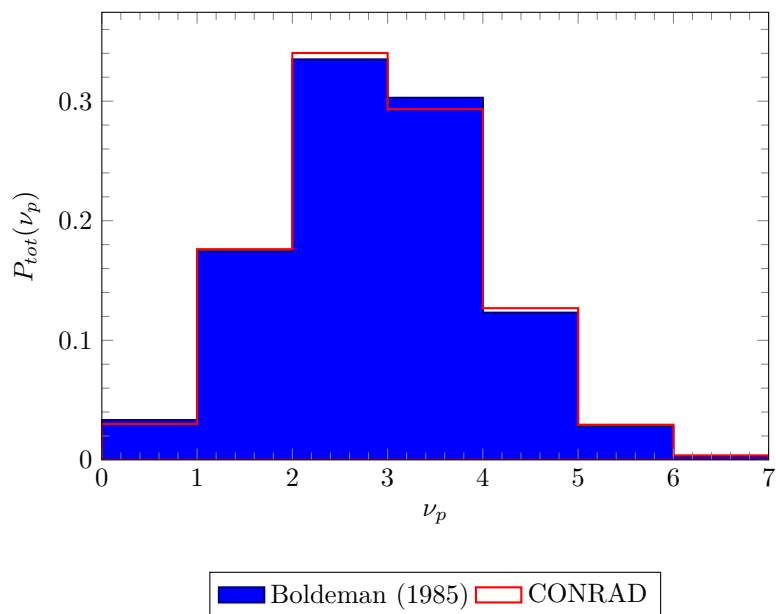


Figure 4.8: Comparison between experimental (from Boldeman [Boldeman and Hines, 1985]) and CONRAD-evaluated total prompt neutron emission probabilities, $P_{tot}(\nu_p)$ for the thermal fission of ^{235}U . It provides the probability that a certain number of prompt neutrons are globally emitted by the fissioning system.

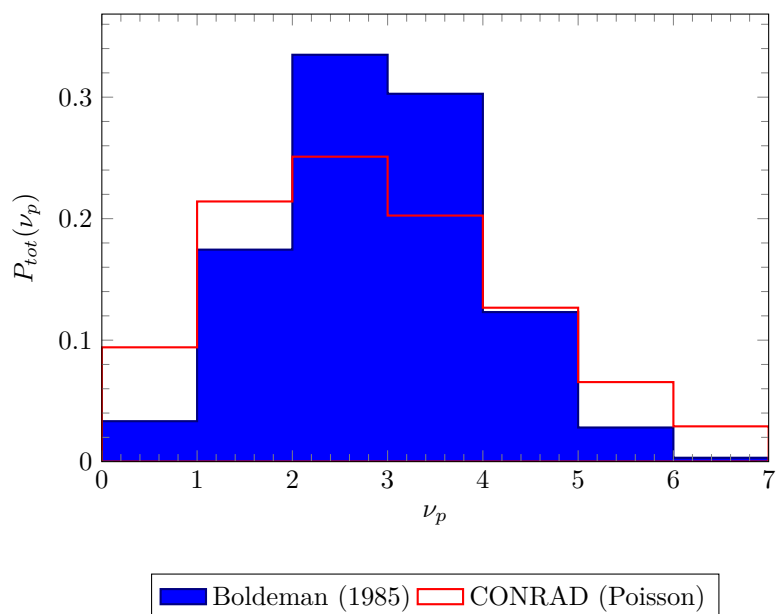


Figure 4.9: Comparison between experimental (from Boldeman [Boldeman and Hines, 1985]) and CONRAD-evaluated total prompt neutron emission probabilities, $P_{tot}(\nu_p)$ for the thermal fission of ^{235}U . In this case the Poisson distribution was used to calculate prompt neutron emission probabilities.

In Tab. 4.3 different prompt neutron multiplicities are provided, comparing CONRAD to JEFF-3.1.1 and experimental values. We obtained a satisfactory representation for the total multiplicity and for the number of prompt neutron emitted by both light and heavy fragments.

Parameter	Exp. Ave.	CONRAD
$\bar{\nu}_P$	2.42	2.42
$\bar{\nu}_P^H$	1.01	1.02
$\bar{\nu}_P^L$	1.42	1.40

Table 4.3: Prompt neutron multiplicities calculated by CONRAD for the thermal fission of ^{235}U . As experimental data we picked the JEFF-3.1.1 evaluated value for the total number of prompt neutron emitted by the fissioning system, and the measurements performed by Nishio of the prompt neutron multiplicities for heavy ($\bar{\nu}_P^H$) and light ($\bar{\nu}_P^L$) fragments [Nishio et al., 1998].

The most difficult task in the present work was to represent JEFF-3.1.1 error bars through the rigorous propagation of model parameter uncertainties. The present evaluation, in fact, is mostly based on experimental data and uses FY models only for interpolation/extrapolation purposes. In our case FY are entirely calculated using models, and the associated uncertainties derive directly from the sandwich rule applied to the model parameter covariance matrix. To solve this issue we firstly performed a sensitivity analysis to find out which are the most influent parameters on FY uncertainties. It turned out to be that Brose fission mode parameters, $\sigma_Z(140)$, $\Delta Z(140)$, $F_N(140)$ and $F_Z(140)$ are the most sensitive parameters.

Reproducing the uncertainties for all the FY dataset became therefore an extremely hard task. We focused on the most important FY from the point of view of applications. To check if the uncertainties provided by CONRAD were plausible, elementary fission decay heat calculations were performed as shown further in the chapter. As already mentioned, we focused on ^{135}Te and ^{135}I , whose FY are the most sensitive in reactivity loss calculations, since their decay produces ^{135}Xe , a well-known neutron absorber. We marginalized a 15% uncertainty on the norm for the Tellurium FY distribution and 21% on Iodine FY⁹. These values were taken observing JEFF-3.1.1 FY uncertainties. As explained in Sec. 1.5, marginalization enhances the uncertainty of model parameters to include the contributions coming from some nuisance parameters, whose uncertainty is fundamental for the data evaluation process but they do not participate directly to the physical models (e.g. measurement norm or background). Only the most sensitive model parameters covariances have been involved in the marginalization, excluding Super Long ones, since they were too sensitive to norm variations.

⁹Different covariance matrices are obtained if different nuclei and uncertainties are chosen in the marginalization procedure. Each statistical methodology leads to specific outcomes which could show non-negligible discrepancies. This choice was justified by the satisfactory results obtained in the uncertainty propagation problems proposed in Chapter 6.

In Figs. 4.10, 4.11, 4.12 and 4.13 isotopic and isomeric independent FY are shown. Average values are mostly reproduced by CONRAD, especially for the most relevant FY. Even if we focused on Tellurium and Iodine FY uncertainties, we got reasonable values also for other isotopes.

In Fig. 4.10, the isotopic distribution for Iodine is shown. Thanks to the marginalization technique the uncertainties of the most significant yields can be well reproduced by CONRAD. The only issue that came up was the non-physical uncertainty (more than 100% in some cases) for very low FY. This was due essentially to the uncertainty propagation of model parameters on very low values (of the order of magnitude of 10^{-5}). However, the most application-sensitive FY uncertainties were quite well reproduced, as it will be clearly shown in Chapter 6.

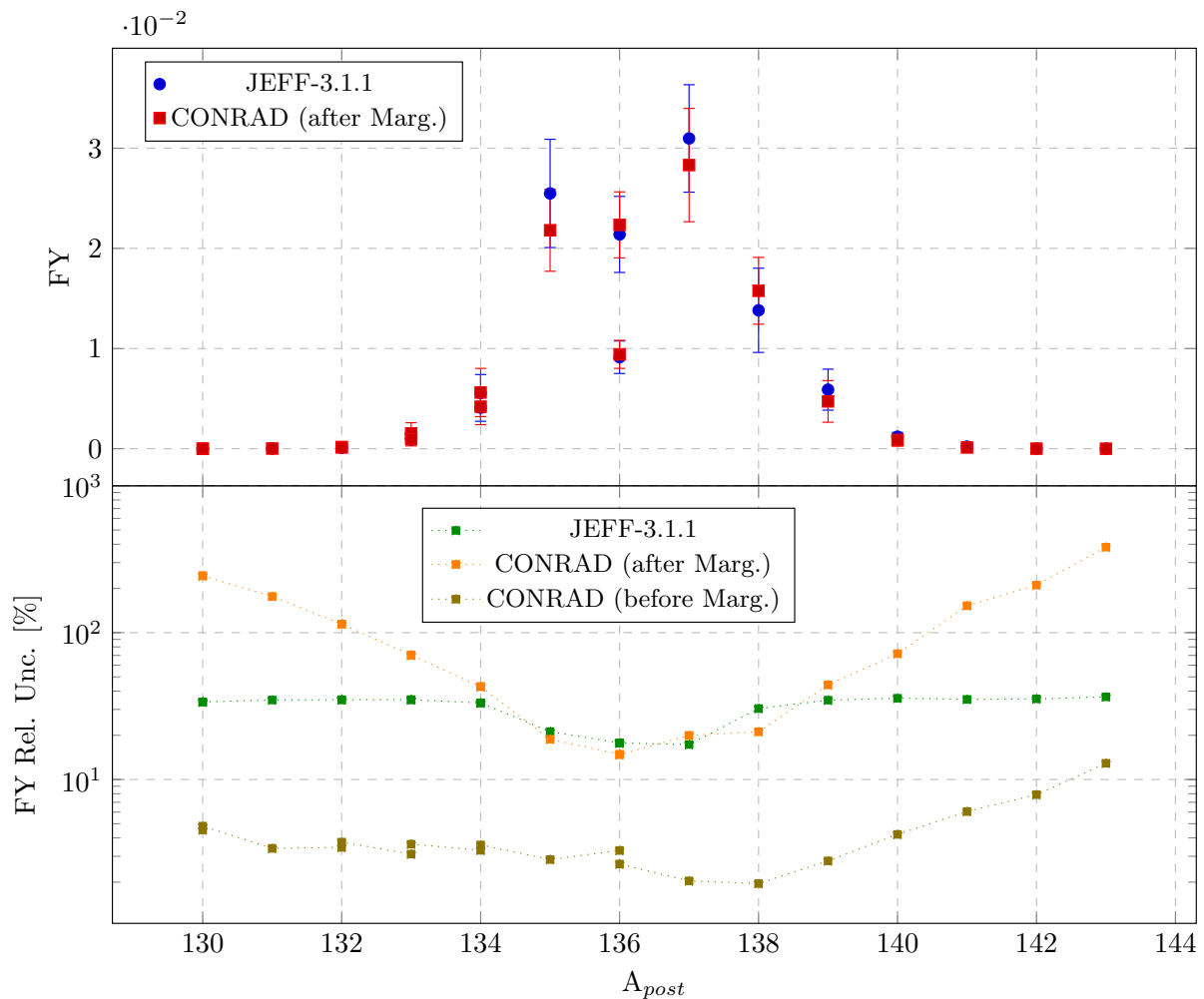


Figure 4.10: Isotopic distribution for the independent FY for the charge $Z=53$ (Iodine). The marginalization techniques allows to reproduce JEFF-3.1.1 uncertainties for the most significant yields.

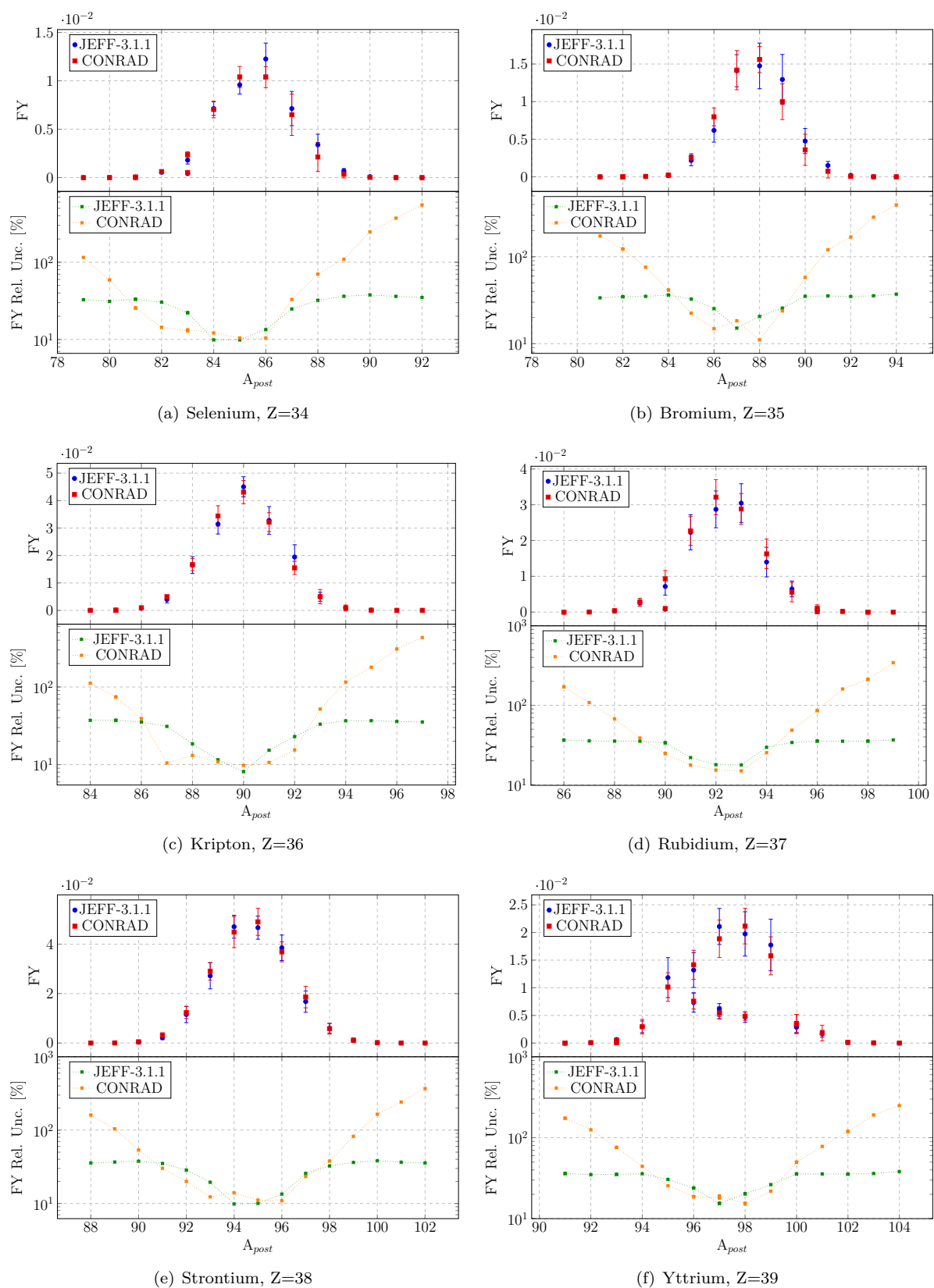
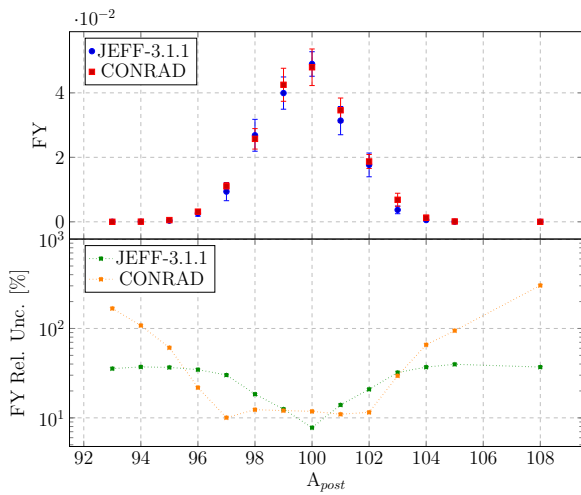
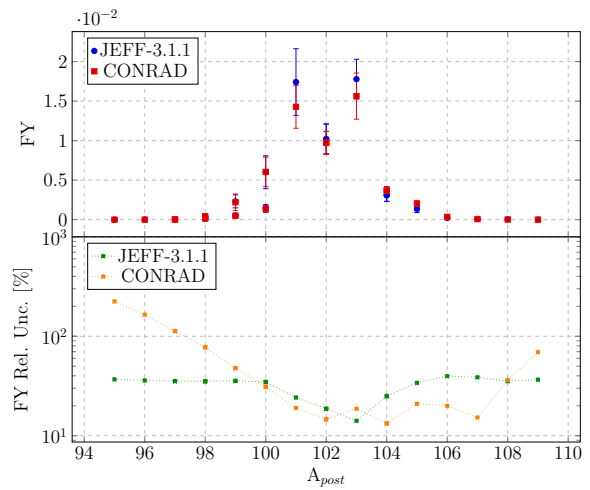


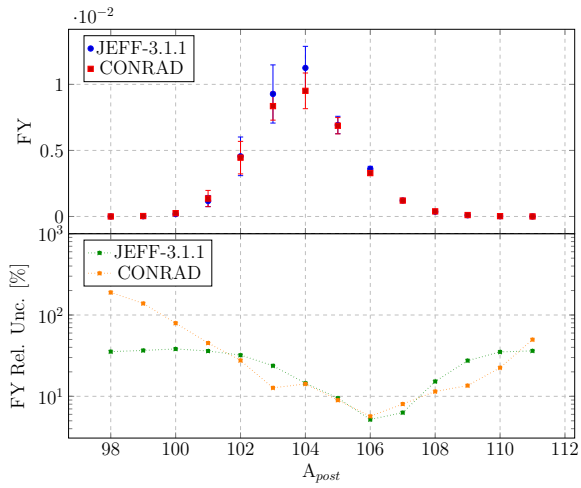
Figure 4.11: Independent isotopic and isomeric FY (top) with their relative uncertainties (bottom) for the thermal fission of ^{235}U , from Z=34 up to Z=39.



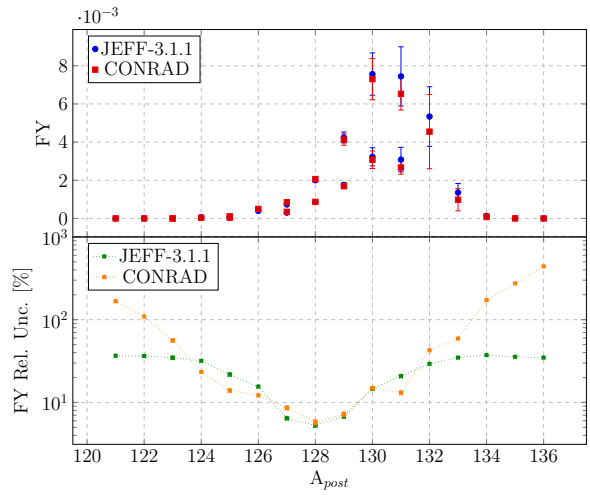
(a) Zirconium, Z=40



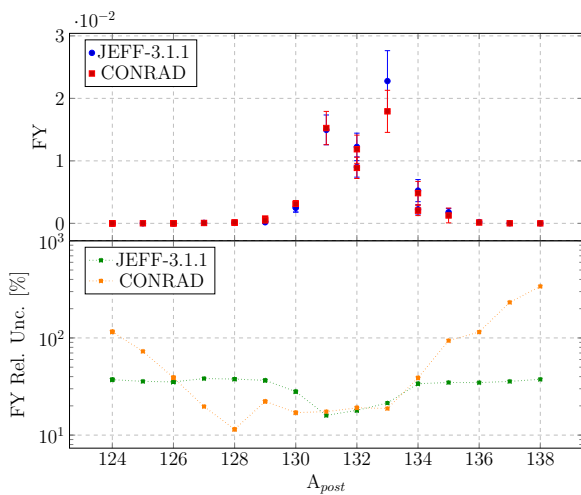
(b) Niobium, Z=41



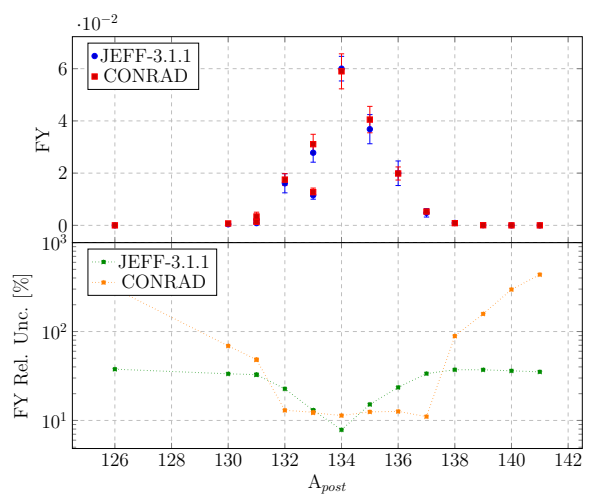
(c) Molybdenum, Z=42



(d) Tin, Z=50



(e) Antimony, Z=51



(f) Tellurium, Z=52

Figure 4.12: Independent isotopic and isomeric FY (top) with their relative uncertainties (bottom) for the thermal fission of ^{235}U , from Z=40 up to Z=42 and from Z=50 up to Z=52.

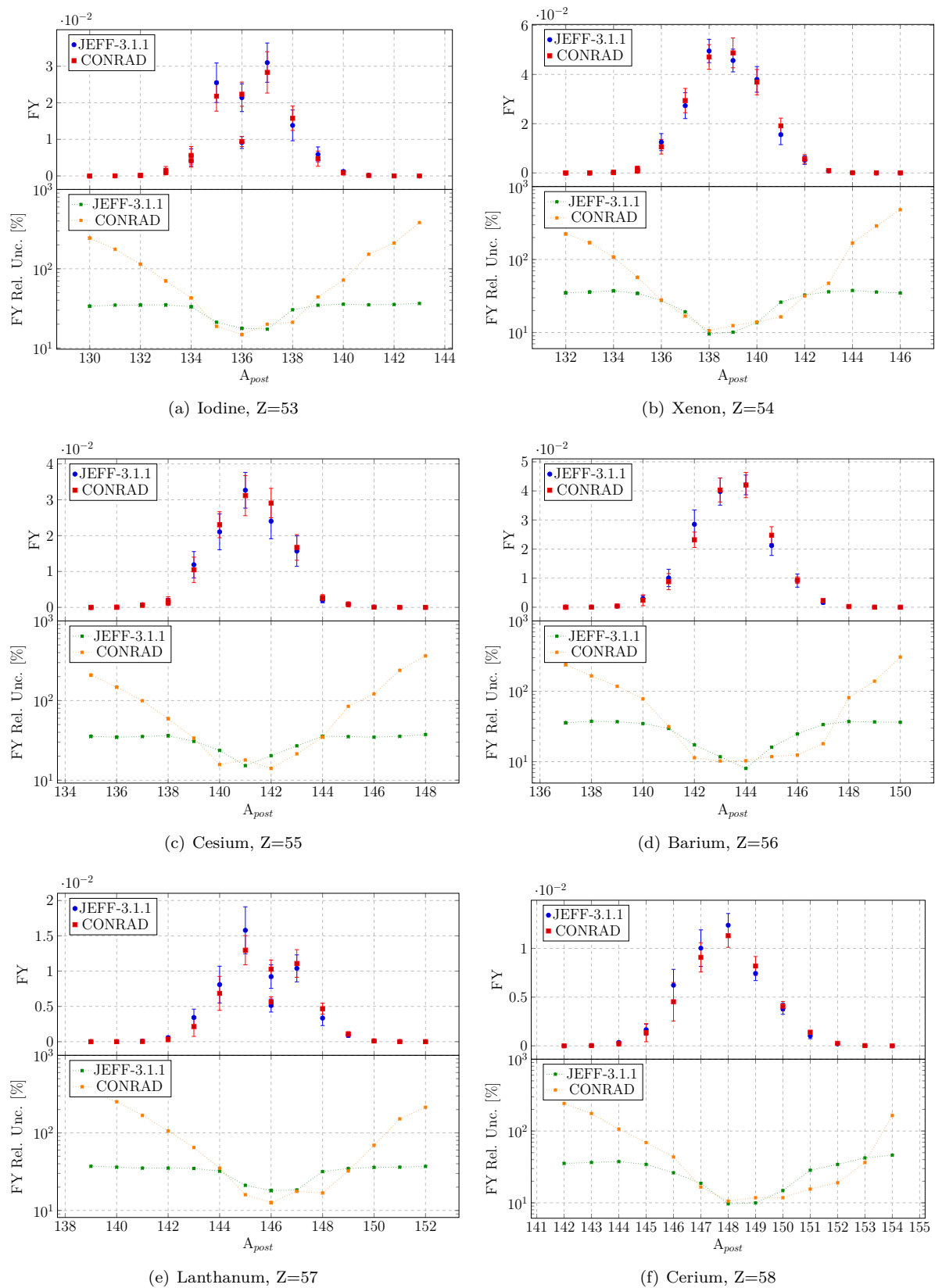


Figure 4.13: Independent isotopic and isomeric FY (top) with their relative uncertainties (bottom) for the thermal fission of ^{235}U , from $Z=53$ up to $Z=58$.

The encouraging aspect of such procedure is its capability to represent completely independent experiments on miscellaneous fission quantities and evaluated FY data at the same time, with a satisfactory degree of accuracy. Different fission measurables are in fact simultaneously reproduced by the models and their physical assumptions are reflected in the correlations we generated, which are showed in Figs. 4.14 and 4.15. Nevertheless, deducing physical meanings in the covariance matrices shown hereinafter is not so straightforward. For the independent mass FY, the anti-correlations between competing fission modes can be detected, as the total correlated regions in the very asymmetric and in the symmetric domains, where the Standard II and the Super Long dominate respectively. The production of two complementary light and heavy fission fragments, induce positive correlations on the second diagonal. For the isotopic independent correlation matrix, understanding the physical and the mathematical reason for the structures we observe is even more difficult. A certain pattern can be detected in the matrix and it has been zoomed in Fig. 4.15. The normalization and the odd-even effect parameters F_Z and F_N are probably responsible for the alternation of correlated and anti-correlated regions.

In Fig. 4.15 the FY related to different fission product isotopes and isomers have been ordered for ascending charge, mass and isomeric state. Therefore the pattern we observe is strictly related to the kind of ordering we choose.

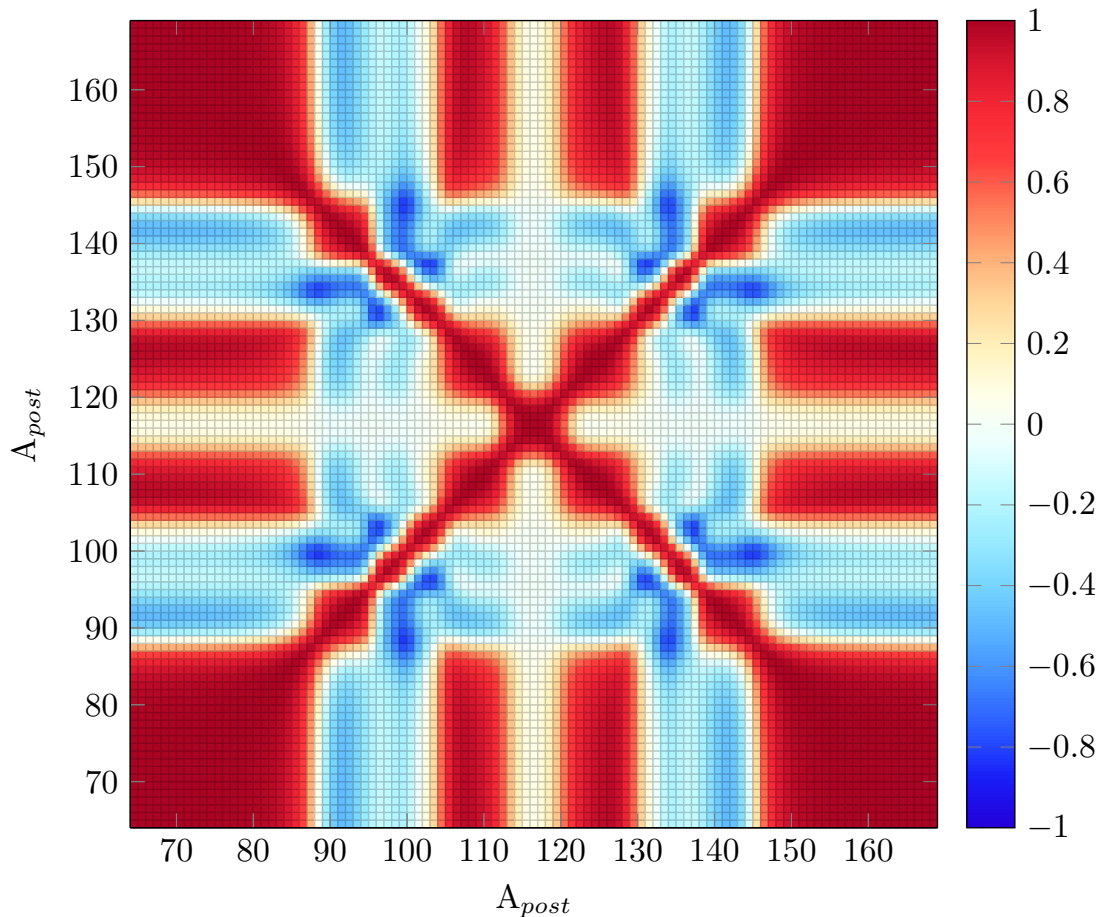


Figure 4.14: Independent mass FY covariance matrix for the thermal fission of ^{235}U .

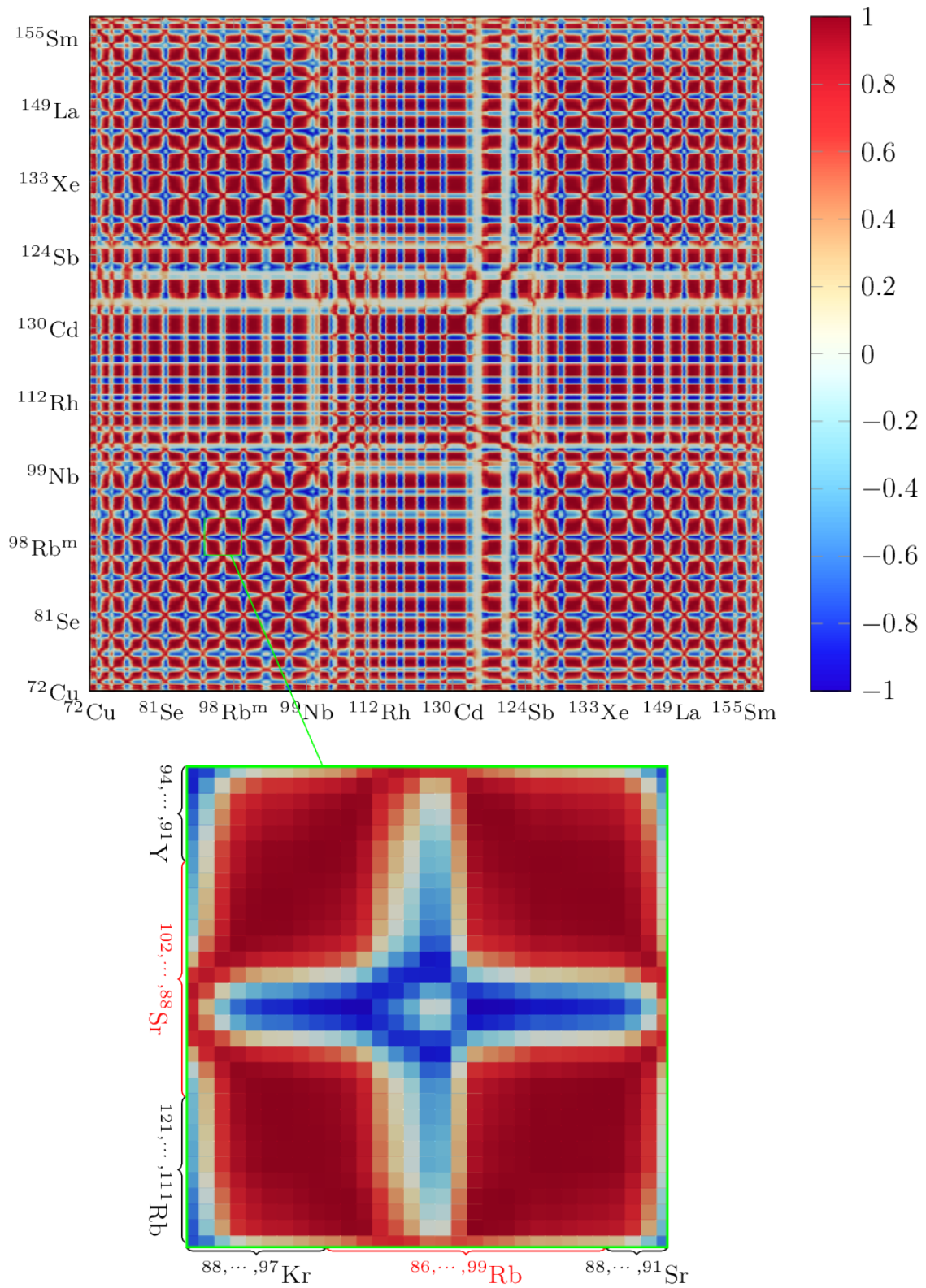


Figure 4.15: Independent isotopic FY covariance matrix for the thermal fission of ^{235}U . Fission yields are ordered in ascending charge, mass and isomeric states. In this case only FY greater than 10^{-7} have been considered.

In Fig. 4.16 the decay heat uncertainty for the elementary thermal neutron induced fission event is presented, considering JEFF-3.1.1 ^{235}U FY. The most significant contributions have been emphasized using different colors, providing the fission products whose independent FY are the most sensitive to the elementary fission decay heat. Sensitivities for the elementary fission have been calculated using the CYRUS code [Benoit, 2012], and are based on direct perturbation calculations as explained in Chapter 5. Let us consider for instance the yield related to ^{137}I and ^{137}Xe , whose sensitivities become relevant starting from 1×10^9 s. The main reason lies on the fact that the decay heat around 10^9 s is significantly generated by the decay of ^{137}Cs ¹⁰. ^{137}Cs belongs obviously to the same decay chain of 137 amu and its cumulative yield is mostly due to the independent ones related to ^{137}I and ^{137}Xe , which are of the order of 10^{-2} .

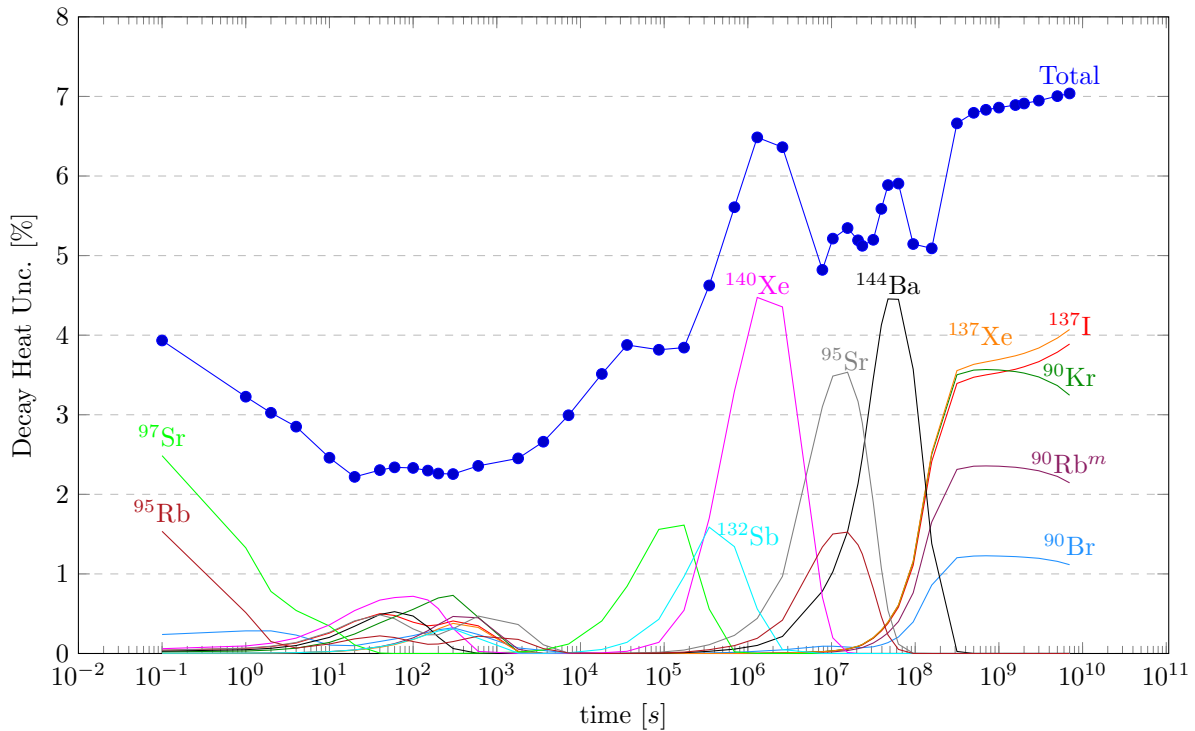


Figure 4.16: Decay heat uncertainty for the elementary thermal neutron induced fission of ^{235}U . The total uncertainty is given by the propagation of JEFF-3.1.1 FY. In the figure, the most significant contributions have been emphasized with different colors.

In Fig. 4.17 the decay heat uncertainty as a function of time for the elementary thermal fission of ^{235}U is presented. The propagation of JEFF-3.1.1 FY uncertainties on the decay heat has been compared to what we obtain from CONRAD-generated FY, with and without including correlations. As said in the introduction of the present section, the main objectives are to reproduce both averages and uncertainties of the JEFF-3.1.1 FY library. Performing elementary fission decay heat uncertainty propagation of FY allowed us to see if CONRAD was actually capable to provide variances in agreement with the existing evaluated data.

As shown in the figure, for the thermal fission of ^{235}U , this seems to be the case. This means that most of the isotopes presented in Fig. 4.16 present uncertainties close to what we can retrieve in JEFF-3.1.1.

¹⁰The half life of ^{137}Cs is around $30\text{ y} = 9.46 \times 10^8\text{ s}$.

Including correlations between FY has as main effect a significant uncertainty reduction, except for the starting phase of the cooling time. In the very first seconds, in fact, the decay heat is mainly characterized by several isotope decays which have evidently correlated independent FY. Having high uncertainty at the beginning of the cooling time is finally quite reasonable, we are very far from the stability line in the nuclide chart, and many contributions participate to the decay heat determination.

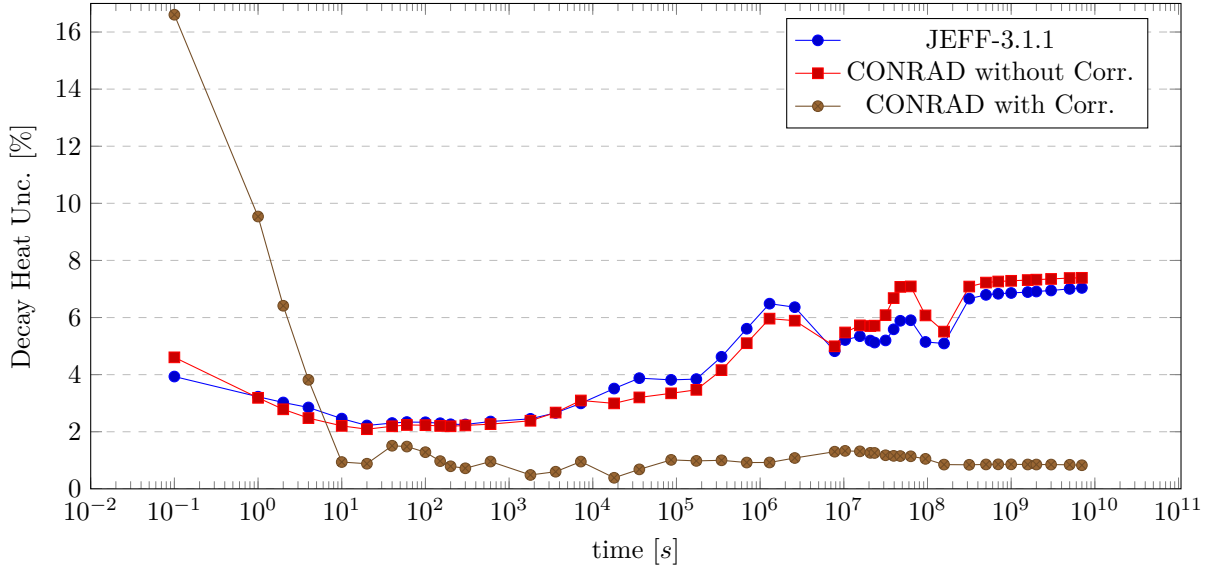


Figure 4.17: Decay heat uncertainty as a function of time for the elementary thermal fission of ^{235}U . The propagation of JEFF-3.1.1 FY uncertainties on the decay heat has been compared to what we obtain from CONRAD-generated FY, with and without including correlations.

Isotope	^{235}U		^{239}Pu		^{241}Pu	
	Cum. Yield	Rel. Unc.	Cum. Yield	Rel. Unc.	Cum. Yield	Rel. Unc.
Sr-92	0.06034	1.1%	0.029988	2.2%	0.022889	5.2%
Rh-103	0.03103	2.7%	0.069481	1.2%	0.065384	4.9%
Cs-133	0.06597	1.6%	0.069948	1.8%	0.066140	2.7%
Cs-137	0.06221	1.1%	0.065881	1.2%	0.062843	2.2%
Ba-140	0.06314	1.5%	0.053220	1.1%	0.057561	1.9%
Ce-143	0.05954	1.4%	0.047550	1.1%	0.043805	2.1%
Nd-148	0.01681	0.7%	0.016583	1.0%	0.018812	3.4%
Sm-151	0.00420	1.7%	0.007757	2.3%	0.008565	28%
Eu-153	0.00148	4.8%	0.003803	7.9%	0.003953	57%

Table 4.4: List of the most significant cumulative FY for applications [Serot et al., 2004a]. The yield values and uncertainties are taken from JEFF-3.1.1 and refer to the thermal fission of ^{235}U , ^{239}Pu and ^{241}Pu .

Once independent FY are calculated, they can be multiplied by the Q-matrix, as explained in Chapter 2, to obtain cumulative yields. Cumulative FY have an important role in nuclear reactor applications. Some of them, such as the cumulative yield of ^{148}Nd , are for instance burn-up indicators, since they do not exhibit a high capture cross section [Suyama and Mochizuki, 2005]. Furthermore, cumulative yields are important in many other applications such as burn-up credit calculations and fission rate normalization

for gamma peak-check experiments. According to Ref. [Serot et al., 2004a], we can list the most relevant cumulative yields for applications (we picked those greater than 10^{-3}), which are provided in Tab. 4.4.

In Fig. 4.18, cumulative FY have been plotted for the isotopes in Tab. 4.4. JEFF-3.1.1 averages and uncertainties are quite well represented by CONRAD calculations. Only for three application-oriented cumulative FY, $C(^{148}\text{Nd})$, $C(^{151}\text{Sm})$ and $C(^{153}\text{Eu})$, discrepancies have been detected on their associated uncertainty (see Tab. 4.5).

Isotope	CFY JEFF-3.1.1	Rel. Unc. JEFF-3.1.1	CFY CONRAD	Rel. Unc. CONRAD
Sr-92	0.06034	1.1%	0.06045	1.3%
Rh-103	0.03103	2.7%	0.03095	2.6%
Cs-133	0.06597	1.6%	0.06522	2.2%
Cs-137	0.06221	1.1%	0.06224	1.5%
Ba-140	0.06314	1.5%	0.06316	1.3%
Ce-143	0.05954	1.4%	0.05997	1.2%
Nd-148	0.01681	0.7%	0.01678	2.5%
Sm-151	0.00420	1.7%	0.00412	5.5%
Eu-153	0.00148	4.8%	0.00134	8.3%

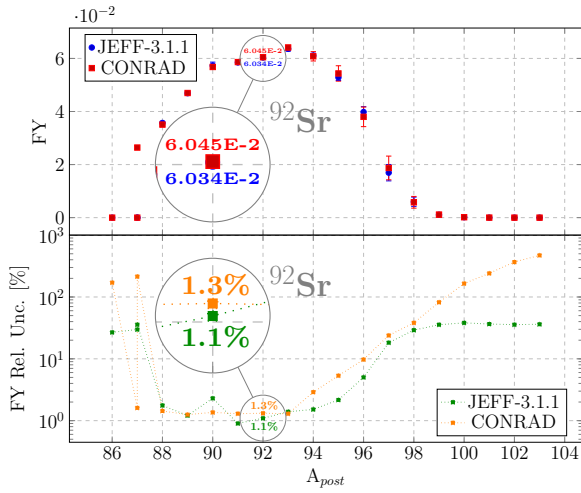
Table 4.5: List of the most significant cumulative FY for applications [Serot et al., 2004a]. The values are referring to the thermal fission of ^{235}U . Under-estimated uncertainties have represented in blue, while in red we show the over-estimations. Average values are instead quite well reproduced.

It has to be emphasized that, as already mentioned in Sec. 4.1, some cumulative FY present uncertainties which are not compatible to what we find for independent FY. Accurate and reliable chain and cumulative FY measurements are in fact available, and probably they have been used to reduce uncertainty on JEFF-3.1.1 cumulative yields (such as $C(^{148}\text{Nd})$), without being included in the independent yield evaluation, which instead reflects properly the experimental data available on post-neutron yields.

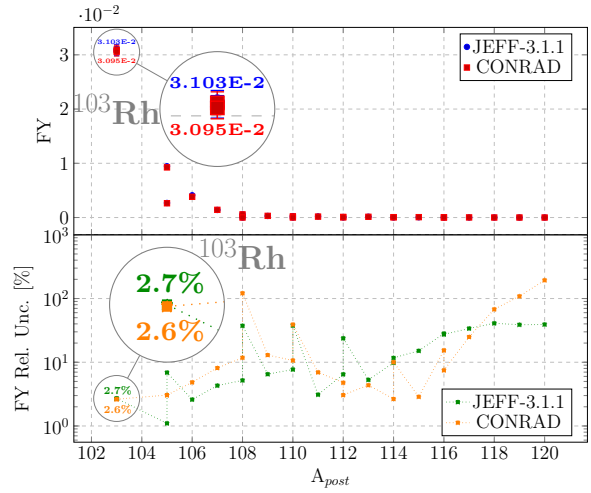
For JEFF-3.1.1 the evaluator has in fact decided to perform two separate evaluations that reproduce independently the respective experimental data, without introducing any correlations. For application purposes, correlations are necessary to quantify properly the uncertainty on integral reactor parameters. Such correlations must also build the link between independent and cumulative yield uncertainties, preserving the already existing both independent and cumulative variance information.

If we look at Tab. 4.6, it is clear that uncertainty of the order of 0.8% on the cumulative ^{148}Ce yield cannot be achieved by the uncertainty propagation of independent yields related to the parent isotopes in the 148-decay chain. As shown in Fig. 4.19, the β^- -decay is prevalent, and the most significant contribution to ^{148}Ce cumulative yield is due to its own independent, provided with an uncertainty of 10%, which surely cannot produce a final 0.8%.

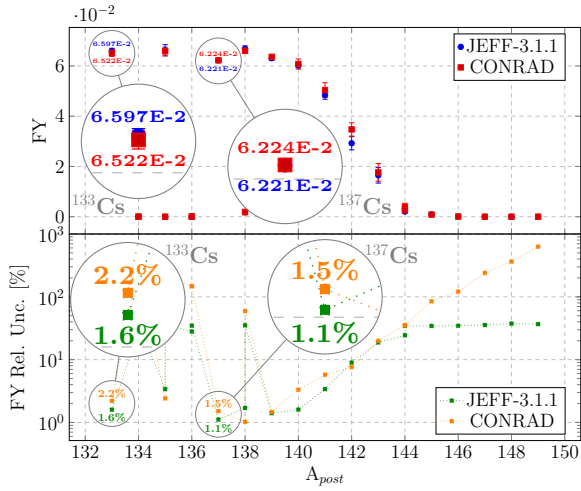
A possible solution to such problem, in order to provide covariances which are fully consistent with the JEFF-3.1.1 evaluation, could be the direct adjustment of independent yields according to cumulative data as also done in Ref. [Fiorito et al., 2016]. The independent yields can be in fact seen as correlated parameters and adjusted through a GLS procedure, to correct discrepancies.



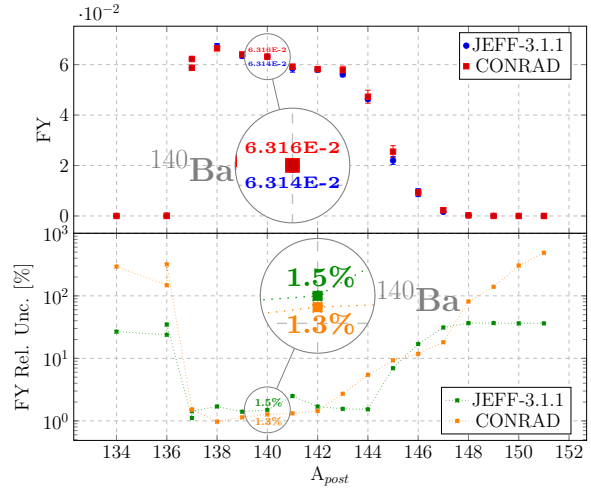
(a) Strontium, Z=38



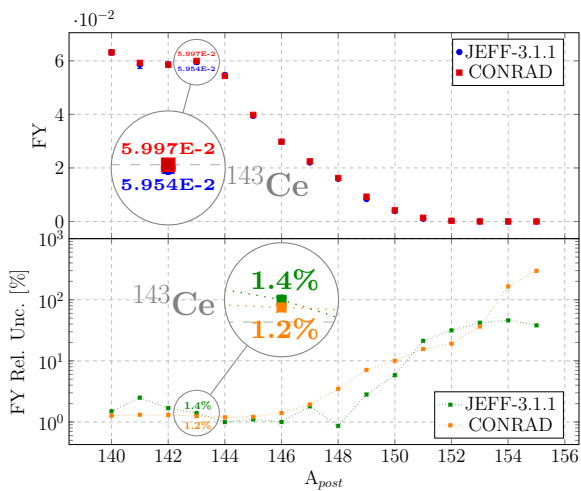
(b) Rhodium, Z=45



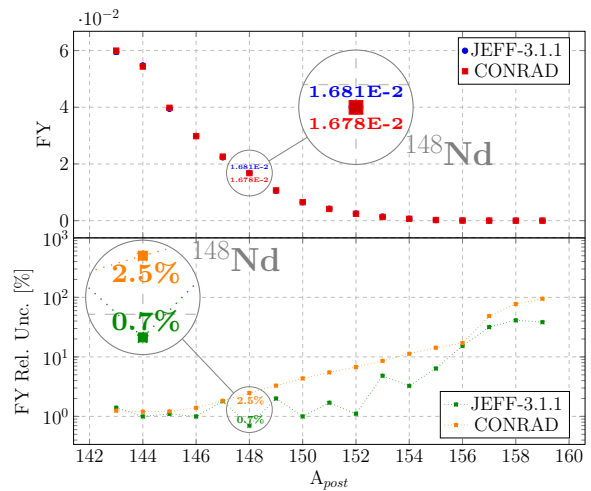
(c) Cesium, Z=55



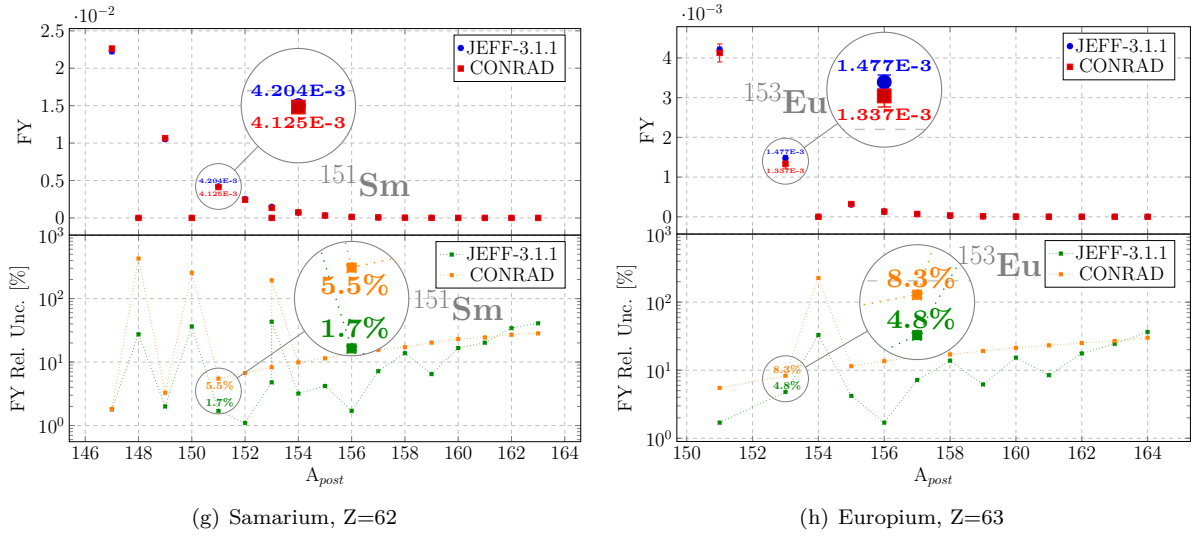
(d) Barium, Z=56



(e) Cerium, Z=58



(f) Neodmium, Z=60


 Figure 4.18: Cumulative FY for the thermal fission of ^{235}U .

Isotope	Independent Yield	Relative Unc.	Cumulative Yield	Relative Unc.
Cs-148	1.5827e-7	37%	1.5827e-7	37%
Ba-148	2.1441e-4	37%	2.1456e-4	37%
La-148	0.003344	32%	0.003558	23%
Ce-148	0.01238	10%	0.015951	0.8%
Pr-148	1.6257e-4	35%	0.016144	0.8%
Nd-148	1.0961e-5	37%	0.016808	0.7%

 Table 4.6: Example of cumulative-independent uncertainty inconsistency in JEFF-3.1.1 FY library. The cumulative yield for ^{148}Ce is mostly due to its independent yield, which decays β^- two times. The uncertainty on ^{148}Ce independent yield of 10% does not reflect the final accuracy of 0.8% we have on the cumulative, which should be instead of the order of 9%.

Promising results were obtained for ^{148}Nd , which is an important burn-up monitor, returning a perfect correspondence between CONRAD and JEFF-3.1.1 uncertainties. CONRAD independent yields, provided with the covariances shown so far, were taken as adjustable parameters, but only those with masses equal to $(148 \pm 2)\text{amu}$ were actually fitted. The GLSM has been applied using JEFF-3.1.1 $C(^{148}\text{Nd})$ as an experimental data point and the Q-matrix as theoretical model. The CONRAD ^{148}Nd uncertainty, which previously was of 2.5%, became 0.7% as in JEFF-3.1.1. No significant variations were observed in the relative uncertainties. The most important one set in for the independent yield of ^{148}Ce , that from 10.6% decreased to 10.2%. An interesting result was a diffused slight modification of the final independent yields correlation matrix. No significant deviations from the previous matrix were observed, however, the combination of such results induced an impressive uncertainty reduction of ^{148}Nd uncertainty. Such methodology turned out to be then a powerful tool to obtain the right uncertainty on application sensitive cumulative FY, and it can be certainly applied to solve differences between CONRAD and JEFF for the most significant fissioning systems for applications.

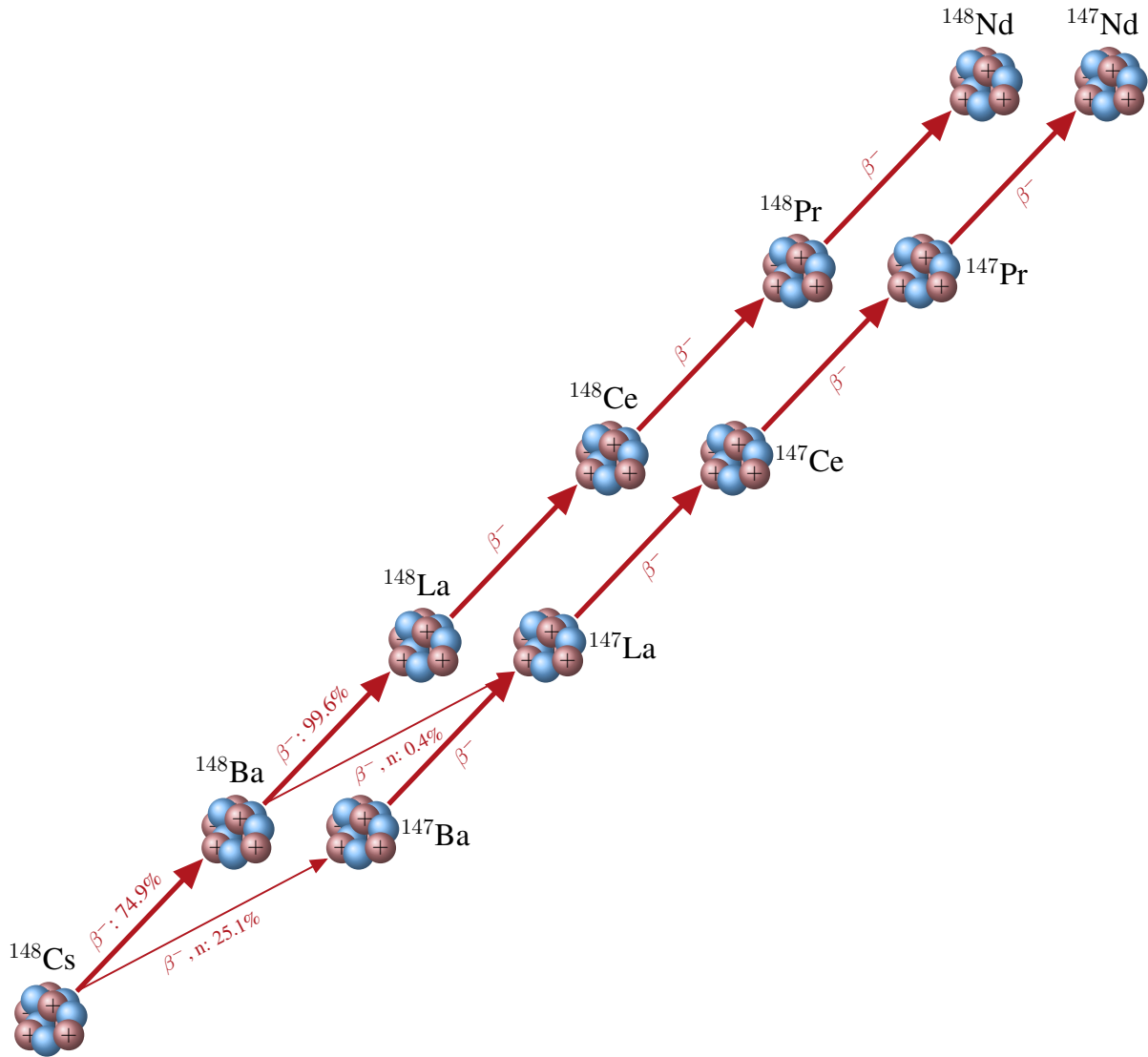


Figure 4.19: Decay scheme for isotopes with mass equal to 148, giving ^{148}Nd .

4.4 Pu-239 Thermal Fission

Let us now continue with the thermal fission of ^{239}Pu . The procedure we adopted was almost the same we showed for ^{235}U and it will not be repeated. Only the final results we got from CONRAD calculations will be presented.

For the Brosa fission mode parameters, prior values were retrieved from Ref. [Dematté, 1996], assigning the same relative prior uncertainties we saw so far, for the previous fissioning system. Priors and adjusted values are provided in Tab. 4.7, recalling that posterior uncertainties are given after performing the analytical marginalization. The table shows as no significant modifications of the priors has occurred during the GLS adjustment. As we found for $^{235}\text{U}(n_{th}, f)$, only the posterior Standard I weight turned out to be significantly enhanced. A non-negligible variation has been observed also for the position of the Standard fission modes in the mass domain, a 1-*amu* shift is in fact given by CONRAD comparing to the literature.

Parameter	Prior BE	Prior Unc. [%]	Posterior BE	Posterior Unc. [%]
$D_{St.I}^*$	14.97	5	16.56	0.7
$D_{St.II}^*$	20.96	5	21.82	1.3
$\sigma_{St.I}^*$	3.73	10	3.30	3.2
$\sigma_{St.II}^*$	6.48	10	6.05	3.1
σ_{SL}^*	15.8	10	10.75	8.4
$N_{St.I}$	0.248	10	0.363	8.8
N_{SL}	0.005	20	0.007	13.1

* Expressed in [amu].

Table 4.7: Fission mode parameters best estimates (BE) and uncertainties before (prior) and after (posterior) the analysis using CONRAD for the thermal fission of ^{239}Pu .

In Tab. 4.8 Wahl and Madland-England model parameters are provided. As priors we picked those related to ^{235}U , since no detailed lists of values have been found in the literature. Posterior averages and uncertainties are also given. In this case, since we do not have any term of comparison, no conclusions can be drawn on the results we got from CONRAD.

Parameter	Prior BE	Prior Unc. [%]	Posterior BE	Posterior Unc. [%]
$\sigma_Z(140)$	0.566	20	0.461	26.1
$\Delta Z(140)$	-0.487	20	-0.536	10.8
σ_{50}	0.356	20	0.525	2.4
$F_N(140)$	1.076	20	1.088	10.7
$F_Z(140)$	1.207	20	1.151	18.9
$SL50$	0.191	20	0.349	0.93
ΔZ_{max}	0.699	20	0.514	1.2
$\sigma_Z SLW$	-0.045	20	-0.057	3.5
$\Delta Z SLW$	0.0049	20	-0.0043	14.6
$F_Z SLW$	0.039	20	0.086	18.6
$F_N SLW$	0.159	20	1.498	8.8
J_{rms}^L	7.5	10	7.57	0.6
J_{rms}^H	7.5	10	7.45	1.4

Table 4.8: Wahl and Madland-England parameters best estimates (BE) and uncertainties before (prior) and after (posterior) the analysis using CONRAD, for the thermal fission of ^{239}Pu .

The only possibility we had to check the quality of our calculations is observing the mass and isotopic independent FY data representation. In Figs. 4.20 and 4.21 CONRAD calculated mass FY are compared to JEFF-3.1.1. As previously seen, no uncertainty information for mass yields are available in JEFF, so they have been retrieved from JANIS-4.0, which performs a simple uncertainty propagation without any correlation.

The adjustment of JEFF-3.1.1 FY data taken as pseudo-experimental values had been performed together with miscellaneous fission quantities files retrieved in the EXFOR database. Fitting the average numbers of prompt neutron emitted by a primary fission fragment and including the prompt neutron emission probability model in present calculations gave us the possibility to obtain a quite satisfactory representation of the most important FY also for the thermal fission of ^{239}Pu .

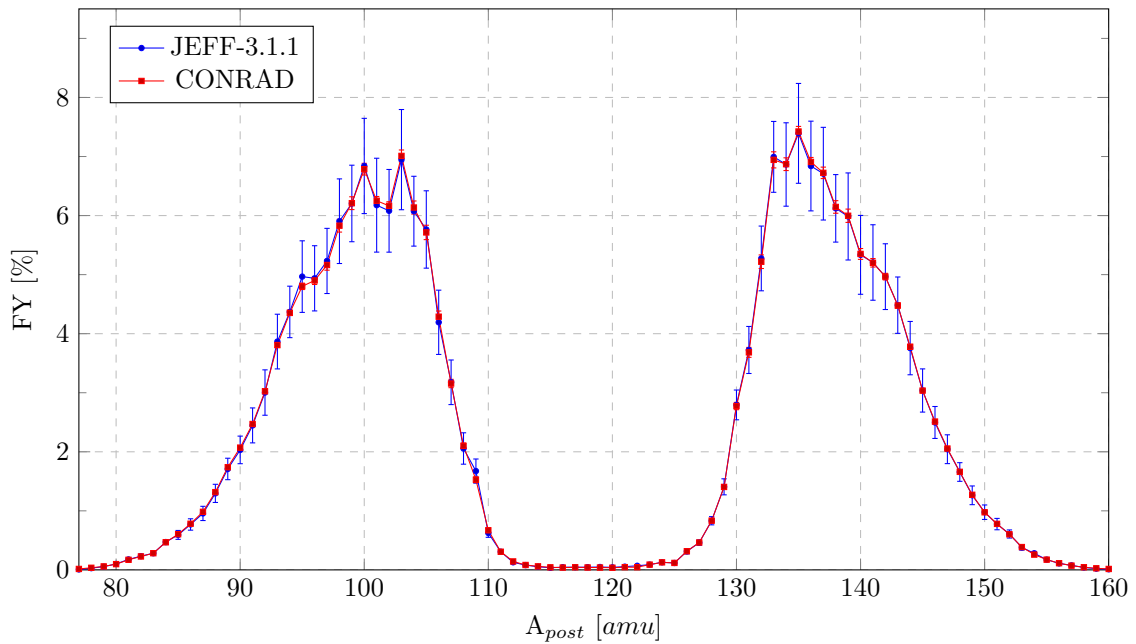


Figure 4.20: Comparison between JEFF-3.1.1 and CONRAD independent mass FY for the thermal fission of ^{239}Pu in linear scale. FY model parameters have been adjusted using CONRAD to reproduce the JEFF-3.1.1 evaluated library and generate covariances. The convolution between the pre-neutron model based on Brosa fission modes and the saw-tooth curve allows a satisfactory representation of the available FY data.

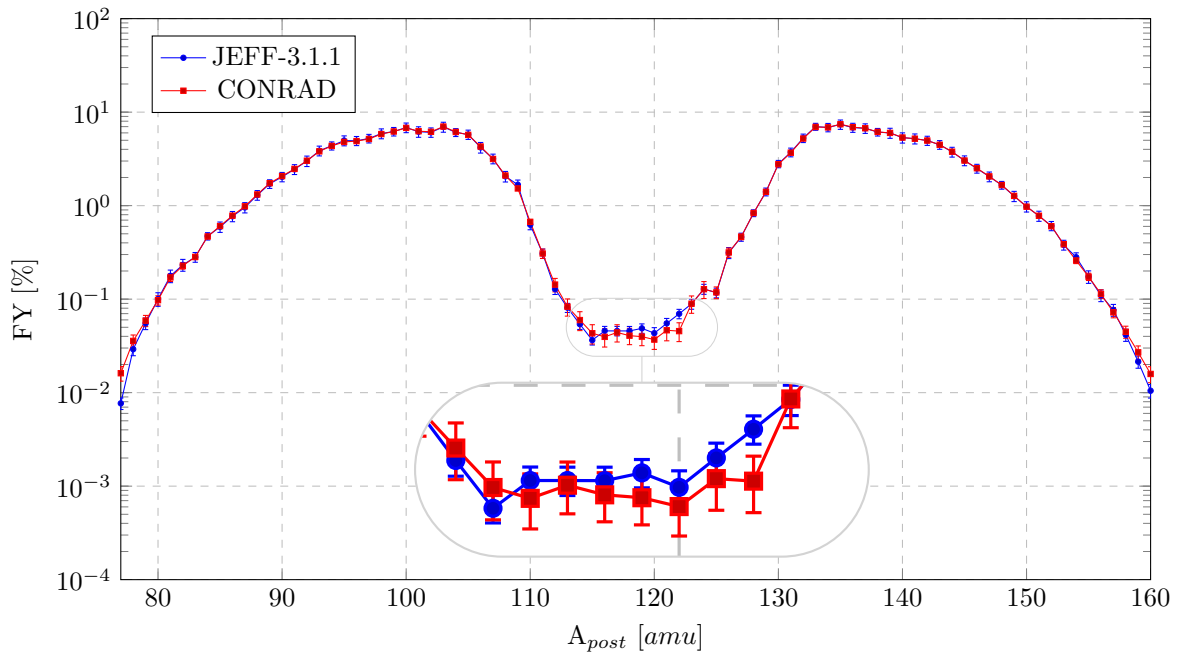


Figure 4.21: Comparison between JEFF-3.1.1 and CONRAD independent mass FY for the thermal fission of ^{239}Pu in logarithmic scale. FY model parameters have been adjusted using CONRAD to reproduce the JEFF-3.1.1 evaluated library and generate parameters covariances. The convolution between the pre-neutron model based on Brosa fission modes and the saw-tooth curve allows a satisfactory representation of the available FY data even in the symmetry region.

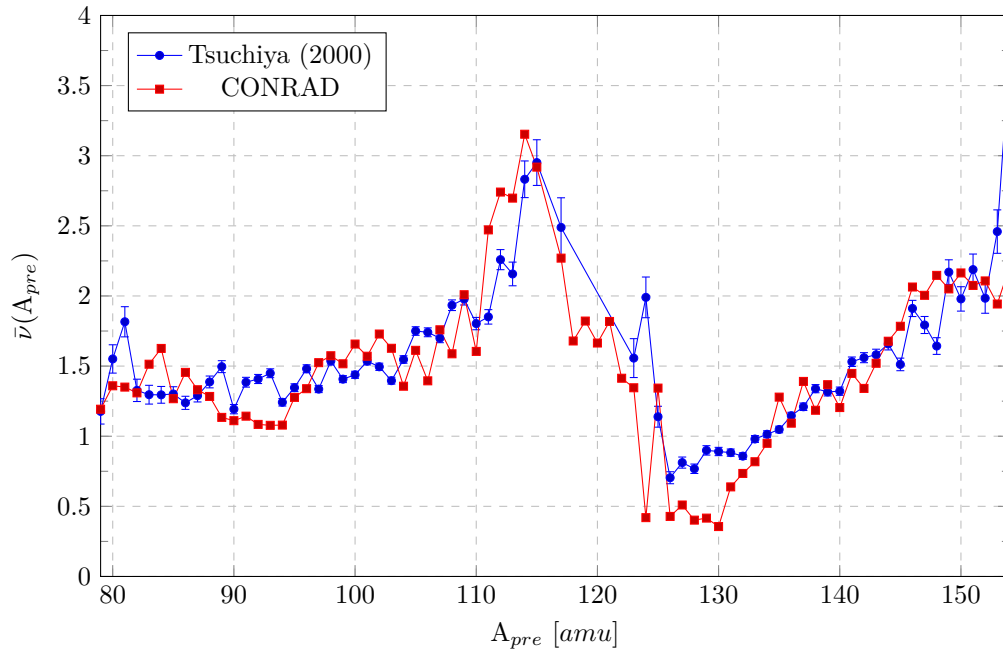


Figure 4.22: Comparison between experimental (from Tsuchiya [Tsuchiya et al., 2000]) and CONRAD-adjusted average number of prompt neutrons emitted as function of the pre-neutron fragment mass for the thermal fission of ^{239}Pu .

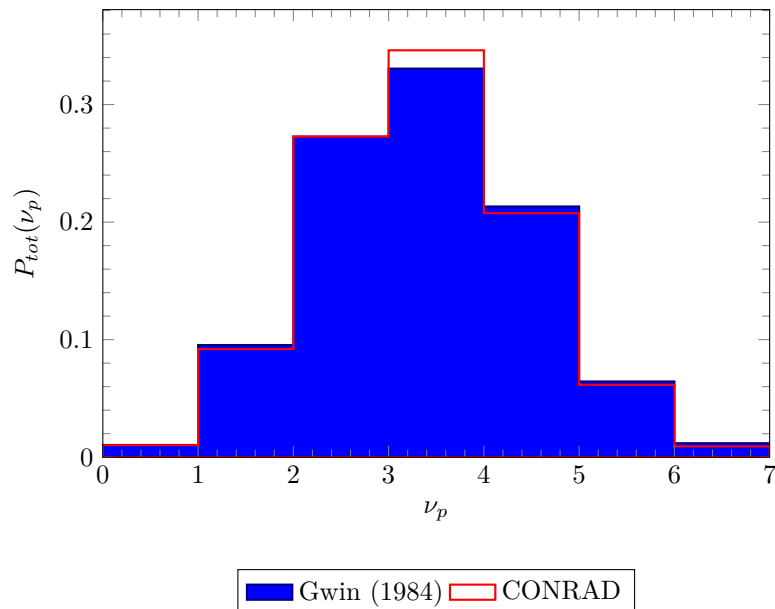


Figure 4.23: Comparison between experimental (from Gwin [Gwin et al., 1984]) and CONRAD-evaluated total prompt neutron emission probabilities, $P_{tot}(\nu_p)$ for the thermal fission of ^{239}Pu . It provides the probability that a certain number of prompt neutrons are globally emitted by the fissioning system.

In Fig. 4.22, the comparison between the experimental saw-tooth curve provided by Tsuchiya¹¹ (see Ref. [Tsuchiya et al., 2000]) and the values calculated by CONRAD is provided. For the thermal fission of ^{239}Pu , significant deviations from the experimental data came up¹². The average number of prompt neutrons emitted by primary fragments are responsible for the asymmetries we find in the mass yield distribution. To represent JEFF-3.1.1 with the available models, such saw-tooth deviations became necessary. It has to be emphasized, by the way, that the saw-tooth experimental data are unfortunately characterized by difficult measurement conditions, and different data sets present relevant discrepancies, especially for $^{239}\text{Pu}(n_{th}, f)$ system. If we look for example at the experimental data available for such fissioning system in Fig. 4.24, it is clear that the knowledge we can infer from measurements is affected by large uncertainty.

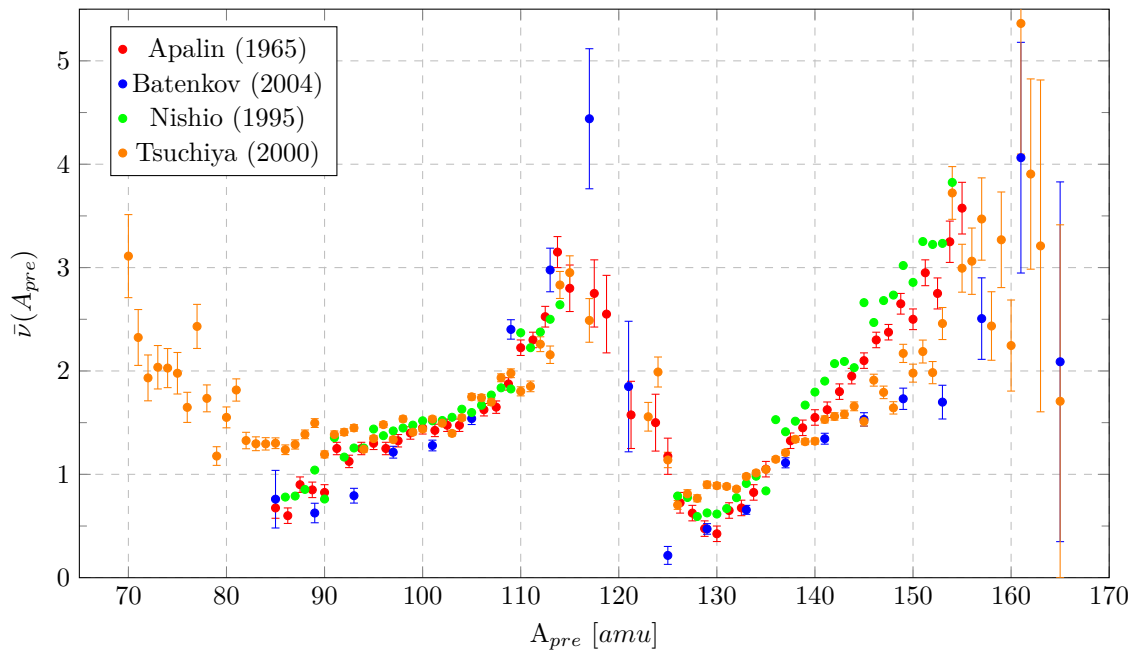


Figure 4.24: Average number of prompt neutron emitted by a fission fragment of mass A_{pre} for the thermal neutron-induced fission of ^{239}Pu , from different experiments (Refs. [Apalin et al., 1965, Nishio et al., 1995, Tsuchiya et al., 2000, Batenkov et al., 2004]).

Seeing how CONRAD is able to represent JEFF-3.1.1, to preserve a saw-tooth trend for the average number of prompt neutrons emitted and to represent nicely experimental data on the total probability $P(\nu)$, as shown in Fig. 4.23, made us to be quite confident on our methodology to generate consistently physics-based covariance matrices for FY. Furthermore the total $\bar{\nu}_P$ multiplicity was respected. A value of 2.87 for the average number of prompt neutrons emitted was obtained, in agreement with both evaluated and experimental data.

The correlation matrices for mass and isotopic independent yields are shown in Figs. 4.25 and 4.26. For mass FY, the competition of the three fission modes can be distinguished. For the isotopic matrix the repetition of a quite regular pattern suggests that it is probably due to the normalization of the isotopic distribution which produces the alternation of highly correlated and anti-correlated regions.

¹¹We chose Tsuchiya's data set because it was the most complete, covering almost the whole mass domain.

¹²The reduced χ^2 is equal to 36, however discrepancies between different experimental data exist and, furthermore, probably under-estimated variances are provided by Tsuchiya, including only the statistical component.

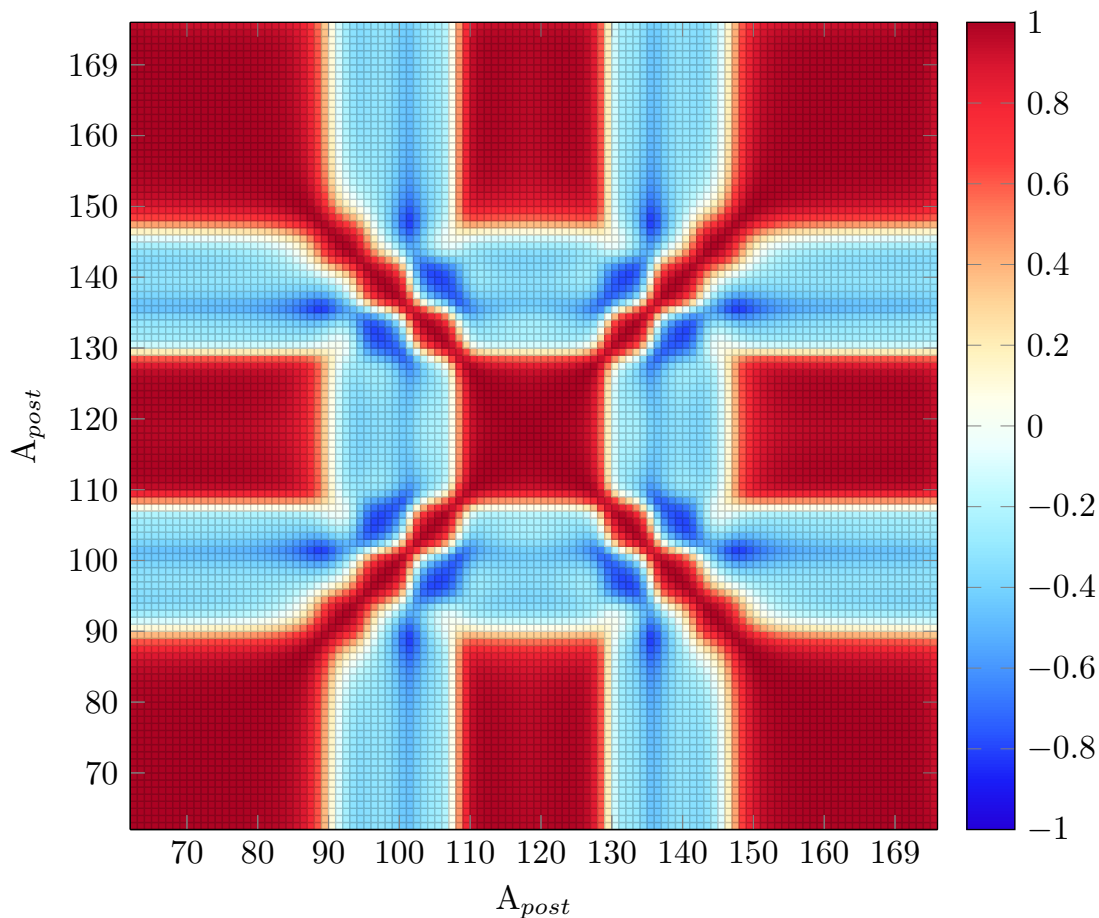


Figure 4.25: Independent mass FY covariance matrix for the thermal fission of ^{239}Pu .

Even for ^{239}Pu we found some difficulties to reproduce JEFF-3.1.1 uncertainties in our calculation. In the marginalization process, we assigned 26.5% and 16.5% of uncertainty to the norm of Tellurium and Iodine isotopic distributions respectively. As previously seen, the rigorous propagation of the model parameter covariance matrix allows a satisfactory representation of the uncertainty related to the most significant yields ($\geq 10^{-2}$), providing on the other hand over-estimated values for lower yields.

We repeated the exercise of evaluating the decay heat uncertainty due to an elementary fission event for the thermal fission of ^{239}Pu (see the results in Fig. 4.27). CONRAD-calculated uncertainties are quite in agreement with JEFF-3.1.1 and the impact of correlations is similar to what we obtained for the thermal fission of ^{235}U . As it will be clearer in Chapter 6, this procedure allowed us to represent both the averages and the uncertainty of the most sensitive yields for the nuclear reactor applications we considered in the present dissertation, giving us some feeling on the reliability of the covariance results we produced.

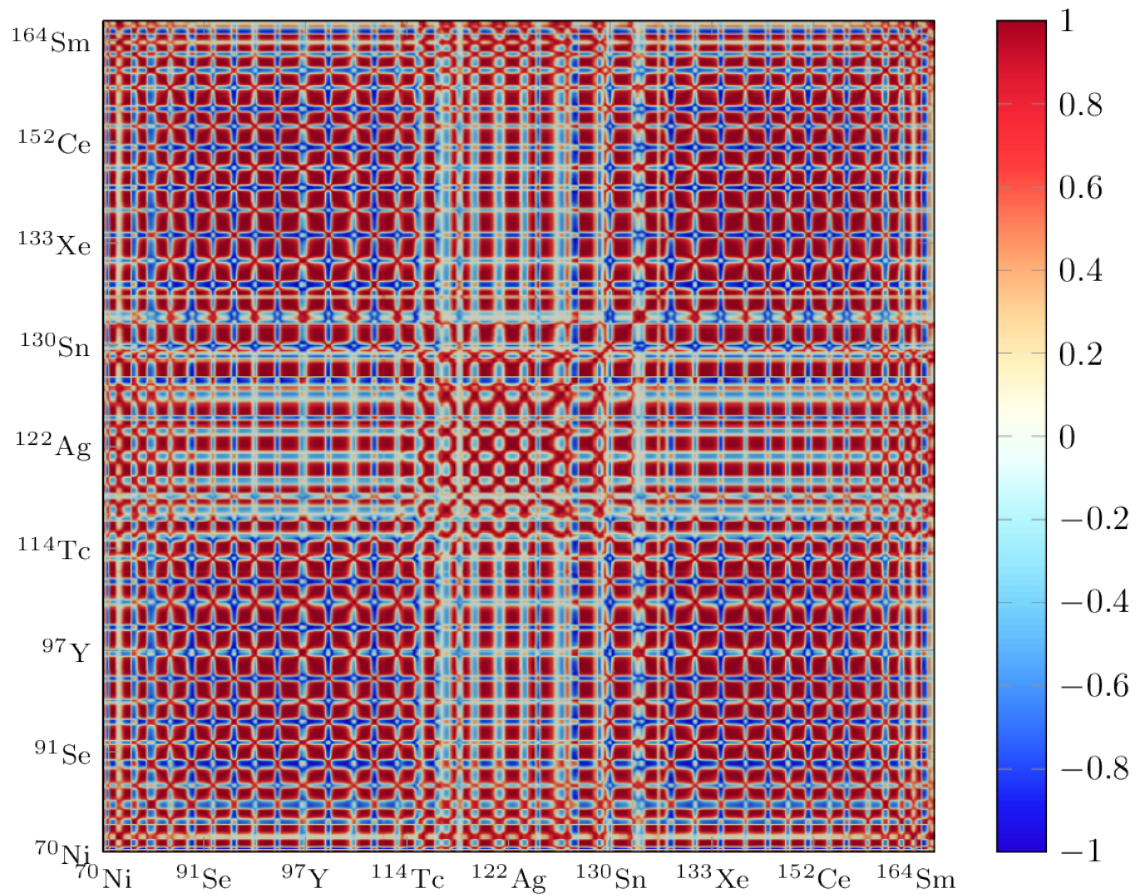


Figure 4.26: Independent isotopic FY covariance matrix for the thermal fission of ^{239}Pu . Fission yields are ordered in ascending charge, mass and isomeric states. In this case only FY greater than 10^{-7} have been considered.

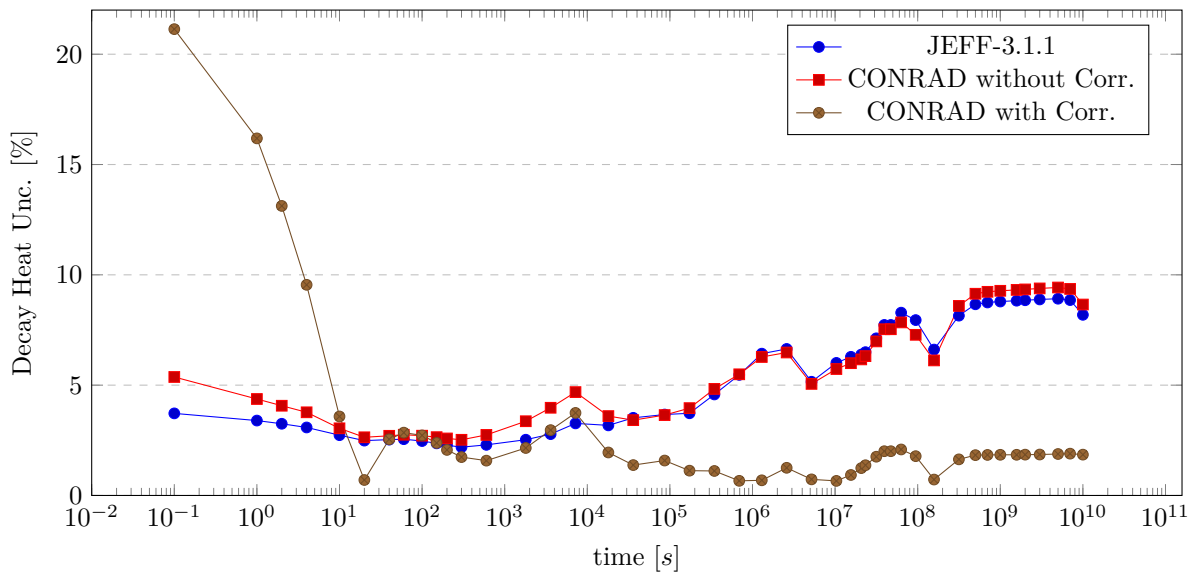


Figure 4.27: Decay heat uncertainty as a function of time for the elementary thermal fission of ^{239}Pu . The propagation of JEFF-3.1.1 FY uncertainties on the decay heat has been compared to what we obtain from CONRAD-generated FY, with and without including correlations.

Cumulative FY calculations can be performed once the parameters for independent FY are known and the Q-matrix has been built. Without presenting all the results, even for ^{239}Pu , we obtained a quite good agreement with the evaluation. Concerning the most important cumulative yields for applications, in Tab. 4.9 both averages and uncertainties have been listed for JEFF-3.1.1 and CONRAD.

Isotope	CFY JEFF-3.1.1	Rel. Unc. JEFF-3.1.1	CFY CONRAD	Rel. Unc. CONRAD
Sr-92	0.029988	2.2%	0.030334	1.2%
Rh-103	0.069481	1.2%	0.070111	1.4%
Cs-133	0.069948	1.8%	0.069440	1.9%
Cs-137	0.065881	1.2%	0.062294	1.4%
Ba-140	0.053220	1.1%	0.053410	1.7%
Ce-143	0.047550	1.1%	0.047080	1.0%
Nd-148	0.016583	1.0%	0.016609	1.5%
Sm-151	0.007757	2.3%	0.007795	3.6%
Eu-153	0.003803	7.9%	0.003866	5.9%

Table 4.9: List of the most significant cumulative FY for applications [Serot et al., 2004a]. The values are referring to the thermal fission of ^{239}Pu . Under-estimated uncertainties have represented in blue, while in red we show the over-estimations. Average values are instead quite well reproduced.

As it can be read in the table, averages present particularly good results. Some under-estimations have been observed for $C(^{92}\text{Sr})$ and $C(^{153}\text{Eu})$ (in blue in Tab. 4.9). Viceversa, over-estimations have been obtained for $C(^{140}\text{Ba})$ and $C(^{151}\text{Sm})$ (in red in the table). For the thermal fission of ^{239}Pu , acceptable results have been obtained for the cumulative yield of ^{148}Nd , which is an important burn-up indicator.

4.5 Pu-241 Thermal Fission

As next fissioning system we treat the thermal fission of ^{241}Pu . We adopted the same procedure presented before. JEFF-3.1.1 data have been used as pseudo-experimental data on which we adjusted model parameter values. The hardest difficulty we met in such fissioning system was the absence of an experimental saw-tooth curve, as it will be better explained later on.

Let us start with the Brosa fission mode parameters. In Tab. 4.10 prior and posterior values are presented as usual.

Parameter	Prior BE	Prior Unc. [%]	Posterior BE	Posterior Unc. [%]
$D_{St.I}^*$	13.7	5	15.9	0.7
$D_{St.II}^*$	18.1	5	21.1	0.7
$\sigma_{St.I}^*$	2.5	10	3.6	2.4
$\sigma_{St.II}^*$	5.9	10	6.8	2.0
σ_{SL}^*	15.0	10	18.6	2.5
$N_{St.I}$	0.307	10	0.417	4.3
N_{SL}	0.005	20	0.005	17.2

* Expressed in [amu].

Table 4.10: Fission mode parameters best estimates (BE) and uncertainties before (prior) and after (posterior) the analysis using CONRAD for the thermal fission of ^{241}Pu .

No priors for the thermal neutron induced fission of ^{241}Pu were found in literature for

Brosa fission modes. For this reason we picked $^{242}\text{Pu}(\text{SF})$ values from Ref. [Schillebeeckx et al., 1992]. Significant deviations can be observed in the adjusted parameters. The reliability of such deviations cannot be effectively quantified since no terms of comparison are available at the moment.

The same conclusions can be drawn from Tab. 4.11 for Wahl parameters, where, as priors, we used those related to the thermal neutron induced fission of ^{235}U provided in Ref. [Wahl, 2000].

Parameter	Prior BE	Prior Unc. [%]	Posterior BE	Posterior Unc. [%]
$\sigma_Z(140)$	0.566	20	0.42772	27.3
$\Delta Z(140)$	-0.487	20	-0.54682	6.2
σ_{50}	0.356	20	0.37634	2.0
$F_N(140)$	1.076	20	0.90814	13.6
$F_Z(140)$	1.207	20	1.1886	19.3
$SL50$	0.191	20	0.2918	5.4
ΔZ_{max}	0.699	20	0.50533	0.8
$\sigma_Z SLW$	-0.045	20	1.1268	1.5
$\Delta Z SLW$	0.0049	20	0.0014324	20.0
$F_Z SLW$	0.039	20	0.14725	12.0
$F_N SLW$	0.159	20	-0.23086	1.3
J_{rms}^L	7.5	10	7.5163	1.0
J_{rms}^H	7.5	10	7.5826	1.0

Table 4.11: Wahl and Madland-England parameters best estimates (BE) and uncertainties before (prior) and after (posterior) the analysis using CONRAD, for the thermal fission of ^{241}Pu .

In Figs. 4.28 and 4.29, independent mass FY are plotted performing a comparison between JEFF-3.1.1 and CONRAD data. Even in the present case, a good agreement has been found for the most significant FY, greater than 10^{-2} .

The saw-tooth adjustment has been performed starting from experimental values obtained by Tsuchiya for the thermal neutron induced fission of ^{239}Pu [Tsuchiya et al., 2000]. Significant variations can be observed even if unrealistic values are not provided by CONRAD. The quite high value for mass 113 can be, in fact, considered plausible if we look, for instance, at the experimental data obtained by Batenkov for the saw-tooth related to $^{239}\text{Pu}(n_{th}, f)$, given in Fig. 4.24.

A satisfactory agreement with the experimental data provided by Gwin for the thermal fission of ^{241}Pu (see Ref. [Gwin et al., 1984] and Fig. 4.31) has been obtained calculating the total prompt neutron emission probability with CONRAD¹³. This result was quite encouraging, and gave a little more confidence on the analysis performed for this fissioning system. For the prompt neutron multiplicity $\bar{\nu}_P$ a calculated value of 2.95 turned out to be not so far from evaluated and experimental values which are close to 2.92.

Again, the possibility to obtain physics-based reasonable results on FY and on total independent fission miscellaneous quantities induced us to consider such methodology applicable even for this last fissioning system. The associated covariance matrices for mass and isotopic independent yields are presented in Figs. 4.32 and 4.33, exhibiting the same patterns seen before.

¹³Despite the reduced uncertainty levels for the central values (of the order of magnitude of 1%), an extraordinary agreement was reached with a reduced χ^2 of 1.1.

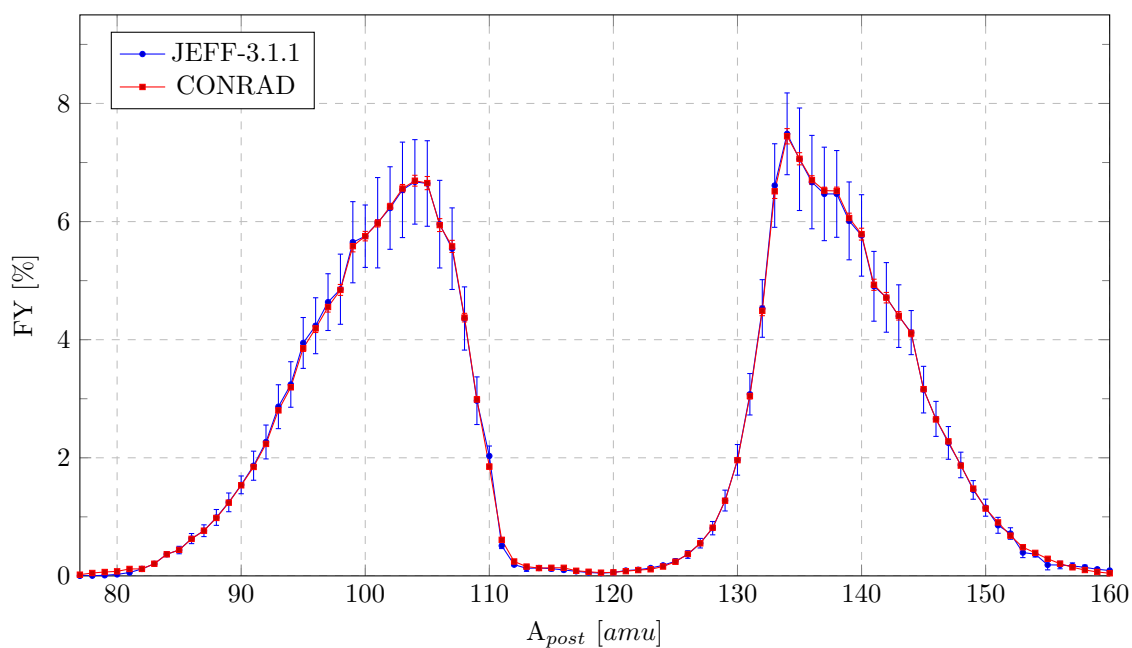


Figure 4.28: Comparison between JEFF-3.1.1 and CONRAD independent mass FY for the thermal fission of ^{241}Pu in linear scale. FY model parameters have been adjusted using CONRAD to reproduce the JEFF-3.1.1 evaluated library and generate covariances. The convolution between the pre-neutron model based on Brosa fission modes and the saw-tooth curve allows a satisfactory representation of the available FY data.

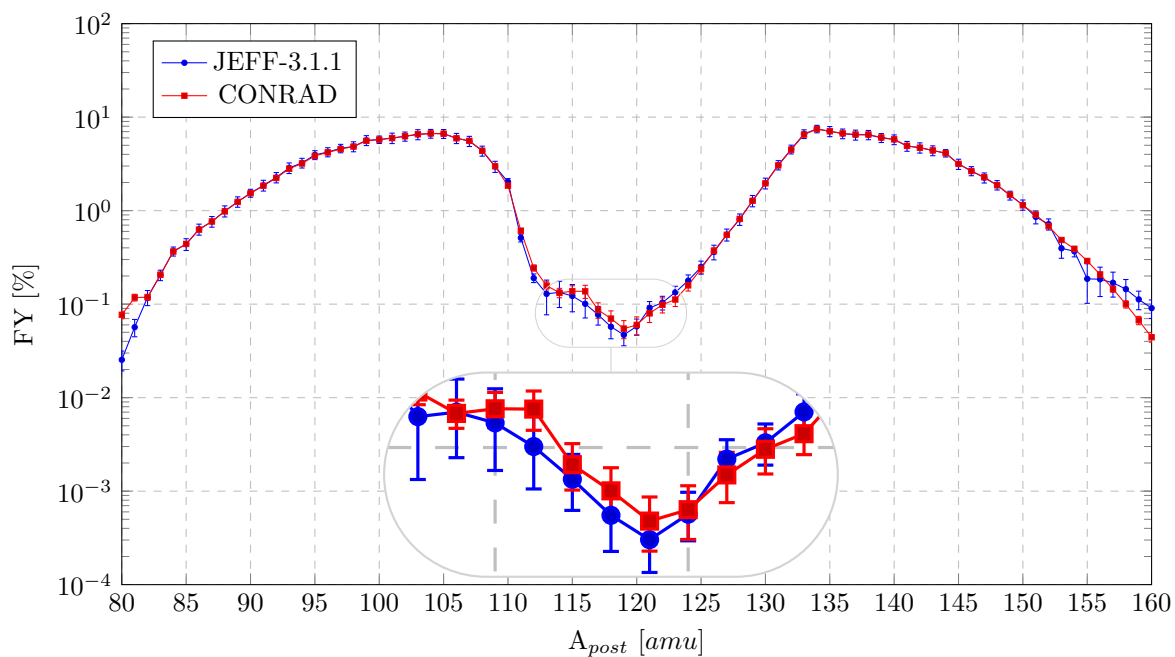


Figure 4.29: Comparison between JEFF-3.1.1 and CONRAD independent mass FY for the thermal fission of ^{241}Pu in logarithmic scale. FY model parameters have been adjusted using CONRAD to reproduce the JEFF-3.1.1 evaluated library and generate covariances. The convolution between the pre-neutron model based on Brosa fission modes and the saw-tooth curve allows a satisfactory representation of the available FY data even in the symmetry region.

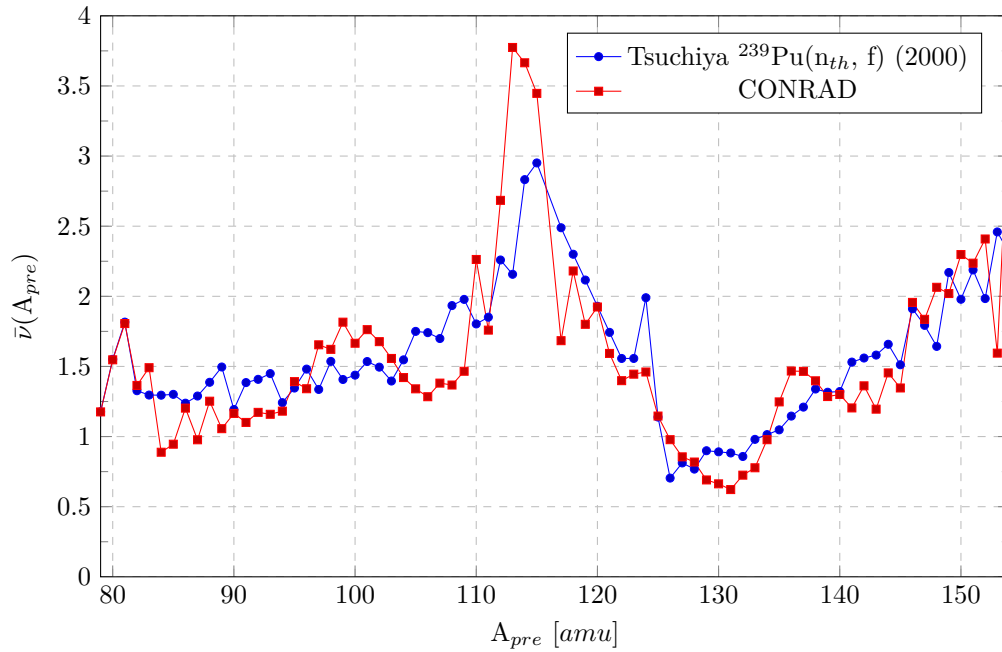


Figure 4.30: Comparison between prior (from Tsuchiya [Tsuchiya et al., 2000] experimental values measured for the thermal fission of ^{239}Pu) and CONRAD-adjusted average number of prompt neutrons emitted as function of the pre-neutron fragment mass, for the thermal fission of ^{241}Pu .

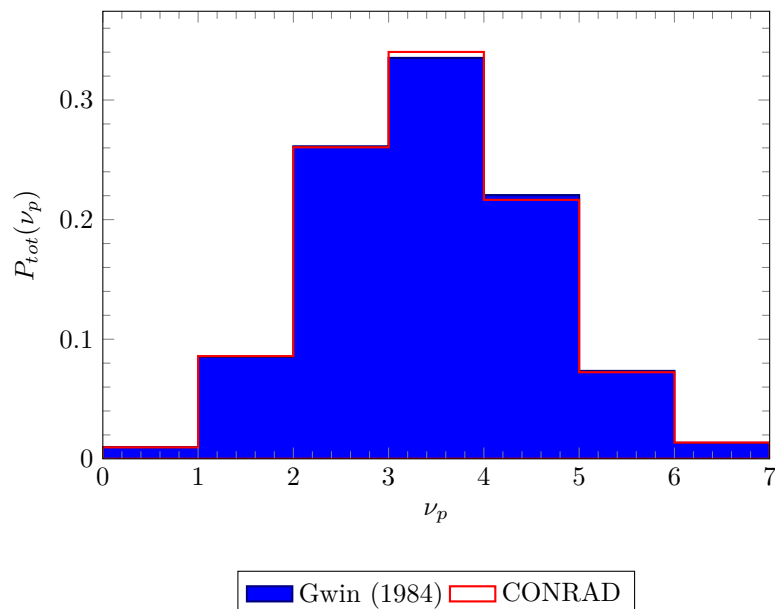


Figure 4.31: Comparison between experimental (from Gwin [Gwin et al., 1984]) and CONRAD-evaluated total prompt neutron emission probabilities, $P_{tot}(\nu_p)$ for the thermal fission of ^{241}Pu . It provides the probability that a certain number of prompt neutrons are globally emitted by the fissioning system.

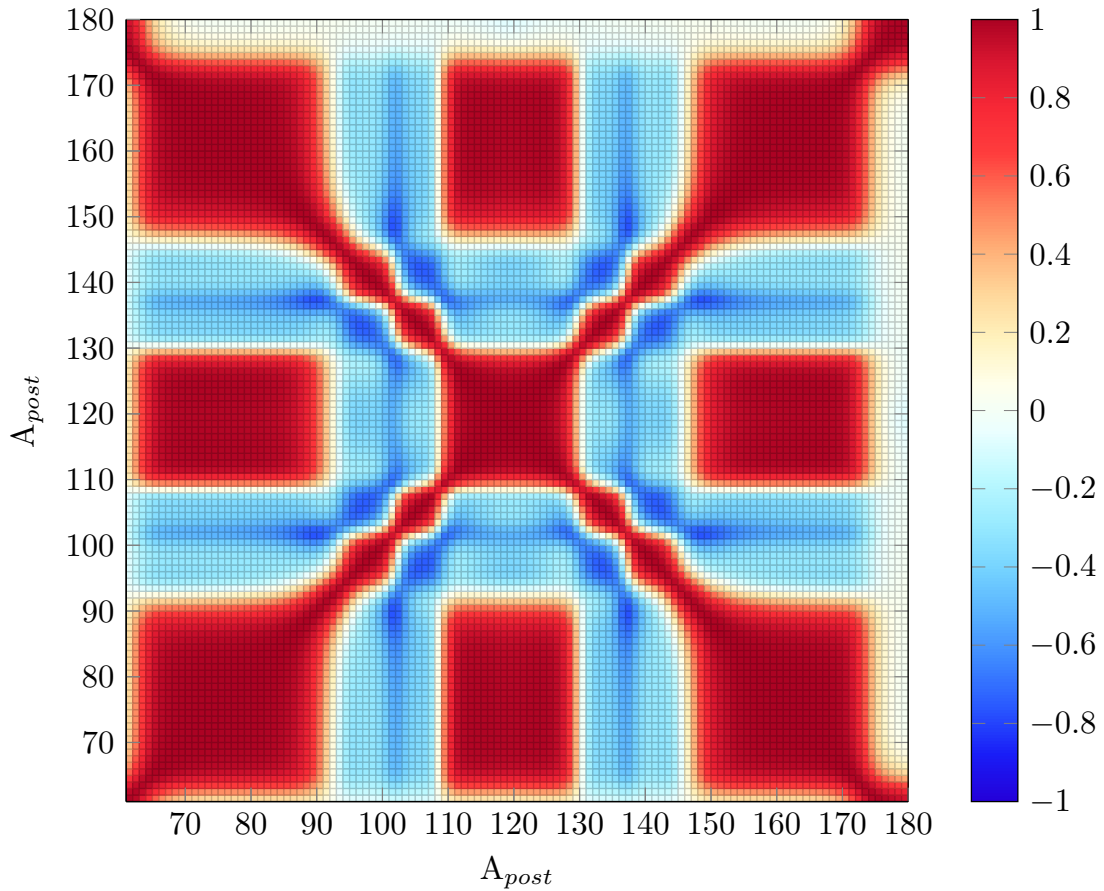


Figure 4.32: Independent mass FY covariance matrix for the thermal fission of ^{241}Pu .

As previously seen for other fissioning systems, the elementary fission calculation was performed also for $^{241}\text{Pu}(n_{th},f)$ to test uncertainties (see Fig. 4.34). We marginalize a 26% and a 19% uncertainty on the norm concerning Iodine and Tellurium distributions respectively. The error bars we obtained allowed us to observe satisfactory results on the elementary fission decay heat, except for very large times ($\sim 10^9$ s).

The reason of such discrepancy for that time interval resides mostly on the uncertainty we obtain from CONRAD for the independent yield of ^{137}I . Similarly to what we observed for the elementary fission of ^{235}U ; ^{137}I , ^{137}Xe , ^{90}Kr and ^{90m}Rb are the fission products with the most sensitive independent yield to the decay heat calculation for large times. While for ^{137}Xe , ^{90}Kr and ^{90m}Rb , CONRAD uncertainties are very close to those evaluated in JEFF-3.1.1, this is not the case for $Y(^{137}\text{I})$. For ^{137}I we have a JEFF-3.1.1 independent FY uncertainty of 14.4%, considerably lower than the value of 23.9% obtained with CONRAD. This can be taken as explanatory example of how hard was to represent uncertainties for JEFF-3.1.1 using model parameters and rigorous Bayesian techniques.

Once independent yield parameters are evaluated, we can proceed with the usual cumulative yields calculation. Even in this case, which has quite relevant implications on existing applications, we looked at the most significant cumulative FY for practical purposes. In Tab. 4.12 averages and uncertainties are provided for the present fissioning system.

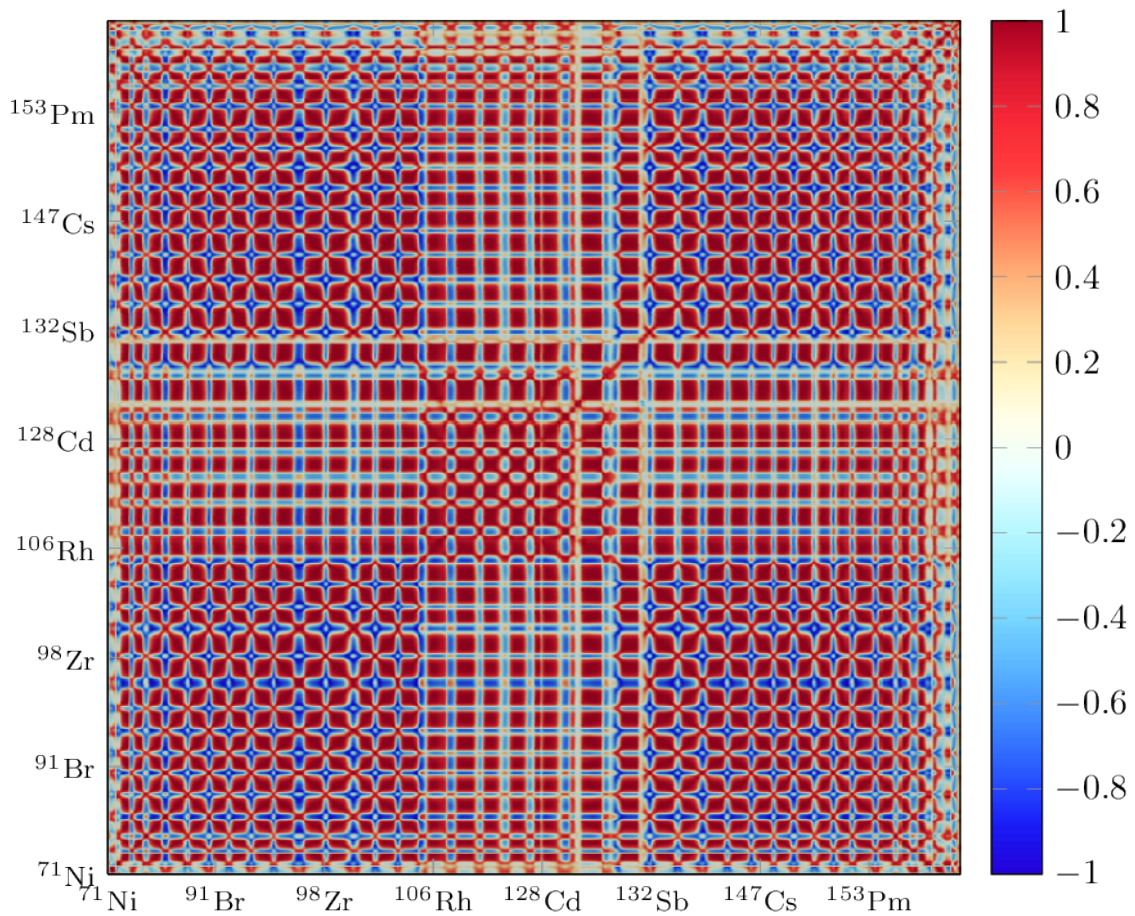


Figure 4.33: Independent isotopic FY covariance matrix for the thermal fission of ^{241}Pu . Fission yields are ordered in ascending charge, mass and isomeric states. In this case only FY greater than 10^{-7} have been considered.

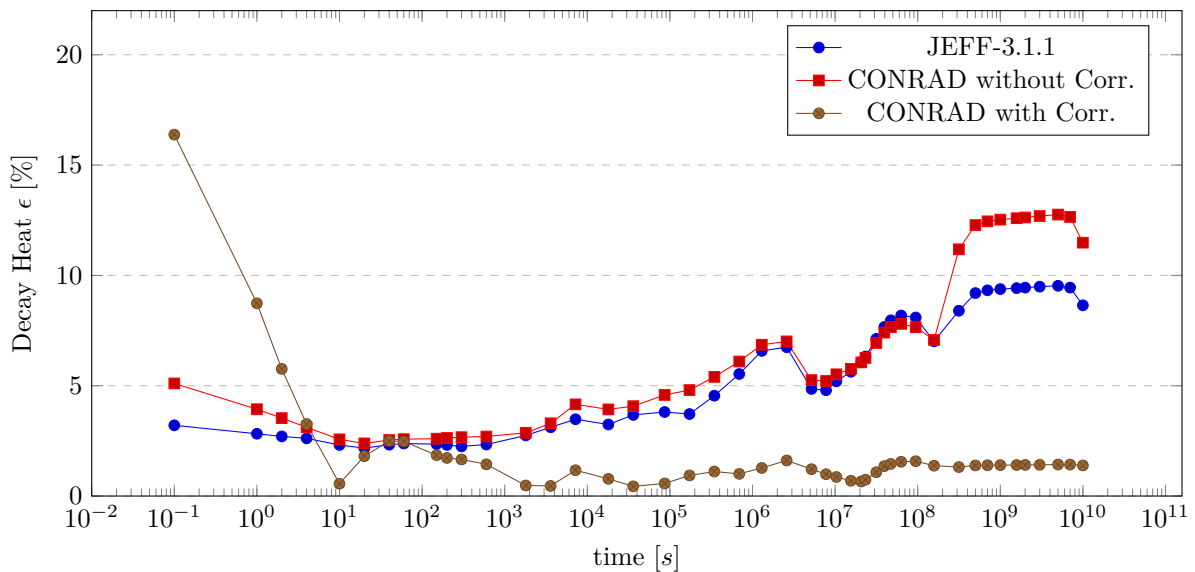


Figure 4.34: Decay heat uncertainty as a function of time for the elementary thermal fission of ^{241}Pu . The propagation of JEFF-3.1.1 FY uncertainties on the decay heat has been compared to what we obtain from CONRAD-generated FY, with and without including correlations.

Isotope	CFY JEFF-3.1.1	Rel. Unc. JEFF-3.1.1	CFY CONRAD	Rel. Unc. CONRAD
Sr-92	0.022889	5.2%	0.022571	1.3%
Rh-103	0.065384	4.9%	0.065609	1.1%
Cs-133	0.066140	2.7%	0.065160	1.9%
Cs-137	0.062843	2.2%	0.062294	1.0%
Ba-140	0.057561	1.9%	0.057720	1.7%
Ce-143	0.043805	2.1%	0.043865	1.6%
Nd-148	0.018812	3.4%	0.018698	1.5%
Sm-151	0.008565	28%	0.009052	2.8%
Eu-153	0.003953	57%	0.004855	4.0%

Table 4.12: List of the most significant cumulative FY for applications [Serot et al., 2004a]. The values are referring to the thermal fission of ^{241}Pu . Under-estimated uncertainties have been represented in blue. Average values are instead quite well reproduced.

While average values were quite well represented, some issues were discovered for the uncertainties that were all under-estimated. In particular for ^{151}Sm and ^{153}Eu huge differences were observed, probably due to both under-estimation and over-estimation of chain yields uncertainty in CONRAD calculations and JEFF evaluation respectively¹⁴.

4.6 U-238 Fast Fission

We tried also to treat a fast neutron induced fissioning system such as U238F¹⁵. This case was particularly difficult, since no experimental data were available to perform miscellaneous fission quantities calculations and adjustment. The prior saw-tooth, the fission mode and the Wahl parameters were picked from ^{235}U and no data on total prompt neutron emission probability were used as term of comparison. Only the total prompt neutron emission multiplicity was checked, as it will be explained later.

Parameter	Prior BE	Prior Unc. [%]	Posterior BE	Posterior Unc. [%]
$D_{St.I}^*$	15.8	10	15.6	0.3
$D_{St.II}^*$	23.1	10	24.1	0.3
$\sigma_{St.I}^*$	2.60	10	2.7	0.9
$\sigma_{St.II}^*$	4.95	10	4.63	1.1
σ_{SL}^*	5.05	10	4.23	4.1
$N_{St.I}$	0.162	10	0.392	1.7
N_{SL}	0.002	20	0.004	2.7

* Expressed in [amu].

Table 4.13: Fission mode parameters best estimates (BE) and uncertainties before (prior) and after (posterior) the analysis using CONRAD for the fast neutron induced fission of ^{238}U .

The fission modes parameters are given in Tab. 4.13. The average values seem reasonable, even if uncertainties are clearly under-estimated. A possible reason is the saw-tooth adjustment. Adjusting the saw-tooth values give high flexibility to the models, which have great capacity of FY representation. In such case, the Bayes theorem sees an almost

¹⁴For ^{241}Pu the discrepancies in ^{148}Nd uncertainty are surely less pronounced than those we see for ^{235}U .

¹⁵The 400 keV neutron induced fission is indicated with this notation in JEFF, while T stands for thermal and H for high energy ($\sim 14\text{MeV}$).

perfect coincidence between experimental data (in our case the mass FY derived from JEFF-3.1.1) and the model calculation, then an uncertainty reduction of adjusted model parameters is unavoidable. No model defects are seen by the theorem, as previously said, the theoretical model is assumed by the Bayes learning process as true prior knowledge. The marginalization technique allowed us to enhance error bars on Wahl model parameters and introduce systematic uncertainties and correlations, which should be necessarily present in FY evaluations. A 28% and a 16% uncertainty have been assigned to Iodine and Tellurium FY distribution norms respectively. The Wahl and Madland-England parameter averages and uncertainties are listed in Tab. 4.14¹⁶.

Parameter	Prior BE	Prior Unc. [%]	Posterior BE	Posterior Unc. [%]
$\sigma_Z(140)$	0.566	20	0.484	18.4
$\Delta Z(140)$	-0.487	20	-0.413	1.13
σ_{50}	0.356	20	0.419	0.7
$F_N(140)$	1.076	20	0.893	5.0
$F_Z(140)$	1.207	20	1.049	18.4
$SL50$	0.191	20	0.341	4.5
ΔZ_{max}	0.699	20	0.357	1.4
$\sigma_Z SLW$	-0.045	20	-0.029	21.1
$\Delta Z SLW$	0.0049	20	0.0040	24.1
J_{rms}^L	7.5	10	7.76	2.3
J_{rms}^H	7.5	10	7.93	1.4

Table 4.14: Wahl and Madland-England parameters best estimates (BE) and uncertainties before (prior) and after (posterior) the analysis using CONRAD for the fast neutron induced fission of ^{238}U .

In Figs. 4.35 and 4.36 mass FY for JEFF and CONRAD are shown. The adjustment of saw-tooth values in Fig. 4.37 gave us the possibility to have a decent representation of the most significant FY. It has to be emphasized that in this case the saw-tooth proposed by CONRAD presents some particular deviations that should be further investigated, even if a saw-tooth trend is roughly maintained.

The total prompt neutron multiplicity has been checked and compared to existing evaluated data. A value of 2.51 has been obtained for the present fissioning system, slightly higher than the evaluated one in JEFF-3.1.1, equal to 2.41 for 400 keV neutrons.

In Fig. 4.38 the correlation matrix for independent mass FY for the fast neutron induced fission of ^{238}U is shown. As before, the competition between Brosa fission modes is visible and produces the alternation of adjacent correlated and anti-correlated regions. The isotopic correlation matrix has not been included, but it presents similar patterns as we saw for the thermal fissioning systems.

¹⁶Performing the adjustment of Wahl parameters related to very asymmetric mass domains was not so successful. Averages and uncertainties for $F_N SLW$ and $F_Z SLW$ showed not reasonable results.

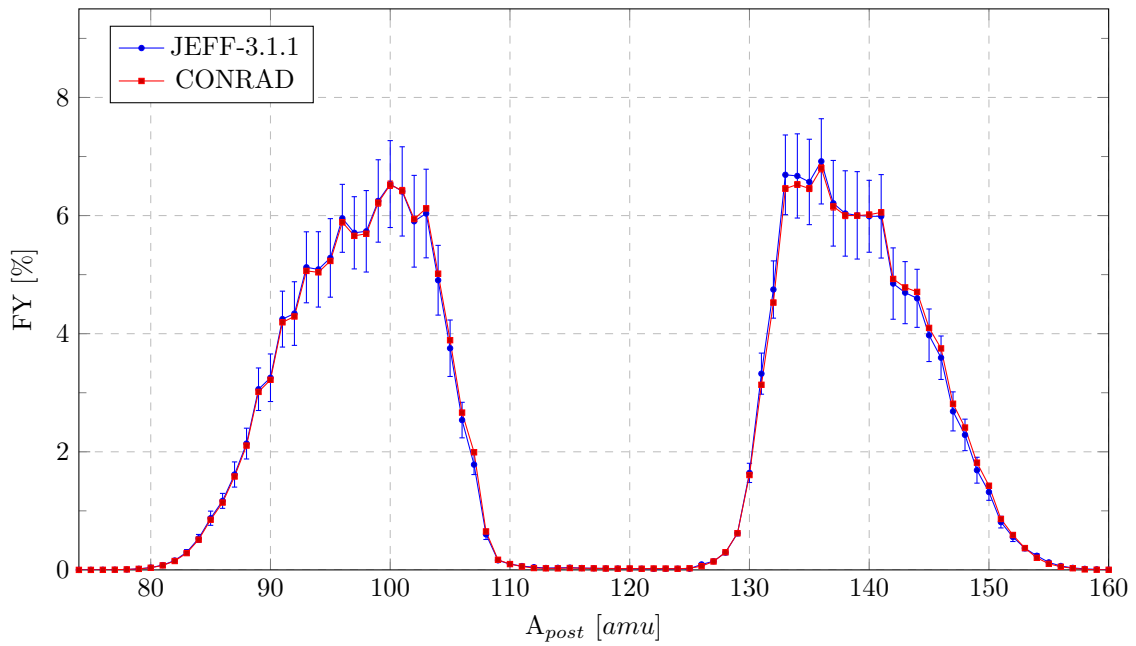


Figure 4.35: Comparison between JEFF-3.1.1 and CONRAD independent mass FY for the fast fission of ^{238}U in linear scale. FY model parameters have been adjusted using CONRAD to reproduce the JEFF-3.1.1 evaluated library and generate covariances. The convolution between the pre-neutron model based on Brosa fission modes and the saw-tooth curve allows a satisfactory representation of the available FY data.

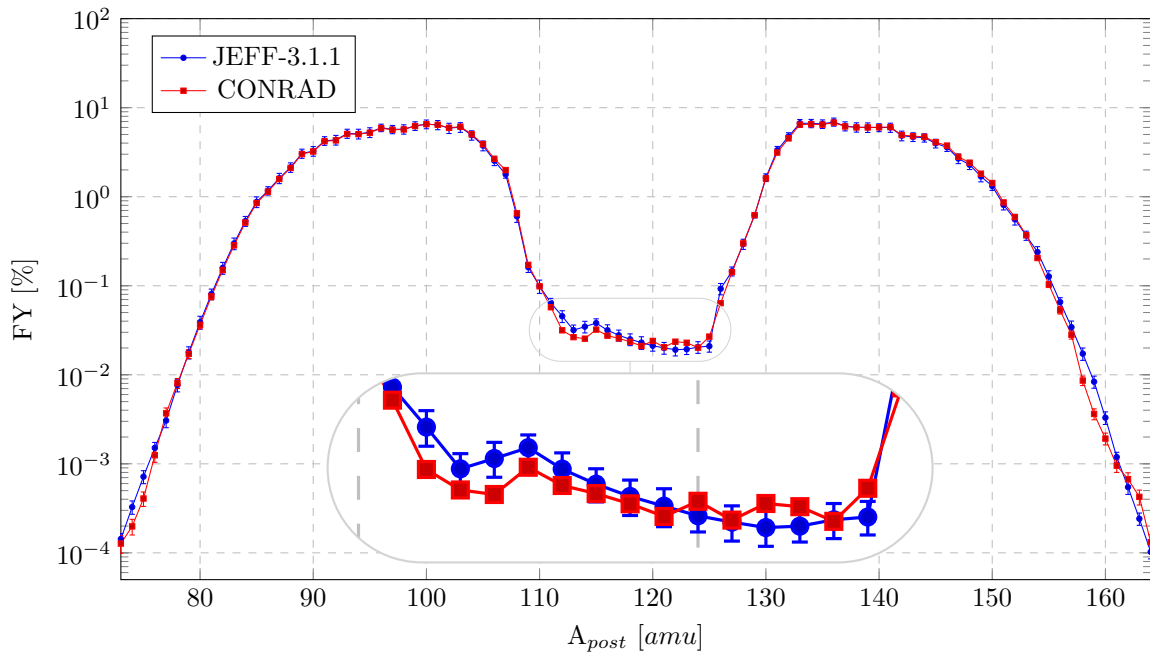


Figure 4.36: Comparison between JEFF-3.1.1 and CONRAD independent mass FY for the fast fission of ^{238}U in logarithmic scale. FY model parameters have been adjusted using CONRAD to reproduce the JEFF-3.1.1 evaluated library and generate covariances. The convolution between the pre-neutron model based on Brosa fission modes and the saw-tooth curve allows a satisfactory representation of the available FY data even in the symmetry region.

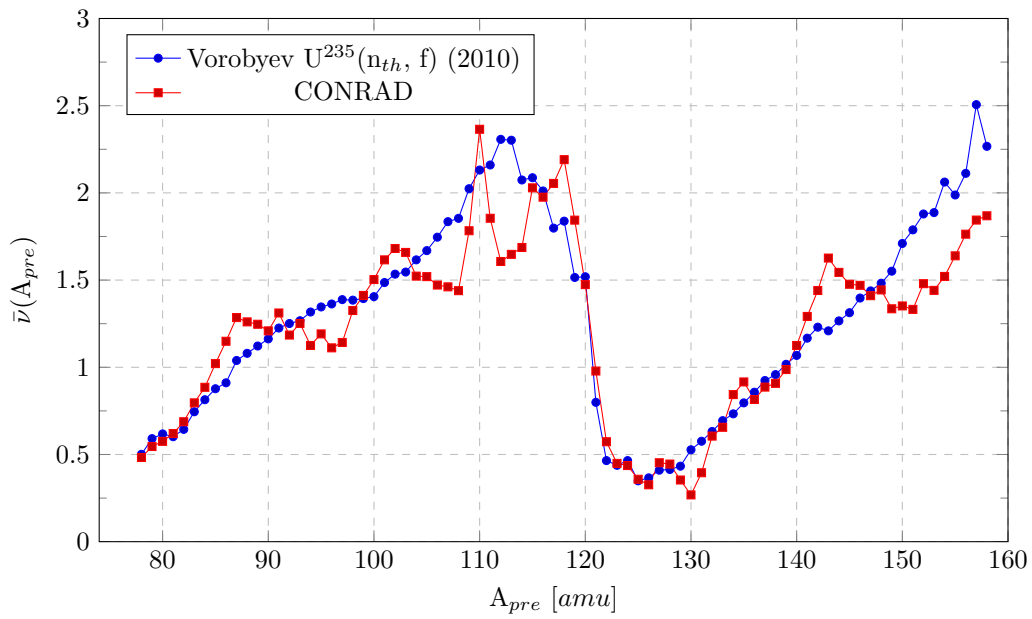


Figure 4.37: Comparison between prior (from Vorobyev [Vorobyev et al., 2010] experimental values measured for $^{235}\text{U}(n_{th}, f)$ and CONRAD-adjusted average number of prompt neutrons emitted as function of the pre-neutron fragment mass, for the fast fission of ^{238}U .

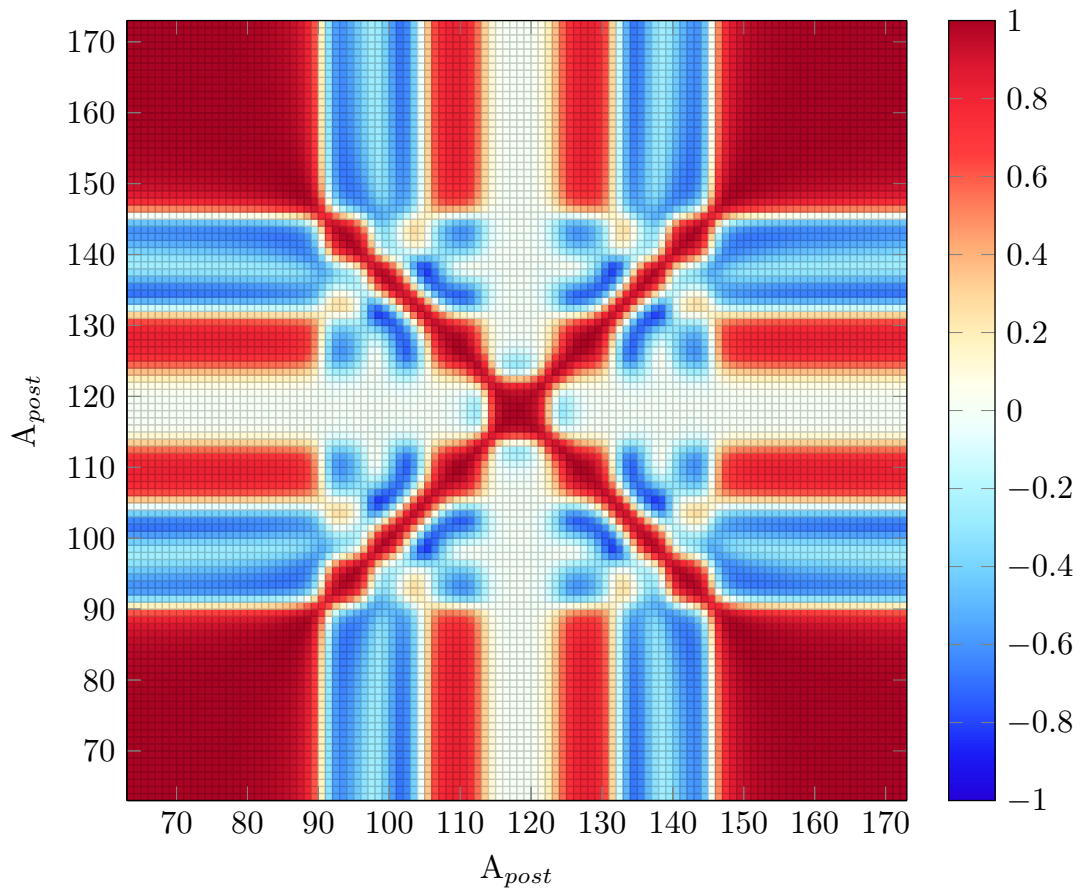


Figure 4.38: Independent mass FY covariance matrix for the fast fission of ^{238}U .

The elementary fission decay heat uncertainty estimation has been performed also for the present fissioning system. Fig. 4.39 tells us that the most sensitive FY uncertainties were well represented, even if we found a similar issue to the one we saw for the thermal neutron induced fission of ^{241}Pu for times of the order of 10^9 s. The problem still resides in the independent FY uncertainty for ^{137}I . CONRAD presents in fact a 19% of uncertainty which is greater than the value proposed in JEFF-3.1.1, of about 13%.

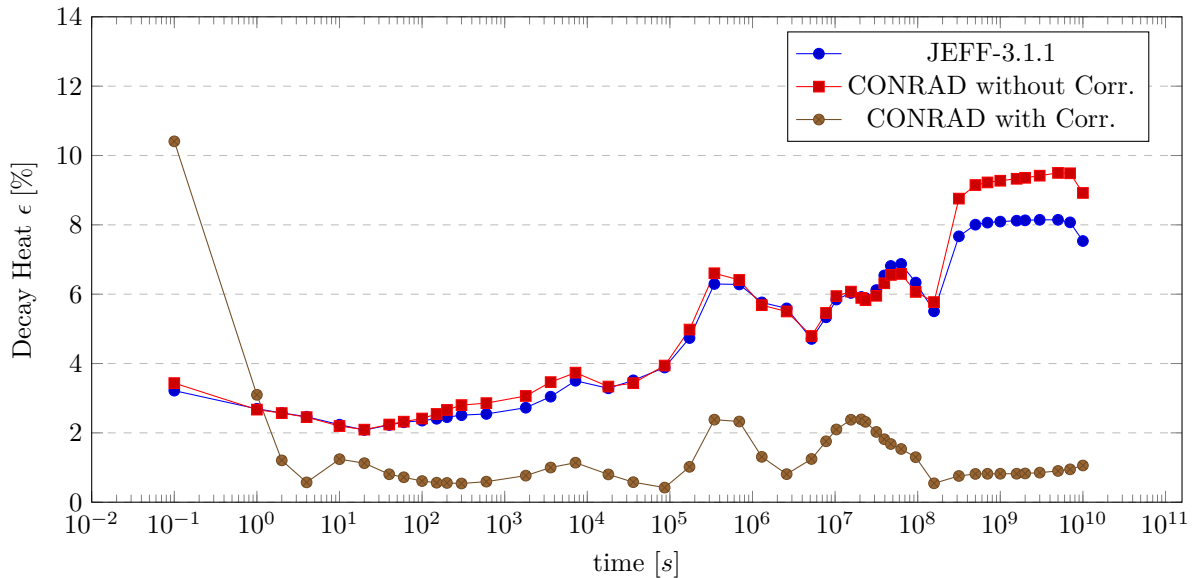


Figure 4.39: Decay heat uncertainty as a function of time for the elementary fast fission of ^{238}U . The propagation of JEFF-3.1.1 FY uncertainties on the decay heat has been compared to what we obtain from CONRAD-generated FY, with and without including correlations.

In Appendix D, some details are provided on elementary fission decay heat calculations to see if CONRAD FY can produce the same results obtainable with JEFF.

In Appendix E, some other fissioning systems have been considered. The results have not been included here since firstly they are not definitive, but also to do not burden the reading of the present chapter. In the next final section some general conclusions and remarks of the author are discussed.

4.7 Conclusions and Final Remarks

In the present Chapter some results on FY covariances and model parameters adjustment for the most important fissioning systems have been provided.

In Sec. 4.1 the general features of JEFF-3.1.1 FY evaluation have been briefly described. This evaluation, which is the last available at the present moment, has been taken as reference in our calculations. The main goal was in fact to reproduce evaluated data and provide associated covariance matrices.

The methodology adopted to generate covariances for FY has been presented in Sec. 4.2. It is based on the Bayesian techniques described in Chapter 1 and implemented in CONRAD. The GLSM allowed us to adjust the model parameters introduced in Chapter 2 for FY and the analytical marginalization was employed to take into account systematic errors

and provide satisfying uncertainties. The theoretical models were the same used for the evaluation, adding a special treatment for the prompt neutron emission performed by pre-neutron fission fragments. The Brosa model has been, in fact, consistently applied to pre-neutron distributions and a simplified model has been considered to take into account prompt neutron evaporation probabilities. Since no predictive physical models are available, the Wahl and Madland-England models have been used for isotopic and isomeric distributions, as done in JEFF-3.1.1 evaluation to fill gaps in the experimental data. The Q-matrix obtained by JEFF-3.1 decay data was used to finally calculate cumulative FY.

Some results have been proposed for the thermal neutron induced fission of ^{235}U , ^{239}Pu and ^{241}Pu , and for the fast neutron induced fission of ^{238}U . For ^{235}U and ^{239}Pu we can claim that physically consistent covariance matrices were generated in agreement with the JEFF-3.1.1 evaluation. The adjustment of model parameters and of the saw-tooth curve allowed to reproduce simultaneously evaluated FY data and independent experimental miscellaneous quantities such as the prompt neutron emission probability and multiplicity. The saw-tooth curves obtained by CONRAD presented slight deviations from the experimental data considered, hence, since this kind of data is not really well known especially for ^{239}Pu , this gave a certain confidence on the methodology. Completely independent data were represented by the models with a sufficient degree of accuracy, making the covariance data suitable to be associated to the JEFF-3.1.1 library.

For ^{241}Pu , saw-tooth experimental data were not available. This is certainly a drawback of the procedure, even if some priors from other fissioning systems can be used, as we did considering the Tsuchiya's experiment for ^{239}Pu . The favorable results we obtained on the prompt neutron emission probability and multiplicity made us to think to have promising covariances also for this fissioning system. For ^{238}U , the total absence of experimental data on the saw-tooth curve and on the prompt neutron emission probability makes the whole analysis more difficult. Nevertheless, covariances have been generated with the same procedure, providing reasonable results that can be employed when no better data are available.

We focused not only on the averages but also on the uncertainties. In this work in fact we meant to reproduce both average and variances proposed in JEFF-3.1.1 evaluation. Reproducing uncertainties for all the FY data set by propagating rigorously model parameters was not an easy task. In JEFF-3.1.1, FY are evaluated mostly by weighted averages of experimental results, and models are only used to fill gaps in interpolation-extrapolation processes. Furthermore, the great flexibility given by the adjustment of the saw-tooth curve played an important role in uncertainty determination. The Bayes theorem, in fact, assumes the theoretical model as true prior information. If experimental data affected by low uncertainties are almost perfectly reproduced by the theoretical model (which was the case taking JEFF-3.1.1 as pseudo-experimental information), model parameter uncertainties drop down necessarily in a Bayesian learning process. To compensate such effect and introduce systematic errors we adopted the analytical marginalization. Reproducing all the uncertainties was not possible, so we focused on Tellurium and Iodine isotopes which have the most important FY in reactivity loss estimation purposes.

To check globally the quality of the uncertainties produced we performed elementary fission decay heat calculations, discovering that CONRAD was sufficiently close to JEFF-3.1.1 evaluation for problem-sensitive FY. It has to be emphasized that probably some compensation effects took place. Some under-estimated uncertainties may be compensated by over-estimated ones, but globally the results were acceptable. We looked also at the impact of correlations. For the elementary fission a relevant uncertainty reduction was

observed for the decay heat uncertainty, even if, in the very beginning of the cooling time, correlations between different decaying isotopes enhance it considerably.

The marginalization technique was applicable since JEFF-3.1.1 data were assimilated with a diagonal variance matrix, taking into account only statistical uncertainties. However, recent efforts to estimate experimental covariances for FY are underway (e.g. Ref. [Kessedjian, 2015]) and they should be consistently taken into account in a comprehensive evaluation process able to incorporate experimental correlations when provided.

Special consideration goes to the saw-tooth curve adjustment. The lack of a model for the saw-tooth is a drawback for such procedure. Saw-tooth averages are probably correlated data and cannot be adjusted separately. Complementary fission fragments, in fact, dissipate fission excitation energies by a competition between prompt neutron and γ emissions. The average number of prompt neutrons emitted by a primary fragment depends therefore on its excitation energy just after the scission event. Correlations then probably exist between complementary light and heavy fragments, due to the fission excitation energy repartition law, which is still under investigation by nuclear physicists. This issue represents certainly a model defect which should be taken into account. As mentioned in Chapter 1, considering model defects is not straightforward and requires often a certain degree of personal speculation. The enhancement of the uncertainty due to model defects is surely a point to be developed in the future.

Some attentive readers may also rise issues on the simultaneous utilization of mass and independent yields of the same evaluation as pseudo-experimental data in a Bayesian learning process. The Bayes theorem in fact states that new experimental evidence should be independent from prior knowledge and experiments. This is surely a licit observation, but the aim of this entire work was to propose a possible solution to a very hard problem since no powerful and predictive physical theoretical models exist for FY. We just took existing and widely used models, and show that, if properly used, they are able to represent both evaluated and experimental data, producing covariance information.

Some words were spent also for cumulative yields. Once independent yields model parameters were calculated and the associated covariances were generated, cumulative FY can be evaluated using the Q-matrix. We focused mainly on those yields which are more significant for nuclear reactor applications. Average values were nicely represented, but some issues were discovered for some cumulative yields such as the one related to ^{148}Nd for the thermal fission of ^{235}U . ^{148}Nd is in fact a burn-up indicator, and its cumulative yield plays a fundamental role in burn-up monitoring and fuel qualification activities. Nevertheless, discrepancies in JEFF-3.1.1 evaluation between the uncertainties provided for independent and cumulative yields were shown, which make harder the task to have a satisfying representation of the whole data set by rigorous uncertainty propagation.

The next chapters will be devoted to the uncertainty propagation of FY data for applications. This gave us the possibility to determine the impact of the covariances we generated on real cases and see if they provide reasonable results. In particular a test problem as the PWR-pin cell and a whole reactor, such as the JHR, will be considered, using both Monte Carlo and deterministic techniques.

Part II

Uncertainty Propagation

Chapter 5

Uncertainty Propagation Methodologies

Contents

5.1	Introduction	140
5.2	Deterministic Sensitivity Estimation	142
5.2.1	Local Sensitivity Analysis: First Derivative Based Methods	143
5.2.2	Few Words on Global Sensitivity Analysis	144
5.3	Monte Carlo Uncertainty Propagation	146
5.3.1	General Features	147
5.3.2	Nuclear Data Monte Carlo Sampling	148
5.3.3	The Latin Hypercube Sampling	149
5.3.4	The Sample Size Determination	150
5.4	The URANIE-APOLLO-MENDEL Coupling	156
5.4.1	The URANIE Platform	156
5.4.2	Reactivity and Decay Heat Uncertainty Propagation	157
5.5	Conclusions	159

TO be safe and sustainable, modern and future nuclear systems require accurate knowledge on integral reactor parameters with reduced ranges of uncertainty. An important activity of sensitivity analysis and uncertainty quantification is then necessary to understand how much confidence we have on our predictions and if we have any margin of improvement.

The previous part of present dissertation was devoted to covariance generation methodologies for fission product yields. Some results have been provided for several thermal and fast neutron induced fission yields, proposing covariance information to be possibly associated to existing libraries, which have, at moment, incomplete uncertainty information (limited in many cases to only variances).

In this following chapter the sensitivity analysis and the uncertainty quantification methodologies will be presented. The main goal is to design uncertainty propagation techniques which are at the same time simple and suitable to treat burn-up calculations. Hereinafter we present two methodologies. The former is based on a deterministic approach. A straightforward way to generate sensitivities is in fact based on the calculation of finite incremental ratios based on direct perturbations. Such methodology introduces strong approximations, since it assumes a perfect linearity of the problem we are treating, but

offers an extraordinary flexibility and simplicity which turned out to be useful in covariance testing on applications. The latter is instead based on a Monte Carlo uncertainty quantification, which considers nuclear data as random variables to be sampled and used in different independent calculations.

These methods allowed us to generate results on FY covariance propagation for some reactor applications, presented further in Chapter 6.

5.1 Introduction

What we are interested in is to propagate nuclear data uncertainty in burn-up calculations. The main goal of the present doctoral dissertation is in fact to generate covariance matrices for nuclear data of interest in the reactivity loss uncertainty estimation of the JHR.

A common way to propagate nuclear data is using the conventional law for uncertainty propagation (see Chapter 1):

$$\mathbf{C}_k = \mathbf{S}^\dagger \mathbf{C}_\Sigma \mathbf{S}, \quad (5.1)$$

where \mathbf{C}_k is again the covariance matrix for a generic quantity of interest k , \mathbf{C}_Σ is a generic nuclear data covariance matrix, such as the one concerning the independent yields of the thermal fission of ^{235}U , and \mathbf{S} is the sensitivity matrix, collecting all the sensitivity coefficients of the vector \vec{k} to the nuclear data $\vec{\Sigma}$. Such equation was derived truncating at the first order the Taylor expansion of the functional $\vec{k} = \vec{k}(\vec{\Sigma})$, so the sensitivity matrix is nothing else than the associated Jacobian.

In nuclear reactor physics, as in other fields of science, there are different ways to calculate sensitivity coefficients. Once nuclear data covariance matrices are available, the uncertainty quantification problem can be then reduced to the determination of the sensitivity coefficients. We need to keep in mind that, even if sensitivities are calculated by sophisticated methods which take into account non-linear effects, the sandwich formula was derived assuming a linear approximation that cannot be ignored.

But, for depletion calculations (which are those ones we are interested in), how much is correct to assume linear approximations for nuclear data functionals? Let us look at the equations describing our physical problem.

For the neutron transport we have the well known Boltzmann equation, which can be written in the integro-differential form

$$\begin{aligned} \frac{1}{v} \frac{\partial \varphi(\vec{r}, E, \vec{\Omega}, t)}{\partial t} = & -\vec{\Omega} \cdot \vec{\nabla} \varphi(\vec{r}, E, \vec{\Omega}, t) - \sum_k N_k(\vec{r}, t) \sigma_k(E) \varphi(\vec{r}, E, \vec{\Omega}, t) \\ & + \sum_k N_k(\vec{r}, t) \int_0^\infty dE' \int_{4\pi} d\vec{\Omega}' \sigma_{s,k}(E' \rightarrow E, \vec{\Omega}' \rightarrow \vec{\Omega}) \varphi(\vec{r}, E', \vec{\Omega}', t) \\ & + \frac{1}{4\pi} \sum_k N_k(\vec{r}, t) \int_0^\infty dE' \nu_{p,k}(E') \sigma_{f,k}(E') \chi_{p,k}(E' \rightarrow E) \phi(\vec{r}, E', t) \\ & + \frac{1}{4\pi} \sum_k \nu_{p,sf,k} \lambda_{sf,k} N_k(\vec{r}, t) \chi_{p,sf,k}(E) + \frac{1}{4\pi} \sum_k \nu_{d,k} \lambda_{d,k} N_k(\vec{r}, t) \chi_{d,k}(E) + S_{ext}(\vec{r}, E, \vec{\Omega}, t). \end{aligned} \quad (5.2)$$

The variation of the neutron population $n(\vec{r}, E, \vec{\Omega}, t)$ in Eq. 5.2 for an elementary phase space volume $d\vec{r} \cdot dE \cdot d\vec{\Omega}$, with $\varphi(\vec{r}, E, \vec{\Omega}, t) = n(\vec{r}, E, \vec{\Omega}, t)v$ the angular flux, is given by the difference between loss and productions in the system which are due to

- i) $\vec{\Omega} \cdot \vec{\nabla} \varphi(\vec{r}, E, \vec{\Omega}, t) d\vec{r} dE d\vec{\Omega}$, that is the leakage term taking into account the disappearance of neutrons with energy included into the bin between E and $E + dE$ and flight direction in $d\vec{\Omega}$ around $\vec{\Omega}$ streaming out of the geometrical elementary volume $d\vec{r}$, in the interval of time dt .
- ii) $\sum_k N_k(\vec{r}, t) \sigma_k(E) \varphi(\vec{r}, E, \vec{\Omega}, t) d\vec{r} dE d\vec{\Omega}$ is the total reaction rate. It includes absorption (capture and fission) and scattering, that make the neutron to leave the elementary phase volume. The $N_k(\vec{r}, t)$ are the nuclide concentrations¹.
- iii) $\sum_k N_k(\vec{r}, t) \int_0^\infty dE' \int_{4\pi} d\vec{\Omega}' \sigma_{s,k}(E' \rightarrow E, \vec{\Omega}' \rightarrow \vec{\Omega}) \varphi(\vec{r}, E', \vec{\Omega}', t) d\vec{r} dE d\vec{\Omega}$ is a production term giving the contribution coming from neutrons which assume an energy and a direction included in the elementary phase volume $d\vec{r} dE d\vec{\Omega}$, after a scattering collision. $\sigma_{s,k}(E' \rightarrow E, \vec{\Omega}' \rightarrow \vec{\Omega})$ is in fact the double differential transfer cross section for the nuclide k .
- iv) $\frac{1}{4\pi} \sum_k N_k(\vec{r}, t) \int_0^\infty dE' \nu_{p,k}(E') \sigma_{f,k}(E') \chi_{p,k}(E' \rightarrow E) \phi(\vec{r}, E', t) d\vec{r} dE d\vec{\Omega}$ is the positive contribution coming from neutron induced fission. Prompt neutrons, with multiplicity $\nu_{p,k}(E)$, are assumed to be emitted isotropically² with a fission spectrum $\chi_{p,k}(E' \rightarrow E)$.
- v) $\frac{1}{4\pi} \sum_k \nu_{p,sf,k} \lambda_{sf,k} N_k(\vec{r}, t) \chi_{p,sf,k}(E) d\vec{r} dE d\vec{\Omega}$ is the analogous term regarding spontaneous fission, where $\lambda_{sf,k}$ is the associated decay constant and $\chi_{p,sf,k}(E)$ is the related prompt neutron energy distribution. In most of the cases, this term is negligible.
- vi) $\frac{1}{4\pi} \sum_k \nu_{d,k} \lambda_{d,k} N_k(\vec{r}, t) \chi_{d,k}(E) d\vec{r} dE d\vec{\Omega}$ is the delayed neutron contribution coming from the decay of the fission products which is governed by the constant $\lambda_{d,k}$. $\chi_{d,k}(E)$ is the delayed neutron spectrum for the nuclide k .
- vii) $S_{ext}(\vec{r}, E, \vec{\Omega}, t) d\vec{r} dE d\vec{\Omega}$ is the external source.

The $d\vec{r} dE d\vec{\Omega}$ elementary phase volume has been dropped in Eq. 5.2.

Such equation is in principle linear because no neutron-neutron interactions are considered. However, it must be coupled to those relations governing the time evolution of the concentrations $N_k(\vec{r}, t)$ of the atomic nuclei, whose modifications in the system depend on the irradiation conditions, and so on the neutron flux. The generalized Bateman formulation [Bateman, 1910] is a system of coupled differential equations describing the burn-up of the reactor constituents during depletion. They can be expressed as follows

$$\frac{dN_k(\vec{r}, t)}{dt} = \sum_{m \neq k} \zeta_{m \rightarrow k}(\vec{r}, t) N_m(\vec{r}, t) + \sum_{m \neq k} \lambda_{m \rightarrow k} N_m(\vec{r}, t) - \lambda_k N_k(\vec{r}, t) - \zeta_k(\vec{r}, t) N_k(\vec{r}, t), \quad (5.3)$$

where the different terms are

¹The macroscopic cross section $\Sigma_k(\vec{r}, E, t) = N_k(\vec{r}, t) \sigma_k(E)$ is here explicit to show better the connection with the Bateman equation (see further) and highlight how the depletion calculation is a coupled Bateman-Boltzmann problem.

²This assumption is almost true, even if a certain degree of anisotropy can be observed for prompt neutron emission.

- i) $\sum_{m \neq k} \zeta_{m \rightarrow k}(\vec{r}, t) N_m(\vec{r}, t)$. It gives the production of nuclides k due to neutron interactions with other constituents of the matter. The transfer probability is given by the integrated reaction rates for different interactions

$$\zeta_{m \rightarrow k}(\vec{r}, t) = \sum_q \int_0^\infty \sigma_{q, m \rightarrow k}(E) \phi(\vec{r}, E, t) dE. \quad (5.4)$$

$\sigma_{q, m \rightarrow k}(E) = \sigma_{q, m}(E) \Pi(m \rightarrow k)$, where $\sigma_{q, m}(E)$ is the cross section for the reaction q related to the nuclide m , while $\Pi(m \rightarrow k)$ is the probability to get the nuclide k as product of the nuclear reaction. For fission, $\Pi(m \rightarrow k)$ is nothing else than the FY for the product k .

- ii) $\sum_{m \neq k} \lambda_{m \rightarrow k} N_m(\vec{r}, t)$ is the production rate due to the decay towards the considered nuclide k .
- iii) $\zeta_k(\vec{r}, t) N_k(\vec{r}, t)$ is the reaction rate related to the disappearance of the nuclide k . ζ_k is then given by

$$\zeta_k(\vec{r}, t) = \sum_q \int_0^\infty \sigma_{q, k}(E) \phi(\vec{r}, E, t) dE. \quad (5.5)$$

- iv) $\lambda_k N_k(\vec{r}, t)$ takes finally into account the loss rate due to the radioactive decay of the nuclide k we are considering.

As it is shown in the Eqs. 5.2 and 5.3, the neutron transport and the nuclei concentration systems of equations are linear, if they are taken separately. Nevertheless, a coupling between the flux and the nuclide concentrations exists, even if the problem still is well posed. Such coupling can introduce non-linearity issues in the calculation of sensitivity coefficients, since the conventional perturbations theories used in reactor physics (see Appendix F) are not directly applicable.

Some methodologies to calculate sensitivities coefficients in depletion problems are actually available, and they can give even reliable results (see Ref. [Williams, 1979]). However, they are not widely implemented in neutron transport codes and sensitivities during depletion are hardly retrievable.

For our purposes, which mainly include the covariance generation, testing and propagation, we decided to find the best compromise between simplicity and effectiveness. We developed two simple methods able to give us a first grasp on the impact of the covariances we generated, with enough flexibility to avoid intense implementation efforts, but at the same time capable to give reliable responses. In the next sections, these methods will be presented.

5.2 Deterministic Sensitivity Estimation

Sensitivity analysis can tell us how uncertainty in the output of a model can be apportioned to different sources of uncertainty in the model input [Saltelli et al., 2008]. It can identify critical regions in the input domain, establish research priorities and highlight margins of improvement, which can have both economic and safety significant impacts.

As proposed in the uncertainty propagation law, the first concept of sensitivity comes from the definition of the Jacobian operator. Indeed the derivative $\partial Y / \partial X_i$ of an output Y

versus an input X_i gives the quantification of how much the output changes due a variation of the input. Derivative-based methods are immediate to be implemented and perform a straightforward sensitivity analysis. Nevertheless, derivative based methods do not offer any warranty when we treat uncertain parameters and non-linear problems. Derivatives are local operators which describe the model in the infinitesimal domain around the point where they are calculated. Global methods, on the other hand, explore the entire input hyperspace and allow more reliable but also more expensive sensitivity techniques. In the following sections of the present dissertation, some essential features of the most important general sensitivity techniques will be provided. Most of them will be briefly introduced for a sake of completeness. The conventional perturbation theories used in reactor physics to calculate sensitivity coefficients are, on the other hand, described in Appendix F. For our purpose only local-finite-difference methods will be actually used to observe the outcome of nuclear data covariance matrices in burn-up applications.

5.2.1 Local Sensitivity Analysis: First Derivative Based Methods

The Jacobian operator for sensitivity coefficients is surely the most intuitive and it accomplishes its task for uncertainty propagation purposes, but it does not give any information on the ranking of the input parameters³. If for example the reactor k_{eff} has the same derivative compared to different cross sections, the two sensitivity coefficients will be the same, regardless if one of the two nuclear data have different relative uncertainties or they are correlated.

Furthermore, this last sensitivity definition turns to be useful only when the form of the functional describing the physical problem can be written analytically and is differentiable. When the output of interest is a code response, an alternative way to proceed is to perform a relative finite difference calculation to estimate sensitivity coefficients:

$$S_{k_j}^{\Sigma_i} = \frac{\Delta k_j / k_j(\vec{\Sigma})}{2 \cdot \Delta \Sigma_i / \Sigma_i} = \frac{[k_j(\Sigma_1, \dots, \Sigma_i + \Delta \Sigma_i, \dots, \Sigma_n) - k_j(\Sigma_1, \dots, \Sigma_i - \Delta \Sigma_i, \dots, \Sigma_n)] / k_j(\vec{\Sigma})}{2 \cdot \Delta \Sigma_i / \Sigma_i}. \quad (5.7)$$

For our goals, we performed the uncertainty propagation for FY according to the following procedure. We firstly calculated sensitivity coefficients performing perturbations of one standard deviations. This allows to estimate sensitivity coefficients more accurately, since it also considers contributions given by small yields with high standard deviations, which otherwise would be neglected using fixed perturbations of few percents. Furthermore, considering 1- σ perturbations allows to attenuate eventual non-linear effects, which are not detectable by few percent increments. Considering for instance the decay heat at $t = 1$ y

³To have a more solid definition of the sensitivity coefficient, capable to give directly indication about its relevance on the final output uncertainty, a sigma-normalized derivative formula can be used

$$S_{k_j}^{\Sigma_i} = \frac{\sigma_{\Sigma_i} \partial k_j}{\sigma_{k_j} \partial \Sigma_i}, \quad (5.6)$$

where the relative sensitivity coefficient $S_{k_j}^{\Sigma_i}$ takes into account input parameter Σ_i contributions on the output parameter k_j uncertainty. σ_{Σ_i} and σ_{k_j} are input-output standard deviations. The drawback of such definition is that the output standard deviation has to be known, that is not the case for uncertainty propagation purposes.

we can calculate the sensitivity to ^{135}Te as

$$S_{DH_{1y}}^{Y(^{135}\text{Te})} = \frac{\Delta DH_{1y} / DH_{1y}(\vec{Y})}{2 \cdot \Delta Y_i / Y_i} = \frac{[DH_{1y}(Y_{72\text{Cu}}, \dots, Y_{135\text{Te}} + \sigma_{Y_{135\text{Te}}}, \dots, Y_{162\text{Sm}}) - DH_{1y}(Y_{72\text{Cu}}, \dots, Y_{135\text{Te}} - \sigma_{Y_{135\text{Te}}}, \dots, Y_{162\text{Sm}})] / DH_{1y}(\vec{Y})}{2 \cdot \sigma_{Y(^{135}\text{Te})} / Y(^{135}\text{Te})}. \quad (5.8)$$

To obtain the relative uncertainty on the decay heat relative covariances are required. CONRAD provides the correlation matrix \mathbf{R} that simply is

$$(R)_{i,j} = \frac{(C)_{i,j}}{\sigma_{Y_i} \sigma_{Y_j}}, \quad (5.9)$$

the relative decay heat uncertainty vector is given by

$$\vec{\sigma}_{DH}^{rel} = \sqrt{\mathbf{S}_{DH}^\dagger \mathbf{C}_{fy}^{rel} \mathbf{S}_{DH}} \quad (5.10)$$

where

$$(C_{fy}^{rel})_{i,j} = (R)_{i,j} \sigma_i^{rel} \sigma_j^{rel}. \quad (5.11)$$

In the next sections some other deterministic methods are presented for a sake of completeness, but this last method was extensively applied in the present work. This was due essentially to the simplicity of this method and to the possibility to compare results with the CYRUS code for simple cases. The reader who is not interested in such methods can directly jump to the next section describing Monte Carlo uncertainty propagation methods, which have been also used in this doctoral work.

5.2.2 Few Words on Global Sensitivity Analysis

In this section we are going to introduce briefly two techniques which are quite important in global sensitivity analysis, even if not used in the present work:

- i) The Elementary Effect Method, which is used in the Morris screening;
- ii) Variance Decomposition, at the basis of the Sobol-Saltelli algorithm.

The main features will be presented hereinafter to explain essentially why such techniques were not employed for our purposes. We do not pretend to be exhaustive, leaving the reader to the consultation of dedicated references [Saltelli et al., 2004, Saltelli et al., 2008] for further details.

5.2.2.1 Elementary Effects

In 1991 Morris proposed a less-expensive way to establish parameter priorities with a small number of sample points properly distributed. It is based on elementary effect (EE) calculations and it is a way of screening a few important factors among the many that can be inputs of the model we are considering. Morris proposed the construction of two sensitivity measures able to give indications if the parameters are significant in the determination of the response uncertainty, and if they present some non-linear effects, interacting with other parameters of the model. Such measures are not quantitatively relevant but depict qualitatively the parameter hierarchy, providing a restricted list of

most important parameters. This reason induced us to do not apply such methods, since we were interested in a quantitative estimation of the uncertainty on reactor parameters.

An elementary effect is defined as follows. Let us consider a response function Y of k parameters x_1, \dots, x_k . The input space is divided in elementary steps, such that we have a p -level discretization of the input domain Ω . For a given $\vec{x} \in \Omega$, we can define the elementary effect as

$$EE_i = \frac{Y(x_1, \dots, x_{i-1}, x_i + \Delta, \dots, x_k) - Y(x_1, \dots, x_{i-1}, x_i, \dots, x_k)}{\Delta}. \quad (5.12)$$

Δ is the variation step we make x_i to assume and it is a value belonging to $\{1/(p-1), \dots, 1 - 1/(p-1)\}$, supposing that, such variation still gives vectors in Ω . Basically the present method imposes a domain decomposition in variation steps, where the different variables can assume only discrete points which are equidistant of the quantity Δ . Morris methodology suggests to build a number r of different piece-wise trajectories in the hyperspace Ω . Each trajectory corresponds to $(k+1)$ model excursions and yields the computation of an elementary effect for each parameter x_i . Trajectories are built in the following manner. An initial vector \vec{x}_0 is selected in the domain Ω . This is only the vector originating all the elementary effects and it is not part of the trajectory itself. The starting point is chosen randomly picking a parameter x_i and varying this component of a factor Δ , obtaining $\vec{x}_1 = \vec{x}_0 \pm \vec{e}_i \Delta$, where \vec{e}_i is a zero vector with only the i -th component equal to 1. The second point is chosen varying another random component $j \neq i$ of the quantity Δ , starting from \vec{x}_1 . The entire procedure is repeated until all the k components x_i are modified of a quantity Δ . Once a certain number r of trajectories is built⁴, we can calculate single elementary effect for the j -th trajectory and the parameter i

$$EE_i^j(\vec{x}_{(l)}) = \frac{[Y(\vec{x}_{(l+1)}) - Y(\vec{x}_{(l)})]}{\Delta}, \quad (5.13)$$

where $\vec{x}_{(l)}$ is the point of the trajectory from which we decide to increment the i -th component of a factor Δ ⁵. Morris indicators are calculated by the following formulas

$$\mu_i = \frac{1}{r} \sum_{j=1}^r EE_i^j \quad (5.14)$$

$$\sigma_i^2 = \frac{1}{r-1} \sum_{j=1}^r (EE_i^j - \mu_i)^2 \quad (5.15)$$

The first factor indicates the impact of single parameters on the output response. σ_i^2 , on the other hand, provides information on how much non-linear effects and parameter interactions are significant.

5.2.2.2 Variance Decomposition

Variance-based methods are really important in sensitivity analysis and find applications in several fields of science such as Mechanical Engineering, Risk Analysis and Nuclear Engineering; examples are given in Refs. [Borgonovo, 2006, Arwade et al., 2010, Abdel-Khalik, 2013].

⁴See Ref. [Saltelli et al., 2008] for more details.

⁵If such component is decremented of a factor Δ , signs are inverted.

Let us consider a general model $Y = Y(x_1, \dots, x_i, \dots, x_k)$, function of k input parameters. Thanks to Hoeffding theorem, Sobol demonstrated that the variance for a given response can be decomposed as

$$Var(Y) = \sum_{i=1}^k V_i + \sum_{i=1}^k \sum_{j>i}^k V_{i,j} + \dots + V_{1,2,\dots,k} \quad (5.16)$$

with

$$V_i = Var(E(Y|x_i)) \quad (5.17)$$

$$V_{i,j} = Var(E(Y|x_i, x_j)) - V_i - V_j \quad (5.18)$$

$$V_{1,2,\dots,d} = Var(E(Y|x_1, x_2, \dots, x_k)) - \sum_{r=1}^k V_r \quad (5.19)$$

V_i indicates the variance contribution of the first order, due exclusively to the parameter i . Second order terms identify variance contribution coming from parameter interactions. Such interaction are only due to model features. In fact to perform such variance decomposition uncorrelated parameters are needed. This is necessary since variance decomposition is based on Hoeffding finite series expansion, which requires a family of orthogonal functions belonging to the Hilbert space. Such orthogonality is guaranteed for variance decomposition only if model parameters are not correlated.

Sobol sensitivity indexes are defined as

$$S_i = \frac{Var(E(Y|x_i))}{V(Y)} \quad (5.20)$$

which are a direct expression of the importance of variable i relatively to the output Y . Sobol first, and successively Saltelli with some improvements, proposed a Monte Carlo procedure to calculate Sobol indexes (See Ref. [Saltelli et al., 2008]).

Since the variance decomposition method supposes uncorrelated random variables, we abandoned such technique even if it is quite used in other field of science.

5.3 Monte Carlo Uncertainty Propagation

Modern Monte Carlo codes such as MCNP [Goorley et al., 2015], TRIPOLI-4 [Truchet et al., 2015] and SERPENT [Aufiero et al., 2015] can provide sensitivity coefficients thanks to recent developments of perturbation tools able to calculate the solution to the adjoint equation, but they do not provide any solution for depletion calculations. Therefore these methods were not considered in the present dissertation. What we propose, on the other hand, is a direct Monte Carlo uncertainty propagation procedure for nuclear data, which is simple to implement and gives a large flexibility.

The first part of this section will be devoted to general theoretical and practical aspects of the method. The second part of the section will be, on the other hand, the description of what was realized to accomplish the main tasks of the present work. We used the URANIE platform [Gaudier, 2010], a set of libraries we employed as Monte Carlo sampling engine. To estimate uncertainties for neutronic parameters, such as reactivity and decay heat, URANIE was coupled to APOLLO2 and MENDEL.

5.3.1 General Features

The Monte Carlo uncertainty propagation proposed here is quite standard in modern nuclear technology. The first step is the identification of the most important uncertain input parameters, defined as $\vec{x} = (x_1, \dots, x_k)$, which can be of any kind, such as models, boundary conditions, initial conditions etc. In our case we sample nuclear data, more specifically FY data if we mean to test the covariance matrices we propose. The uncertain parameters should be provided with a probability distribution (PDF), and possibly with correlations when they are available. A Monte Carlo sampling strategy is then used to generate a sample of size N from such input hyperspace, that should be representative of averages and covariances of the original PDFs. These sets of sampled input data are then propagated to a simulation tool to provide an equal number of quantities of interest, such as the k_{eff} of a nuclear reactor.

Once the sample of the code outputs has been collected, averages, uncertainties and output correlations can be inferred by statistical procedures. In this way a simple uncertainty propagation of nuclear data is consistently performed for any general code we are interested in. The sampling method has the advantage that burn-up and thermo-hydraulics feedback effects are easily considered in complicated light water reactor core analysis [Kinoshita et al., 2014].

The drawbacks of such method are certainly the computational cost behind many calculations (of the order of 1000), that can take several days to be performed for whole reactor geometries. A second drawback is the hypothesis about the PDFs used for nuclear data, which, in principle, should be as general as possible. Furthermore statistical errors are involved in the uncertainty estimation since it is a stochastic approach, they can be reduced increasing the sample size and so the number of calculations.

The Monte Carlo uncertainty propagation method has been quite used in nuclear reactor technology in the last 15 years, so it is not a novelty introduced by the present doctoral work. Some examples are the XSUSA Monte Carlo sampling tools for nuclear data [Zwermann et al., 2009] developed at GRS⁶ and adopted by ORNL⁷ for the SAMPLER tool of SCALE-6.1 [Williams et al., 2013]. The method has been adopted also by many other organizations and research teams in several works and for different purposes [Cabellos et al., 2011, Hernández Solís et al., 2013, Martínez et al., 2014, Diez et al., 2015], with and without using the tools mentioned so far.

An interesting alternative is the Total Monte Carlo method (TMC) [Koning and Rochman, 2008], developed at NRG, which does not perform any direct sample on nuclear data averages and covariances. It consists on the generation of a set of different ENDF files using TENDL, sampling the nuclear reaction model parameters. These files are then used for different Monte Carlo reactor calculations (using MCNP for instance), whose outputs are post-processed to find integral reactor parameter uncertainties.

In the following section we describe how we perform direct Monte Carlo samplings of the CONRAD-correlated FY nuclear data using the URANIE platform.

⁶Gesellschaft für Anlagen- und Reaktorsicherheit (GRS)

⁷Oak Ridge National Laboratory (ORNL)

5.3.2 Nuclear Data Monte Carlo Sampling

The first task we need to accomplish is to sample nuclear data preserving the correlations we have found using CONRAD. Nuclear data are usually provided in the form of expected values and covariance matrix. For our purposes, we suppose Gaussian or Log-normal distributions for the nuclear data we sample.

The basic idea behind the generation of N sampled correlated parameters \vec{x} , is to perform a Monte Carlo sampling of an equal number of independent random variables $\vec{\xi}$ (e.g. normal or uniform distributions) and to find a transfer function \vec{F} capable to represent the original PDFs and correlations for \vec{x} . In formulas we have then [Žerovnik et al., 2011]

$$\vec{x}^{(m)} = \vec{F}(\vec{\xi}^{(m)}), \quad (5.21)$$

where \vec{F} depends on parameter distributions and correlations.

Due to its linearity, for normal distributions the sample of correlated variables is given by [Žerovnik et al., 2011]

$$\vec{x}^{(m)} = \mathbf{A} \cdot \vec{\xi}^{(m)} + \vec{\mu}, \quad (5.22)$$

where \mathbf{A} is defined such that the mean values, standard deviations and correlations of \vec{x} are preserved. $\vec{\mu}$ is the average values vector and $\vec{\xi}$ are zero mean normal distributions with unitary standard deviation (standard normal distributions). The matrix \mathbf{A} needs to satisfy the following relationship [Žerovnik et al., 2011]:

$$\begin{aligned} C_{ij} &= \lim_{M \rightarrow \infty} \frac{1}{M-1} \sum_{m=1}^M (x_i^{(m)} - \mu_i)(x_j^{(m)} - \mu_j) = \lim_{M \rightarrow \infty} \frac{1}{M-1} \sum_{m=1}^M \sum_{k,l=1}^n A_{i,k} \xi_k^{(m)} A_{j,l} \xi_l^{(m)} \\ &= \sum_{k,l=1}^n A_{i,k} A_{j,l} \lim_{M \rightarrow \infty} \frac{1}{M-1} \sum_{m=1}^M \xi_k^{(m)} \xi_l^{(m)} = \sum_{k,l=1}^n A_{i,k} A_{j,l} \delta_{kl} = \sum_{k=1}^n A_{i,k} A_{j,k}, \end{aligned} \quad (5.23)$$

where C_{ij} are the absolute covariances of the parameters x_i and x_j . Therefore, to generate a sample able to reproduce the given distributions and the associated correlations we can simply write

$$C_{ij} = \sum_{k=1}^n A_{i,k} A_{j,k} = \sum_{k=1}^n A_{i,k} (A^\dagger)_{kj} = (AA^\dagger)_{ij} \quad (5.24)$$

Therefore, a $\mathbf{C} = \mathbf{A}\mathbf{A}^\dagger$ decomposition can be performed using the Cholesky methodology. Since \mathbf{C} is a symmetric positive-definite matrix, it can be written as

$$\begin{aligned} \mathbf{C} &= \mathbf{\Sigma}^\dagger \mathbf{D} \mathbf{\Sigma}, \\ &= (\mathbf{\Sigma}^\dagger \sqrt{\mathbf{D}}) (\sqrt{\mathbf{D}} \mathbf{\Sigma}), \\ &= (\sqrt{\mathbf{D}} \mathbf{\Sigma})^\dagger (\sqrt{\mathbf{D}} \mathbf{\Sigma}) \end{aligned} \quad (5.25)$$

then we have the definition for matrix $\mathbf{A} = (\sqrt{\mathbf{D}} \mathbf{\Sigma})^\dagger$.

For a Log-normal distribution we can use the same procedure converting the covariance matrix \mathbf{C} to the equivalent covariance matrix for the normal distribution $\tilde{\mathbf{C}}$, and after

apply the Cholesky decomposition and the standard normal sampling seen so far. The covariance matrix is given by [Žerovnik et al., 2011]

$$\tilde{C}_{ij} = \ln\left(\frac{C_{ij}}{\langle x_i \rangle \langle x_j \rangle} + 1\right). \quad (5.26)$$

5.3.3 The Latin Hypercube Sampling

The Latin Hypercube Sampling (LHS) method is an alternative way to perform random sampling which provides a faster convergence to the original distribution. Let us describe the procedure for a uniform distribution defined in the $[0, 1]$ domain. If N is the sample size, the range of each input parameter can be divided into N intervals. The procedure consists in taking only one sampling for each hypercube given by different intervals belonging to different sampled parameters [Kinoshita et al., 2014]. Let us take as example two parameters x and y to be sampled. Each $[0, 1]$ domain is subdivided in N intervals, then for a 2-D case the hyperspace is just a surface, which is divided in $N \times N$ little areas, as given in Fig. 5.1 for $N = 9$.

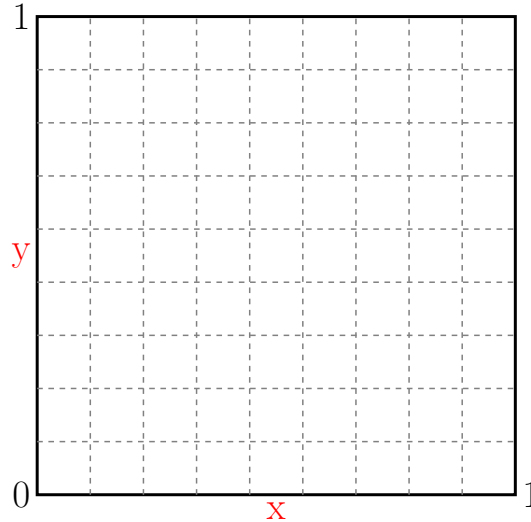


Figure 5.1: Example of subdivision of the sampling domain.

The intervals for each parameter can be ordered and labeled by cardinal numbers $1, 2, \dots, N$. For both the random variables, the two lists of numbers are shuffled to generate two random strings in order to have random coordinates in the sampling hyperspace. In the example proposed, we can shuffle the two lists of $1, \dots, 9$ numbers to get for example⁸

5 6 7 4 9 1 3 8 2
4 6 5 3 8 9 1 2 7

These two strings gives N coordinates in the starting domain hyperspace where perform N independent samplings of the random variables. The first row represents coordinates for x and the second for y . Therefore we have $a = (5, 4)$, $b = (6, 6)$, $c = (7, 5)$ etc. areas where to perform distinct random samplings. For instance, after the sampling, we can get

0.50 0.60 0.72 0.36 0.92 0.08 0.23 0.79 0.22
0.44 0.64 0.51 0.32 0.87 0.95 0.11 0.15 0.72

⁸The example is taken from Ref. [Kinoshita et al., 2014].

which are reported in Fig. 5.2 with labels A=(0.50, 0.44), B=(0.60, 0.64), C=(0.72, 0.51) etc.

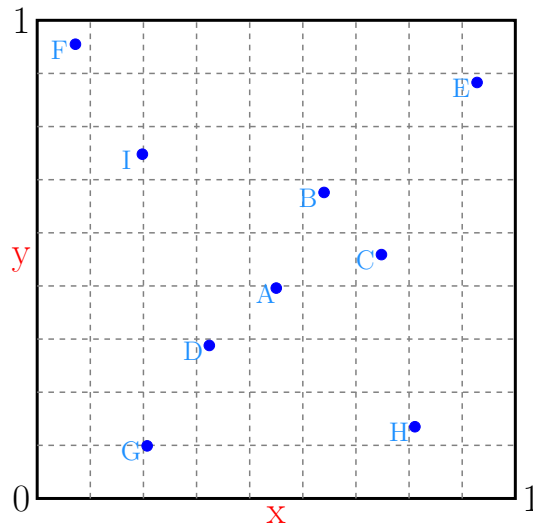


Figure 5.2: Example of LHS sampling (reproduced from [Kinoshita et al., 2014]).

To reproduce correlated distributions, we start by sampling a normal Gaussian with a unitary standard deviation. To do so, we need the inverse of the cumulative distribution (CDF). If r is the uniform random number in the interval $(0, 1)$, sampled with a LHS procedure, then we have

$$z = F^{-1}(r) \quad (5.27)$$

where z is the random number which obeys to the standard normal distribution and

$$F(z) = \int_{-\infty}^z f(t)dt. \quad (5.28)$$

The LHS allowed us to perform a sort of intelligent sampling, covering all the entire domain even for small sample size. This special case of stratified sampling [Kinoshita et al., 2014] yields in fact a faster convergence if compared to standard random sampling (SRS), reducing the stochastic error influence on the uncertainty evaluation.

5.3.4 The Sample Size Determination

In the previous sections we have seen how a Monte Carlo uncertainty propagation method can be set up for a general reactor physics problem. A correlated multi-variate distribution can be sampled, we saw for instance the correlated sampling of Gaussian distributions based on the Cholesky decomposition of the covariance matrix.

But how many calculations with different sampled nuclear data we need? A good practice, widely used in several nuclear reactor applications, is to look at the averages for input and output distributions to check convergence. The convergence of Monte Carlo methods is, in fact, following the law $1/\sqrt{N}$ and it does not depend on the number of input parameters.

However if we want actually quantify how much the output joint probability distribution

is represented by the sample size we choose, statistical reasoning can be set-up resorting to the construction of non-parametric tolerance regions. The *tolerance interval* method has been commonly used in the field of nuclear reactor safety for the assessment of code output uncertainties [Guba et al., 2003]. This approach was firstly proposed by the GRS for the utilization of the SUSAN code [Glaeser et al., 1994]. To better understand the basic idea let us take a general example in the safety analysis framework, which can be considered strictly related to the main goals proposed by the present doctoral dissertation.

In safety analysis there are two approaches [Guba et al., 2003]. The former is called *conservatism*. It demonstrates that a non so realistic but rather unfavorable situation is safe, the more realistic conditions will be necessarily safer. An alternative approach, the *best estimate*, can be the investigation of the real situation, demonstrating that no safety margins can be violated. In this case the calculated values should be accompanied with uncertainty ranges, that should not overcome safety limits with a non-negligible probability.

Let us suppose to analyze a certain accident with a simulation code which takes \vec{x} as input parameters. Let us call \vec{y} the p -dimensional vector, output of the code, which collects the safety-related parameters provided with technologically relevant bounds. The system is considered safe if all the calculated variables belong to a given set of intervals [Guba et al., 2003]

$$\mathcal{S}_T = \{[L_T^{(j)}, U_T^{(j)}], j = 1, \dots, p\} \quad (5.29)$$

determined by technology. As well known, input parameters, numerical algorithm, mathematical models and physical approximations introduce bias and uncertainties. Input data can be considered as probability distributions which in principle can assume any value. Output responses are affected necessarily by input uncertainties. In principle, a best estimate calculation can be performed. If the \vec{y}_0 calculated response, given by the nominal \vec{x}_0 is in the safety bound included in \mathcal{S}_T , then the system could be considered safe. Nevertheless, a more rigorous approach might be to consider the system safe for the conditions \vec{x} , if all the calculated \vec{y} are in the safety domain \mathcal{S}_T for each $x \in \mathcal{X}$, where \mathcal{X} is the set of all possible values of \vec{x} .

In principle \mathcal{X} could be the entire real domain, if for instance input parameters are considered as random variables with Gaussian distributions. Despite of such domain can be confined by realistic limits fixed by engineering reasoning, if a possible value of \vec{x} produces a \vec{y} value outside \mathcal{S}_T , the system should be considered unsafe even if the nominal parameters give safe conditions. If the input variables are random, output vectors are still random variables with a certain probability distribution which can assume in principle values on an infinite domain. Since we can only perform a limited number of calculations, even if the every calculated outputs are safe, there is a non-zero probability that the state is actually unsafe. Performing N calculations we can infer the characteristics of such probability distribution as shown for the Monte Carlo uncertainty propagation. Reactor safety analysis physicists proposed the *tolerance interval method* to calculate the confidence we have that a certain portion of the output distribution is left out by the finite number of calculations we make. The level of confidence expresses the probability that our system is actually limited by certain boundaries and so it provides a degree of acceptability to the licensing authority.

This approach is similar to what we want to accomplish for uncertainty propagation

purposes. We perform a certain number of calculations and, from the outputs, we infer the characteristics of the response probability distribution. We want to use the tolerance interval method to determine the level of confidence we have on the assumption that a certain probability contents of the unknown response distribution is covered by the outputs we generated.

For a given set of sampled quantities y_1, \dots, y_N , the *tolerance interval method* is based on the construction of two functions $L = L(y_1, \dots, y_N)$ and $U = U(y_1, \dots, y_N)$ called (lower and upper) *tolerance limits* [Wilks, 1941, Wilks, 1942, Wald, 1943, Wilks, 1962, Guba et al., 2003] such that

$$\mathcal{P}\left\{\int_L^U g(y)dy > \gamma\right\} = \beta, \quad (5.30)$$

which says that β is the probability that at least a fraction γ of the output populations is contained in the tolerance limits. β is called *level of confidence*. There are several theories about setting the tolerance limits according to observed samples. The first work comes from Wilks [Wilks, 1941, Wilks, 1942] who gave the sample size determination for a given setting of tolerance limits, in the case of univariate output. Wald [Wald, 1943] extended the Wilks theory for multi-variate outputs. From a safety point of view, for given probability and confidence provided by the licensing authority, we can determine the tolerance limits for a sample size and see if those limits are included in the safety domain \mathcal{S}_T . For our uncertainty propagation purposes, we can set the tolerance limits and the coverage of the output population we want to obtain and see the level of confidence we get with a certain sample size.

Ackermann, Abt and Guba [Ackermann and Abt, 1984, Guba et al., 2003] provided a summary on how to design the sample size following the theories provided by Wilks, Wald and Tukey [Wald, 1943, Tukey, 1947]. We refer to the case where nothing is known about the output distribution, except perhaps that it is continuous. This case is well-known as the non-parametric tolerance regions construction for the continuous case. This seems to be quite the case for uncertainty propagation purposes. We do not know anything about the output distribution and we want to know the level of confidence of our calculations.

Let us take an univariate unknown output distribution $g(y)$. Let us call y_1, \dots, y_N the calculated output values generated by an equal number of sampling from the input hyperspace. We can arrange the outputs in ascending order where

$$y_1 = \min_{1 \leq k \leq N} y_k \quad (5.31)$$

$$y_N = \max_{1 \leq k \leq N} y_k. \quad (5.32)$$

We can define $y_0 = -\infty$ and $y_{N+1} = +\infty$. As showed by Wilks and after summarized by Wald and Guba (Refs. [Wilks, 1941, Wald, 1943, Guba et al., 2003]), for given probability content $\gamma < 1.0$ and level of confidence $\beta < 1.0$, two tolerance limits can be built as random functions $L(y_1, \dots, y_N)$ and $U(y_1, \dots, y_N)$ such that

$$\int_L^U g(y)dy > \gamma. \quad (5.33)$$

For $0 \leq r \leq s \leq N$, if we build $L = y_r$ and $U = y_s$ as tolerance limits, it can be proved (Refs. [Wilks, 1941, Wald, 1943]) that for the level of confidence β we have

$$\beta = 1.0 - I_\gamma(s - r, N - s + r + 1) = \sum_{j=0}^{s-r-1} \binom{N}{j} \gamma^j (1 - \gamma)^{N-j}, \quad (5.34)$$

where $I_\gamma(s - r, N - s + r + 1)$ is the Pearson's notation for the incomplete Beta function of the random variable γ and with shape parameters $(s - r)$ and $(N - s + r + 1)$ which can be expressed as [Guba et al., 2003]

$$I_\gamma(j, k) = \int_0^\gamma \frac{u^{j-1} (1-u)^{k-1}}{B(j, k)} du \quad (5.35)$$

$$B(j, k) = \frac{(j-1)!(k-1)!}{(j+k-2)!}. \quad (5.36)$$

Once we perform the sampling, then we proceed with the calculations, we may think to take as tolerance limits the first and the last calculated values, $L = y_1$ and $U = y_N$ respectively. In such case $r = 1$ and $s = N$ and we get the level of confidence of a *two-sided tolerance region* by the expression

$$\beta = 1 - \gamma^N - (N - 1)(1 - \gamma)\gamma^{N-1} \quad (5.37)$$

which gives the probability that our sample covers the γ fraction of the whole output population with a sample size of N . We could imagine to seek just the level of confidence of *one-sided* tolerance region, making L to tend to $-\infty$. In that case $L = y_0 = -\infty$ and we have

$$\beta = 1 - \gamma^N \quad (5.38)$$

that is equivalent to what we could obtain for a left tolerance limit taking $U = y_{N+1} = +\infty$. A right one-sided tolerance limit can be useful for safety applications. If we want for example to find out if the system is safe in specific accidental conditions, we need to respect an upper-bound limit such as maximum temperature that will give us the technological limit U_T . In that case we can perform the calculation for $\gamma = 0.95$ and $\beta = 0.95$ for instance and find the value for N . For that sample size we take y_N as the maximum calculated value. If $U = y_N < U_T$ the system is safe and we will have a 5% of probability with a 95% level of confidence that such limit will be overcome anyway.

The practical case we are going to treat concerns the uncertainty determination for multiple correlated parameters whose probability distribution is not known. To determine the sample size, we need to extend the theory seen so far to multi-variate output distributions. So we want to build non-parametric tolerance regions for the multi-variate case, supposing the output distribution continuous.

Let us now consider $\vec{y} = y_1, \dots, y_p$ distinct variables. If they were statistical independent, we would apply the results obtained so far. Since decay heat and k_{eff} values at different time and burn-up respectively are clearly correlated output variables, because they are connected by the evolution of the system during the cooling time and the depletion, we need to add new considerations summarized hereinafter (See Ref. [Guba et al., 2003]). Sampling the input hyperspace and calculate the p outputs for each sampled hypervector

gives the construction of a $p \times N$ matrix \mathbf{Y} . Setting tolerance limits for a multi-variate distribution means to find random functions $L_j = L_j(\mathbf{Y})$ and $U_j = U_j(\mathbf{Y})$, with $j = 1, \dots, N$ such that

$$\mathcal{P}\left\{\int_{L_1}^{U_1} \cdots \int_{L_p}^{U_p} \vec{g}(y_1, \dots, y_p) dy_1 \cdots dy_p > \gamma\right\} = \beta. \quad (5.39)$$

Since we do not know anything about $\vec{g}(\vec{y})$, we need to resort to techniques which allow the determination of tolerance regions for observed \vec{y} . We can follow a similar procedure to what we saw so far arranging the first row of matrix \mathbf{Y} in ascending order of magnitude, $y_1^{(1)}, \dots, y_1^{(N)}$. We select two integer r_1 and s_1 such that

$$L_1 = y_1^{(r_1)}, \quad (5.40)$$

$$U_1 = y_1^{(s_1)}, \quad (5.41)$$

$$y_1^{(s_1)} > y_1^{(r_1)}. \quad (5.42)$$

We take the elements in the second row included between the $(r_1+1)^{th}$ and the $(s_1-1)^{th}$, and we sort them in ascending order of magnitude to obtain $y_2^{(1)}, \dots, y_2^{(s_1-r_1-1)}$. From these we choose $r_2 \geq r_1$ and $s_2 \leq s_1 - r_1 - 1$ for L_2 and U_2 and we continue for all the p rows. Finally we get the p -dimensional tolerance hyperspace

$$\mathcal{T} = [L_1, U_1] \times [L_2, U_2] \times \cdots \times [L_p, U_p] \quad (5.43)$$

where

$$L_j = y_j^{(r_j)}, \quad (5.44)$$

$$U_j = y_j^{(s_j)}, \quad (5.45)$$

$$r_j \geq r_{j-1} \geq \cdots \geq r_1 \quad (5.46)$$

$$r_j < s_j \leq s_{j-1} - r_{j-1} - 1 \quad (5.47)$$

$$j = 2, \dots, p. \quad (5.48)$$

Once we have these tolerance limits the following theorem can be proved

$$\beta = 1 - I_\gamma(s_p - r_p, N - s_p + r_p + 1). \quad (5.49)$$

The choice of $r_p = 1$ and $s_p = N - 2(p - 1)$ is commonly adopted in several applications. This leads to [Guba et al., 2003]

$$\beta = 1.0 - I_\gamma(N - 2p + 1, 2p) = \sum_{j=0}^{N-2p} \binom{N}{j} \gamma^j (1 - \gamma)^{N-j} \quad (5.50)$$

for the two-sided tolerance region and

$$\beta = 1.0 - I_\gamma(N - p + 1, p + 2) = \sum_{j=0}^{N-p} \binom{N}{j} \gamma^j (1 - \gamma)^{N-j} \quad (5.51)$$

for the one-sided tolerance region.

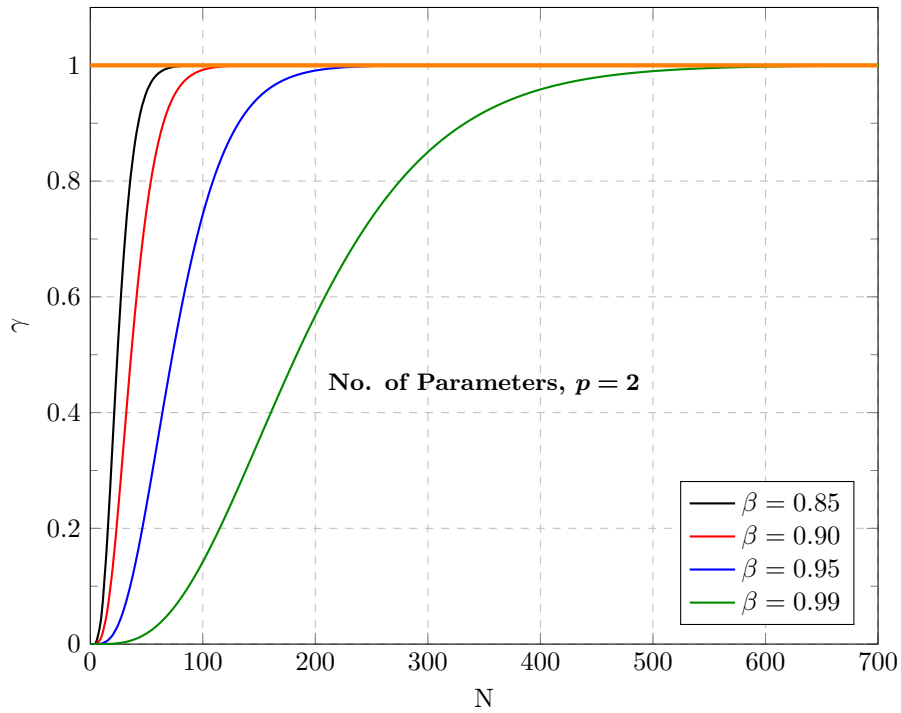


Figure 5.3: Sample size for different level of confidence β and probability content γ for $p = 2$ parameters.

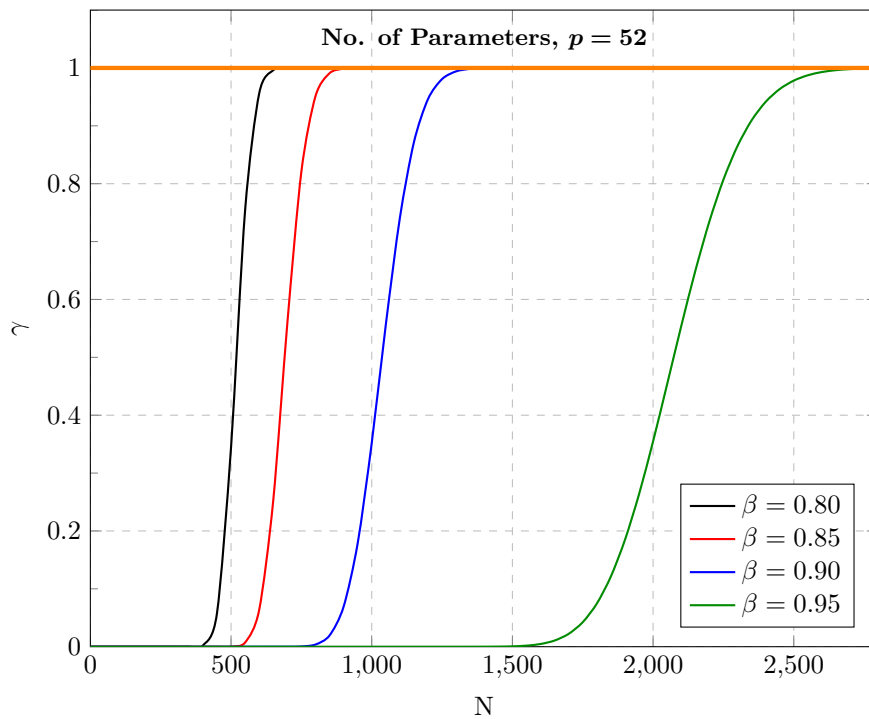


Figure 5.4: Sample size for different level of confidence β and probability content γ for $p = 52$ parameters.

In Figs. 5.3 and 5.4 some numerical results are given for $p = 2$ and $p = 52$. The latter has been taken since is the number of burn-up steps chosen in the JHR calculation scheme, as it will be clearer in Chapter 6. The level of confidence and the number of parameters play a significant role in sample size determination. For high β and p , a large number of calculations are needed to achieve a probability content γ of at least 90%. Nevertheless, the formulas proposed are quite conservative. It can be demonstrated [Guba et al., 2003] that for highly correlated parameters Eq. 5.50 overestimates the sample size. Furthermore, what we obtain from this kind of statistical treatment is the number of samples required to cover more than a portion γ of the entire unknown output population with a level of confidence β . We do not know the actual probability content, what we know is that is greater than γ with a certain probability β .

Scheffé and Tukey proposed an approximation of Eq. 5.50 which can be equivalently used to estimate the level of confidence of our calculations. The sample size for a given level of confidence β that we finally have a probability content of γ for the output population can be determined by [Sheffé and Tukey, 1944, Ackermann and Abt, 1984]

$$N = m \frac{\left(\frac{\chi_{\beta, 2m}^2}{2m} - 1 \right) \sqrt{\gamma} + 1}{1 - \gamma}, \quad (5.52)$$

where $\chi_{\beta, 2m}^2$ is the β -quantile⁹ of the χ^2 distribution with $2m$ degrees of freedom, where m is the number of tolerance regions. For two-sided tolerance regions constructions, m will be equal to the double of the number of output parameters p . This formula was born for single output treatment, but as explained in Ref. [Sheffé, 1943], it can be used to determine the sample size for multi-variate cases as faster method to evaluate the sample size than Eq. 5.50. In Chapter 6, some numerical applications of FY uncertainty propagations on reactivity loss and decay heat will be presented.

5.4 The URANIE-APOLLO-MENDEL Coupling

In this section we describe briefly what we actually implement in order to effectively perform the Monte Carlo uncertainty propagation for our purposes. We decided to use the URANIE platform [Gaudier, 2010], a set of libraries based on the ROOT framework¹⁰. URANIE has been coupled to APOLLO2 and MENDEL to post-process reactivity and decay heat calculations for different set of sampled nuclear data.

5.4.1 The URANIE Platform

URANIE is a set of libraries written in C++ for uncertainty, optimization and sensitivity analysis. The main features of URANIE can be summarized as follows:

- i) Design of experiments. This set of libraries allow the sampling of different statistical distributions using different techniques, such as the LHS. These libraries have been used in this work to sample nuclear data distributions, preserving correlations (see Cholesky decomposition method in Sec. 5.3.2).
- ii) Clustering methods.

⁹With β -quantile we mean $\int_0^\beta \chi_{2m}^2(x) dx$.

¹⁰ROOT is a modular scientific software framework that provides tools for data analysis and processing.

- iii) Surrogate models (polynomial, artificial neural network, kriging, etc.).
- iv) Non-intrusive spectral projection such as the generalized chaos polynomials method.
- v) Uncertainty inverse quantification methods.
- vi) Sensitivity analysis tools, such as the local derivative-based methods, the Sobol coefficients estimation, the Morris method etc.
- vii) Multi-criteria optimization procedures.

In the present work URANIE was essentially used as Monte Carlo sampling engine and as interface for data mining. It can in fact well handle different parallel calculations on PC and cluster machines. No sensitivity analysis tools were used for our purposes and the coupling with reactor physics code was built up by the candidate, implementing C++ scripts to provide to the URANIE C++ interpreter.

5.4.2 Reactivity and Decay Heat Uncertainty Propagation

In this section we describe the procedure we adopted to estimate uncertainty for decay heat and reactivity loss, using Monte Carlo propagation. In Fig. 5.5 the flow-chart of the procedure we set-up for the Monte Carlo FY uncertainty propagation is given. The CONRAD-generated correlation matrices for independent yields are given as input to URANIE to sample FY data. FY can be supposed as Gaussian or Log-normal distributions. Normally Log-normal distributions are preferable for FY since very low values can occur, and the related Gaussian distributions can present non-negligible negative tails.

Once URANIE has generated N FY files, where N is the sample size, sampled data are employed directly to generate an equal number of MENDEL input files. MENDEL solves the Bateman equation acquiring directly independent fission yields. Nevertheless, to calculate the contribution coming from neutron-nuclei interactions, self-shielded cross sections and fluxes are needed. These data are provided by APOLLO2 through the generation of MENDEL-readable files, called SAPHYBS.

As already explained in Sec. 3.3.2.5, independent FY are not directly used by APOLLO2 for neutronic calculations. CONRAD is able to generate FY data for APOLLO2 once the list of fission products used in the calculation is provided. Such procedure can take place thanks to the generation of a special-purpose Q-matrix as explained in Sec. 3.3.2.5. Just as reminder, the APOLLO2 Q-matrix is nothing else than a standard Q-matrix obtained by a special branching ratio matrix \mathbf{B} with APOLLO2 fission products considered as stable nuclei. The radioactive decay of such products will be in fact correctly incorporated during the depletion calculation. Such partial cumulative FY are then provided to APOLLO2 to perform the depletion calculation solving the time dependent Boltzmann equation with a quasi-static method.

Decay heat and reactivity are finally post-processed to find the associated uncertainties due to FY. In the next section we propose some results on applications using the Monte Carlo procedure just proposed and the deterministic method based on direct perturbation calculations to estimate sensitivity coefficients.

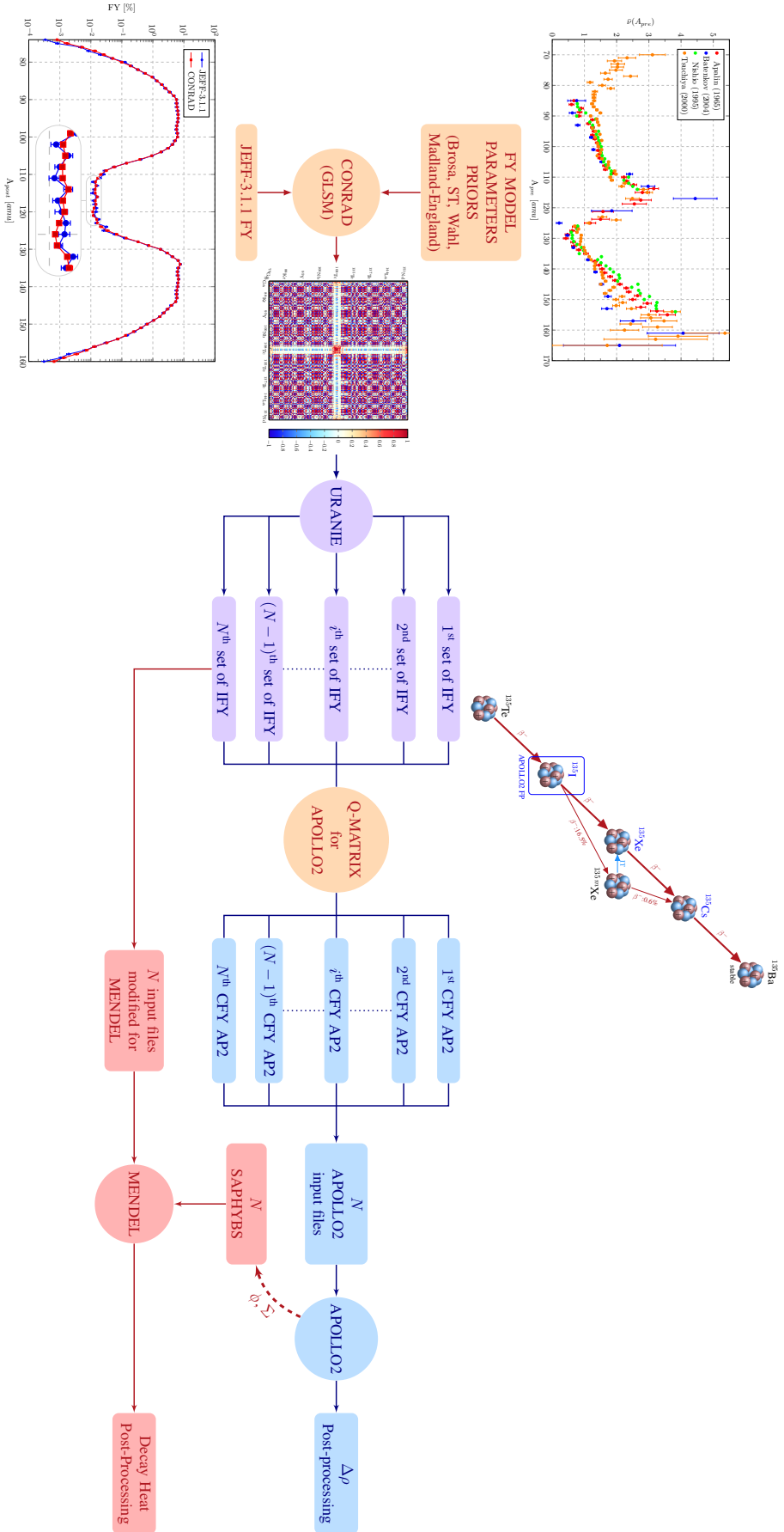


Figure 5.5: Schematic representation of the URANIE-APOLLO2-MENDEL coupling for Monte Carlo uncertainty propagation.

5.5 Conclusions

In this chapter we have seen the methodologies we propose to propagate nuclear data uncertainties in depletion calculations for our purposes. We want to test and see the impact of the FY covariance matrices we calculated using CONRAD and to do that we resort to two methods. Since estimating reliable sensitivity coefficients using the solution of the adjoint equations for the neutron transport and the nuclei concentrations is not trivial at all and for our purposes we decided to adopt easy-to-implement techniques.

The first method we use is deterministic and employs the well-known uncertainty propagation law or sandwich rule. To calculate sensitivities a very flexible and straightforward procedure is based on finite differences obtained by one-sigma perturbation calculations.

Since the direct perturbation method relies on a non-negligible linear approximation and since the coupled Boltzmann-Bateman problem can possibly hide some important non-linearities we decided to set-up also a Monte Carlo method to propagate FY uncertainties. The main features of the method has been presented in Sec. 5.3, including the description of correlated random variable sampling techniques and the LHS for random number generation. The sample size issue has been treated, proposing some statistical reasoning to assign a certain level of confidence to our calculations. The tolerance region theory, commonly applied in nuclear reactor safety calculations, has been proposed to estimate the probability to cover a certain fraction of the output population and will be applied in the next chapter.

In the next chapter we will see some practical results on applications. The FY covariances generated using CONRAD will be propagated to see the impact on decay heat and reactivity for some simple test-case geometries and for whole reactors such as the JHR.

Chapter 6

Uncertainty Quantification on Nuclear Reactor Applications

Contents

6.1	Reactor Applications Description	162
6.1.1	The PWR Pin-Cells	162
6.1.2	JHR Calculations in Reference Configuration	165
6.2	Sensitivity Coefficients Validation	166
6.3	FY Covariance Matrices Testing	171
6.3.1	U-235 Thermal Fission	171
6.3.2	Pu-239 Thermal Fission	184
6.3.3	Pu-241 Thermal Fission	189
6.3.4	U-238 Fast Fission	192
6.4	Conclusions	193

THE uncertainty quantification of integral reactor parameters is a fundamental task for safety and economic purposes. It presumes the combination of sensitivity and covariance information to evaluate the impact of nuclear data on the final target outcomes. To do so, sensitivity and uncertainty propagation techniques are required. In Chapter 5, we proposed two methods. The first one is based on direct perturbations to perform sensitivity coefficient calculations. Estimating sensitivities using simple finite differences supposes the model to be perfectly linear. To *validate* such method in depletion calculations, where the neutron balance equation is coupled to the nuclei concentrations evolution, the second method consisted in a Monte Carlo uncertainty procedure. Monte Carlo uncertainty propagation techniques have the capability to represent a wide range of problems, even those affected by strong non-linearities. They are relatively straightforward to implement and based on recognized statistical principles. The major drawback is that many calculations (of the order of 1000) are generally required. They also need assumptions on the basic nuclear data distributions sampled and they add to the final outcome uncertainty a certain stochastic component that must be reduced as much as possible.

Once the reference configuration of the reactor problem we analyze and the uncertainty propagation strategies are available, nuclear data correlations should be collected. To demonstrate the reliability of FY covariances we evaluated using CONRAD, and to test their impact on real applications, we propagate JEFF-3.1.1 and CONRAD FY uncertainty information in simple test-case problems and on JHR loss of reactivity. This allowed also

to determine if the FY covariances seen in Chapter 4 are actually suitable to be included in the JHR uncertainty estimation analyses.

6.1 Reactor Applications Description

In this chapter FY covariance matrices generated using CONRAD are tested to verify their reliability and impact on reactor applications. We are interested in reactivity loss and decay heat uncertainties. Reactivity in a nuclear reactor decreases mainly due to the fissile actinides burn-up. However a relevant contribution is given by neutron absorbing fission products, which have high capture cross sections. Fission products have an important impact on reactor neutronics, this is the reason why FY can significantly affect the reactor neutron balance. Reactivity loss uncertainty due to FY data must be then estimated for safety and economic purposes. The reactivity loss during depletion determines in fact the cycle length, that, in the case of the JHR, is only 27 days in nominal conditions. The reactivity loss can be calculated once the k_{eff} is known, using the following simple formula

$$\Delta\rho(t) = \rho(t) - \rho^{BOL} = \frac{k_{eff}(t) - 1}{k_{eff}(t)} - \frac{k_{eff}^{BOL} - 1}{k_{eff}^{BOL}} = \frac{1}{k_{eff}^{BOL}} - \frac{1}{k_{eff}(t)}, \quad (6.1)$$

where ρ is the reactivity and with ρ^{BOL} we indicate its Beginning Of Life (BOL) value.

The decay heat, on the other hand, has been analyzed only in pin-cell applications for covariance testing purposes. Radioactive fission products in exhausted fuel assemblies continue to decay releasing heat that has to be dissipated. Determining the decay heat uncertainty due to nuclear data is certainly a fundamental task from the safety point of view.

Before proceeding with the results on integral reactor parameter uncertainties due to FY, let us describe the applications we actually considered in the calculations. We performed analyses for a UOX-PWR pin-cell, a MOX-PWR pin-cell and the JHR bare core in reference configuration.

6.1.1 The PWR Pin-Cells

Fig. 6.1 shows a schematic representation of the UOX and MOX pin-cells used in APOLLO2 calculations.

Both cell calculations have been performed solving the 281-groups approximation of the transport Boltzmann equation through a quasi-static method of collision probabilities [Reuss, 2008, Hébert, 2009], implemented in APOLLO2. APOLLO2 generates MENDEL-readable files called SAPHYBS, which collect fluxes and self-shielded cross sections collapsed in one energy group for the nuclei concentration evolution calculations.

Both pin cells are characterized by a 1.26 cm pin pitch. The fuel radius, neglecting material thermal expansion, is 0.4063 cm. The external radius of the cladding, still ignoring zircalloy thermal expansion, is 0.475 cm. The fuel-cladding gap is 0.0067 cm (see Fig. 6.1). For both calculations, we supposed a fuel and cladding temperatures of 600 °C and 300 °C respectively. They are cooled by 151 bar-pressurized light water at 300 °C, with 600 ppm of Boron.

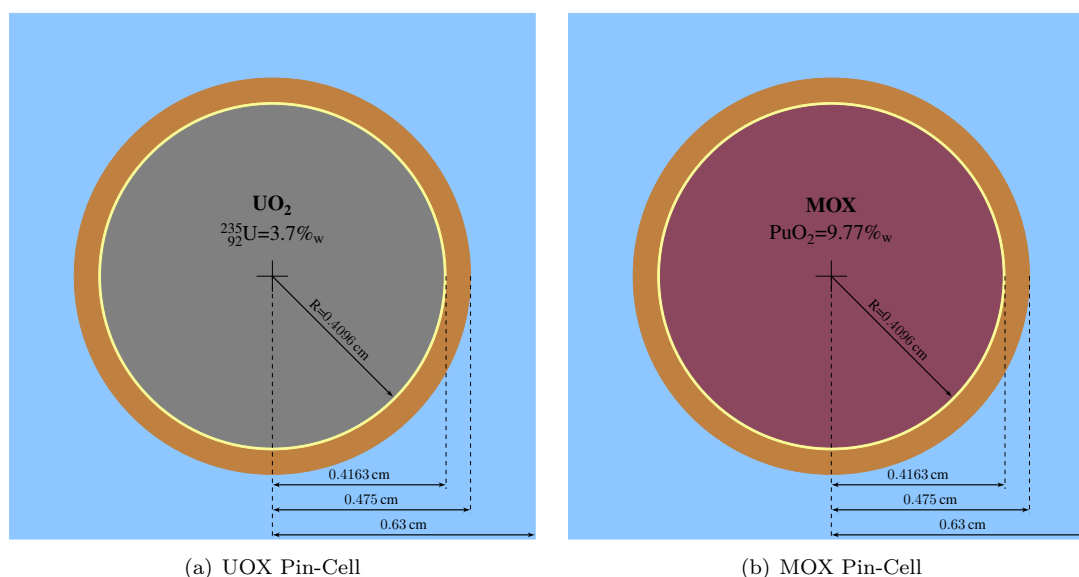


Figure 6.1: Schematic representation of the UOX and MOX pin-cells.

The UOX-pin-cell fuel is 3.7%_w-enriched in ^{235}U ¹. 0.0366%_w and 0.00025%_w are respectively the ^{234}U and ^{236}U contents, the remaining portion is of course ^{238}U , for a UO_2 density of 10.96 g/cm³. For a fuel specific power of 38 W/g, the end-of-cycle burn-up chosen for this calculation scheme is of 45 000 MW d/t, subdivided in 54 calculation steps for the quasi-static evolution problem. Once the SAPHYBS are provided, MENDEL calculates the decay heat for a 45 000 MW d/t burned fuel in 45 instants of time, from 0.1 s to 7.0×10^9 s.

The MOX²-pin-cell presents a Uranium-Plutonium Oxides mixture fuel, with a 9.77%_w of Pu content. The isotopic concentrations for PuO_2 are given in Tab. 6.1, for a density of 11.46 g/cm³. For its characteristics, this kind of fuel allowed us to test covariance matrices for Plutonium isotopes in a more comprehensive way.

Isotope	Concentrations [% _w]
^{238}Pu	2.5
^{239}Pu	54.5
^{240}Pu	25.2
^{241}Pu	8.6
^{242}Pu	7.9
^{241}Am	1.3
Total	100

Table 6.1: Isotopic fraction for the PuO_2 contained in the MOX fuel.

For a fuel specific power of 39.68 W/g, the end-of-cycle burn-up chosen for this calculation scheme is of 49 200 MW d/t, subdivided in 59 calculation steps for the quasi-static evolution problem. The same cooling times picked for the UOX cell were chosen to perform decay heat calculations.

¹The fuel characteristics are important since our main goal is to propagate FY covariances, investigating the differences

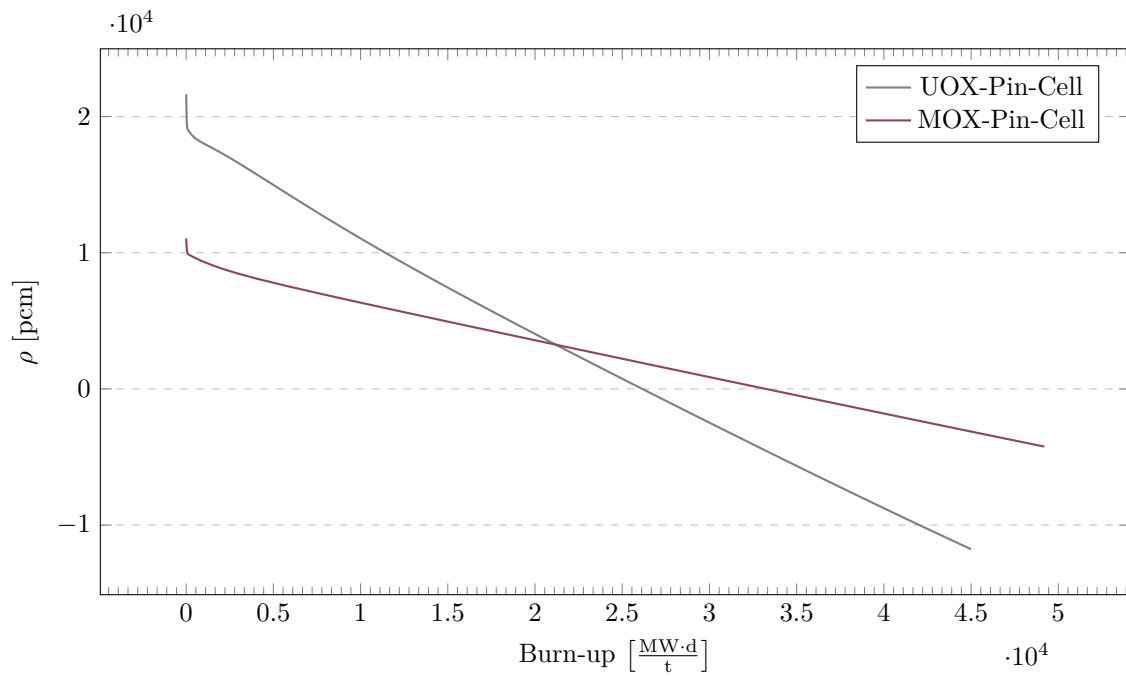


Figure 6.2: Nominal reactivity values in pcm as function of burn-up for the UOX and MOX pin-cells evolution.

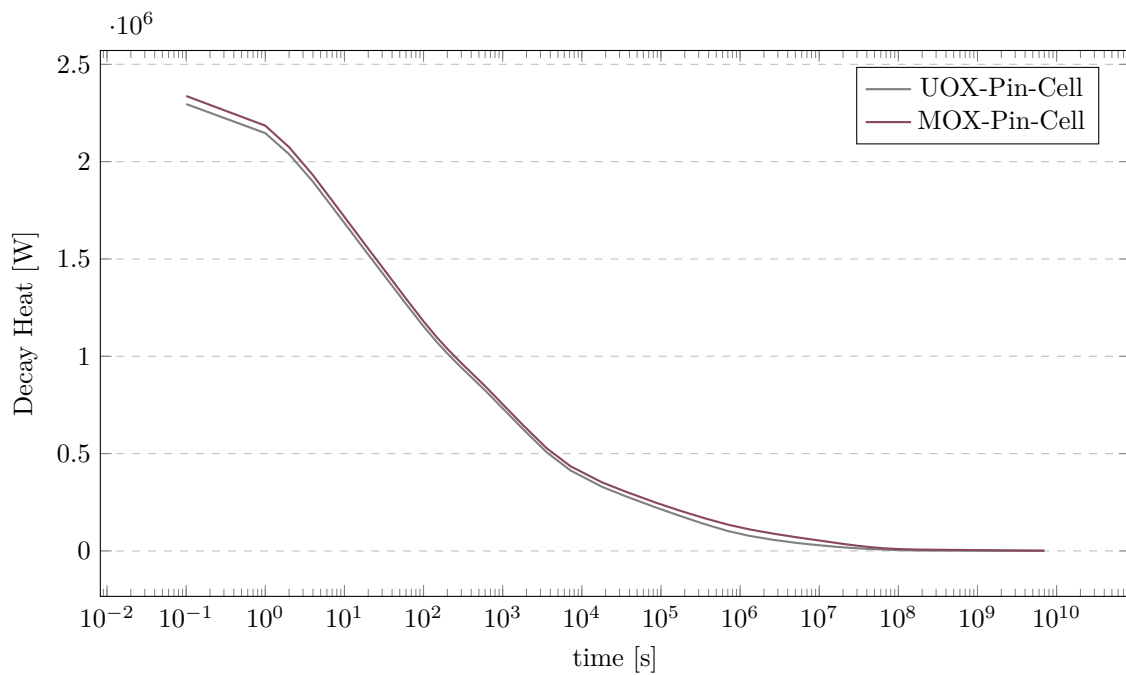


Figure 6.3: Nominal decay heat values in W as function of time for the UOX and MOX pin-cells evolution.

Nominal values for the UOX and MOX pin-cells reactivity loss and decay heat are provided in Figs. 6.2 and 6.3. Since lattice calculations for the PWR pin cells were taken into account, with zero current boundary conditions, $k_\infty < 1.0$ values were reached during the cell evolution, yielding to negative reactivity values. Except for the initial burn-ups, PWR cell reactivity seems to decrease linearly during depletion. This allows us to find a proportional correlation between reactivity loss and cycle length uncertainty.

6.1.2 JHR Calculations in Reference Configuration

The JHR was conceived to perform several simultaneous in-core and in-reflector irradiation experiments, yielding to many possible machine configurations. For our purposes, we decided to perform reactivity uncertainty propagation for the bare core in reference configuration. Without any experiments and with the hafnium control bars totally withdrawn, the reference geometry is constituted by 37 cylindrical assemblies with a 27%-enriched U_3Si_2Al fuel, releasing a nominal power of 100 MW.

The simulation platform (neutronics code and nuclear data), dedicated to JHR, is called HORUS3D/N³ (HOrowitz Reactor simulation Unified System [Döderlein et al., 2008]) and it has been developed in the last ten years by CEA-Cadarache. The HORUS3D package gathers all the necessary tools, specifically dedicated to the JHR design and safety studies. Several modules are devoted to different tasks, neutronics (HORUS3D/N), radiative transport (/P), fuel cycle (/Cy), core and system thermo-hydraulics (/Th and /Sys) [Vaglio-Gaudard et al., 2014].

HORUS3D/N relies on APOLLO2 and CRONOS2 [Lautard et al., 1990] performing a deterministic 2-step reactor calculation, using JEFF-3.1.1 evaluated nuclear data. During the lattice calculation step, self-shielded and depleted cross sections, obtained by 172-groups Collision Probability (CP) 2D calculations, are collapsed in 6 energy groups. For the reflector, the lattice phase is performed by 20-groups Method of Characteristics⁴ (MOC, see Ref. [Hébert, 2009]) 2D calculations, due to its heterogeneity⁵. The second step consists in a 3D full core diffusion calculation on a hexagonal spatial mesh using the cross sections homogenized and collapsed during the first step.

The numerical validation of the neutronic calculation scheme has been performed using two kinds of reference calculations. For the JHR-Beginning of Life (BOL) configuration, the modeling biases have been estimated comparing the 3D multi-group 2-steps deterministic calculation to a 3D continuous-energy Monte Carlo TRIPOLI4 run. During depletion, biases have been assessed comparing HORUS to a fine mesh 22-groups APOLLO2-MOC calculation [Vaglio-Gaudard et al., 2014]. The 22-groups MOC bare core configuration, with 37 fuel assemblies, has been then chosen to perform FY uncertainty propagation and to test CONRAD covariances.

Performing 22-groups MOC calculations with a refined unstructured mesh requires considerable memory and time resources. The uncertainty propagation methodologies

between conventional existing nuclear technologies and highly enriched experimental facilities, such as JHR.

²Mixed Oxide fuel, made of depleted Uranium (0.3%-enriched) and Plutonium oxides.

³N stands for Neutronics.

⁴The Method of Characteristics solves iteratively the characteristic form of the Boltzmann equation over tracks crossing the whole domain. A multi-group approximation is generally used to simplify the energy description and the spatial domain is subdivided in regions with piece-wise homogeneous nuclear properties [Hébert, 2009].

⁵The MOC is generally preferred to the CP when the number of spatial regions is greater than one hundred.

proposed so far in Chapter 5 demand for numerous runs, especially if we think about the Monte Carlo technique.

If we want to perform Monte Carlo uncertainty propagation with a statistically relevant confidence, we need at least 1000 calculations to cover more than 90% of the output population. Sensitivities estimation through direct perturbations, on the other hand, require $2N+1$ runs, where N is the number of FY analyzed. A single 22-groups MOC reference calculation demands for 8 Gb of memory, taking about 40 h to be performed on a conventional machine. To make JHR uncertainty propagation feasible, MOC parameters have been modified to decrease the required computational efforts and save time. A coarser mesh has been then adopted and the quadrature parameters for the flux numerical integration over the characteristic have been modified. This induced to have a 200 pcm bias on the k_{eff} , which has been maintained during the whole fuel cycle in the depletion calculation, requiring roughly 4 Gb of memory and 30 h of computational time⁶. In Fig. 6.4 the modified MOC reactivity as a function of the fuel burn-up is presented.

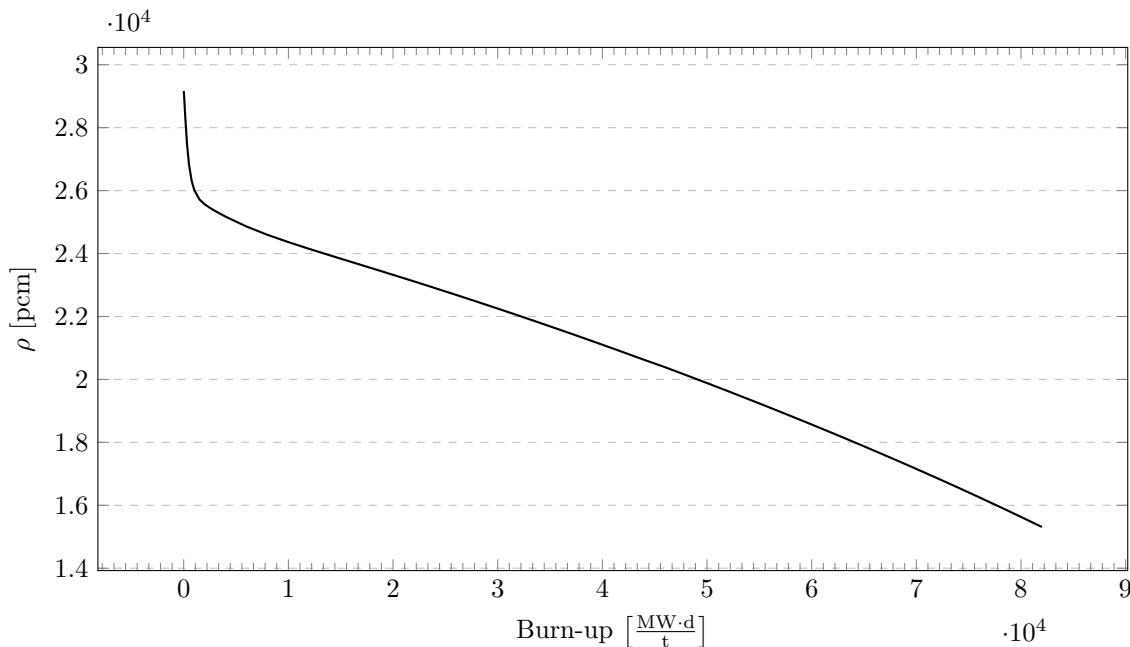


Figure 6.4: Nominal reactivity values in pcm as function of burn-up for the JHR evolution.

6.2 Sensitivity Coefficients Validation

As explained in Chapter 5, two main methods were chosen to perform FY uncertainty propagation. Direct perturbation sensitivities have been used in the sandwich formula (see Eq. 5.10) to estimate reactor parameter covariances, propagating JEFF-3.1.1 evaluated data and CONRAD results. Since the coupled Boltzmann-Bateman system of differential equations numerically solved in depletion calculations could present some non-linearities which might not be caught by direct perturbations, a Monte Carlo methodology was set up to test the validity of the sensitivities we calculated.

⁶The actual motivation of changing MOC parameters derived from the available computational capacity. JHR calculations have been performed on a 128-CPU cluster, whose processors have only 5 Gb of dedicated memory. A so long calculation, in fact, could not be performed multiple times on personal work-stations.

Monte Carlo uncertainty propagation methods require a sample size of the order of one thousand to converge to the output distribution. Sensitivity estimations through direct perturbations demand for $2N+1$ calculations, where N is the number of input parameters. For the thermal neutron induced fission of ^{235}U , the number of FY in the evaluated JEFF-3.1.1 library is about 900. To considerably reduce the number of calculations for sensitivity assessments, only the uncertainties of the most significant FY ($\geq 10^{-4}$) were propagated⁷. The impact of FY data derives, in fact, from the physical properties of the fission products they refer to. FY sensitivities to reactivity loss are, for instance, related to fission product capture macroscopic cross sections, which depends on nuclei concentrations. As confirmed by CYRUS results and by the sensitivities calculations we performed during the present work, only those fission products which present a quite significant yield are actually affecting reactivity and decay heat calculations.

Let us start from the uncertainty propagation of ^{235}U thermal neutron induced FY on the reactivity loss and decay heat of a UOX pin-cell. In such case the highest number of correlated outcomes we are interested in is 54. 54 is in fact the number of steps performed by APOLLO2 in the quasi-static calculation scheme chosen for this type of pin-cell. We are interested to evaluate the reactivity loss uncertainty during the all depletion cycle. Therefore, all the k_∞ values, at different burn-up steps, have been considered⁸. The number of decay heat values are instead calculated at 45 time instants. Decay heat can be considered correlated in some sense to k_{eff} . They both depend, in fact, on the irradiation conditions and on the materials characterizing the reactor assemblies. If for instance a FY for a neutron absorber is also unstable, contributing significantly to the decay heat after shut down, it will be certainly a non-negligible source of correlation. However, for a sake of simplicity, we did not considered cross correlations between decay heat and reactivity, focusing only on reactivity in sample size determination.

The approximated formula proposed by Scheffé and Tukey (see Refs. [Sheffé and Tukey, 1944, Ackermann and Abt, 1984] and Eq. 5.52) has been used for $p = 54$ parameters. It can provide the sample size in few seconds, using advanced calculation platform such as *Mathematica*. It is completely equivalent to what might be obtained from Eq. 5.50, the two formulas have been tested, providing same results.

Using Eq. 5.52 as a two-sided tolerance region formula, the number of tolerance regions (called m in Eq. 5.52) for 54 parameters are then 108. In Tab. 6.2, the sample sizes for the reactor problems presented so far are provided. For the UOX-pin-cell we propose to use 2504 calculations applying the Monte Carlo methodology. This allows a 95% level of confidence that a fraction greater than 0.95 of the output population, made of 54 values, will be covered by the Monte Carlo calculations with different sampled FY.

⁷This brings the number of FY from about 900, contained in JEFF-3.1.1, to 247, for the thermal fission of ^{235}U .

⁸The pin-cell calculation we perform for this uncertainty propagation test can be thought as the first step lattice calculation for reactor physics analysis. The leakage term is imposed to make the $k_{eff} = 1.0$. To see effects on reactivity due to FY variations, k_∞ values have been post-processed.

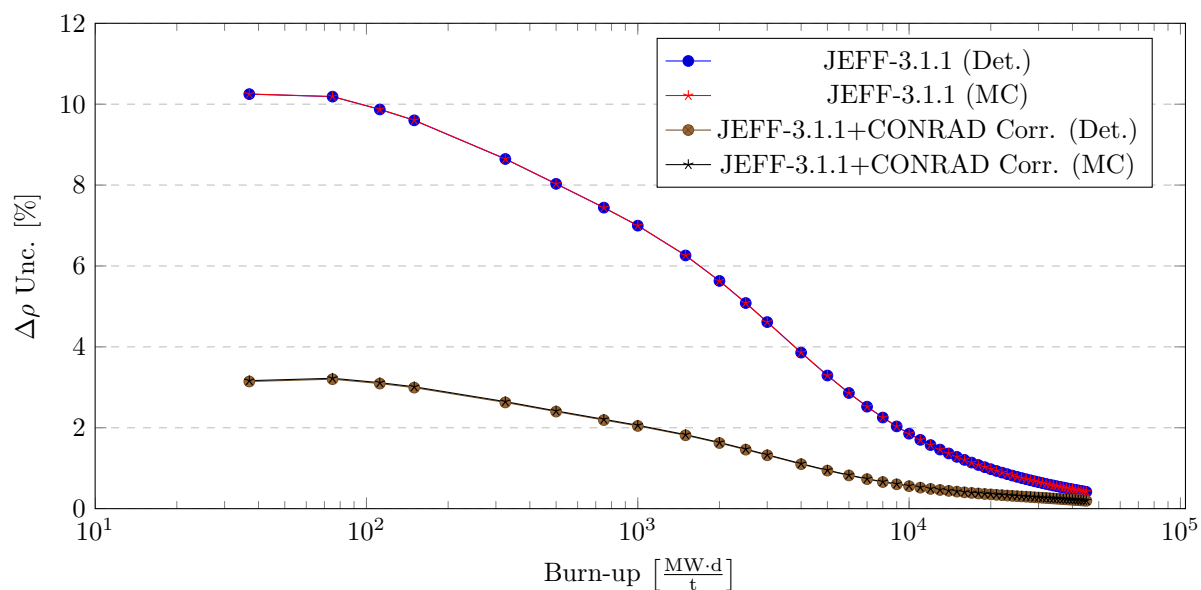


Figure 6.5: Reactivity loss uncertainty as function of burn-up for the propagation of ^{235}U thermal neutron induced FY on a UOX-pin-cell calculation. The results obtained using the sandwich formula (Det.) applied on sensitivities which were deduced from direct perturbations are in excellent agreement with Monte Carlo estimates (MC).

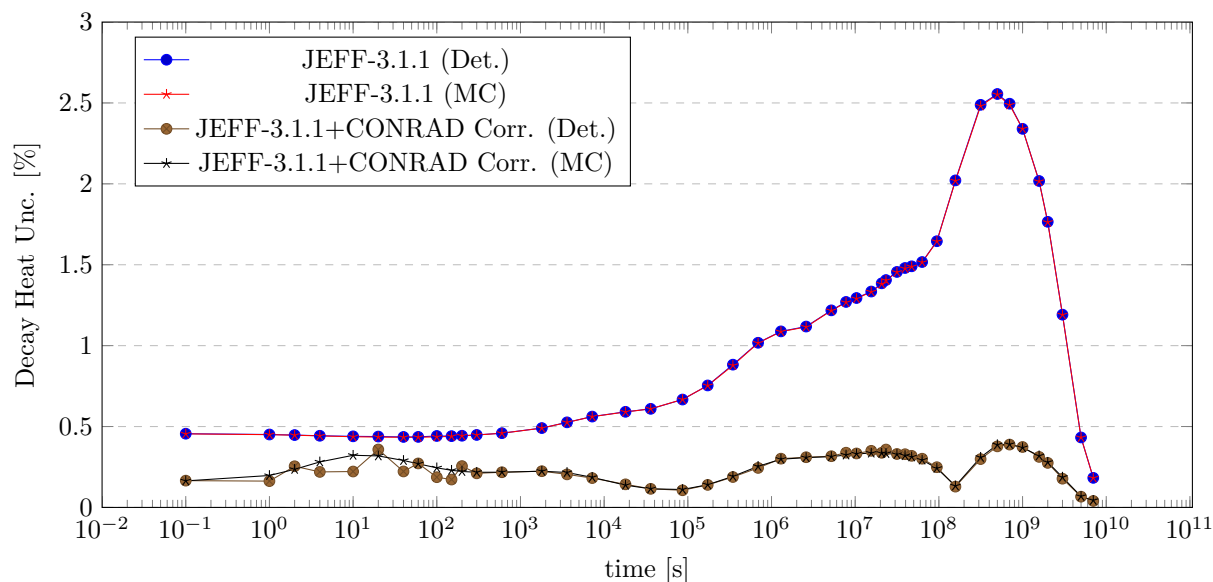


Figure 6.6: Decay heat uncertainty as function of time for the propagation of ^{235}U thermal neutron induced FY on a UOX-pin-cell calculation. The results obtained using the sandwich formula (Det.) applied on sensitivities which were deduced from direct perturbations are in excellent agreement with Monte Carlo estimates (MC).

	$\beta = 0.90$			$\beta = 0.95$			$\beta = 0.99$		
	$\gamma = 0.90$	$\gamma = 0.95$	$\gamma = 0.99$	$\gamma = 0.90$	$\gamma = 0.95$	$\gamma = 0.99$	$\gamma = 0.90$	$\gamma = 0.95$	$\gamma = 0.99$
$p = 52$									
N	1166	2339	11720	1204	2418	12124	1289	2571	12906
$p = 54$									
N	1208	2423	12145	1247	2504	12556	1323	2660	13351
$p = 59$									
N	1314	2635	13205	1355	2719	13633	1434	2881	14460

Table 6.2: Application of the Scheffé and Tukey formula $N = m \frac{\left(\frac{\chi_{\beta, 2m}^2 - 1}{2m}\right) \sqrt{\gamma+1}}{1-\gamma}$ to PWR-pin-cells and JHR cases. The parameter values we look at are 52, 54 and 59 in the three quasi-static calculations.

In Figs. 6.5 and 6.6 reactivity loss and decay heat uncertainty calculations for the UOX-pin-cell are shown. We propagated JEFF-3.1.1 evaluated ^{235}U thermal neutron induced FY uncertainties on integral reactor parameters with and without correlations⁹. In the Monte Carlo uncertainty propagation we supposed FY distributed as Gaussian functions centered in JEFF-3.1.1 evaluated best estimates and provided with standard deviation equal to the associated evaluated uncertainty. To fully validate sensitivities, we considered also the case of highly correlated yields including CONRAD correlation results, but maintaining JEFF-3.1.1 variances. We obtained excellent agreement in both cases, with and without including CONRAD correlations. Only for the decay heat uncertainty (see Fig. 6.6) we observed slight negligible differences in the case correlations were included¹⁰.

To see if the two uncertainty propagation methods were effectively equivalent, we compared also correlation matrices on reactivity loss and decay heat. To do so, the Frobenius matrix norm (given in Eq. 6.2) was used to quantify how much the matrices were close. Once the difference matrices were calculated for decay heat and reactivity loss performing a term-by-term subtraction, the following norm was applied:

$$\|\mathbf{A}\|_{\mathcal{F}} = \sqrt{\sum_{i=1}^m \sum_{j=1}^m |A_{ij}|^2} \quad (6.2)$$

where \mathbf{A} is a generic $m \times m$ square matrix. In Fig. 6.7 the reactivity loss and the decay heat difference matrices are shown. No significant discrepancies were found especially for reactivity. This was also confirmed by the calculated norms. For the reactivity loss difference matrix a Frobenius norm of 0.29 was found. This is telling reasonably that the matrix is close to zero, especially if compared to single reactivity matrix norms of 43.3 and 43.4 respectively for the sandwich rule and the Monte Carlo method. For decay heat things went slightly different as saw also for the uncertainty values. A norm of 4.1 was found for the difference matrix, while 26.2 and 26.4 were the norms for sandwich rule and Monte Carlo matrices.

⁹We propagate JEFF-3.1.1 variances including CONRAD correlations. Doing so is not perfectly rigorous, however, the final goal here is to verify that the two methodologies are equivalent with both diagonal and full variance-covariance matrices.

¹⁰The impact of CONRAD correlations will be discussed further in the next dedicated sections.

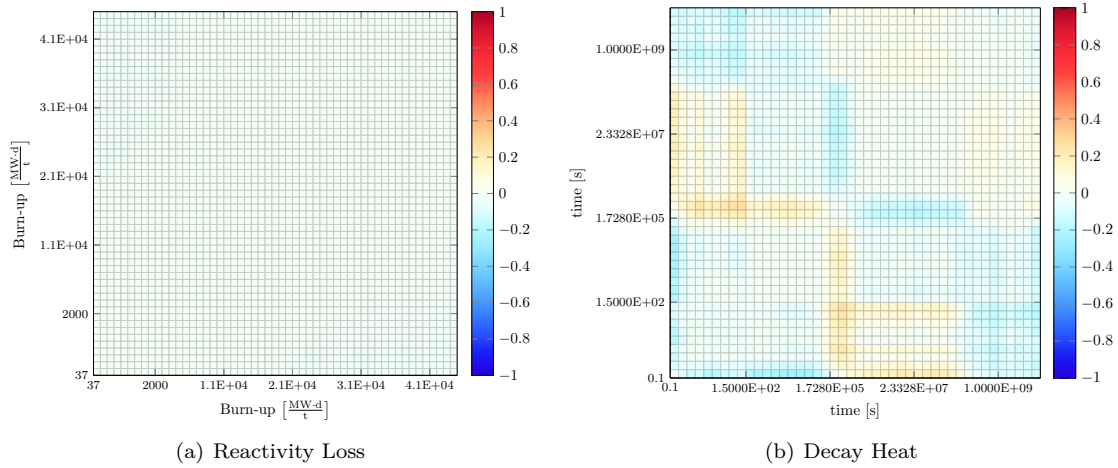


Figure 6.7: Difference correlation matrices for reactivity loss (left) and decay heat (right) for the UOX pin-cell. The two matrices have been obtained subtracting term-by-term the correlation matrices obtained using the sandwich formula and the Monte Carlo uncertainty propagation.

Since the JHR is the target application, we repeated the same exercise for its reactivity loss to see if the sensitivities calculated for the ^{235}U thermal neutron induced FY are validated by the Monte Carlo uncertainty propagation. As explained in Section 6.1.2, performing Monte Carlo uncertainty analysis using the reference MOC calculation scheme is not straightforward and requires significant efforts in term of computational cost and time. Therefore, we decided to perform the lowest number of calculations provided in Tab. 6.2, taking a sample size of 1166 for the Monte Carlo method. It provides, for 52 parameters, a confidence of 90% of covering a 90%-fraction of the output population.

The analysis of the two correlation matrices and of the reactivity loss uncertainty (see Fig. 6.8), obtained by the application of the sandwich formula and the Monte Carlo method, led to the same conclusions drawn for the UOX-pin-cell. No significant discrepancies were noticed, a norm of 0.63 was obtained for the difference matrix. The two correlation matrices showed a norm of 46.3 and 46.5 for the sandwich formula and the Monte Carlo method respectively.

The comparison between a Monte Carlo uncertainty propagation and the simple application of the sandwich rule induced us to accept linear approximations as precise enough for our purposes. For the PWR-pin-cell and the JHR problems in fact, FY uncertainty propagation does not present any non-linearity issues that can justify an extensive use of the Monte Carlo method, which is quite time consuming, even if it is straightforward to implement and based on statistical recognized principles. In the next sections, results on FY uncertainty propagation are presented, adopting the sensitivities calculated as explained so far and the application of the sandwich formula.

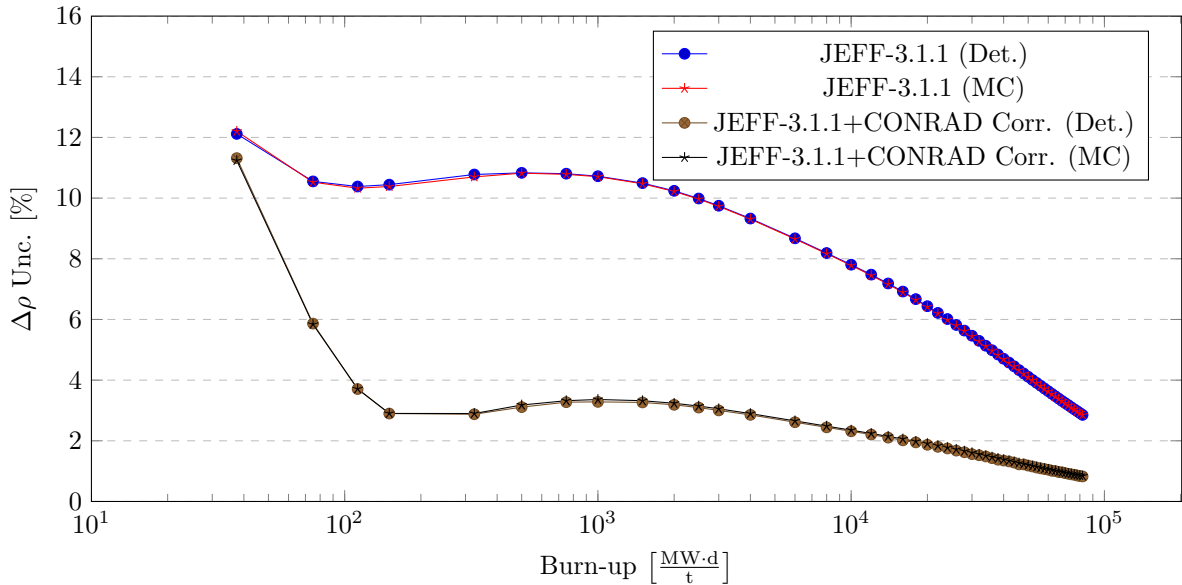


Figure 6.8: Reactivity loss uncertainty as function of burn-up for the propagation of ^{235}U thermal neutron induced FY on JHR MOC calculation. The results obtained using the sandwich formula (Det.) applied on sensitivities which were deduced from direct perturbations are in excellent agreement with Monte Carlo estimates (MC).

6.3 FY Covariance Matrices Testing

In Chapter 4 we saw some results on FY covariance matrices using the CONRAD code. In this section, some results obtained by the yield uncertainty propagation of the most significant fissioning systems are presented. In particular, we study the impact of CONRAD covariances on target engineering parameters for the applications described so far. This allowed us to draw some conclusions on the reliability of the uncertainty information we generated and to understand if such information are applicable in JHR reactivity loss analyses.

6.3.1 U-235 Thermal Fission

Let us start testing the covariances generated for thermal neutron induced fission of ^{235}U . The first application we look at is the UOX-pin-cell. In Fig. 6.9 the reactivity loss uncertainty obtained by JEFF-3.1.1 ^{235}U thermal FY variances propagation is shown. The total uncertainty is presented together with the most significant FY contributions, emphasized with different colors. Performing direct perturbation sensitivity assessments allowed us in fact to distinguish single FY impact on final parameter uncertainties, which is not possible for Monte Carlo methods, unless distinct calculations are performed.

The analysis showed that the most significant contributions to reactivity loss uncertainty come from ^{135}Te and ^{135}I independent FY. The reason why these two independent FY are so important becomes clear if we look at their decay products and times. In Fig. 6.10 the capture cross section for ^{135}Xe is shown.

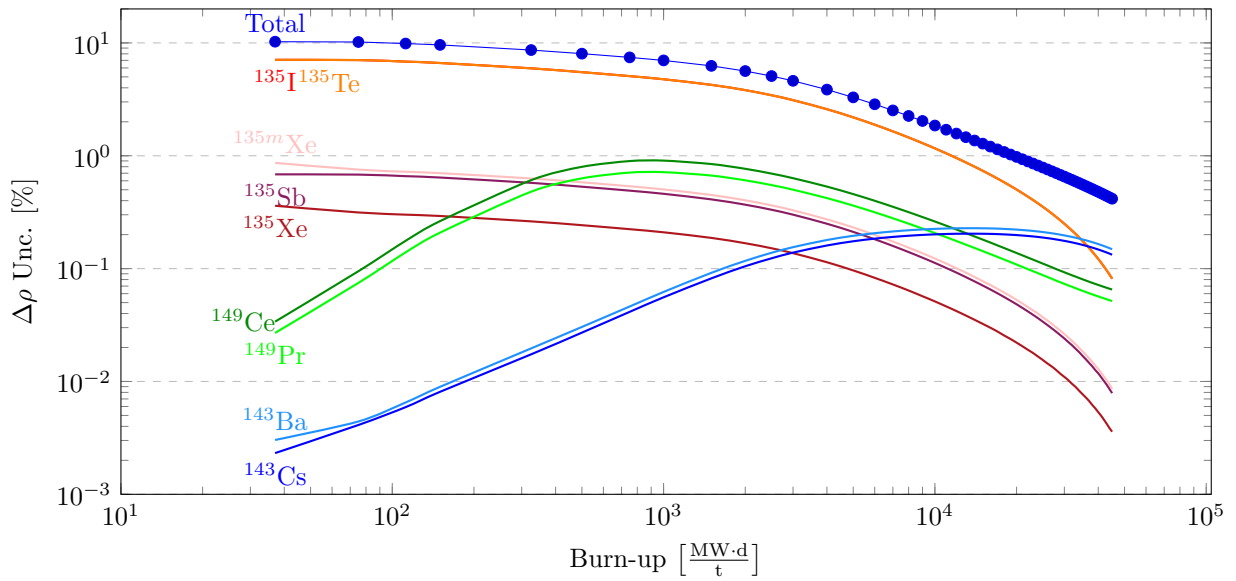


Figure 6.9: UOX-pin-cell reactivity loss uncertainty due to the yields of the thermal neutron induced fission of ^{235}U . The total uncertainty is given by the propagation of JEFF-3.1.1 FY. In the figure, the most significant contributions have been emphasized with different colors.

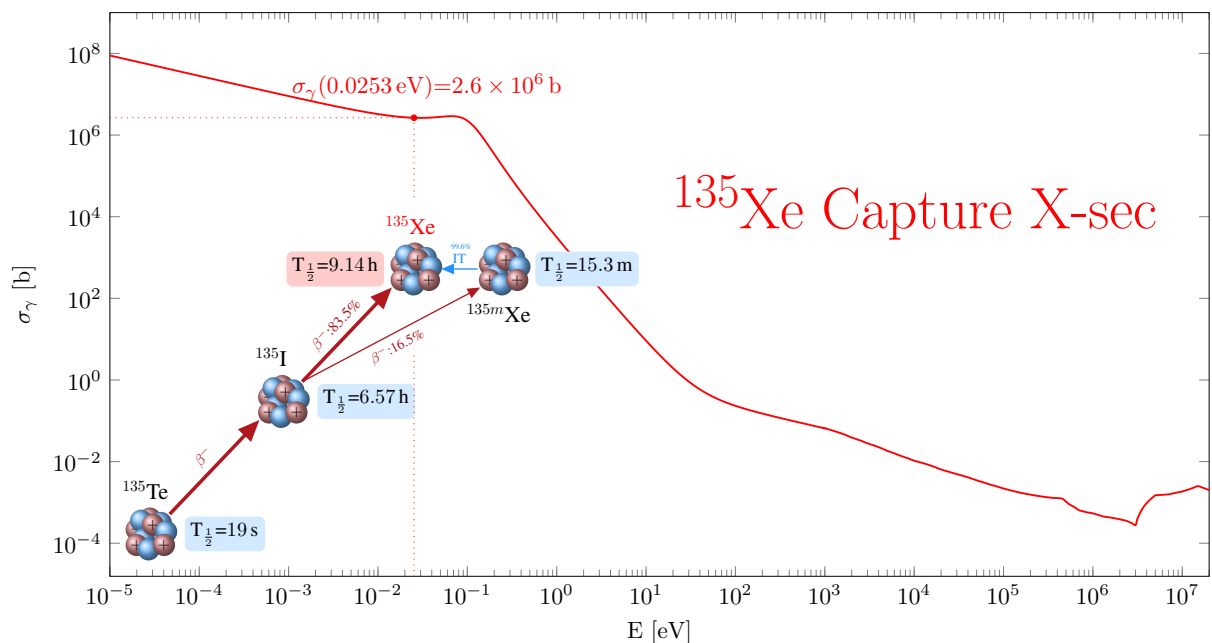


Figure 6.10: ^{135}Xe JEFF-3.1.1 evaluated capture cross section. ^{135}Xe is mainly given by Tellurium and Iodine decay. ^{135}Te and ^{135}I have independent FY of respectively 3.6828E-02 and 2.5486E-02.

^{135}Xe is in fact the most significant fission product neutron absorber. Its independent FY is of only 6.9118E-04, however it is mainly produced by the radioactive decay of ^{135}Te and ^{135}I , which have independent FY of respectively 3.6828E-02 and 2.5486E-02, and by the isomeric transition of $^{135\text{m}}\text{Xe}$, which has a FY of 1.6686E-03. ^{135}Xe build-up plays a crucial role in thermal reactor start-up operations. For conventional Light Water Reactor (LWR) applications the Xenon concentration sees an initial growing phase which reaches equilibrium after about 30 h [Stacey, 2007].

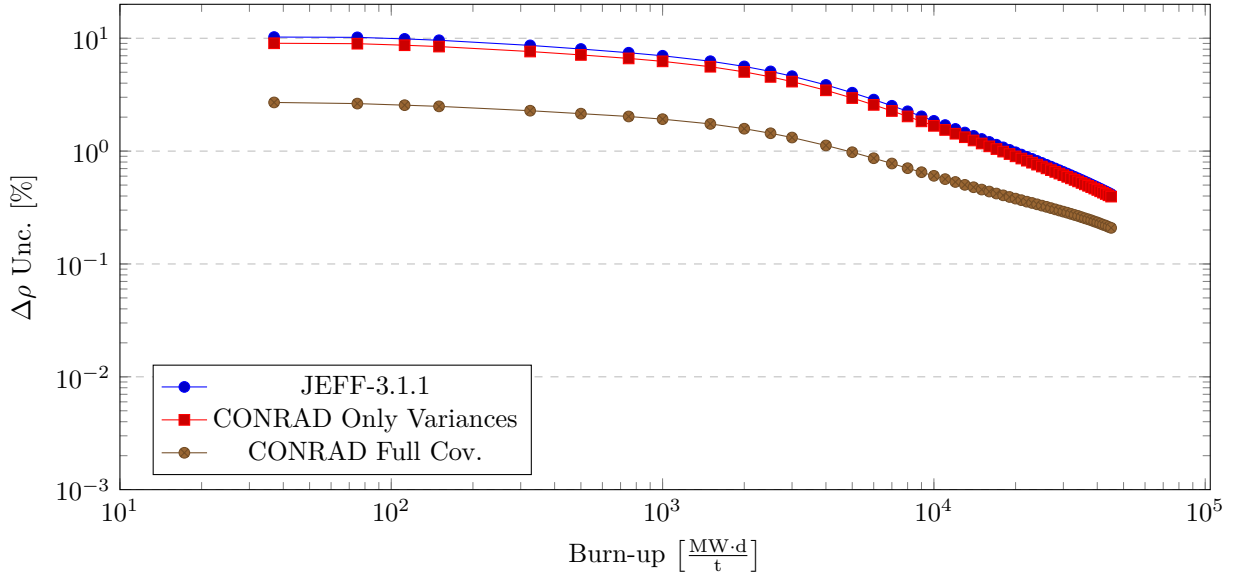


Figure 6.11: Relative reactivity loss uncertainty as a function of burn-up for a PWR-UOX pin-cell. The propagation of JEFF-3.1.1 $^{235}\text{U}(n_{th}, f)$ FY uncertainties on the reactivity loss has been compared to what we obtain from FY uncertainties generated by CONRAD, with and without including correlations.

Other independent FY participate to reactivity loss uncertainty, even if in a lesser extent. ^{149}Ce and ^{149}Pr independent FY, for instance, are respectively equal to 7.4359E-03 and 2.0839E-03. They both decay β^- , so they are the principal contributors to the formation of another relevant neutron absorbing nuclide, ^{149}Sm .

In Fig. 6.11 the relative reactivity loss uncertainty as a function of burn-up for the UOX pin-cell is presented. The propagation of JEFF-3.1.1 $^{235}\text{U}(n_{th}, f)$ FY uncertainties on the reactivity loss has been compared to what we obtained from CONRAD. To see if CONRAD was actually able to well reproduce application-sensitive independent JEFF FY uncertainties, we firstly propagate only the variances. Satisfactory results were obtained, showing, however, a very slight underestimation of CONRAD variances. The full CONRAD covariance matrix has been also propagated on the pin-cell reactivity loss, inducing a strong uncertainty reduction¹¹, probably due to existing anti-correlations between ^{135}Te and ^{135}I .

Since reactivity is mostly affected by only those nuclides presenting high capture cross sections, the only FY involved in its sensitivity analysis were those related to neutron poisons precursors. To see if CONRAD is actually capable to well represent a wide range of FY data, the decay heat uncertainty has been considered. In Fig. 6.12 the contributions to the decay heat of the UOX PWR-pin-cell are presented in different colors, considering JEFF-3.1.1 uncertainties. As it is well depicted by the figure, many fission products are

¹¹The reactivity loss uncertainty due to ^{235}U FY assumes no significant values at the end of the cycle, passing from 0.4% (JEFF diagonal variance matrix) to 0.2% (CONRAD full covariance matrix).

responsible for the final decay heat and so several FY have significant sensitivities. The labels refer to the fission products whose yield is relevant for the decay heat estimation. They must not be confused with the decaying fission products. In fact, those independent FY are important, because they are precursor of nuclides emitting high energy particles or photons.

Fig. 6.13 shows how CONRAD can represent globally the decay heat uncertainty if compared to JEFF-3.1.1 results. This suggests us that, even if in the marginalization process characterizing the covariance matrix generation (see Chapter 4) we mainly focused on Tellurium and Iodine uncertainties, a wider range of product yields are actually nicely represented by the parameter covariance matrices obtained from CONRAD. Furthermore, also in this case, an impressive uncertainty reduction was observed including the full covariance matrix. Finding a precise reason to such reduction with so many sensitive parameters is not straightforward at all. However, as explained afterwards, a global anti-correlation between FY is certainly prevalent.

Applying the sandwich formula allowed us to estimate covariance matrices for target reactor parameters. In Fig. 6.14 and 6.15 correlation matrices for the UOX-pin-cell reactivity loss are shown propagating respectively JEFF uncertainty and the full CONRAD covariance matrix. Adding FY correlations does not change significantly the reactivity loss matrix, while, for decay heat, if we compare the results presented in Figs. 6.16 and 6.17 some new structures appear.

The propagation of CONRAD covariances for the UOX pin-cell decay heat and reactivity parameters showed an important uncertainty reduction. A possible and plausible explanation can be found on the anti-correlations that clearly exist for nuclides belonging to the same decay chain. The chain yields, which are the cumulative yields of stable nuclides, differ from independent mass yields of only few percent, since the β^- decay is always prevalent. Therefore, nuclides in the same decay chain have roughly the same mass. In the analyses we assigned uncertainties on the mass yields which were reasonably close to characteristic statistical uncertainties in mass yields measurements. This explains the high anti-correlations between isotopic and isomeric yields related to fission products belonging to the same chain and then with the same mass. Their sum have to be equal to a very well known value, which is the mass yield itself. The normalization to one of the isobaric distribution is then an important source of correlation in isotopic and isomeric independent fission yields covariance matrices. This result seemed to be reasonable, since chain yields are effectively well known quantities and the same anti-correlation effect was highlighted also by other authors treating the same problem (see Ref. [Fiorito et al., 2014] for instance). A further confirmation of this effect was also found analyzing more specifically the results obtained for the JHR, and in particular investigating the ^{135}I cumulative yield contribution.

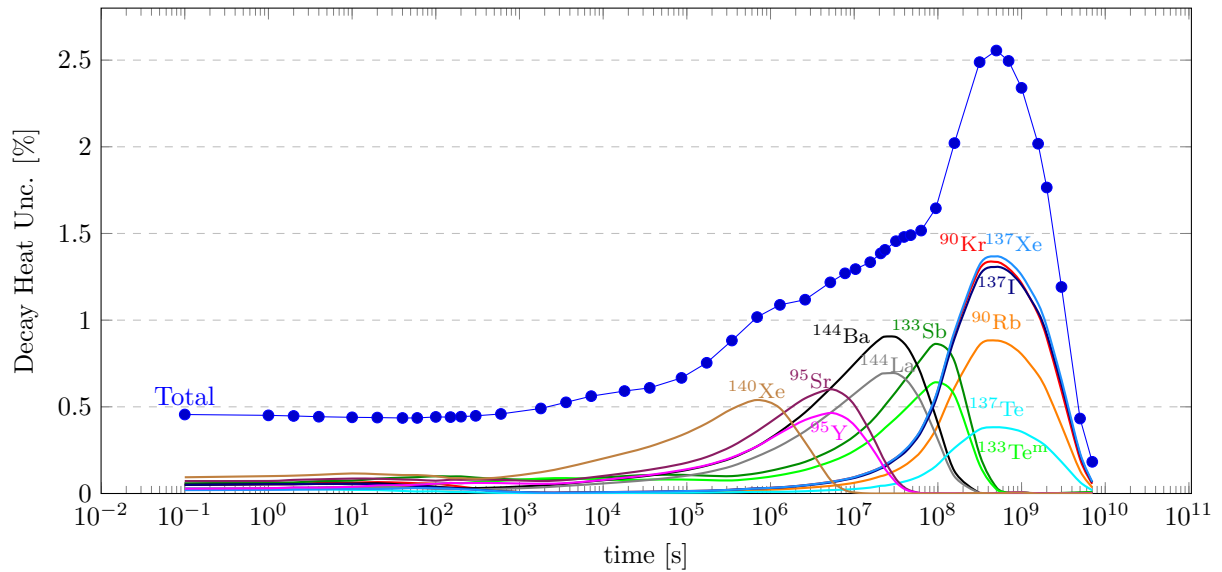


Figure 6.12: UOX-pin-cell decay heat uncertainty due to the yields of the thermal neutron induced fission of ^{235}U . The total uncertainty is given by the propagation of JEFF-3.1.1 FY. In the figure, the most significant contributions have been emphasized with different colors.

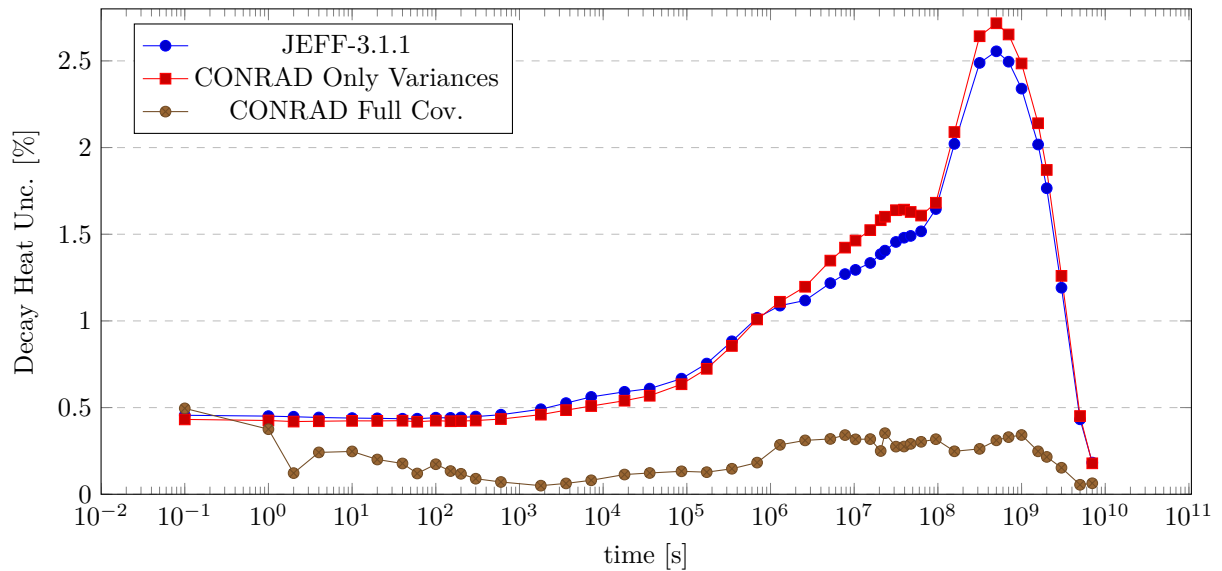


Figure 6.13: Decay heat uncertainty as a function of time for a PWR-UOX pin-cell. The propagation of JEFF-3.1.1 $^{235}\text{U}(n_{th}, f)$ FY uncertainties on the decay heat has been compared to what we obtain from FY uncertainties generated by CONRAD, with and without including correlations.

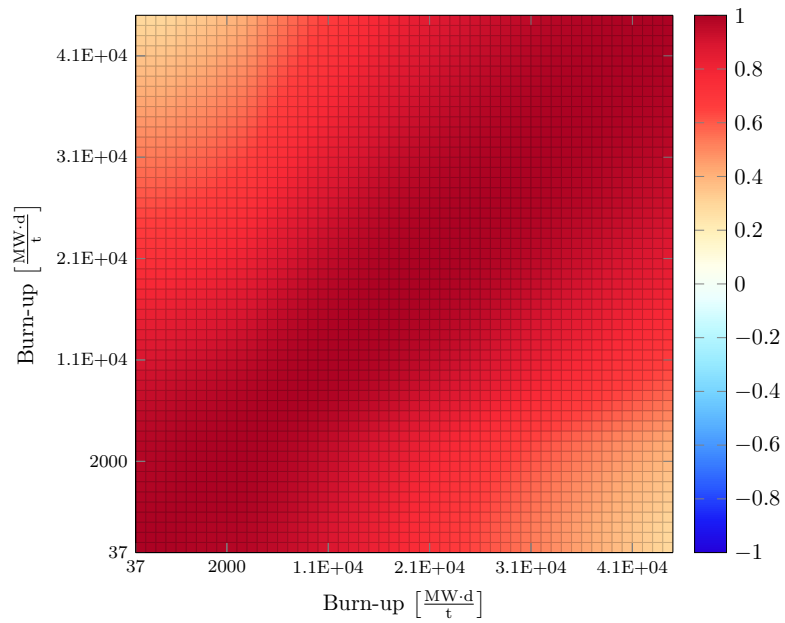


Figure 6.14: Correlation matrix for the UOX-pin-cell reactivity loss obtained from JEFF-3.1.1 $^{235}\text{U}(n_{th}, f)$ FY uncertainty propagation.

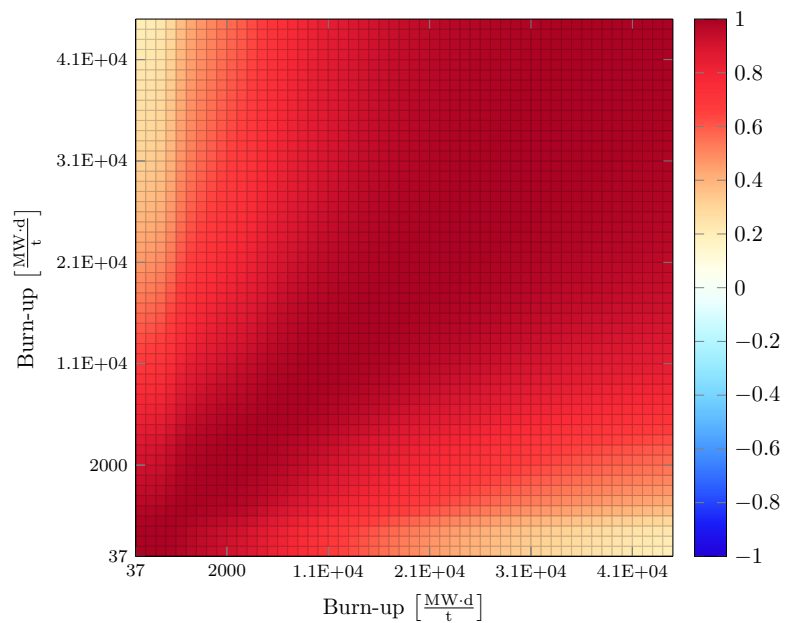


Figure 6.15: Correlation matrix for the UOX-pin-cell reactivity loss obtained from CONRAD $^{235}\text{U}(n_{th}, f)$ FY uncertainty propagation.

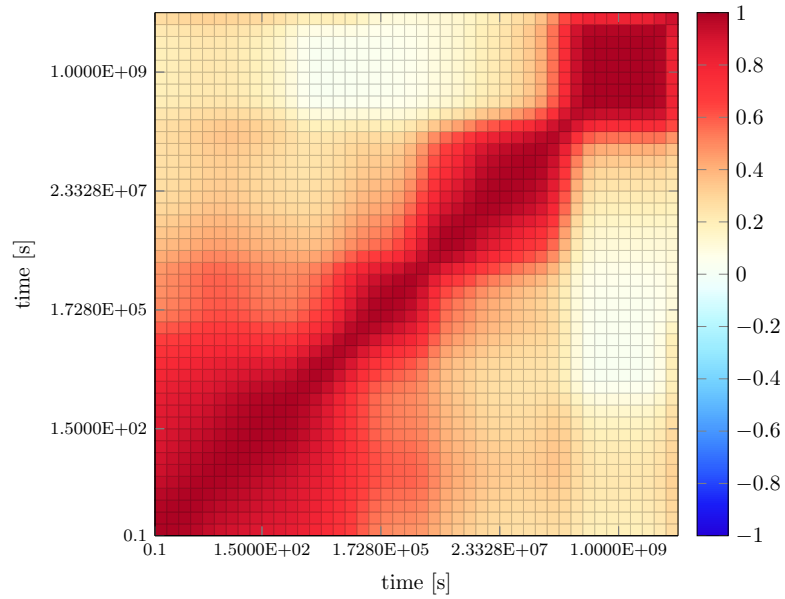


Figure 6.16: Correlation matrix for the UOX-pin-cell decay heat obtained from JEFF-3.1.1 $^{235}\text{U}(n_{th}, f)$ FY uncertainty propagation.

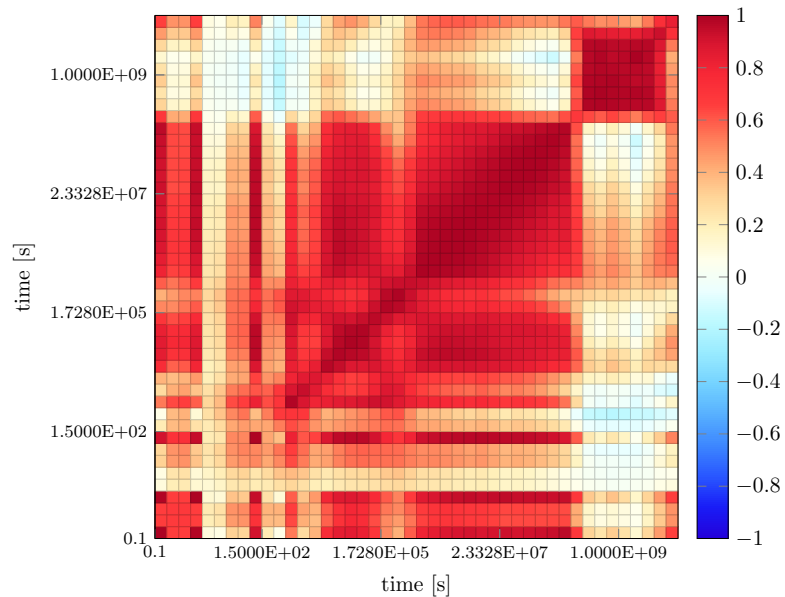


Figure 6.17: Correlation matrix for the UOX-pin-cell decay heat obtained from CONRAD $^{235}\text{U}(n_{th}, f)$ FY uncertainty propagation.

Let us then evaluate the impact of ^{235}U covariances on the JHR reactivity loss uncertainty. The uncertainty propagation of FY uncertainties on the JHR allowed us to test covariances but also to have a first grasp on their effect on reactor reactivity. Again, in Fig. 6.18 the different contributions coming from the most significant yields are showed with different colors.

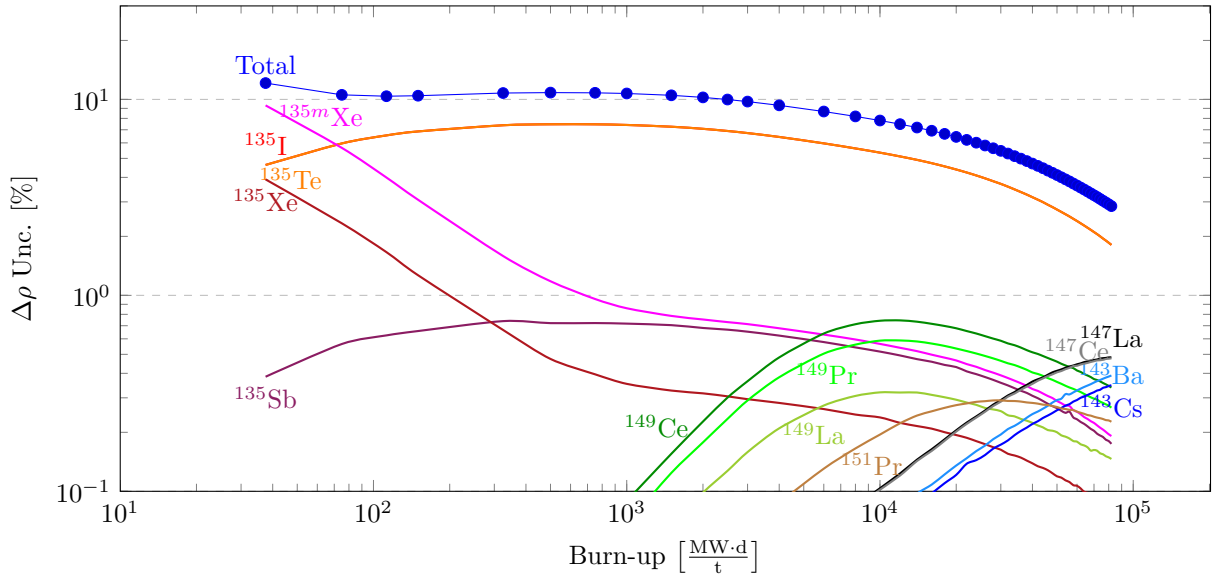


Figure 6.18: JHR reactivity loss uncertainty due to the yields of the thermal neutron induced fission of ^{235}U . The total uncertainty is given by the propagation of JEFF-3.1.1 FY. In the figure, the most significant contributions have been emphasized with different colors.

Again, the most sensitive yields are those related to the 135 amu decay chain. However, the higher fission rates reached in this 27%-enriched fuel produced some differences if compared to what we observed for the UOX-pin-cell. The sensitivity analysis demonstrates, in fact, a more significant impact of $^{135\text{m}}\text{Xe}$. Even if its FY value is lower than those related to Tellurium and Iodine isobars, having higher fluxes in the reactor induces enhanced $^{135\text{m}}\text{Xe}$ production rates whose fission yield is affected by higher uncertainty. This higher uncertainty plays obviously an important role in reactivity loss sensitivity analysis, augmenting $^{135\text{m}}\text{Xe}$ ranking. Furthermore, Tellurium and Iodine contributions are more intense compared to the conventional pin-cell. This translates into a greater reactivity loss uncertainty during the whole fuel cycle.

In Fig. 6.19 the comparison between JEFF and CONRAD results is proposed. CONRAD ^{235}U FY variances, if propagated through JHR reactivity loss calculations, provide results slightly lower (roughly 0.3% less) but anyway close to what can be obtained using JEFF-3.1.1. The only significant difference is the uncertainty of $^{135\text{m}}\text{Xe}$ which causes an over-estimation in the initial phase of the fuel cycle.

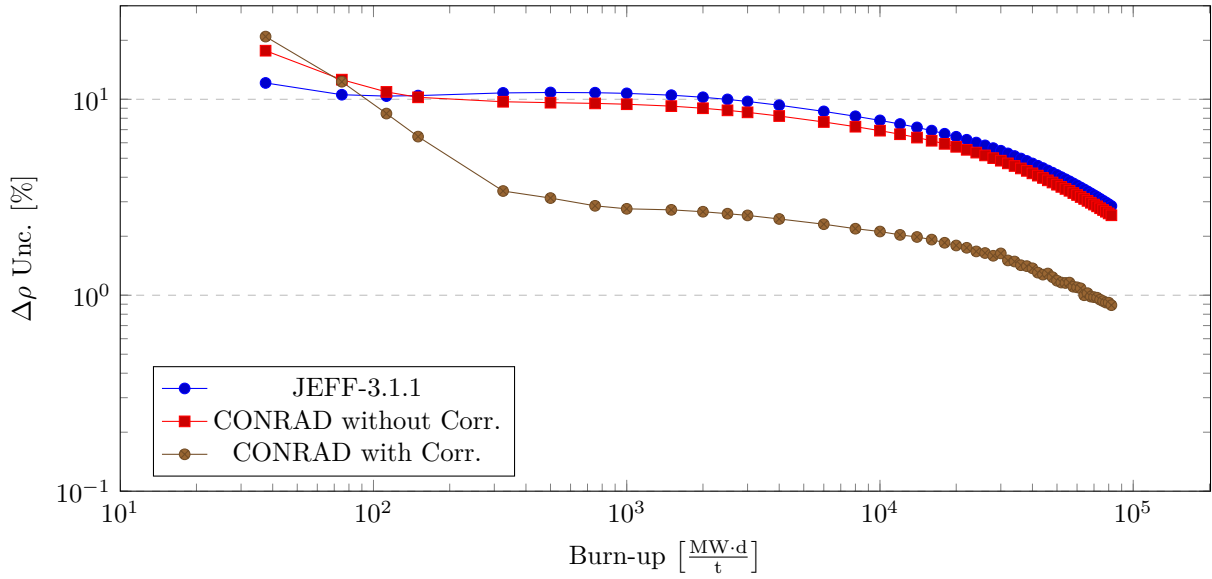


Figure 6.19: Relative reactivity loss uncertainty as a function of burn-up for the JHR. The propagation of JEFF-3.1.1 $^{235}\text{U}(n_{th}, f)$ FY uncertainties on the reactivity loss has been compared to what we obtain from FY uncertainties generated by CONRAD, with and without including correlations.

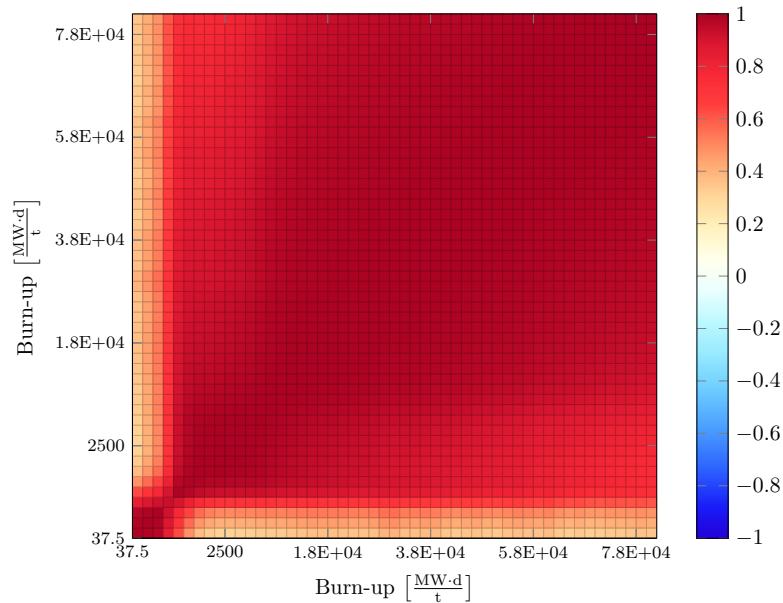


Figure 6.20: Correlation matrix for the JHR reactivity loss obtained from CONRAD $^{235}\text{U}(n_{th}, f)$ FY uncertainty propagation.

JEFF-3.1.1 $^{135\text{m}}\text{Xe}$ independent yield presents, in fact, an uncertainty of 35%, much lower than what calculated by CONRAD which is about 55%. That is confirming the problem encountered in Chapter 4 of overestimating small ($\simeq 10^{-3}$) FY uncertainties. Performing the analysis with the full CONRAD covariance matrix causes again a considerable uncertainty reduction. At the end of the cycle, the JHR reactivity loss uncertainty due to JEFF-3.1.1 ^{235}U thermal FY is equal to 2.85%, while 2.56% is what is obtained using CONRAD variances. Including correlations the final uncertainty descends to 0.89%.

Reactivity uncertainty was also analyzed to see the effects of fission yields on its uncertainty. While knowing reactivity loss margins of variation is related to exploitation optimization purposes, since it affects the cycle length (of 27 days for the JHR in nominal conditions), reactivity is a safety related parameter and its uncertainty is fundamental for writing the final report. For a burn up of 82 GW d t^{-1} , the uncertainty due to JEFF-3.1.1 ^{235}U thermal FY has been found to be of 395 pcm at 1σ . We tested also CONRAD correlations maintaining JEFF variances. The anti-correlations existing between Iodine and Tellurium isotopes reduced uncertainty to 116 pcm.

Nevertheless, the results mentioned so far are in contrast with a preliminary study carried on JEFF-3.1.1 ^{235}U FY uncertainties, which claimed a 141 pcm uncertainty on reactivity for the 27%-enriched fuel, burned at 81 GW d t^{-1} [Vaglio-Gaudard, 2014]. To understand the reason of such difference, which cannot reside on the different enrichments, we need firstly to better understand how the reactivity is affected by fission product concentrations and hence yields.

The reactivity loss in a nuclear reactor is mainly due to two different causes: the burn-up of fissile materials and the build-up of poisoning neutron absorbers. As mentioned so far, the main neutron absorbers can be identified in ^{135}Xe and ^{149}Sm . The principal one, the ^{135}Xe , reaches its equilibrium concentration after an interval of time depending on reactor flux and specific power characteristics. In a conventional LWR it is about after 30 h. Therefore the neutron absorption in a reactor by Xenon poisoning will be proportional to its capture reaction rate given by $\sigma_{\gamma} X \phi$, where X is ^{135}Xe concentration. But why do we observe a decreasing reactivity loss uncertainty in FY error propagation? The reason why uncertainty decreases from about 12% to about 3% for the JHR and from 10% to about 0.4% for the UOX-pin-cell is quite straightforward. The reactivity loss nominal value increases due to the fissile fuel burn-up. On the other hand, the poisoning contribution due to ^{135}Xe keeps constant. Therefore its associated uncertainty will be relatively smaller for increasing burn-up, highlighting the predominance of fuel consumption.

But why for a high-flux material testing reactor such uncertainty is so high? And furthermore why this uncertainty propagation was in contrast with preliminary reactivity analyses? Answering to these questions is still quite straightforward.

For higher fission rates, the neutron absorber concentrations will be also higher inducing higher capture rates. The reason why the uncertainty due to ^{235}U FY is still relevant¹² even for very high burn-ups can be possibly identified looking at ^{135}Xe concentration evolution equation.

The Bateman equation for ^{135}Xe can be written as follows

¹²A 2.85% uncertainty due to only ^{235}U FY can be considered quite important if compared to 3.4% found propagating neutron absorbers and actinides cross sections [Vaglio-Gaudard, 2014].

$$\frac{dX(t)}{dt} = Y_{Xe}\Sigma_f\phi + 0.835 \cdot \lambda_I I(t) + 0.994 \cdot \lambda_{Xe^m} X^m(t) - (\lambda_{Xe} + \sigma_{Xe}^\gamma \phi) X(t), \quad (6.3)$$

where $X(t)$ is the ^{135}Xe concentration, Y_{Xe} the associated independent FY, λ_{Xe} its decay constant and σ_{Xe}^γ the capture cross section. With λ_I we indicated the decay constant for ^{135}I , whose concentration is given by $I(t)$. $X^m(t)$ is the concentration of the first metastable state of ^{135}Xe and λ_{Xe^m} is the associated decay constant. The 0.835 and 0.994 are simply the branching ratios for the 135 amu decay chain.

A similar equation can be written also for ^{135}I concentration:

$$\frac{dI(t)}{dt} = Y_I \Sigma_f \phi + \lambda_{Te} T(t) - \lambda_I I(t), \quad (6.4)$$

where λ_{Te} and $T(t)$ are the decay constant and the nuclei concentration for ^{135}Te . These equations are evidently coupled to those concerning the relative precursors. In Chapter 3 we have seen that APOLLO2 has a specific list of neutronics relevant fission products. In this case, simplifications can be in fact done, looking at the decay chains and times. ^{135}Te decays in ^{135}I in 19s. Considering the reactor inventory evolution characteristic time, a first simplification could be to consider ^{135}Te , and its precursors, decaying without any delay after a fission event. This is equivalent to replace in the reactor calculations the independent yield of ^{135}I with its cumulative. This is exactly what is done in APOLLO2. ^{135}Te is not in the fission products list and the APOLLO2 ^{135}I yield is equal to its cumulative. A second simplification made in APOLLO2 is to neglect the existence of the first metastable state of ^{135}Xe , including its independent yield in Y_{Xe} and supposing ^{135}I all decaying towards the ^{135}Xe ground state. This is, in fact, what we called in Chapter 3 a semi-cumulative FY (Y'_{Xe} in the following equations) for ^{135}Xe , because the metastable yield contribution is already included.

The previous equations can be then simplified and rewritten as follows

$$\begin{cases} \frac{dX(t)}{dt} = Y'_{Xe} \Sigma_f \phi + \lambda_I I(t) - \kappa X(t) \\ \frac{dI(t)}{dt} = C_I \Sigma_f \phi - \lambda_I I(t) \end{cases} \quad (6.5)$$

where $\kappa = (\lambda_{Xe} + \sigma_{Xe}^\gamma \phi)$ and C_I is the ^{135}I cumulative yield. Defining $\tilde{I}(s) = \mathcal{L}\{I(t)\}$ and $\tilde{X}(s) = \mathcal{L}\{X(t)\}$ the Laplace integral transforms of the two concentration functions, we have

$$\begin{cases} \tilde{I}(s) = \frac{C_I \Sigma_f \phi}{s(s + \lambda_I)} + \frac{I(0)}{(s + \lambda_I)} \\ \tilde{X}(s) = \frac{X(0)}{(s + \kappa)} + \frac{Y'_{Xe} \Sigma_f \phi}{s(s + \kappa)} + \lambda_I \left(\frac{C_I \Sigma_f \phi}{s(s + \lambda_I)(s + \kappa)} + \frac{I(0)}{(s + \lambda_I)(s + \kappa)} \right). \end{cases} \quad (6.6)$$

Applying the inverse Laplace transform $\mathcal{L}^{-1}\{\bullet\}$ to the first equation we have¹³

$$I(t) = I(0)e^{-\lambda_I t} + \frac{C_I \Sigma_f \phi}{\lambda_I} (1 - e^{-\lambda_I t}). \quad (6.7)$$

Proceeding in the same way also for $X(t)$ we obtain¹⁴

$$X(t) = X(0)e^{-\kappa t} + \frac{(Y'_{Xe} + C_I) \Sigma_f \phi}{\kappa} (1 - e^{-\kappa t}) + \frac{(C_I \Sigma_f \phi - \lambda_I I(0))}{(\lambda_I - \kappa)} (e^{-\lambda_I t} - e^{-\kappa t}). \quad (6.8)$$

The equilibrium concentration X^{eq} is then given by

$$X^{eq} = \frac{(Y'_{Xe} + C_I) \Sigma_f \phi}{\lambda_{Xe} + \sigma_{Xe}^2 \phi}. \quad (6.9)$$

It is clear from Eq. 6.9 that the ^{135}Xe concentration at the equilibrium is strongly dependent on its independent yield and on ^{135}I cumulative one. This last equation confirms furthermore that the reactivity loss contribution coming from this poisoning fission product is mostly constant during the all cycle time. The reactivity decrement due to fuel burn-up, on the other hand, becomes predominant after a certain burn-up making the uncertainty due to FY relatively smaller and decreasing with the fuel consumption. This can be seen clearer in we plot the reactivity loss uncertainty in a linear scale as shown for the JHR in Fig. 6.21.

A plausible explanation for JHR higher reactivity loss uncertainty can be found still looking at Eq. 6.9. For a 27%-enriched high flux reactor, in fact, the fission rate at the numerator dominates the capture rate at the denominator which leads to higher equilibrium Xenon concentration. The impact of fission products on the neutronics is then more significant and this translates in an enhanced reactivity uncertainty.

In the present work we consistently propagated the independent yields uncertainty reproducing APOLLO2 FY. This allowed us to perfectly identify the main responsible of target parameter uncertainty performing independent yields sensitivity analyses. The cumulative yield of ^{135}I is then a summation of independent yields contributions coming from ^{135}I itself, ^{135}Te , ^{135}Sb and ^{135}Sn . In Tab. 6.3 the relative uncertainties for such independent yields are provided.

¹³ The result can be obtained once the residues are calculated

$$\text{Res} \left[\frac{C_I \Sigma_f \phi}{s(s + \lambda_I)}, s = 0 \right] = \lim_{s \rightarrow 0} \frac{C_I \Sigma_f \phi}{(s + \lambda_I)} = \frac{C_I \Sigma_f \phi}{\lambda_I}, \quad \text{Res} \left[\frac{C_I \Sigma_f \phi}{s(s + \lambda_I)}, s = -\lambda_I \right] = \lim_{s \rightarrow -\lambda_I} \frac{C_I \Sigma_f \phi}{s} = -\frac{C_I \Sigma_f \phi}{\lambda_I}.$$

¹⁴ To find it we need the following residues:

$$\begin{aligned} \text{Res} \left[\frac{Y'_{Xe} \Sigma_f \phi}{s(s + \kappa)}, s = 0 \right] &= \lim_{s \rightarrow 0} \frac{Y'_{Xe} \Sigma_f \phi}{s + \kappa} = \frac{Y'_{Xe} \Sigma_f \phi}{\kappa}, & \text{Res} \left[\frac{Y'_{Xe} \Sigma_f \phi}{s(s + \kappa)}, s = -\kappa \right] &= \lim_{s \rightarrow -\kappa} \frac{Y'_{Xe} \Sigma_f \phi}{s} = -\frac{Y'_{Xe} \Sigma_f \phi}{\kappa} \\ \text{Res} \left[\frac{\lambda_I C_I \Sigma_f \phi}{s(s + \lambda_I)(s + \kappa)}, s = 0 \right] &= \lim_{s \rightarrow 0} \frac{\lambda_I C_I \Sigma_f \phi}{(s + \lambda_I)(s + \kappa)} = \frac{C_I \Sigma_f \phi}{\kappa}, \\ \text{Res} \left[\frac{\lambda_I C_I \Sigma_f \phi}{s(s + \lambda_I)(s + \kappa)}, s = -\lambda_I \right] &= \lim_{s \rightarrow -\lambda_I} \frac{\lambda_I C_I \Sigma_f \phi}{s(s + \kappa)} = \frac{C_I \Sigma_f \phi}{\lambda_I - \kappa}, \\ \text{Res} \left[\frac{\lambda_I C_I \Sigma_f \phi}{s(s + \lambda_I)(s + \kappa)}, s = -\kappa \right] &= \lim_{s \rightarrow -\kappa} \frac{\lambda_I C_I \Sigma_f \phi}{s(s + \lambda_I)} = -\frac{\lambda_I C_I \Sigma_f \phi}{\kappa(\lambda_I - \kappa)}. \end{aligned}$$

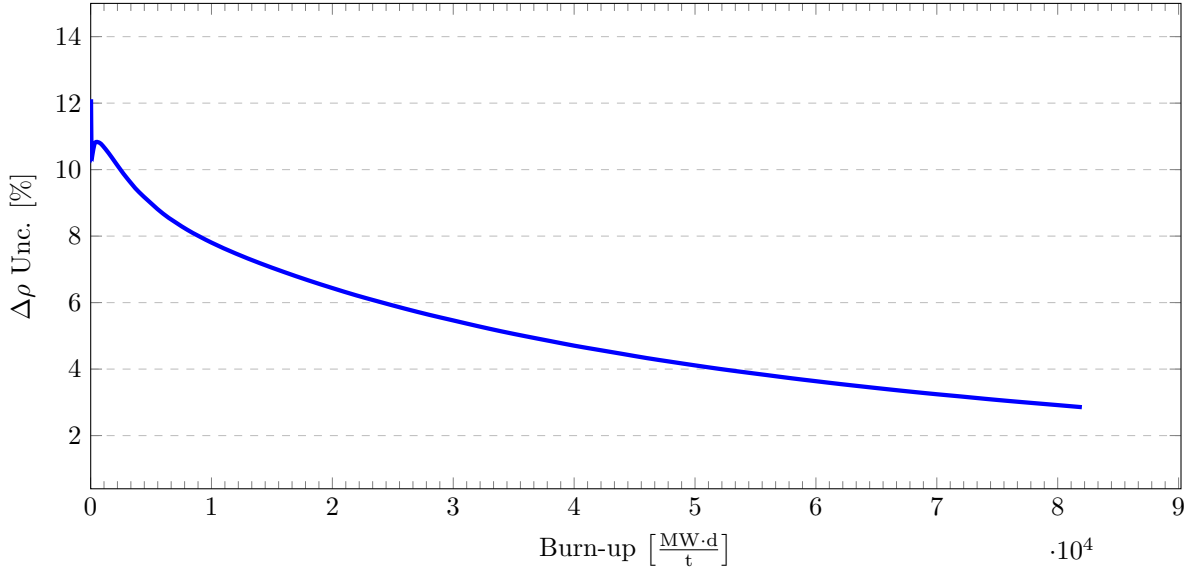


Figure 6.21: Relative reactivity loss uncertainty as a function of burn-up for the JHR in a linear scale.

Isotope	Independent Yield	Relative Unc.	Cumulative Yield	Relative Unc.
Sn-135	6.8852E-06	35.6%	6.8860E-6	35.7%
Sb-135	1.7799E-03	34.8%	1.7850E-3	33.4%
Te-135	3.6828E-02	15.2%	3.8367E-2	7.05%
I-135	2.5486E-02	21.2%	6.3853E-2	3.4%

Table 6.3: The cumulative yield of ^{135}I is roughly given by the sum of the independent yields related to ^{135}Te , ^{135}Sb and ^{135}Sn . Performing the quadratic sum of their uncertainties, which is equivalent to propagate their uncertainty without any correlations, cannot provide the 3.4% found in JEFF-3.1.1.

The cumulative ^{135}I evaluated in JEFF-3.1.1 has a relative uncertainty of 3.4%. Its accuracy derives from experimental measurements which can be precise enough since the associated ^{135}I decay half-life is 6.57 h. This is clearly not reflected in independent yield evaluations, which will never reproduce such low values by rigorous propagations of their diagonal variance matrix, without including correlations. This induces to evident discrepancies in the JEFF-3.1.1 FY library, already seen for ^{148}Nd in Chapter 4.

Propagating JEFF-3.1.1 variances led to 395 pcm because the uncertainty on C_1 was over-estimated. It was in fact calculated automatically by the procedure here proposed through the Q-matrix for APOLLO2. Without correlations the uncertainty was rigorously propagated returning a value clearly different from the evaluated JEFF-3.1.1 one. Including CONRAD anti-correlations between isotopes belonging to the same decay chain allowed to have the right uncertainty on this parameter, then equal to the 3.4% we found in the JEFF-3.1.1 cumulative FY library. That is the reason why with CONRAD a 116 pcm uncertainty is afterwards obtained. The 141 pcm for the 27%-enriched configuration was derived assigning of the JEFF cumulative uncertainty of 3.4% on C_1 .

At a first glance the procedure here proposed can be possibly seen as redundant, just leading finally to the same uncertainty levels found in preliminary analyses. However, the 141 pcm of uncertainty were found only because APOLLO2 simplifies calculations

using a cumulative yield describing the Iodine concentration in a nuclear reactor. Other softwares, such as Monte Carlo codes or MENDEL itself, use independent FY as input nuclear data. The proposed methodology together with the utilization of proper covariance matrices is then the only mean to consistently propagate FY uncertainties in nuclear reactor calculations, which is confirmed by the decay heat analyses we performed in the present work.

6.3.2 Pu-239 Thermal Fission

We repeated the same exercise for the covariance matrix related to the thermal fission of ^{239}Pu . To specifically test the Plutonium covariance matrices, the MOX pin-cell was firstly considered, since different concentrations of Plutonium isotopes are present even in the fresh fuel.

In Fig. 6.22 the MOX pin-cell reactivity loss uncertainty due to the thermal FY of ^{239}Pu is provided, emphasizing the different contributions. Even in this case we can draw the same conclusions we discussed for the thermal fission of ^{235}U . ^{135}Te and ^{135}I independent FY are still the most sensitive parameters and provide the most significant contribution to the final uncertainty. However, for Plutonium, we can clearly see that ^{149}Ce and ^{149}Pr gained more importance, augmenting the level of Samarium in the reactor.

Comparing JEFF and CONRAD variances (see Fig. 6.23) we verified again that the uncertainty for the most sensitive yields are effectively represented by our calculations and, performing a full covariance matrix propagation, we see that uncertainties can be drastically reduced. In Fig. 6.24 the associated correlation matrix is presented.

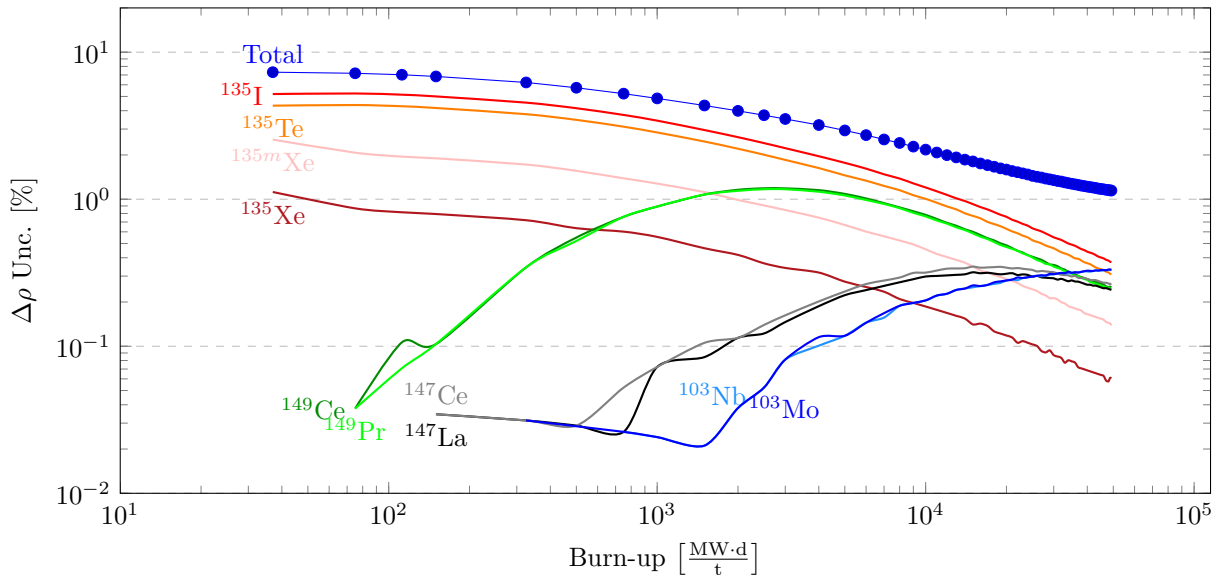


Figure 6.22: MOX-pin-cell reactivity loss uncertainty due to the yields of the thermal neutron induced fission of ^{239}Pu . The total uncertainty is given by the propagation of JEFF-3.1.1 FY. In the figure, the most significant contributions have been emphasized with different colors.

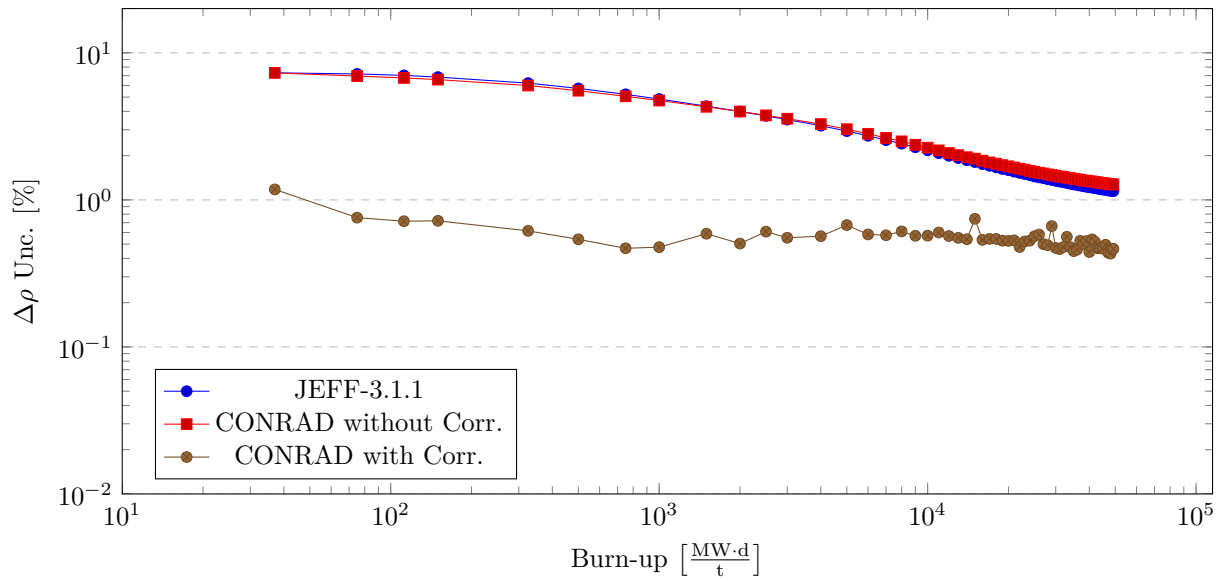


Figure 6.23: Relative reactivity loss uncertainty as a function of burn-up for a PWR-MOX pin-cell. The propagation of JEFF-3.1.1 $^{239}\text{Pu}(n_{th}, f)$ FY uncertainties on the reactivity loss has been compared to what we obtain from FY uncertainties generated by CONRAD, with and without including correlations.

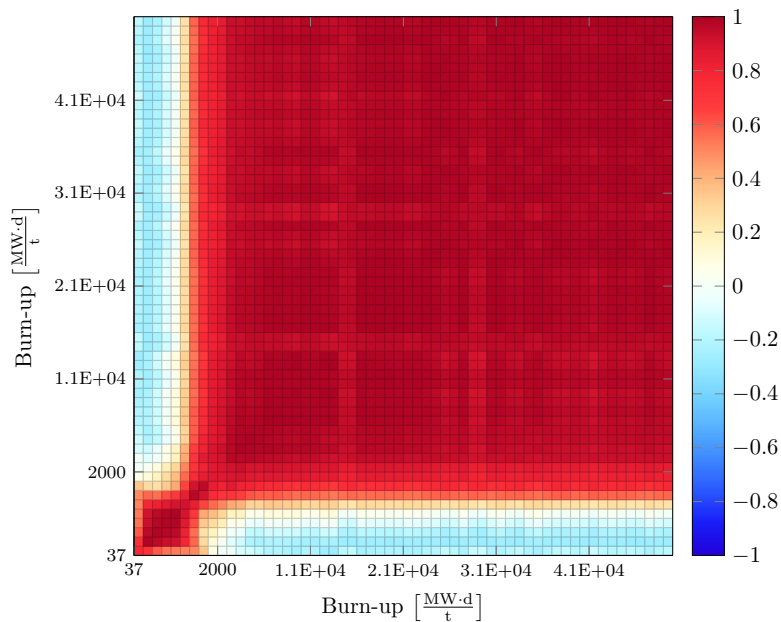


Figure 6.24: Correlation matrix for the MOX pin-cell reactivity loss obtained from CONRAD $^{239}\text{Pu}(n_{th}, f)$ FY uncertainty propagation.

Let us now look at the results we obtained for decay heat propagating ^{239}Pu independent FY, as we did for ^{235}U .

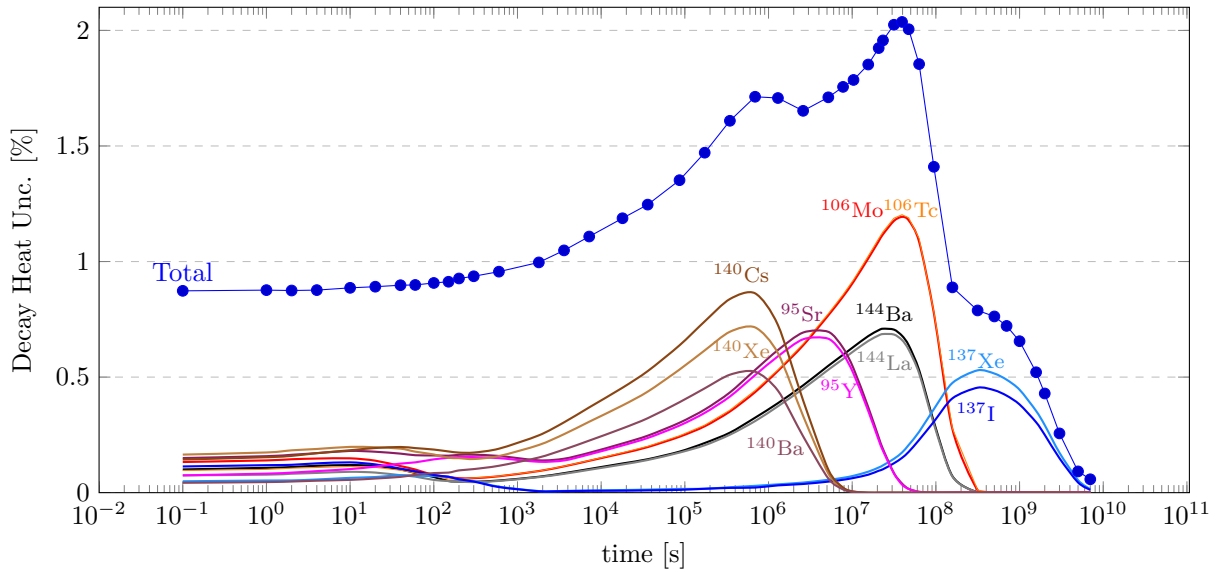


Figure 6.25: MOX-pin-cell decay heat uncertainty due to the yields of the thermal neutron induced fission of ^{239}Pu . The total uncertainty is given by the propagation of JEFF-3.1.1 FY. In the figure, the most significant contributions have been emphasized with different colors.

For ^{239}Pu we find some different most sensitive independent FY parameters such as the isotopes of mass 106 (see Fig. 6.25) which gave a different structure to the decay heat uncertainty trend. The comparison between CONRAD and JEFF variance propagations (see Fig. 6.26) showed however satisfactory agreement. Only in the initial cooling times a slight over-estimation of the decay heat uncertainty was observed for CONRAD variances. It has to be emphasized that, in such interval of time, many isotopes decay. All the fission products far from the stability line have modest half lives, so they dominate the initial cooling phase. They are generally highly correlated, so to find the reason of such effect is not straightforward.

The CONRAD covariance matrix produced again an important uncertainty reduction. The associated decay heat correlation matrix is given in Fig. 6.27. This result is quite interesting because clear blocks are now recognizable, probably due to the anti-correlation of ^{137}Xe and ^{137}I FY with those related to other isotopes intervening at different cooling times.

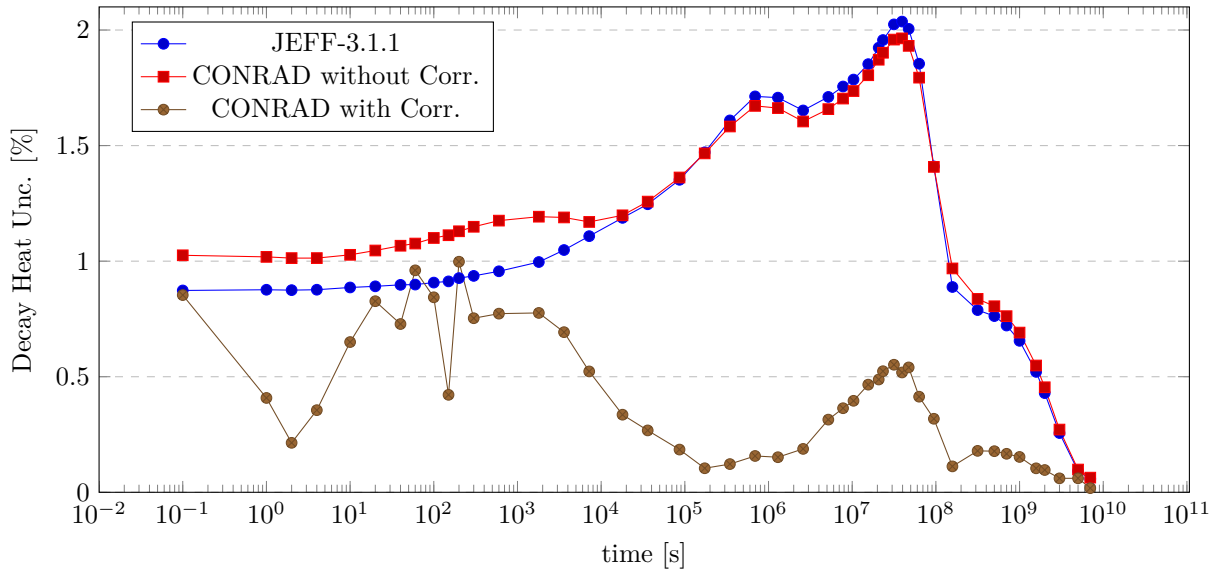


Figure 6.26: Decay heat uncertainty as a function of time for a PWR-MOX pin-cell. The propagation of JEFF-3.1.1 $^{239}\text{Pu}(n_{th}, f)$ FY uncertainties on the decay heat has been compared to what we obtain from FY uncertainties generated by CONRAD, with and without including correlations.

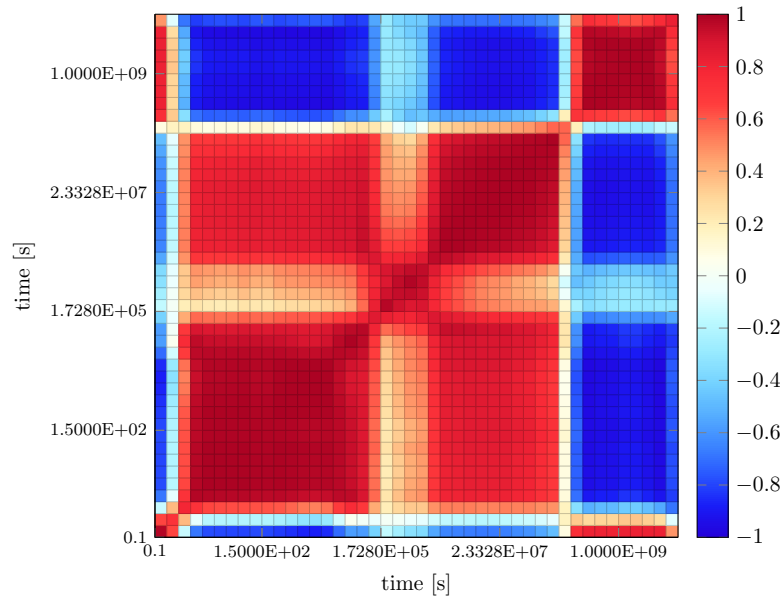


Figure 6.27: Correlation matrix for the MOX-pin-cell decay heat obtained from CONRAD $^{239}\text{Pu}(n_{th}, f)$ FY uncertainty propagation.

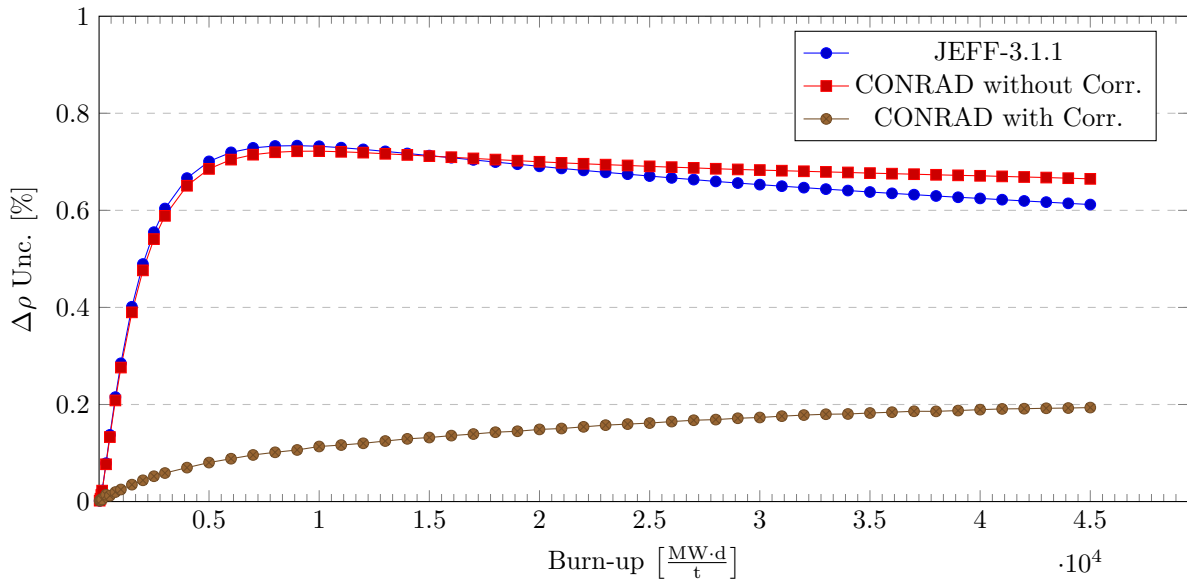


Figure 6.28: Relative reactivity loss uncertainty as a function of burn-up for a PWR-UOX pin-cell. The propagation of JEFF-3.1.1 $^{239}\text{Pu}(n_{th}, f)$ FY uncertainties on the reactivity loss has been compared to what we obtain from FY uncertainties generated by CONRAD, with and without including correlations.

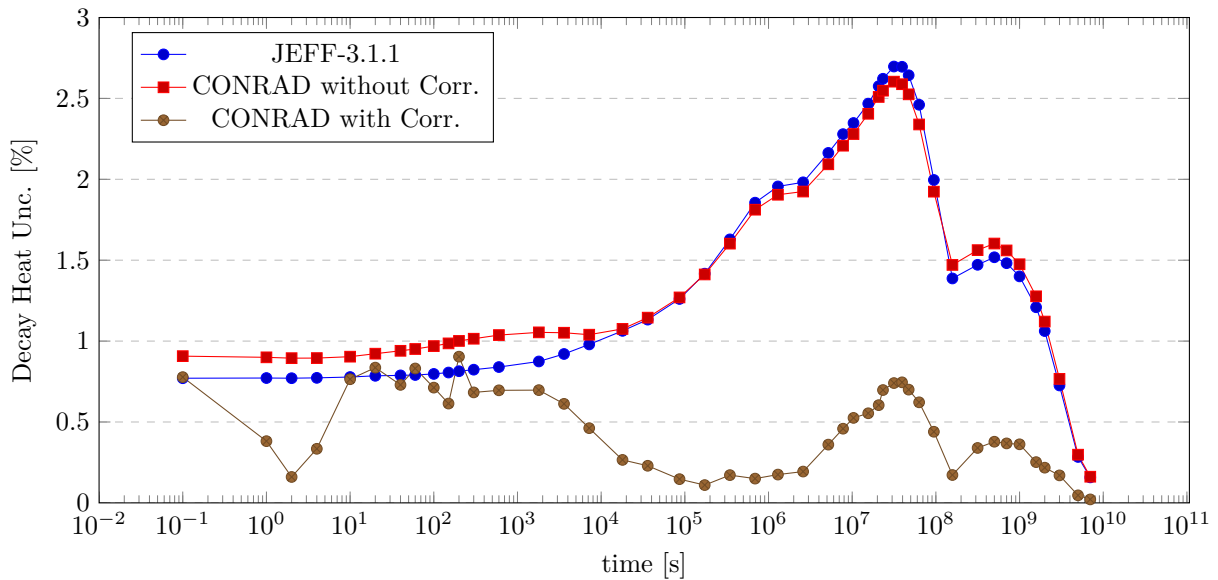


Figure 6.29: Decay heat uncertainty as a function of time for a PWR-UOX pin-cell. The propagation of JEFF-3.1.1 $^{239}\text{Pu}(n_{th}, f)$ FY uncertainties on the decay heat has been compared to what we obtain from FY uncertainties generated by CONRAD, with and without including correlations.

In Figs. 6.28 and 6.29 the UOX pin-cell reactivity loss and decay heat uncertainties due to the thermal FY of ^{239}Pu are provided. Even in this case we can draw the same conclusions we discussed for the MOX pin-cell.

It is nice to see how the physics of the problem is well reflected by the uncertainty analysis. At the beginning of the cycle, no Plutonium exists in UOX fresh fuel and so no uncertainty due to its FY is given. A decay heat uncertainty calculation was also been performed and it is presented in Fig. 6.29.

We checked also the contribution of ^{239}Pu FY on JHR reactivity. No significant effects were found. However the results, given in Fig. 6.30, are consistent with the conclusions we discussed for the PWR pin-cell configurations.

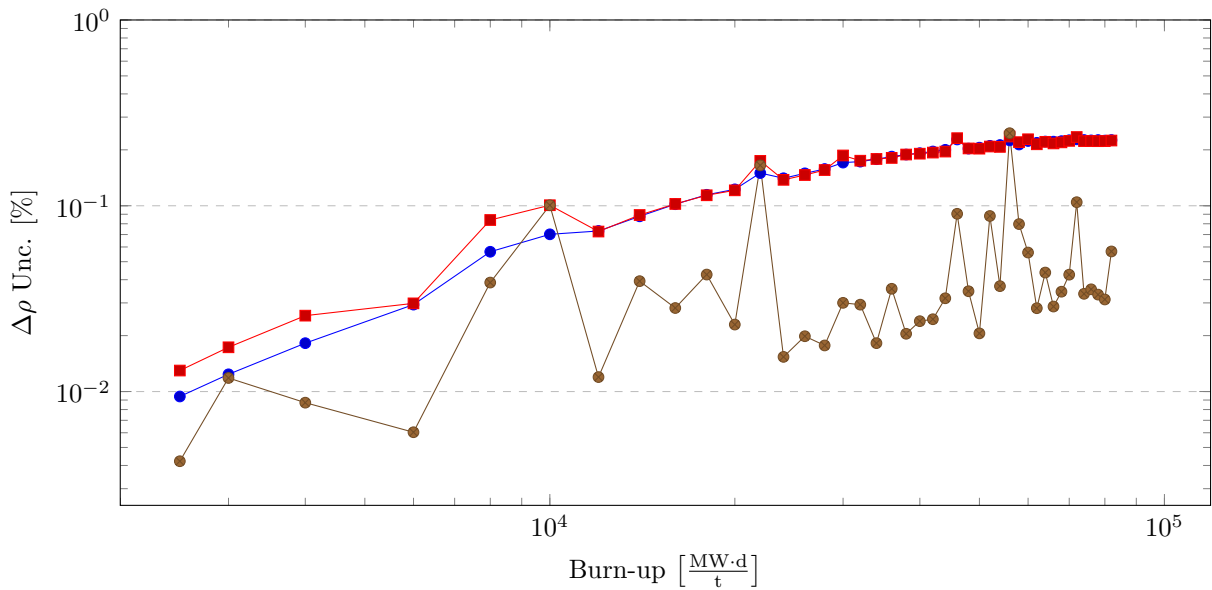


Figure 6.30: Relative reactivity loss uncertainty as a function of burn-up for the JHR. The propagation of JEFF-3.1.1 $^{239}\text{Pu}(n_{th}, f)$ FY uncertainties on the reactivity loss has been compared to what we obtain from FY uncertainties generated by CONRAD, with and without including correlations.

6.3.3 Pu-241 Thermal Fission

Let us now show briefly the results obtained for $^{241}\text{Pu}(n_{th}, f)$. For the MOX pin-cell, results on reactivity loss and decay heat uncertainties are provided in Figs. 6.31 and 6.32. Also in this case we can affirm that CONRAD is quite well reproducing JEFF-3.1.1 variances, even if a slight overestimation can be observed for the decay heat. Including CONRAD covariances still induces strong uncertainty reduction. An oscillating behavior has been reported for the reactivity loss uncertainty at the end of the cycle, which suggests a possible failing of estimating sensitivities using direct perturbations in the case of small target parameter uncertainties.

In Figs. 6.33 and 6.34 the correlation matrix for the reactivity loss and the decay heat propagating CONRAD ^{241}Pu FY covariances are presented. The two matrices present peculiar structures if compared to what we obtained for the other fissioning systems, which should be further investigated.

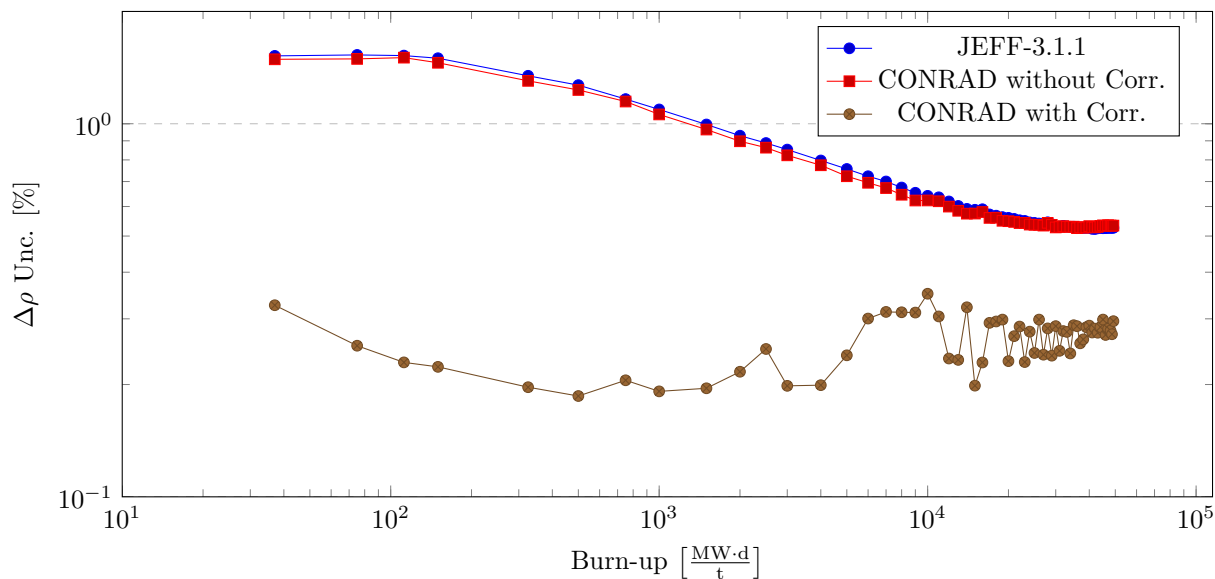


Figure 6.31: Relative reactivity loss uncertainty as a function of burn-up for a PWR-MOX pin-cell. The propagation of JEFF-3.1.1 $^{241}\text{Pu}(n_{th}, f)$ FY uncertainties on the reactivity loss has been compared to what we obtain from FY uncertainties generated by CONRAD, with and without including correlations.

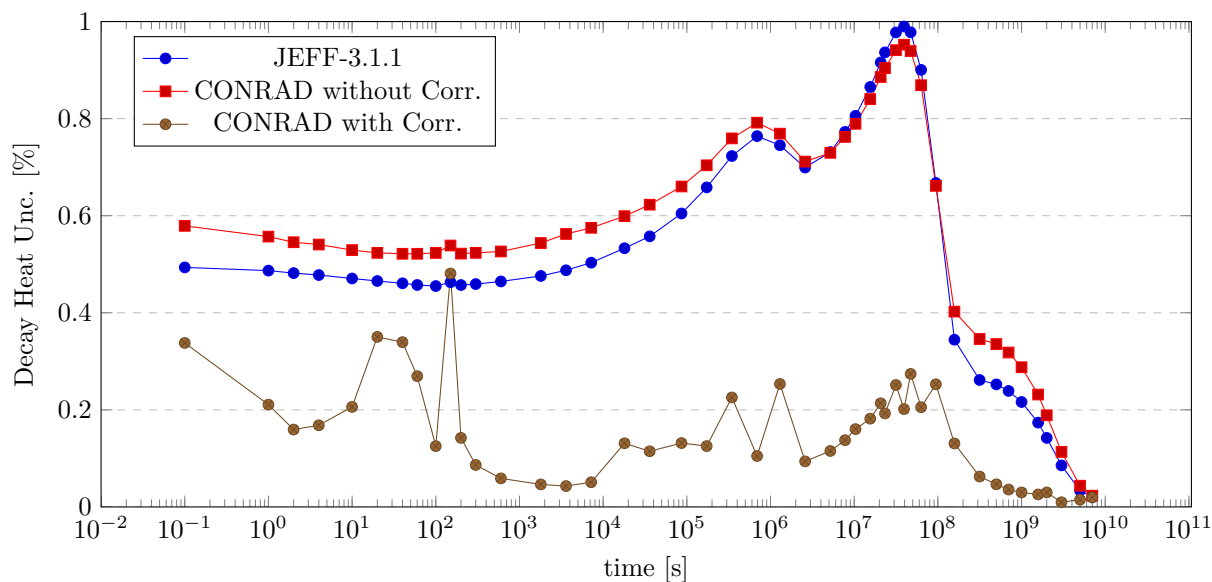


Figure 6.32: Decay heat uncertainty as a function of time for a PWR-MOX pin-cell. The propagation of JEFF-3.1.1 $^{241}\text{Pu}(n_{th}, f)$ FY uncertainties on the decay heat has been compared to what we obtain from FY uncertainties generated by CONRAD, with and without including correlations.

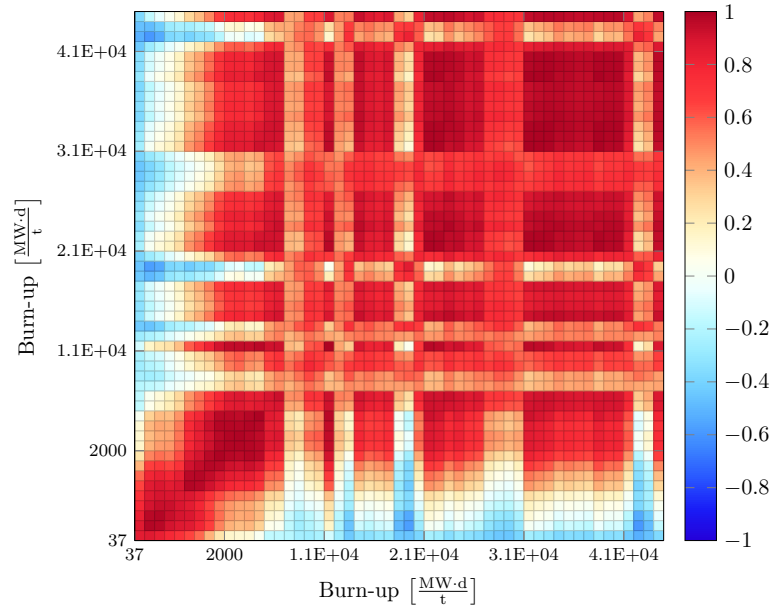


Figure 6.33: Correlation matrix for the MOX pin-cell reactivity loss obtained from CONRAD $^{241}\text{Pu}(n_{th}, f)$ FY uncertainty propagation.

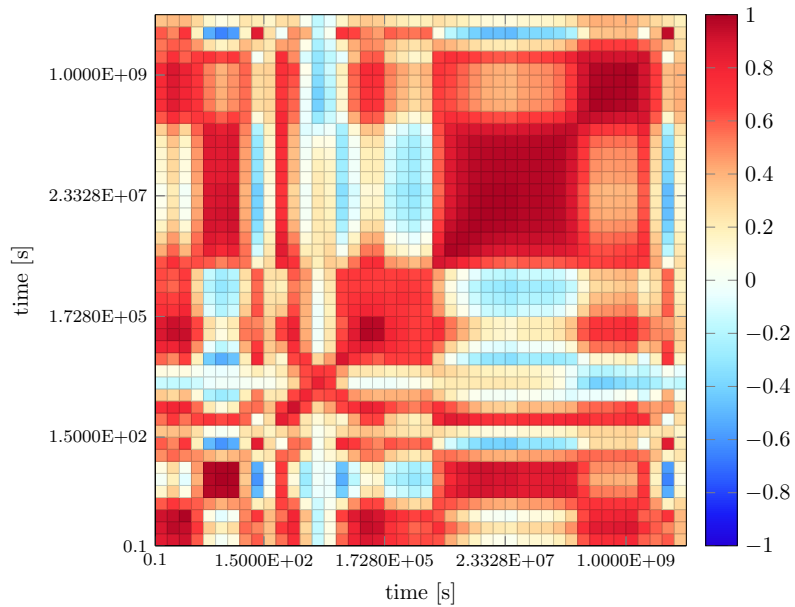


Figure 6.34: Correlation matrix for the MOX-pin-cell decay heat obtained from CONRAD $^{241}\text{Pu}(n_{th}, f)$ FY uncertainty propagation.

6.3.4 U-238 Fast Fission

For the fast fission of ^{238}U , FY covariances were used to see their impact on the applications considered. Even if negligible compared to the thermal fission of ^{235}U , a certain fast fission fraction exist even in thermal reactor applications and the associated FY data can introduce uncertainties, especially in the case of twofold spectrum, available in the JHR.

For the UOX pin-cell geometry no significant contributions were observed to the reactivity loss and decay heat. However, the results showed in Figs. 6.35 and 6.36 enhance the level of confidence we have on the covariances estimated with CONRAD.

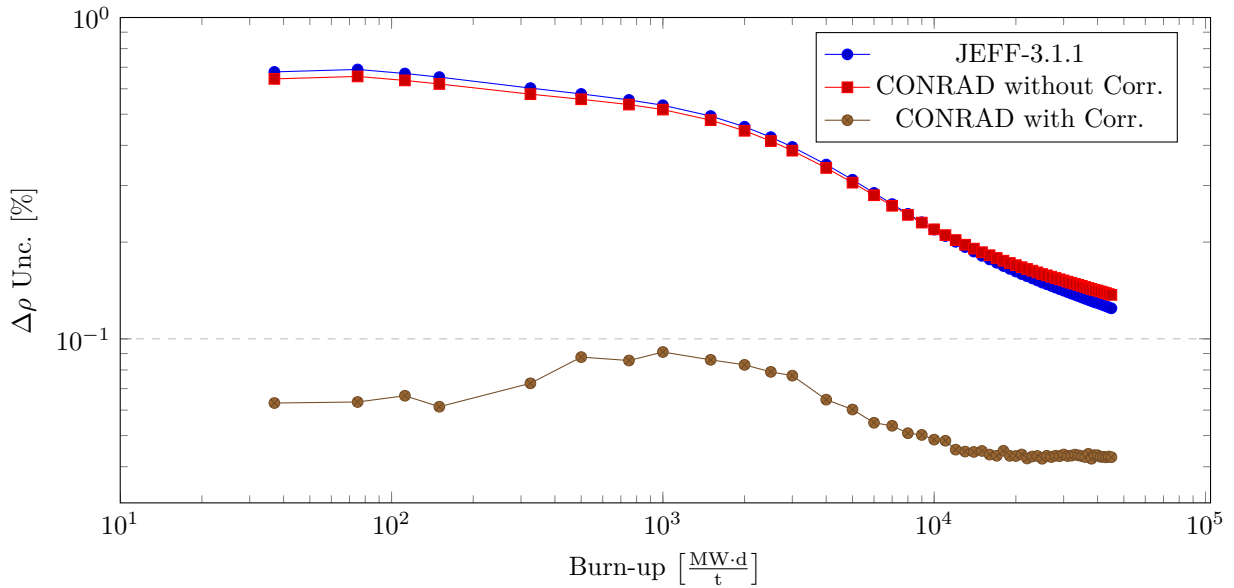


Figure 6.35: Relative reactivity loss uncertainty as a function of time for a PWR-UOX pin-cell. The propagation of JEFF-3.1.1 U238F FY uncertainties on the reactivity loss has been compared to what we obtain from FY uncertainties generated by CONRAD, with and without including correlations.

Also for ^{238}U variances seem to well represent JEFF-3.1.1 values, unless for the application-sensitive yields. CONRAD correlations are globally reducing the uncertainty on the engineering parameters of interest, except for a peak that emerges in decay heat calculations which needs probably further investigations, perhaps performing pin-cell calculations for fast applications. However, a similar behavior was observed for the uncertainty propagation of ^{235}U FY on the MOX pin-cell decay heat, so a common cause might exist.

We checked the influence of ^{238}U yields on JHR reactivity. An expected contribution seemed reasonable since the high flux levels reached in the reactor. Nevertheless, no significant impact was observed, producing an uncertainty due to ^{238}U yields of about 0.1% on the reactivity loss at the end of the cycle. This could be probably due to the high enrichment, which makes the ^{235}U fission events dominate. Also for the JHR CONRAD variances and covariances were tested, returning result in perfect agreement to what verified in the PWR pin-cell calculations.

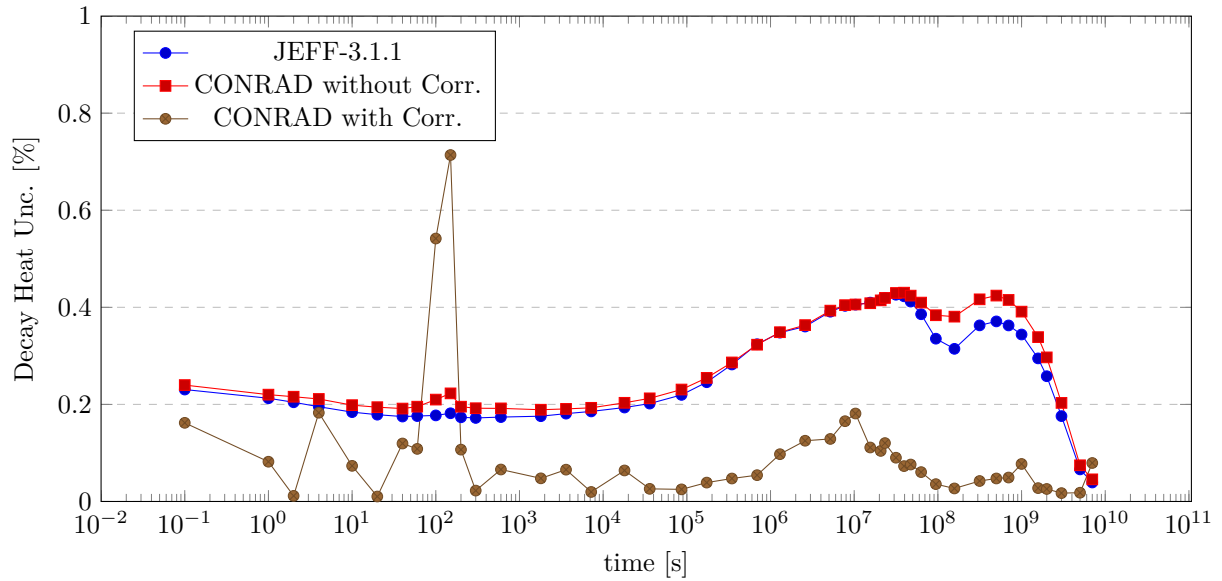


Figure 6.36: Decay heat uncertainty as a function of burn-up for a PWR-UOX pin-cell. The propagation of JEFF-3.1.1 U238F FY uncertainties on the decay heat has been compared to what we obtain from FY uncertainties generated by CONRAD, with and without including correlations.

6.4 Conclusions

The FY covariance matrices presented in Chapter 4 have been tested in nuclear reactor applications, estimating decay heat and reactivity loss uncertainty quantifications for three configurations. Conventional PWR UOX and MOX pin-cells were analyzed as test case to show the impact of correlations and to verify that CONRAD was actually able to reproduce not only JEFF-3.1.1 average values but also variances. The objective to ensure that CONRAD evaluations were consistent to the existing library was attained, unless for the most application-sensitive and then significant FY.

Some results were also obtained for the JHR. In particular the uncertainty propagation of ^{235}U yields led to extremely interesting conclusions. Such application in fact demonstrated and showed clearly the importance of properly including correlations in any uncertainty propagation of independent FY. The anti-correlations caused by the isobaric distribution normalization not only allow an impressive uncertainty reduction but also resolve and eliminate the inconsistencies existing between the evaluated independent and cumulative uncertainties contained in JEFF-3.1.1 library.

The propagation of independent FY without any correlation yielded a 2.85% uncertainty on the reactivity loss at the end of the cycle, reduced afterwards to 0.9% including CONRAD full covariance matrix. Reactivity was also considered, since it is clearly important for safety purposes. The initial JEFF-3.1.1 uncertainty of 395 pcm was brought to 116 pcm by CONRAD correlations.

Satisfactory results were obtained for all the fissioning systems considered. CONRAD seemed to calculate consistent and truthful uncertainty information for the most significant yields for applications. In most cases, the drastic uncertainty reductions observed

found physical explanations, but further investigations may be appropriate especially if safety-oriented utilizations of present results are planned.

Covariance matrices are mathematical objects which contain physical, modeling, experimental and statistical dependencies between the input data we provide to reactor analysis codes. Verifying covariance matrices is quite straightforward. A comprehensive validation is instead a really difficult task, since covariances are not measurable quantities. In this last chapter no validation accomplishment can be claimed. The main object was to verify and test the covariance behaviors on reactor applications, trying to understand if reliable outcomes were achievable. Only a thorough comparison to clean and FY-oriented integral measurements can provide information on the truthfulness of the uncertainty information estimated, verifying that FY uncertainty propagation is effectively in agreement with experimental error bars and providing some elements of validation of the statistical procedure adopted.

Conclusions and Perspectives

The main objective of the present doctoral work has been the generation of covariance information of interest for the Jules Horowitz Reactor (JHR) reactivity loss uncertainty estimation. During depletion, in fact, many new materials appear and fission product nuclear data uncertainty information are often incomplete. In particular, we treated the problem of finding consistent and science-based covariance matrices for fission product yields (FY). Current evaluated FY uncertainty information (contained in ENDF, JEFF, JENDL etc.), in fact, are limited to only variances, without providing any correlation. In the present work we proposed a methodology to evaluate physically consistent FY covariances to be included in JHR reactivity uncertainty quantification analyses, and reliable enough to be associated to the European JEFF-3.1.1 evaluation. We sought then to evaluate general purpose FY variance-covariance matrices demanded by present and future nuclear application optimization and design. Indeed, to meet recent needs on fission yields data, the Working Party on International Nuclear Data Evaluation Co-operation (WPEC) opened a collaboration sub-group (SG-37) for *Improved Fission Product Yields Evaluation Methodologies* [Mills, 2012], capable to produce covariance data including effects from experimental measurements, model parameter fitting and statistical analysis.

Many methodologies exist to generate nuclear data covariance matrices and they have been described in Chapter 1. We decided to resort to the Generalized Least Square Method (GLSM) implemented in CONRAD (COde for Nuclear Reaction Analysis and Data assimilation, developed at CEA-Cadarache) to find simultaneously FY model parameter best estimates and covariances. The main goal was not to provide a new evaluation, but to reproduce consistently JEFF-3.1.1 FY average values and uncertainties, adding correlation information. To do so, we firstly implemented in CONRAD independent FY models at the basis of JEFF-3.1.1 and ENDF/B-VII FY databases, adding a simplified new model to estimate prompt neutron emission probabilities. The Brosa mass FY physical model, used in JEFF-3.1.1 to fill gaps in post-neutron mass FY experiments, was correctly applied to pre-neutron evaporation distributions. It has been then convoluted with prompt neutron emission probabilities to obtain post-neutron data (also called independent fission yields), which allowed to take into account that light and heavy pre-neutron fragments emit a different average number of prompt neutrons. For the prompt neutron emission probability a simple model based on Gaussian distributions has been chosen, since it yielded the best results on total prompt neutron emission probability experimental data compared to other distributions (e.g. Poisson, Log-Normal). Since no physical theories are available to predict isotopic and isomeric fractions, we resorted to the Wahl and Madland-England semi-empirical models. This choice was truly consistent with JEFF-3.1.1 evaluated data, since the models just mentioned were used in JEFF to calculate independent distributions and isomeric ratios in absence of experimental data.

Independent FY model parameters have been adjusted in a GLS procedure using JEFF-3.1.1 as a pseudo-experimental database to represent evaluated FY. To do so, the average numbers of prompt neutrons emitted by pre-neutron fragments (saw-tooth curve) have been included as fitted parameters in the Bayesian learning process. Systematic uncertainties were considered in the covariance generation procedure thanks to analytical marginalization techniques, already implemented in CONRAD. Model parameter variance-covariance matrices have been afterwards propagated to obtain full FY uncertainty information.

CONRAD was also adapted to evaluate not only cross section or fission yield data but also miscellaneous fission quantities. This allowed a comprehensive analysis which included JEFF-3.1.1 evaluated data and experimental measurements on miscellaneous fission quantities such as the total prompt neutron emission probabilities and multiplicities. The results on the thermal neutron induced fission of ^{235}U , ^{239}Pu , ^{241}Pu and on the fast neutron induced fission of ^{238}U (presented in Chapter 4) showed the simultaneous representation of different independent fission related quantities and data sets. The most significant yields in JEFF-3.1.1 were consistently represented by model parameters calculations, providing reasonable results for the saw-tooth curves and returning values in complete agreement with experimental assessments for prompt neutron emission probabilities and multiplicities. Some differences were observed between CONRAD saw-tooth data and experimental measurements, when available. Nevertheless, the bibliographic research on experimental saw-tooth data showed quite relevant discrepancies between different authors which enhanced the confidence on the results we obtained.

Cumulative FY averages and covariances were also calculated thanks to the Q-matrix. The Q-matrix allowed to take into account all the fission product decay mechanisms and branching ratios to provide cumulative and chain yields. CONRAD data were in excellent agreement with the most significant JEFF values, this verified the Q-matrix implementation in CONRAD and validated the independent yield model parameter values obtained by the statistical analysis.

Furthermore, an algorithm able to produce dedicated FY inputs for reactor physics codes has been implemented in CONRAD. It allowed to generate FY data for APOLLO2, but its extension to other deterministic and Monte Carlo calculation tools is quite straightforward.

To provide fully consistent covariance information to existing evaluated data, we checked if CONRAD variances were close enough to what is available in JEFF-3.1.1. Representing the variances for the all FY inventory contained in JEFF-3.1.1 is not straightforward. The main goal was to verify if the variances related to the most application-sensitive FY were actually well taken into account. Different applications were considered to test the impact of CONRAD covariances and to compare the results to what could be previously obtained using diagonal JEFF-3.1.1 variance matrices. A first calculation performed with the CYRUS code showed a good agreement between CONRAD and JEFF variances for the elementary fission decay heat uncertainty.

Some cumulative yields which cover an important role for reactor physics applications were considered. Their average values were perfectly represented by CONRAD. Some issues were found for some cumulative yield uncertainty. An example was the cumulative yield of ^{148}Nd for the thermal fission of ^{235}U . Even if the discrepancies between independent

and cumulative yield uncertainties existing in the JEFF-3.1.1 library have been discussed in Chapter 4, a possible and feasible solution to such problem was proposed.

Reactivity loss and decay heat uncertainties due to FY were also analyzed implementing two different methodologies. The former, deterministic, was based on the estimation of sensitivity coefficients evaluated by simple direct perturbations of independent yields. The latter was instead based on Monte Carlo uncertainty propagations, using URANIE as sampling engine. APOLLO2 and MENDEL were used to calculate reactivity and decay heat for real reactor applications. Firstly simple geometries were considered such as PWR UOX and MOX pin-cell. Successively, the JHR in its reference configuration was analyzed to verify the impact of the covariances generated by CONRAD on the engineering parameters we were interested in.

The Monte Carlo comparison to deterministic calculations did not show any non-linear issues in propagating FY data. Direct perturbations sensitivity estimations have been then validated for the pin-cell and the JHR configurations. Propagating CONRAD uncertainties showed a globally satisfactory agreement to what can be obtained by only using JEFF-3.1.1 variance matrices. This confirmed the consistency between our results and the existing evaluated variances. Including full CONRAD covariance matrices in the analyses showed an impressive uncertainty reduction for all the applications considered. The critical observation of reactor parameter results highlighted the importance of including correlations for FY in any uncertainty propagation analyses and showed the actual reliability of the uncertainty information obtained with CONRAD.

FY covariance results for the JHR reactivity uncertainty quantification have been produced. The propagation of JEFF-3.1.1 ^{235}U thermal FY variances led to 2.85% uncertainty on the reactivity loss at the end of the fuel cycle. Including CONRAD full covariance information the uncertainty was reduced to 0.8%, which can have important consequences on fuel cycle length optimization. The same exercise was repeated also for reactivity which is a safety related reactor parameter. The propagation of JEFF variances led to a reactivity uncertainty of 395 pcm (1σ) at 82 GWd t^{-1} . Such value was reduced to 116 pcm using CONRAD correlations, and the reasons and the reliability of such uncertainty reduction were discussed in Chapter 6.

The testing on applications proved that truthful, consistent and science-based FY covariance matrices have been successfully obtained. Such matrices can be in fact certainly proposed for further JHR uncertainty quantification analyses and as additional uncertainty information to be included in the JEFF project. Moreover, considering the promising results obtained on conventional reactor applications, present covariance results will be likely included in COMAC (COvariance MAtrices from Cadarache) [Archier et al., 2014b], the covariance library used by CEA and its industrial partners. This will provide more data on their impact on applications, providing complete indications on the reliability of such covariances.

At the moment no nuclear data format exists to include FY covariances in any nuclear data library. Even if present covariances, or those proposed by other organizations, are accepted to be associated to the existing or next JEFF FY releases, a specific format is required.

It has to be pointed out that only testing on applications has been achieved in the present work. A comprehensive validation process should include the comparison to clean and FY-oriented integral measurements able to provide information on the truthfulness of the uncertainty information estimated, verifying that FY uncertainty propagation is effectively in agreement with experimental error bars.

The present work has demonstrated that reliable FY covariance matrices can be obtained and a methodology has been proposed, leading to convincing results. Nevertheless, only mostly thermal fissioning systems were actually carefully analyzed and tested on light water reactor applications. Fast fissioning systems can be treated in the same way, generating FY covariance matrices to be applied in Generation IV reactor (e.g. ASTRID) calculations and see the impact of FY nuclear data on future nuclear system safety and exploitation parameters. Some results were obtained here for fast fissioning systems, such as the fast fission of ^{238}U , but further investigations are necessary.

The methodology proposed requires a prior knowledge of the average number of prompt neutrons emitted by pre-neutron fission fragments, the saw-tooth curve. Such information reach satisfactory accuracy for well-known fissioning systems (e.g. $^{235}\text{U}(n_{th}, f)$) but the tough experimental conditions which characterize its measurement unfortunately induce generally high uncertainties, and, for more exotic fissioning systems, it is completely missing. For other fissioning systems than $^{235}\text{U}(n_{th}, f)$ and $^{239}\text{Pu}(n_{th}, f)$ we used in fact shifted or derived saw-tooth curves, obtaining results which could not be validated, since no experimental data are available. Furthermore, no models for the saw-tooth exists and the average number of prompts neutrons emitted by pre-neutron fragments, considered as independent in CONRAD analyses, might be instead possibly correlated due to the excitation energy repartition between light and heavy partners. The energy repartition law is however currently under investigation by the physical community, and so the presented results can be considered a satisfactory accomplishment of the initial objectives using the available analysis means. In any case, future work on this aspect, that can be surely considered a model defect, must be achieved to consider the missing of a saw-tooth theoretical model in our analysis calculations, providing a certain degree of uncertainty coming from the lack of knowledge we have on such information.

Such methodology was born as relatively fast method to respond to the quite urgent demand for FY correlations coming from operating and future nuclear systems optimization and design. During the analyses, the JEFF-3.1.1 evaluated data were assumed as pseudo-experimental measurements, provided with a diagonal variance matrix. Systematic errors were successively taken into account using analytical marginalization techniques on the norms of isotopic and mass distributions. However a new and comprehensive FY evaluation which could take into account correlations from modeling, physics, experiments and statistical analyses is desirable, and its feasibility has been demonstrated by the results obtained here. This must also include the systematic uncertainty information contained in recent FY measurements, which should be considered since the beginning analysis phase in an extensive evaluation process able to include all the available information and produce science-based reliable covariances.

Appendix A

Least-Square Solution Schemes

DIFFERENT formulations we can be found for the *Generalized Least Square* problem for the posterior covariance matrix. Each formulation, in fact, can have advantages and drawbacks depending on the type of applications. We saw in Chapter 1 that, minimizing a cost function or applying the Bayesian procedure to the case of a linear or linearizable theoretical model, we are able to find the following expressions for the model parameter best estimates and covariance matrix:

$$\mathbf{C}_x = (\mathbf{C}_\theta^{-1} + \mathbf{G}^\dagger \mathbf{C}_y^{-1} \mathbf{G})^{-1}, \quad (\text{A.1})$$

and

$$\vec{x}_{BE} = \vec{\theta} + (\mathbf{C}_\theta^{-1} + \mathbf{G}^\dagger \mathbf{C}_y^{-1} \mathbf{G})^{-1} \mathbf{G}^\dagger \mathbf{C}_y^{-1} (\vec{y} - \vec{t}_\theta), \quad (\text{A.2})$$

where we used the same notations assumed in Chapter 1.

The following sections will be devoted to a brief description of other two different arrangements of these equations, which are commonly used in practice.

A.1 The (I + Q)-formulation

The first formulation is the simplest one, it is just a straightforward manipulation of Eq. A.1. Multiplying \mathbf{C}_x^{-1} on the right by \mathbf{C}_θ we obtain

$$\mathbf{C}_x^{-1} \mathbf{C}_\theta = \mathbf{C}_\theta^{-1} \mathbf{C}_\theta + \mathbf{G}^\dagger \mathbf{C}_y^{-1} \mathbf{G} \mathbf{C}_\theta = \mathbf{I} + \mathbf{G}^\dagger \mathbf{C}_y^{-1} \mathbf{G} \mathbf{C}_\theta \quad (\text{A.3})$$

then multiplying on the left by \mathbf{C}_x :

$$\mathbf{C}_x \mathbf{C}_x^{-1} \mathbf{C}_\theta = \mathbf{C}_\theta = \mathbf{C}_x (\mathbf{I} + \mathbf{G}^\dagger \mathbf{C}_y^{-1} \mathbf{G} \mathbf{C}_\theta) \quad (\text{A.4})$$

Calling

$$\mathbf{Q} = \mathbf{G}^\dagger \mathbf{C}_y^{-1} \mathbf{G} \mathbf{C}_\theta, \quad (\text{A.5})$$

we finally have

$$\mathbf{C}_x = \mathbf{C}_\theta (\mathbf{I} + \mathbf{Q})^{-1} \quad (\text{A.6})$$

and

$$\vec{x}_{BE} = \vec{\theta} + \mathbf{C}_\theta (\mathbf{I} + \mathbf{Q})^{-1} \mathbf{G}^\dagger \mathbf{C}_y^{-1} (\vec{y} - \vec{y}_\theta). \quad (\text{A.7})$$

A.2 The $(\mathbf{C}_y + \mathbf{N})$ -formulation

Another formulation for the posterior covariance matrix can be deduced applying the following identity¹:

$$(\mathbf{A} + \mathbf{UBV})^{-1} = \mathbf{A}^{-1} - \mathbf{A}^{-1}\mathbf{U}(\mathbf{I} + \mathbf{BVA}^{-1}\mathbf{U})^{-1}\mathbf{BVA}^{-1}, \quad (\text{A.8})$$

then we can write

$$\mathbf{C}_x = \mathbf{C}_\theta - \mathbf{C}_\theta \mathbf{G}^\dagger (\mathbf{N} + \mathbf{C}_y)^{-1} \mathbf{G} \mathbf{C}_y, \quad (\text{A.9})$$

where

$$\mathbf{N} = \mathbf{G} \mathbf{C}_\theta \mathbf{G}^\dagger. \quad (\text{A.10})$$

Rearranging the model parameter best estimates vector we get [SAMMY, 2008]

$$\begin{aligned} \vec{x}_{BE} &= \vec{\theta} + [\mathbf{C}_\theta - \mathbf{C}_\theta \mathbf{G}^\dagger (\mathbf{N} + \mathbf{C}_y)^{-1} \mathbf{G} \mathbf{C}_y] \mathbf{G}^\dagger \mathbf{C}_y^{-1} (\vec{y} - \vec{y}_\theta) \\ &= \vec{\theta} + [\mathbf{C}_\theta \mathbf{G}^\dagger - \mathbf{C}_\theta \mathbf{G}^\dagger (\mathbf{N} + \mathbf{C}_y)^{-1} \mathbf{G} \mathbf{C}_y \mathbf{G}^\dagger] \mathbf{C}_y^{-1} (\vec{y} - \vec{y}_\theta) \\ &= \vec{\theta} + \mathbf{C}_\theta \mathbf{G}^\dagger [\mathbf{I} - (\mathbf{N} + \mathbf{C}_y)^{-1} \mathbf{N}] \mathbf{C}_y^{-1} (\vec{y} - \vec{y}_\theta) \\ &= \vec{\theta} + \mathbf{C}_\theta \mathbf{G}^\dagger [\mathbf{I} - (\mathbf{N} + \mathbf{C}_y)^{-1} (\mathbf{N} + \mathbf{C}_y - \mathbf{C}_y)] \mathbf{C}_y^{-1} (\vec{y} - \vec{y}_\theta) \\ &= \vec{\theta} + \mathbf{C}_\theta \mathbf{G}^\dagger [\mathbf{I} - (\mathbf{N} + \mathbf{C}_y)^{-1} (\mathbf{N} + \mathbf{C}_y) + (\mathbf{N} + \mathbf{C}_y)^{-1} \mathbf{C}_y] \mathbf{C}_y^{-1} (\vec{y} - \vec{y}_\theta) \\ &= \vec{\theta} + \mathbf{C}_\theta \mathbf{G}^\dagger (\mathbf{N} + \mathbf{C}_y)^{-1} (\vec{y} - \vec{y}_\theta), \end{aligned} \quad (\text{A.11})$$

which can be found in many textbooks concerning this subject (see for example [Smith, 1990]).

¹For further details on derivation and variants see Ref. [Henderson and Searle, 1981].

Appendix B

The ENDF Format

THE ENDF (Evaluated Nuclear Data Format) system has been developed for the storage and retrieval of evaluated data to be used for nuclear technology applications [Obložinský et al., 2010]. It provides representations for neutron cross sections and distributions, photon production from neutron reactions, charged-particle production from neutron reactions, photo-atomic interaction data, thermal neutron scattering data, radionuclide decay data and fission product yields.

The development of nuclear technology applications has essentially driven many features of the nuclear data representation systems, including the choice of materials to be included, the data and the format actually used and the testing and benchmarking activity. An important consequence is that such evaluation has to be *complete* for nuclear reactor applications in terms of materials, nuclear reactions and uncertainty information.

The ENDF libraries are a collection of evaluations in a computer-readable format that can be used by nuclear data processing codes for applications. For this reason the ENDF format has been built and maintained having in mind how such codes work. ENDF files in fact must be processed to generate point-wise and group-averaged cross sections to be used in neutronics calculations, including functions for resonance reconstructions, Doppler broadening and multi-group averaging.

After a brief general description of the main features of ENDF-6 format, which is the one used for JEFF-3.1.1 evaluated nuclear data library, specific attention will be dedicated to the fission yield sub-library.

B.1 ENDF General Features

A library is a collection of material evaluations from a recognized evaluation group [Obložinský et al., 2010]. Each of this collections is identified by an NLIB number. For the European library JEFF (Joint Evaluated Fission and Fusion file) such NLIB number is 2. The different libraries can be characterized by several versions that may imply significant changes. Each version can have several releases, that in general differ for less radical modifications following a library revision. An example is the JEFF library, version 3 and release 1 or 1.1. From that we can identify the specific library we are referring to. In the present work, only the JEFF-3.1.1 library was considered, since it is the most recent release for fission yields¹.

¹The 3.2 release is underway, even if already available for cross sections. The next version will be JEFF-4, that will be probably ready in 2020.

Each library is subdivided in sub-libraries distinguished by the incident particles and data types. The sub-libraries are identified by numbers called NSUB. For incident neutron data NSUB=10.

The sub-libraries contain evaluations for different materials (MAT) and such data are organized in files (MF). Examples are MF=3 for cross section information, MF=4 for angular distributions. Specific files are dedicated to covariance data. MF=32 for resonance parameters covariances, MF=33 for cross section covariances, MF=34 for angular distribution covariances etc. For fission yields, no covariance format is currently available as better explained in the following section (see Tab. B.1). These files are subdivided in sections (MT) describing specific reactions, with numbers from 1 to 999. An example is MT=102 for radiative capture cross sections.

MF	Description
1	General information
2	Resonance parameter data
3	Reaction cross sections
4	Angular distributions for emitted particles
5	Energy distributions for emitted particles
6	Energy-angle distributions for emitted particles
7	Thermal neutron scattering law data
8	Radioactivity and fission-product yield data
9	Multiplicities for radioactive nuclide production
10	Cross sections for radioactive nuclide production
12	Multiplicities for photon production
13	Cross sections for photon production
14	Angular distributions for photon production
15	Energy distributions for photon production
23	Photo- or electro-atomic interaction cross sections
26	Electro-atomic angle and energy distribution
27	Atomic form factors or scattering functions for photo-atomic interactions
28	Atomic relaxation data
30	Data covariances obtained from parameter covariances and sensitivities
31	Data covariances for nu(bar)
32	Data covariances for resonance parameters
33	Data covariances for reaction cross sections
34	Data covariances for angular distributions
35	Data covariances for energy distributions
39	Data covariances for radionuclide production yields
40	Data covariances for radionuclide production cross sections

Table B.1: Definition of file types (MF) in a ENDF sub-library.

A complete description of the ENDF format goes far beyond the objective of this dissertation and of this appendix. Further information and details can be found in Ref. [Obložinský et al., 2010].

B.2 The Fission Product Yields File

Data for the production of fission products are collected in different sub-libraries according to which mechanism induces fission. Examples are the spontaneous fission yields

(NSUB=5), the neutron-induced fission product yields (NSUB=11), photon-induced fission product yields (NSUB=10011) etc.

For the different sub-libraries, included the incident neutron data one (NSUB=10), a specific file (MF=8) is dedicated to describe the properties of the reaction products if they are radioactive. Information concerning the decay of the reaction products (any MT) are normally given in this file (so fission products are included), and if some information are missing they are provided in dedicated sub-libraries. Such radioactive products file contains two sections devoted to independent (MT=454) and cumulative (MT=459) yields. The two formats are identical and a complete set of fission product yield data is given for a specific incident particle energies.

In JEFF, fission yields are generally provided for three energy spectra, thermal, fast (400 keV) and high (14 MeV) using the ENDF-6 data format. Once the energy and the fission target are defined, fission product yields data are mainly characterized by the following four numbers:

- i) Fission product charge and mass numbers identifier ZAFP=(1000Z+A) (e.g. 3.8095E+04 for ^{95}Sr);
- ii) Isomeric state identifier FPS=0.0000E+00 for the ground state and FPS=1.0000E+00 (2.0000E+00) for the first (second) metastable state;
- iii) Fission yield values (independent or cumulative) in scientific notation;
- iv) Fission yield uncertainties in scientific notation.

The peculiar aspect for fission yield evaluation is that uncertainties are self-contained. No specific files are in fact dedicated to fission yield uncertainty or covariance storage. This is a key point for the present work since there is no available format for fission yield covariances.

Cumulative yields values need to be consistent with the decay data library (containing branching ratios which are required for the Q-matrix construction) and the independent ones. No mass yields are provided in the library and are usually derived from isomeric data by nuclear data visualization softwares such as JANIS-4.0.

Appendix C

CONRAD Main Functionalities

IN this Appendix some of the most important functionalities available in CONRAD are synthesized and listed. The objective is not to give an exhaustive code presentation, but to provide a general outline to what CONRAD can perform. To retrieve further details in specific topics, the reading of dedicated references is highly recommended.

C.1 Microscopic Data Assimilation

In CONRAD, several cross section models can be employed in the nuclear data evaluation in the whole $[0, 20 \text{ MeV}]$ -range, depending on the energy of the particles which induce the nuclear reactions and on target nuclei. CONRAD is not just a new R-matrix fitting code such as SAMMY [SAMMY, 2008] or REFIT [Moxon et al., 2010]. It allows modern and comprehensive cross section evaluation for the different energy regions of interest for nuclear applications (*theory* module), providing also the possibility to treat other kind of physical observables such as PFNS or FY [Berge, 2015, Terranova et al., 2015b].

For the resolved resonance region (RRR) the Multi-Level Breit-Wigner and the Reich-Moore formalisms are available. For the unresolved resonance region (URR) the average R-matrix theory can be used and a new Hauser-Feshbach engine adaptable to different reactions has been recently added. Level densities can be obtained using Gilbert-Cameron formulas for instance. Gamma transmission, with the Giant Dipole Resonance Model [De Saint Jean et al., 2007], and fission transmission coefficients, using classical Hill-Wheeler or micro-macroscopic multi-barriers [Tamagno, 2015], can be calculated. For the fast energy region, ECIS [Raynal, 1994] and TALYS [Koning et al., 2007] interfaces are available, even if a new coupled channel optical model tool and new transmission coefficient engines have been included [Tamagno, 2015] to replace the ECIS legacy code. Furthermore, to calculate cross sections at any temperature, a Doppler broadening tool has been implemented, which allows to evoke free gas or crystal lattice models.

For cross sections, an energy grid is generated according to the available experimental values. Theoretical calculations for averages and derivatives are then performed for such grid points and the Bayesian adjustment can be then accomplished. Multi-threading capabilities are available in CONRAD for theoretical model calculations, especially if different energy domains, which are characterized by independent theoretical models, can be identified.

New features have been recently added for analyzing better the fission process. They

concern the study of prompt fission neutron spectra (PFNS) using Maxwell, Watt and Madland-Nix theoretical models [Berge, 2015, Berge et al., 2015] and an interface to the FIFRELIN code [Litaize and Serot, 2010, Regnier, 2013]. Semi-empirical fission yield models (see Chapter 2) have been also included in the theoretical framework of conradlib during the present PhD work, allowing to calculate independent and cumulative fission yields.

In the conradlib framework, a comprehensive treatment of experimental data sets and associated uncertainties is available (*experiment* module). These functionalities allow to assimilate raw experimental uncorrelated data and produce reduced long-range-correlated physical observables, provided with complete and scientifically-based uncertainties (statistical and systematic) [De Saint Jean et al., 2007]. The final covariance matrix is obtained by the following formula

$$\mathbf{C} = \mathbf{S} \cdot \mathbf{S}^\dagger + \mathbf{D}. \quad (\text{C.1})$$

\mathbf{D} is diagonal and represents the statistical fraction of the uncertainty. \mathbf{S} takes into account correlations coming from the raw data reduction process. The latter comes from the functional at the basis of the cross section reconstruction from raw observables which can be for instance [Archier, 2011, Archier et al., 2014a]

- i) Total and differential cross sections;
- ii) Transmissions;
- iii) Capture yields;
- iv) Integral experiments.

This kind of experimental observables can be easily provided by the EXFOR¹ [Otuka et al., 2014] database for instance.

A full time-of-flight treatment is available in CONRAD, and observables can be analyzed using a description in energy or even in time. In most of experimental data analysis resolution functions are necessary [Fröhner, 2000]. Resolution functions $R(E, E')$ give the probability distribution that an event observed at energy E has actually occurred at the energy interval dE' centered in E' , since many sources of energy shifting are affecting time-of-flight measurements. In CONRAD two kinds of resolution functions have been implemented [Archier et al., 2013]. The former is analytical, a χ^2 distribution is in fact normally used to represent time distributions in the target-moderator assembly. The latter has a numerical nature which allows the user to provide distributions calculated via Monte Carlo simulations of the experimental facility. Sample homogeneities are treated as well, we need in fact to correct raw data accounting for sample impurity which always affects measurements [Archier et al., 2013].

Multi-scattering correction modules are available for partial cross sections measurements. If, for instance, neutron capture is the sought nuclear reaction, the interaction of interest can take place after multiple prior scattering collisions which induce neutron energy loss. Therefore multiple scattering corrections are needed, especially for thick target sample. In

¹The Experimental Nuclear Reaction Data (EXFOR) library contains an extensive compilation of experimental data for nuclear interactions, such as neutron or charge-particle induced reactions. On December 2015, the database contained 21079 data files (see <https://www-nds.iaea.org/exfor/exfor.htm>).

CONRAD analytical and Monte Carlo methodologies can calculate correction functionals for cylindrical and spherical geometries [Litaize et al., 2013].

Additional experimental parameters have been included to better describe the measurement process and analysis. Those parameters related to the beam (e.g. flight path, time offset, beam diameter), to the sample description (e.g. areal and volumetric density, geometrical configuration, composition etc.) and to the analytical resolution function (e.g. moderator mean free path) can participate to the Bayesian adjustment as theoretical model parameters do [Archier et al., 2014a]. Their uncertainties can be propagated on nuclear reaction model parameters through marginalization techniques² (see Section 1.5.1).

C.2 Integral Data Assimilation

As schematically shown in Fig. C.1, three types of Integral Data Assimilation (IDA) methodologies have been implemented in the CONRAD framework [Archier, 2011]. Such

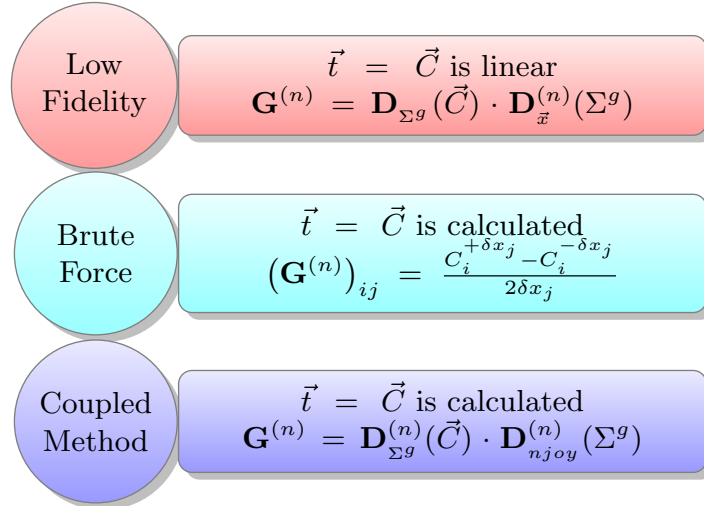


Figure C.1: Integral Data Assimilation methodologies available in CONRAD.

methodologies allow to assimilate directly in the data evaluation process integral data. As already mentioned, in modern nuclear data evaluation, general-purpose integral experiments need in fact to be included in model parameter adjustment process to generate physically consistent cross sections, for a wide range of applications.

Integral experiment data can be included in the evaluation process using the same procedure seen for a general data evaluation process (see Chapter 1). Experimental values \vec{y} are the integral parameters we measure which are normally provided with a covariance matrix \mathbf{C}_y , the theoretical model \vec{t} corresponds to the neutron transport solver adopted which can be indicated as \vec{C} and the derivative matrix is defined as

$$G_{ij} = \frac{\partial C_j}{\partial x_i}, \quad (\text{C.2})$$

²In Chapter 1 we discriminate such experimental additional parameters, whose uncertainties can be propagated through deterministic or Monte Carlo marginalization procedures, using the term *nuisance*.

where $\vec{x} = x_1, \dots, x_N$ is the nuclear reaction model parameter vector and C_j is the j -th calculated integral value. In an iterative GLSM process (see Section 1.4.1.2), the main issue is to dispose of updated calculated values and derivatives. Neutron transport solver are in fact time-consuming tools and a compromise between precision and CPU-time needs to be pursued.

In the *low-fidelity* method (see flow-chart in Fig. C.1), derivatives $(G)_{ij}$ are decomposed in a product of two matrices. The first one, $\mathbf{D}_{\Sigma^g}(\vec{C})$, relies on integral parameter sensibility to multigroup cross sections Σ^g . It can be calculated using perturbation methods commonly implemented in transport codes such as ERANOS2 [Ruggieri et al., 2006] or APOLLO2 [Sanchez et al., 1988], and, in this preliminary approach, it is assumed as constant, not depending on cross section deviations due to the iterative adjustment procedure. The second matrix $\mathbf{D}_{\vec{x}}^{(n)}(\Sigma^g)$ contains the derivative of multigroup cross sections to nuclear reaction model parameters and can be calculated by CONRAD at each n -th iterative step. The theoretical values are updated supposing the neutron transport solver a linear function on nuclear reaction model parameters, hence mathematically

$$\vec{C}^{(n)} = \vec{C}^{(0)} + \mathbf{G}^{(n)}(\vec{x}^{(n)} - \vec{x}^{(0)}). \quad (\text{C.3})$$

The *brute force* method [Archier, 2011] performs $(2N+1)$ transport calculation for each step and for each integral parameter. It calculates directly the theoretical values and derivatives are obtained by finite differences. For each iterative step, ENDF file are then generated by CONRAD, processed and employed in transport calculations. A multi-software interface has been developed in order to handle automatically all these processes and get for each iterative step updated theoretical integral parameters and derivatives. The third method called *coupled* performs one transport and one sensibility calculation for each integral parameter and for each step to obtain $\vec{C}^{(n)}$ and $\mathbf{D}_{\Sigma^g}^{(n)}(\vec{C})$. The $\mathbf{D}_{njoy}^{(n)}(\Sigma^g)$ matrix needed to calculate GLSM derivatives is obtained by finite differences of NJOY [MacFarlane et al., 2000]³ outputs:

$$\left(\mathbf{D}_{njoy}^{(n)}(\Sigma^g)\right)_{ij} = \left(\frac{\partial(\Sigma^g)_i}{\partial x_j}\right)^{(n)} \simeq \left(\frac{(\Sigma^g)_i^{+\delta x_j} - (\Sigma^g)_i^{-\delta x_j}}{2\delta x_j}\right)^{(n)}. \quad (\text{C.4})$$

As already mentioned CONRAD is provided with an *interface* module contained in conradlib set of libraries. Other than handling the communication between different conradlib modules, it can provide and manage different I/O formats. The present ENDF nuclear data format (see Appendix B) is of course available, but XLM output engines are already being conceived for the new GND nuclear data library format [Mattoon et al., 2012]⁴.

In the *analysis* module most of the data analysis methodologies described in Chapter 1 have been implemented [De Saint Jean et al., 2007, Habert, 2009, Privas, 2015]. Deterministic and Monte Carlo parameter adjustments and marginalizations can be performed by CONRAD in the whole energy domain of interest for applications.

³NJOY performs the *processing* phase and it is essentially the conversion of the ENDF cross section file in a binary one which satisfies the needs of neutron transport codes for applications.

⁴The Generalized Nuclear Data format (GND) is meant to replace older formats with a hierarchy based conception, thought to mirror the underlying physics and aligned to modern coding and databases.

Appendix D

Elementary Fission Decay Heat Calculations

IN the present PhD work the main goal is to generate FY covariance matrices which are consistent with the existing JEFF-3.1.1 evaluation, the last available release at present time.

No new evaluation has been meant, the main objective was, in fact, to represent the JEFF library and add consistent and physical covariance data. To do so, semi-empirical models based on physical assumptions and a consistent utilization of the Brosa fission modes to represent pre-neutron distributions were at the basis of a GLS (Generalized Least Square) procedure to simultaneously evaluate model parameter best estimates and covariances. Such covariances have been propagated successively to generate full FY covariance information.

An important task was the representation of JEFF-3.1.1 best estimates. To verify if CONRAD was actually capable to represent the most significant yields, and so the most relevant for nuclear applications, elementary fission decay heat calculations were performed. We used MENDEL to calculate the decay heat released by the several elementary fission products related to the fissioning systems considered in the present dissertations. We performed two types of calculations. Results using JEFF-3.1.1 yields were then compared to those obtained using CONRAD values as input data.

In Figs. [D.1](#) and [D.2](#) JEFF-3.1.1 and CONRAD results are compared for the U235T, Pu239T, Pu241T, U238F, Pu239F and Pu240F fissioning systems. A satisfactory agreement is clearly visible between calculations concerning the same elementary fission, proving the capability of CONRAD to globally represent JEFF values. More precise analyses, performed on microscopic data, showed that the most significant yields are in fact well represented, even if worse agreement exists for lower yields ($\leq 10^{-4}$). However, they induce a negligible impact on applications and their representation goes beyond the purposes prefixed for the present work.

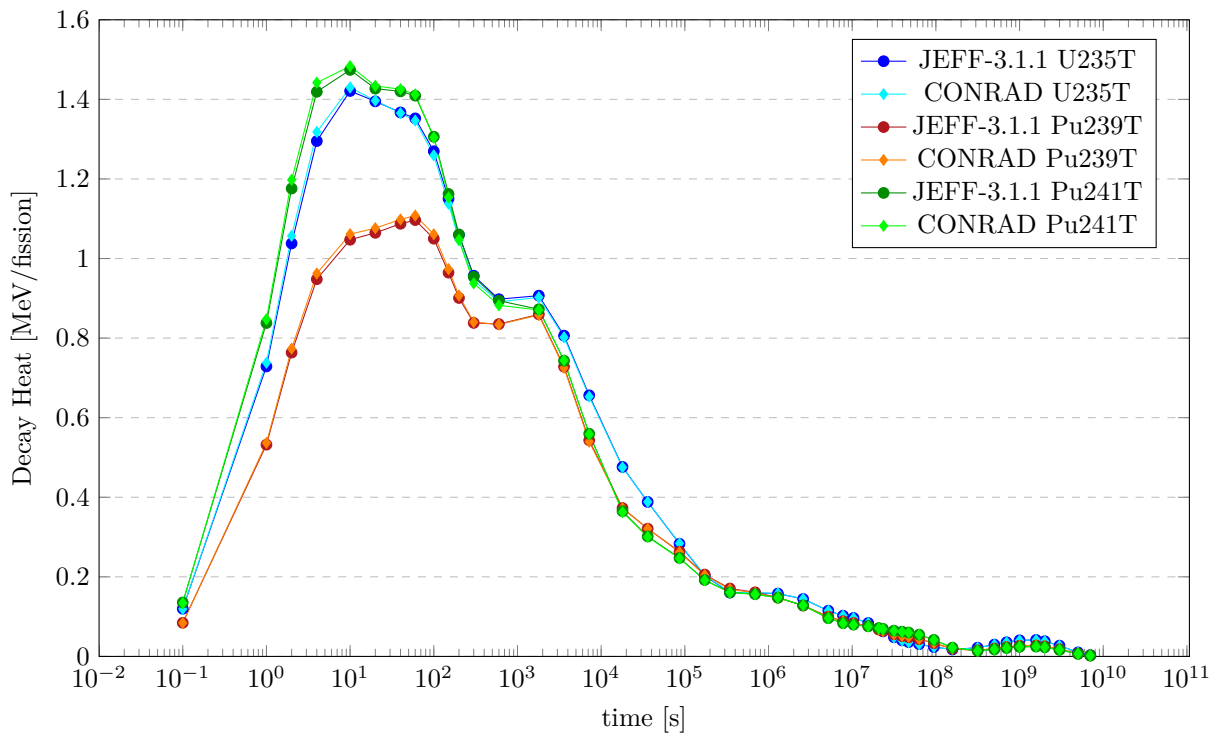


Figure D.1: Comparison between elementary fission decay heat calculations for the thermal fissioning systems U235T, Pu239T and Pu241T, using JEFF-3.1.1 and CONRAD FY values.

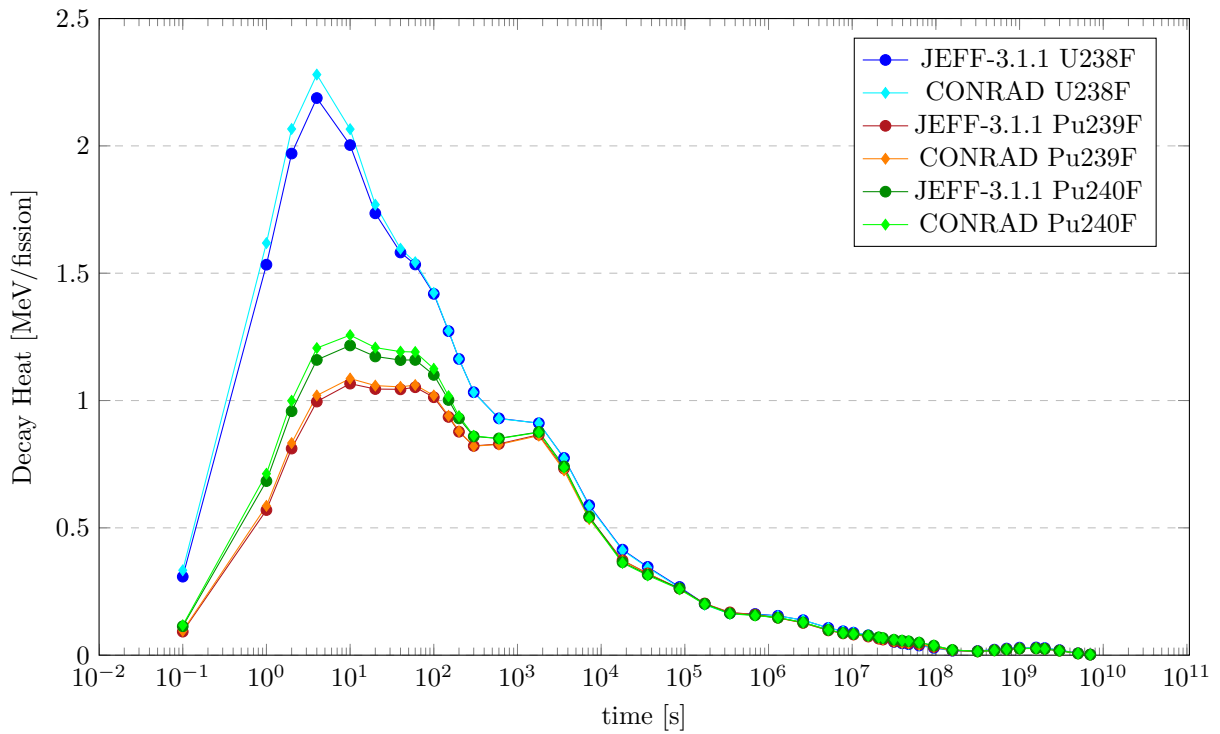


Figure D.2: Comparison between elementary fission decay heat calculations for the fast fissioning systems U238F, Pu239F and Pu240F, using JEFF-3.1.1 and CONRAD FY values.

Appendix E

Complementary Results on FY Covariances

THE JHR is a fascinating nuclear experimental facility oriented to reactor technology research and development. However, it still is a light water reactor so we privileged thermal neutron induced fissioning systems which can find wider applications for operating nuclear systems.

However the generation of FY covariances is a general problem which is of fundamental interest also for Generation IV reactor concepts. For this reason some fast fissioning systems have been considered in this work and some preliminary results are hereinafter presented.

They are preliminary because no covariance testing have in fact been performed using specific fast spectrum reactor test cases but they give quite promising expectations on the possibility to achieve the same results we saw for thermal systems even for fast neutron fissioning ones. In the following sections some results for the fast neutron induced fission of ^{239}Pu and ^{240}Pu are provided.

E.1 Pu-239 Fast Fission

In Chapter 4 a general procedure to generate FY covariances has been discussed and applied for the thermal neutron induced fission of ^{235}U , ^{239}Pu and ^{241}Pu , and for the fast fission of ^{238}U . The same exercise has been repeated for the fast fission of ^{239}Pu to generate independent yields covariance matrices. Again, we used JEFF-3.1.1 evaluated data as pseudo-experimental files in CONRAD and we adjusted FY model parameters including miscellaneous fission quantities as the total prompt neutron multiplicity in the statistical analysis.

Pu239F^1 , has the same difficulties encountered for U238F. No saw-tooth data and no total prompt neutron emission probabilities measurements are available. We used as prior data what has been used for the thermal fission of ^{239}Pu (Pu239T, see Chapter 4). Therefore Tsuchiya's sawtooth values [Tsuchiya et al., 2000] and Dematté fission mode parameters [Dematté, 1996] for Pu239T have been taken as priors for fast neutron induced FY analysis.

¹We can resort to the usual notation, therefore Pu239F refers to the fast fission (~ 400 keV) of ^{239}Pu .

Parameter	Prior BE	Prior Unc. [%]	Posterior BE	Posterior Unc. [%]
$D_{St.I}^*$	14.97	5	15.17	0.4
$D_{St.II}^*$	20.96	5	21.66	1.0
$\sigma_{St.I}^*$	3.73	10	3.1	2.2
$\sigma_{St.II}^*$	6.48	10	6.0	2.6
σ_{SL}^*	15.8	10	9.7	9.2
$N_{St.I}$	0.248	10	0.333	7.3
N_{SL}	0.005	20	0.008	8.9

* Expressed in [amu].

Table E.1: Fission mode parameters best estimates (BE) and uncertainties before (prior) and after (posterior) the analysis using CONRAD for the fast fission of ^{239}Pu .

In Tab. E.1, the fission modes parameters obtained using CONRAD (Posterior) are compared to prior values. The only term of comparison is what obtained for the thermal fission of the same isotope (see Tab. 4.7). Except for a significant difference (~ 1 amu) observed for the position of the Standard I between the two fissioning systems, reasonable values are obtained also for Pu239F. The uncertainties are already taking into account the analytical marginalization process described in Chapter 1.

In Tab. E.2 Wahl and Madland-England model parameters are provided. We used as prior the same file used for Pu239T, as done for mass FY parameters².

Parameter	Prior BE	Prior Unc. [%]	Posterior BE	Posterior Unc. [%]
$\sigma_Z(140)$	0.566	20	0.49855	18
$\Delta Z(140)$	-0.487	20	-0.41021	12
σ_{50}	0.356	20	0.41977	0.75
$F_N(140)$	1.076	20	0.99006	2.4
$F_Z(140)$	1.207	20	1.0485	17.2
$SL50$	0.191	20	0.32562	5.0
ΔZ_{max}	0.699	20	0.49011	0.75
J_{rms}^L	7.5	10	7.9645	0.5
J_{rms}^H	7.5	10	7.952	1.3

Table E.2: Wahl and Madland-England parameters best estimates (BE) and uncertainties before (prior) and after (posterior) the analysis using CONRAD, for the fast fission of ^{239}Pu .

For this fissioning system no Wahl parameters have been adjusted for the very asymmetric regions. Also in this case, uncertainties include norm marginalization for Tellurium and Iodine isomeric distributions, and for the whole mass distribution (1%).

In Figs. E.1 and E.2 the comparison between CONRAD and JEFF-3.1.1 mass distributions is shown, exhibiting an excellent agreement for the most significant FY.

²Another possible way could be using as priors the posterior values obtained from the thermal fission of ^{239}Pu .

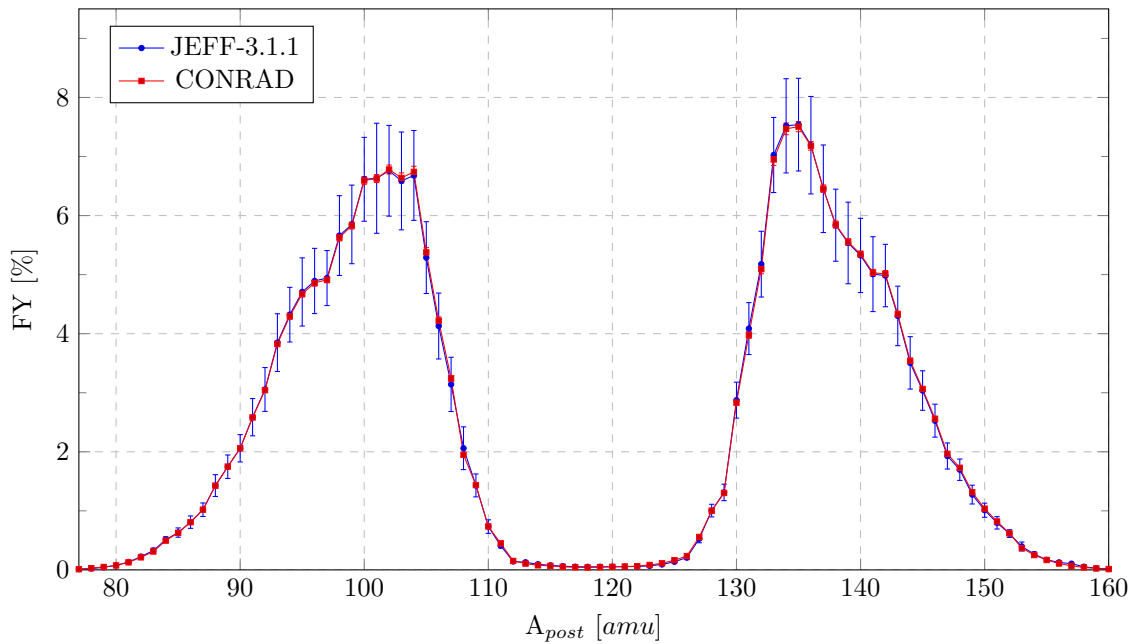


Figure E.1: Comparison between JEFF-3.1.1 and CONRAD independent mass FY for the fast fission of ^{239}Pu in linear scale. FY model parameters have been adjusted using CONRAD to reproduce the JEFF-3.1.1 evaluated library and generate covariances. The convolution between the pre-neutron model based on Brosa fission modes and the saw-tooth curve allows a satisfactory representation of the available FY data.

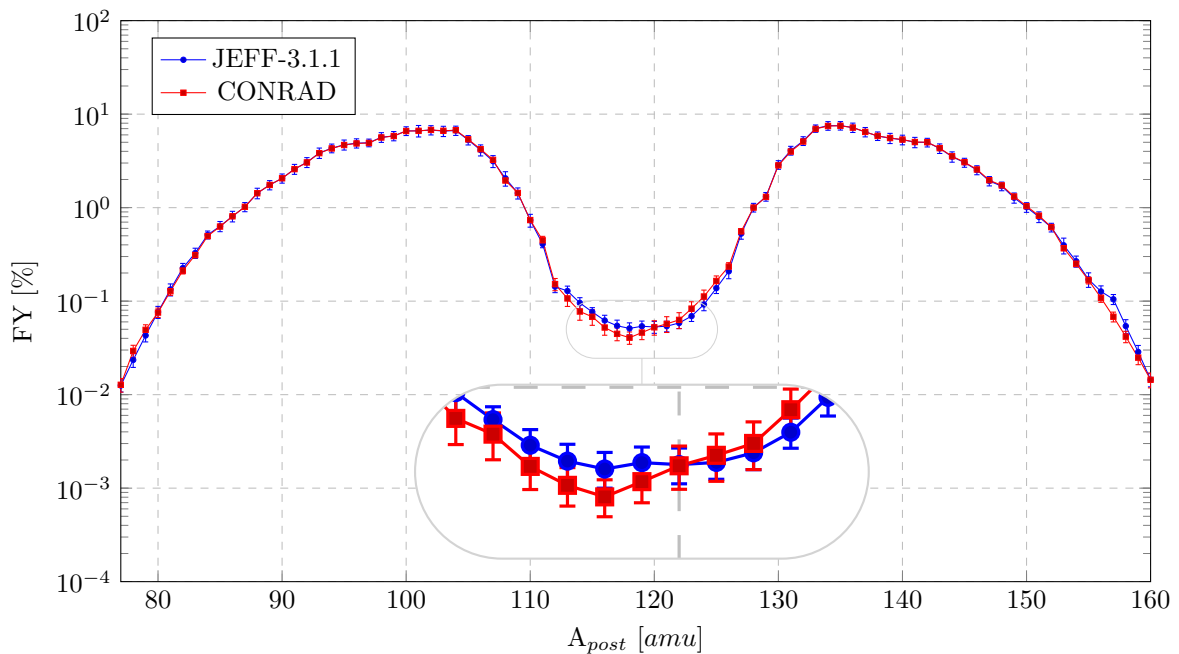


Figure E.2: Comparison between JEFF-3.1.1 and CONRAD independent mass FY for the fast fission of ^{239}Pu in logarithmic scale. FY model parameters have been adjusted using CONRAD to reproduce the JEFF-3.1.1 evaluated library and generate parameters. The convolution between the pre-neutron model based on Brosa fission modes and the saw-tooth curve allows a satisfactory representation of the available FY data even in the symmetry region.

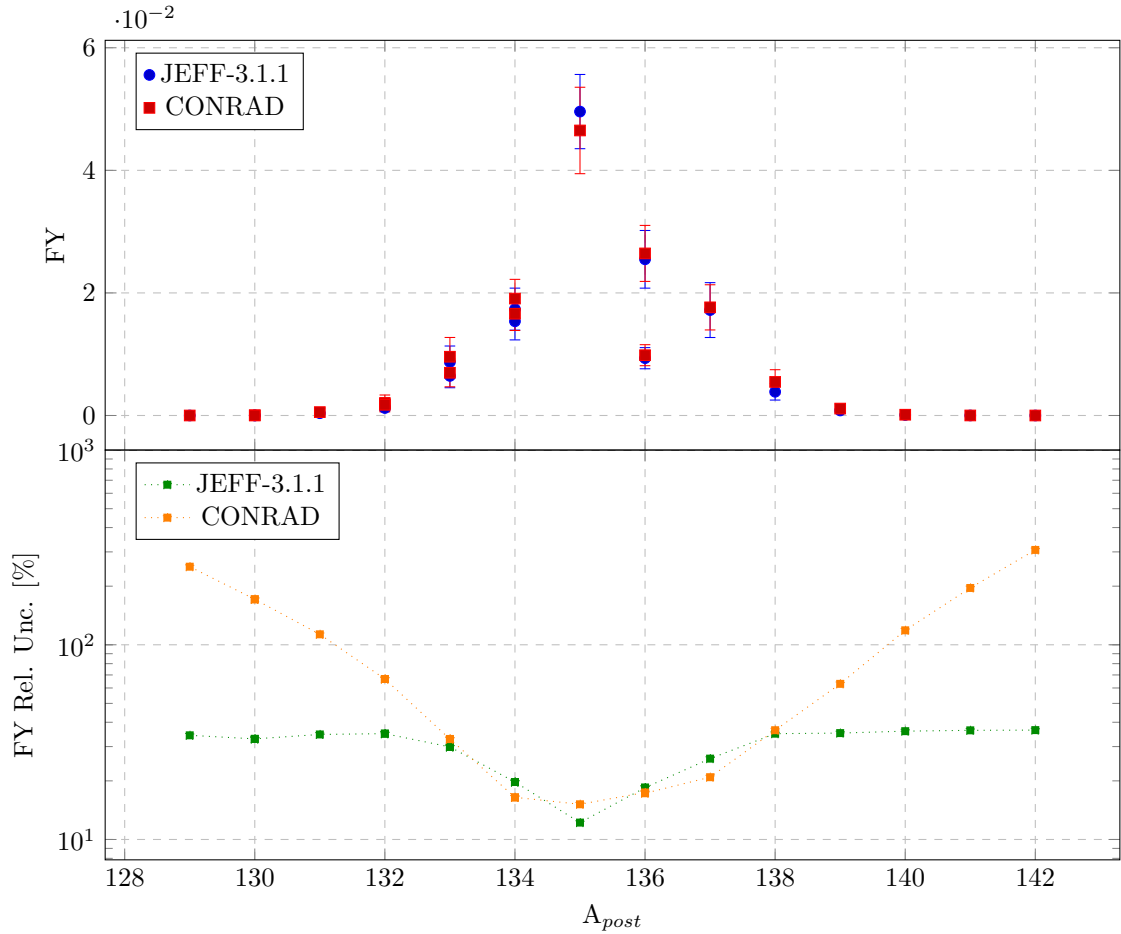


Figure E.3: Comparison between CONRAD and JEFF-3.1.1 independent FY of Iodine isomers for the fast fission of ^{239}Pu . In the figure averages (top) and relative uncertainties (bottom) are presented. Excellent agreement has been found for the most significant FY in average and uncertainty. However, some issues have been noticed for the error bars related to small yields which exhibit unrealistic variances.

Satisfactory results were also obtained for isomeric distributions. In Fig. E.3, only the comparison for the Iodine independent FY are provided to give an idea of the results obtained for yield $\geq 10^{-2}$. Worse results were achieved for smaller yields, as already seen also for better known fissioning systems.

In Fig. E.3, uncertainties are also compared. It is evident that performing a rigorous uncertainty propagation yields unrealistic error bars on smallest FY. This issue still has to be investigated and solved in future perspective of the present work.

A possible solution could be imposing an uncertainty threshold. The impact of such yields on application calculations in fact is not relevant, as demonstrated by sensitivity analyses performed using the tools developed here and the CYRUS code.

Such good representation was possible only adjusting saw-tooth parameters. In Fig. E.4 the comparison between Tsuchiya's experimental values and CONRAD adjusted ones is shown. Experimental values, which were also used as priors, are however referring to the thermal neutron induced fission so they are not representative of the fissioning system considered. Anyway, saw-tooth results seem reasonable and they are not excessively distant from data related to the same target fissioning isotope.

During the statistical analysis, the JEFF-3.1.1 evaluated total prompt neutron multiplicity has been included in the calculation. The CONRAD result of 2.93 is in perfect agreement with the evaluated one (still 2.93), so this is surely increasing the level of confidence on such calculation even if further investigations are required. No prompt neutron probabilities experimental data were available to allow further verifications.

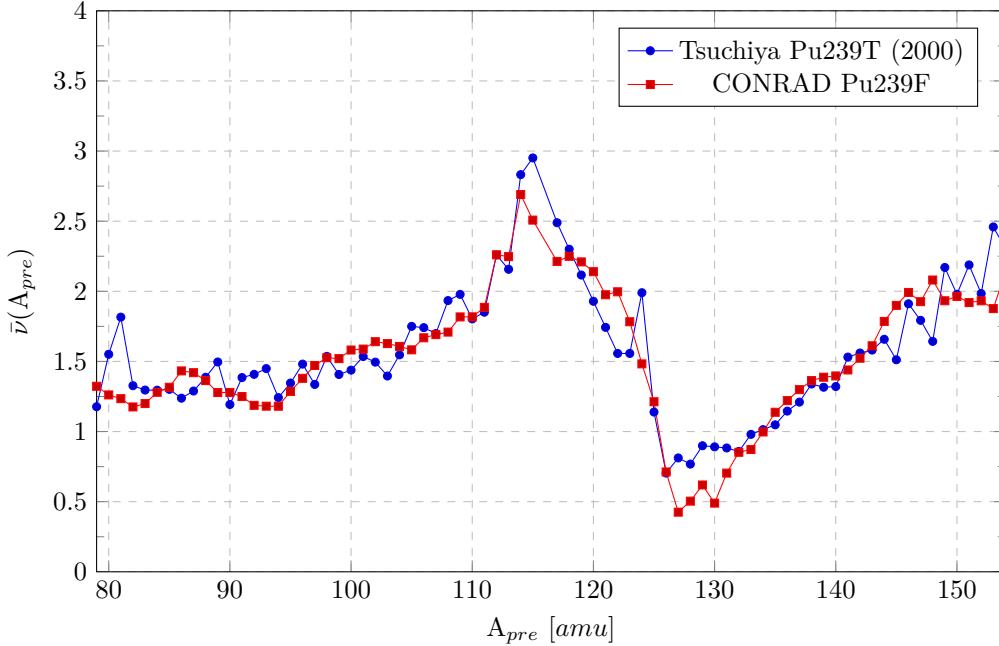


Figure E.4: Comparison between prior (from Tsuchiya [Tsuchiya et al., 2000] experimental values measured for the thermal fission of ^{239}Pu) and CONRAD-adjusted average number of prompt neutrons emitted as function of the pre-neutron fragment mass, for the fast fission of ^{239}Pu .

Even if no application calculations were performed to verify the performances of such covariance matrix, sensitivities for the elementary fission decay heat were calculated using the CYRUS code [Benoit, 2012]. In Fig. E.5 the decay heat uncertainty due to the propagation of fast neutron induced fission yields of ^{239}Pu evaluated in JEFF-3.1.1 is shown, highlighting the different contributions coming from the several evaluated yields (no correlations have been considered). To verify that CONRAD can actually reproduce JEFF-3.1.1 library, we propagated only FY variances without including any correlation. The satisfactory agreement between the two uncertainty propagations (CONRAD without correlations and JEFF-3.1.1) shown in Fig. E.6 indicates that CONRAD replicates globally JEFF variances. Adding correlations and performing the propagation of the full covariance matrix produces the same effects already seen for other fissioning systems, an enhanced uncertainty at the beginning of the cooling time, probably due to the correlations between many decay events, and a significant reduction for longer times due to the anti-correlations existing between isobars.

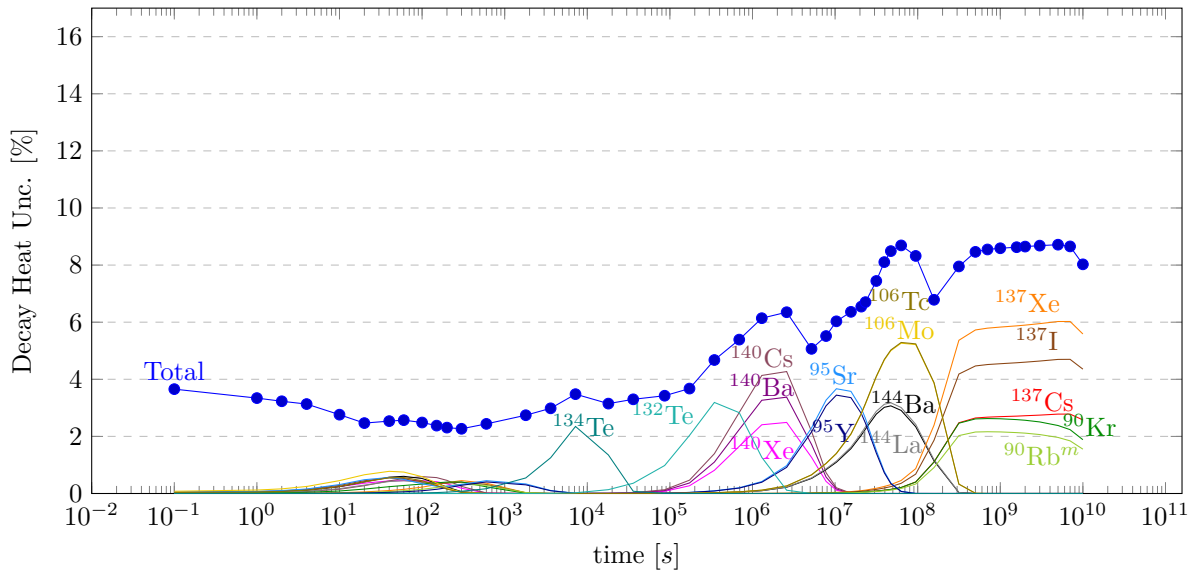


Figure E.5: Decay heat uncertainty for the elementary fast neutron induced fission of ^{239}Pu . The total uncertainty is given by the propagation of JEFF-3.1.1 FY. In the figure, the most significant contributions have been emphasized with different colors.

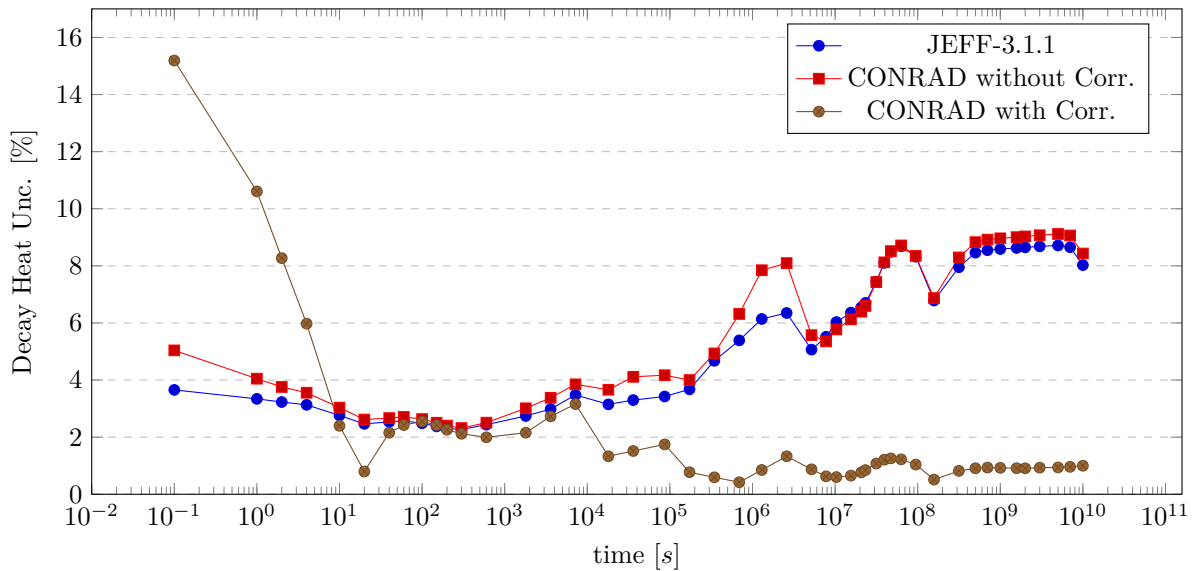


Figure E.6: Decay heat uncertainty as a function of time for the elementary fast fission of ^{239}Pu . The propagation of JEFF-3.1.1 FY uncertainties on the decay heat has been compared to what we obtain from CONRAD-generated FY, with and without including correlations.

E.2 Pu-240 Fast Fission

The same calculation was performed also for Pu240F, with the same prior input files and same prior uncertainties. The preliminary results here shown are meant to prove the feasibility of the covariance generation procedure proposed also for this fissioning systems. Further investigations are therefore desirable and will be done in future work, testing matrices on specific fast spectrum reactor problems.

Parameter	Prior BE	Prior Unc. [%]	Posterior BE	Posterior Unc. [%]
$D_{St.I}^*$	14.97	5	15.30	0.4
$D_{St.II}^*$	20.96	5	21.65	0.3
$\sigma_{St.I}^*$	3.73	10	3.4	1.6
$\sigma_{St.II}^*$	6.48	10	6.1	0.3
σ_{SL}^*	15.8	10	15.7	1.3
$N_{St.I}$	0.248	10	0.359	2.6
N_{SL}	0.005	20	0.005	12.3

* Expressed in [amu].

Table E.3: Fission mode parameters best estimates (BE) and uncertainties before (prior) and after (posterior) the analysis using CONRAD for the fast fission of ^{240}Pu .

In Tab. E.3 and E.4 the values for Brosa fission modes and Wahl parameters are respectively shown. Results in average and uncertainty seem reasonable, even if the terms of comparison available are data concerning the same fissioning target nucleus (e.g. experimental data on spontaneous fission of ^{240}Pu provided by Dematté in Ref. [Dematté, 1996]) or related to other Plutonium fissioning systems.

Parameter	Prior BE	Prior Unc. [%]	Posterior BE	Posterior Unc. [%]
$\sigma_Z(140)$	0.566	20	0.495	19.1
$\Delta Z(140)$	-0.487	20	-0.409	12.6
σ_{50}	0.356	20	0.393	1.0
$F_N(140)$	1.076	20	0.955	3.5
$F_Z(140)$	1.207	20	1.050	18.3
$SL50$	0.191	20	0.348	3.3
ΔZ_{max}	0.699	20	0.491	0.7
J_{rms}^L	7.5	10	7.8	0.8
J_{rms}^H	7.5	10	8.0	1.3

Table E.4: Wahl and Madland-England parameters best estimates (BE) and uncertainties before (prior) and after (posterior) the analysis using CONRAD, for the fast fission of ^{240}Pu .

Parameters uncertainties are still those obtained after marginalization. As done for other fissioning systems, we marginalized only uncertainties related to sensitive parameters.

In Figs. E.7 and E.8 the comparison between CONRAD and JEFF-3.1.1 mass distributions is shown, which are in excellent agreement for the most significant FY. Looking at the central mass domain in Fig. E.8 a quite regular behavior can be observed. Such smooth yield distribution could be provoked by the adoption of semi-empirical models without any prompt-neutron evaporation treatment, to compensate the missing of experimental data.

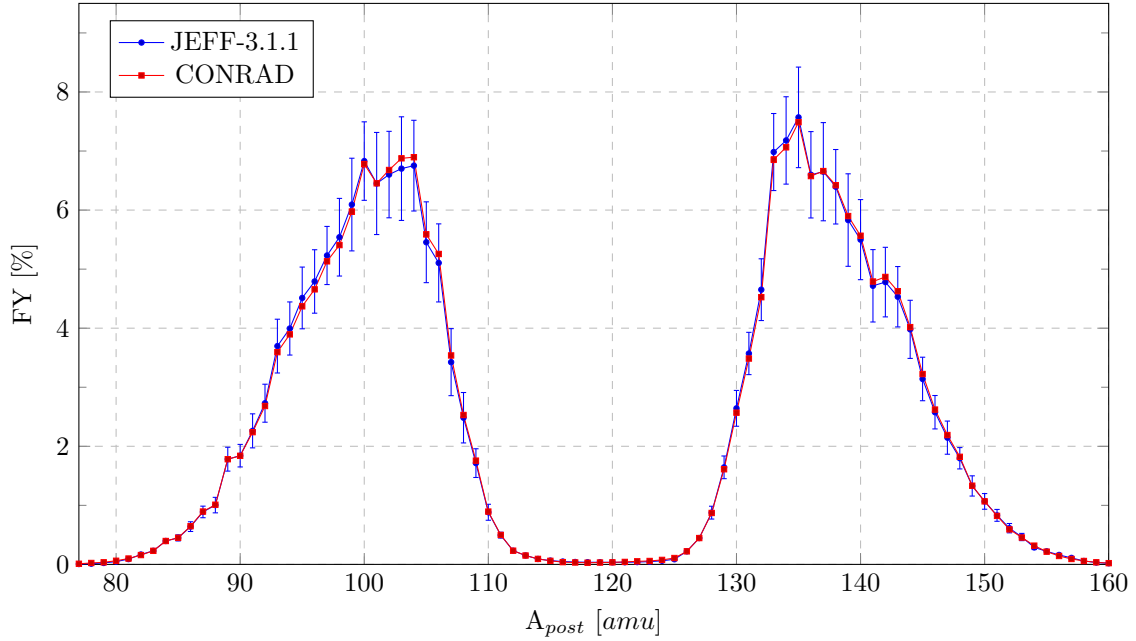


Figure E.7: Comparison between JEFF-3.1.1 and CONRAD independent mass FY for the fast fission of ^{240}Pu in linear scale. FY model parameters have been adjusted using CONRAD to reproduce the JEFF-3.1.1 evaluated library and generate covariances. The convolution between the pre-neutron model based on Brosa fission modes and the saw-tooth curve allows a satisfactory representation of the available FY data.

In Fig. E.9 the comparison between Tsuchiya's experimental values (for Pu239T) and CONRAD adjusted ones is shown. The saw-tooth results seem reasonable and they are not excessively distant from data related to ^{239}Pu .

During the statistical analysis the JEFF-3.1.1 evaluated total prompt neutron multiplicity has been included in the calculation. The CONRAD result of 3.12 is actually quite distant from the evaluated one (still 2.93), and further investigations are required. No prompt neutron probabilities experimental data were available to allow further verifications also in this case.

Satisfactory results were obtained for isomeric distributions. In Fig. E.10, only the comparison for the Iodine independent FY are provided as done for Pu239F. Still worse results were achieved for smaller yields, as already seen also for better known fissioning systems.

We performed the same elementary fission calculations to see if uncertainty results were actually well reproduced by CONRAD. In Fig. E.11 JEFF-3.1.1 FY contributions are shown to see which are the most significant ones in elementary decay heat calculations. Similar results to what we saw for other fissioning systems were obtained also for the fast fission of ^{240}Pu . Also in this case, in fact, covariances induce uncertainty reduction for long cooling times (see Fig. E.12).

Further investigations are surely necessary, including some fast spectrum reactor applications. Such task was not pursued during the present thesis work, but it has been left as future perspective and development.

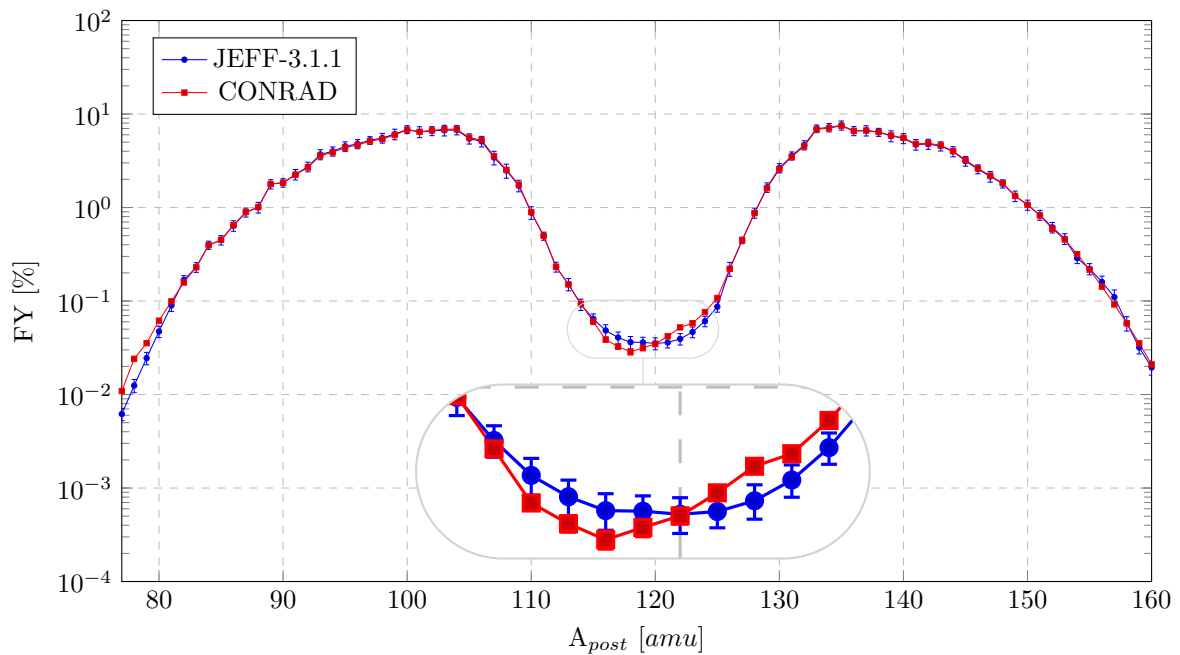


Figure E.8: Comparison between JEFF-3.1.1 and CONRAD independent mass FY for the fast fission of ^{240}Pu in logarithmic scale. FY model parameters have been adjusted using CONRAD to reproduce the JEFF-3.1.1 evaluated library and generate covariances. The convolution between the pre-neutron model based on Brosa fission modes and the saw-tooth curve allows a satisfactory representation of the available FY data even in the symmetry region.

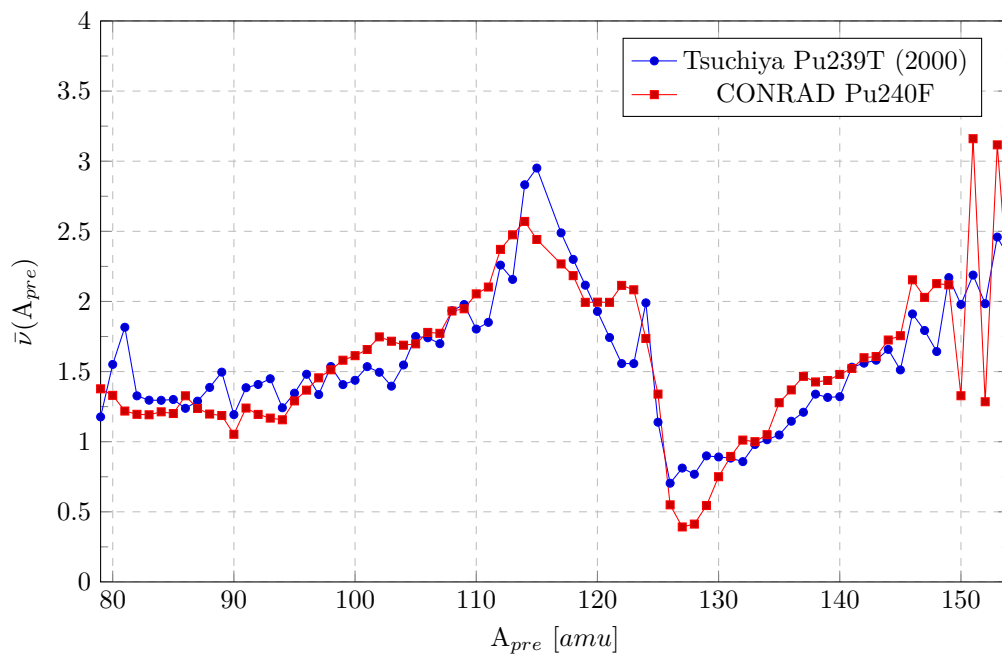


Figure E.9: Comparison between prior (from Tsuchiya [Tsuchiya et al., 2000] experimental values measured for the thermal fission of ^{239}Pu) and CONRAD-adjusted average number of prompt neutrons emitted as function of the pre-neutron fragment mass, for the fast fission of ^{240}Pu .

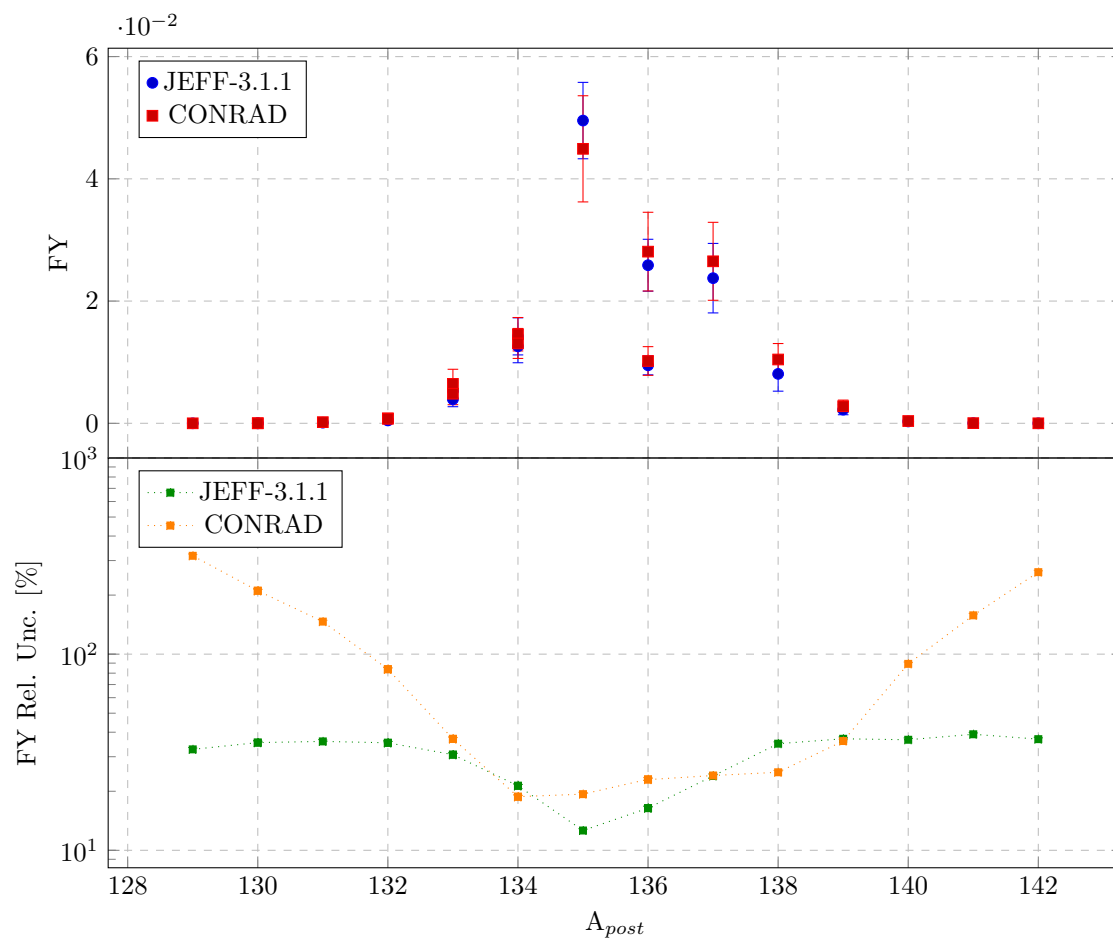


Figure E.10: Comparison between CONRAD and JEFF-3.1.1 independent FY of Iodine isomers for the fast fission of ^{240}Pu . In the figure averages (top) and relative uncertainties (bottom) are presented. Excellent agreement has been found for the most significant FY in average and uncertainty. However, some issues have been noticed for the error bars related to small yields which exhibit unrealistic variances.

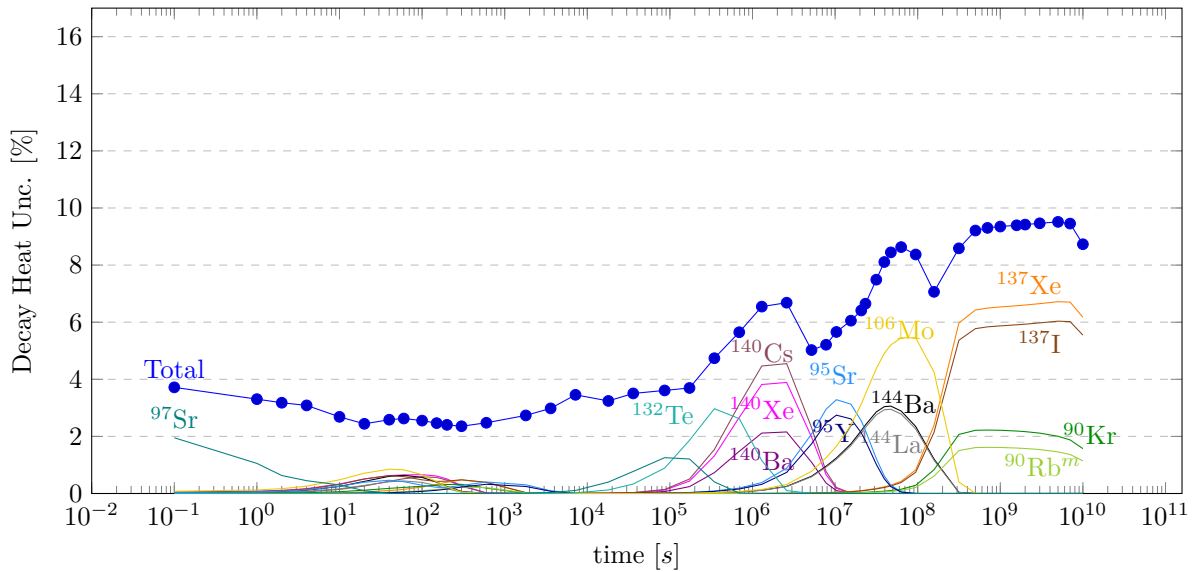


Figure E.11: Decay heat uncertainty for the elementary fast neutron induced fission of ^{240}Pu . The total uncertainty is given by the propagation of JEFF-3.1.1 FY. In the figure, the most significant contributions have been emphasized with different colors.

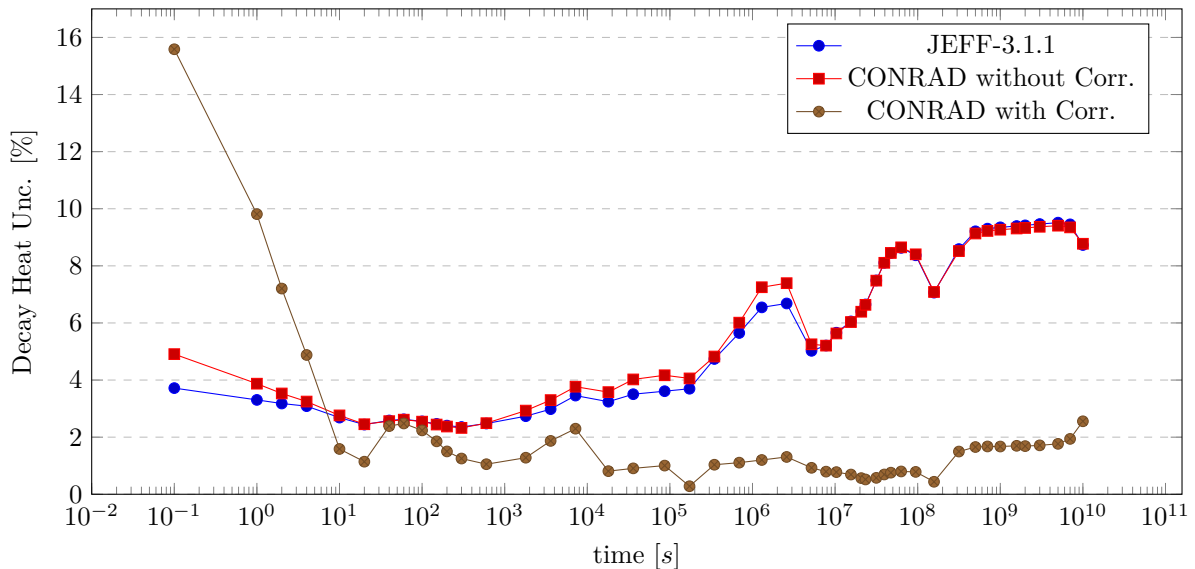


Figure E.12: Decay heat uncertainty as a function of time for the elementary fast fission of ^{240}Pu . The propagation of JEFF-3.1.1 FY uncertainties on the decay heat has been compared to what we obtain from CONRAD-generated FY, with and without including correlations.

Appendix F

Perturbation Theory

Contents

F.1 Introduction	223
F.1.1 Basic Mathematical Concepts	224
F.1.2 Applications of the Perturbation Theory	224
F.2 Neutronic Applications	225
F.2.1 The Standard Perturbation Theory	225
F.2.2 The Generalized Perturbation Theory	226
F.2.3 Equivalent Generalized Perturbation Theory	227
F.3 Nuclide Concentration Applications	228

PERTURBATION theory and variational methods are essential in reactor physics. Perturbation analysis on design parameters, determination of the critical dimensions, evaluation of group constants are in fact possible thanks to the solution of the adjoint equation. For our purposes we will be interested in the sensitivity and perturbation analysis that can be carried out on the modern deterministic core design platforms, showing the impact of the nuclear data uncertainties on important reactor parameters such as k_{eff} , reactivity coefficients and power map distribution.

In this section some elements of perturbation theory and variational methods will be given, focusing on different formulations such as the Standard Theory (ST), the Generalized Perturbation Theory (GPT) and the Equivalent Generalized Perturbation Theory (EGPT). Furthermore an application to the nuclide evolution equation will be discussed.

F.1 Introduction

Perturbation theory was not specifically born as part of nuclear reactor theory, but many more general applications were found in quantum physics and nuclear scientists in the 50's [Weinberg and Wigner, 1958] tried to apply the power of this theoretical approach to the transport of neutrons in a nuclear reactor. In this section some basic definitions are provided in order to give more clarity to the rest of the appendix, without pretending to be exhaustive in perturbation theory description, but giving only some interesting results useful in practice, especially concerning the sensitivity analysis and the determination of sensitivity coefficients.

F.1.1 Basic Mathematical Concepts

Let $\psi(\xi)$ and $\phi(\xi)$ be two functionals of the same variables [Bell and Glasstone, 1970]. The inner product can be defined by the integral

$$\langle \psi, \phi \rangle \equiv \int \psi(\xi)\phi(\xi)d\xi, \quad (\text{F.1})$$

where the integration is performed on the whole domain. If the functionals satisfy certain continuity conditions, then a *Hermitian* or *self-adjoint* operator \mathbf{M} can be defined such that

$$\langle \psi, \mathbf{M}\phi \rangle = \langle \phi, \mathbf{M}\psi \rangle. \quad (\text{F.2})$$

The eigenfunctions of Hermitian operators are orthogonal and the eigenvalues are always real. Nevertheless, even if in neutron transport theory the operators and the functions involved are real, the operator associated to the Boltzmann equation is not self-adjoint. Therefore we need to define an adjoint operator \mathbf{L}^+ to a non-self-adjoint operator \mathbf{L} such that

$$\langle \psi^+, \mathbf{L}\phi \rangle = \langle \phi, \mathbf{L}^+\psi \rangle \quad (\text{F.3})$$

for any arbitrary functional ϕ and ψ [Salvatores, 1988]. If ϕ is an eigenfunction of \mathbf{L} with

$$\mathbf{L}\phi = \lambda\phi, \quad (\text{F.4})$$

we can define the adjoint eigenvalues problem for \mathbf{L}^+

$$\mathbf{L}^+\psi^+ = \eta\psi^+. \quad (\text{F.5})$$

Applying Eq. F.3, we obtain

$$(\lambda - \eta)\langle \psi^+, \phi \rangle = 0, \quad (\text{F.6})$$

where it is clear to see that for $\lambda \neq \eta$ we have $\langle \psi^+, \phi \rangle = 0$.

F.1.2 Applications of the Perturbation Theory

In this section we are going to see the principal applications of perturbation theory. As main motivation for the development of a perturbation theory there is the calculation of reactivity coefficients. In principle it is clear that to estimate the reactivity variations $\Delta\rho$ between two states of the reactor due to any modification in the Boltzmann operator, a direct calculation of the two different conditions can be performed [Salvatores, 1988]. The perturbation theory gives a new possibility to obtain directly the reactivity coefficient through the solution of the adjoint problem, providing also a deeper comprehension of the physical phenomena.

Another application, which is the main one for our purposes, is the sensitivity analysis that can be carried on through the perturbation theory. These methods can yield in fact systematic studies on the effects of basic parameter variations ΔP on integral quantities I . We call them sensitivity coefficients

$$S_i = \frac{\Delta I}{I} / \frac{\Delta P_i}{P_i}. \quad (\text{F.7})$$

We will see in the next sections how the perturbation theory allow us to easily estimate sensitivity coefficients. These coefficients, in the first order approximation, will be independent from the entity of the perturbation on basic parameters and so directly applicable in the uncertainty propagation law, also known sandwich formula.

Perturbation methods are also applied to calculate flux variations due to modification in the Boltzmann operator. An example can be the control rod insertion in a nuclear reactor.

F.2 Neutronic Applications

In this section we are going to show the different formulations applied on three main neutronic applications of the sensitivity analysis [Salvatores, 1988]. The first case is the determination of sensitivity coefficient for the k_{eff} yielding the formulation known as Standard Perturbation Theory (STP). In the second case functionals of the flux are considered, such as the reaction rate or the power map of a nuclear reactor. This formulation takes the name of Generalized Perturbation Theory (GPT). Finally, if reactivity coefficient are considered, the Equivalent Generalized Perturbation Theory (EGPT) can be employed.

F.2.1 The Standard Perturbation Theory

The Boltzmann equation for a critical system ($k_{eff} = 1$), as previously said, can be written in an operational form

$$\mathbf{M}\phi = 0 \quad (\text{F.8})$$

with

$$\mathbf{M} = \mathbf{A} - \mathbf{F} \quad (\text{F.9})$$

where \mathbf{A} is the loss operator, while \mathbf{F} is the production operator.

In this case the inner product is the integration on the phase space. We can define the adjoint operator such that, for given arbitrary vectors v and w , we can find a relation

$$\langle v, \mathbf{M}w \rangle = \langle \mathbf{M}^+v, w \rangle. \quad (\text{F.10})$$

Therefore we can define the adjoint problem associated to the direct one, which has as solution the adjoint flux ϕ^+

$$\begin{aligned} \mathbf{M}^+\phi^+ &= 0, \\ (\mathbf{A}^+ - \mathbf{F}^+)\phi^+ &= 0. \end{aligned} \quad (\text{F.11})$$

If we consider now a perturbation of the critical system which modifies the Boltzmann operator and makes the system no longer critical, we have for the perturbed system

$$\mathbf{M}'\phi' = \left(\mathbf{A}' - \frac{1}{k'}\mathbf{F}' \right)\phi' = 0, \quad (\text{F.12})$$

where

$$\begin{aligned} \mathbf{M}' &= \mathbf{M} + \delta\mathbf{M}, \\ \mathbf{A}' &= \mathbf{A} + \delta\mathbf{A}, \\ \mathbf{F}' &= \mathbf{F} + \delta\mathbf{F}, \\ \phi' &= \phi + \delta\phi. \end{aligned} \quad (\text{F.13})$$

$$(\text{F.14})$$

Let's consider the following two equations:

$$\mathbf{A}^+ \phi^+ - \mathbf{F}^+ \phi^+ = 0 \quad (\text{F.15})$$

and

$$\mathbf{A}' \phi' - \frac{1}{k'} \mathbf{F}' \phi' = 0. \quad (\text{F.16})$$

If we multiply Eq. F.15 by ϕ' and Eq. F.16 by ϕ^+ , and we integrate on the phase space we obtain

$$\langle \mathbf{A}^+ \phi^+, \phi' \rangle - \langle \phi^+, \mathbf{A}' \phi' \rangle - \langle \mathbf{F}^+ \phi^+, \phi' \rangle + \frac{1}{k'} \langle \phi^+, \mathbf{F}' \phi' \rangle = 0. \quad (\text{F.17})$$

Using the adjoint operator properties and $\delta \mathbf{A}$, $\delta \mathbf{F}$ definitions we can sum and subtract the term $\langle \phi^+, \mathbf{F}' \phi' \rangle$ and obtain

$$- \langle \phi^+, \delta \mathbf{A} \phi' \rangle + \langle \phi^+, \delta \mathbf{F} \phi' \rangle = \left(1 - \frac{1}{k'}\right) \langle \phi^+, \mathbf{F}' \phi' \rangle. \quad (\text{F.18})$$

The final expression for the variation of the k_{eff} is

$$\frac{\delta k}{k'} = \frac{1}{I_f} (-\langle \phi^+, \delta \mathbf{A} \phi' \rangle + \langle \phi^+, \delta \mathbf{F} \phi' \rangle), \quad (\text{F.19})$$

where I_f is given by

$$I_f = \langle \phi^+, \mathbf{F}' \phi' \rangle. \quad (\text{F.20})$$

Neglecting higher order contribution, we can write

$$\frac{\delta k}{k'} \cong \frac{1}{I_f} (-\langle \phi^+, \delta \mathbf{A} \phi \rangle + \langle \phi^+, \delta \mathbf{F} \phi \rangle), \quad (\text{F.21})$$

which shows that only the solutions ϕ and ϕ^+ are necessary for $\delta k/k'$. Sensitivity coefficients in the case of the loss operator is given by

$$S_A = \left(\frac{\delta k}{k} \right) / \left(\frac{\delta \mathbf{A}}{\mathbf{A}} \right), \quad (\text{F.22})$$

that gives

$$S_A = -\frac{1}{I_f} \langle \phi^+, \mathbf{A} \phi \rangle, \quad (\text{F.23})$$

and in the case of the fission operator we have

$$S_f = \frac{1}{I_f} \langle \phi^+, \mathbf{F} \phi \rangle. \quad (\text{F.24})$$

The sensitivity coefficients can be then calculated one single time, since they are independent from the perturbation.

F.2.2 The Generalized Perturbation Theory

In this section we are going to spend few words for the case of a linear functional of the flux. Let us consider the reaction rate to describe the generalized perturbation theory. Still considering the inner product as integration on the phase space, we can express the reaction rate as

$$R = \langle \phi, \Sigma_R \rangle. \quad (\text{F.25})$$

For a given critical problem

$$\mathbf{M}\phi = 0, \quad (\text{F.26})$$

we can define an adjoint function as solution of the following inhomogeneous equation

$$\mathbf{M}^+\psi_R^+ = \Sigma_R. \quad (\text{F.27})$$

We can consider now a perturbation $\delta\mathbf{M}$ that leaves the system critical:

$$(\mathbf{M} + \delta\mathbf{M})(\phi + \delta\phi) = 0, \quad (\text{F.28})$$

then, neglecting the second order, we have

$$\delta\mathbf{M}\phi + \mathbf{M}\delta\phi = 0. \quad (\text{F.29})$$

Multiplying by ψ_R^+ and integrating on the phase space we have

$$\langle \psi_R^+, \mathbf{M}\delta\phi \rangle = -\langle \psi_R^+, \delta\mathbf{M}\phi \rangle, \quad (\text{F.30})$$

$$\langle \mathbf{M}^+\psi_R^+, \delta\phi \rangle = -\langle \psi_R^+, \delta\mathbf{M}\phi \rangle. \quad (\text{F.31})$$

From the definition of the reaction rate and of the adjoint problem we have

$$\delta R = \langle \Sigma_R, \delta\phi \rangle = \langle \mathbf{M}^+\psi_R^+, \delta\phi \rangle, \quad (\text{F.32})$$

then we can write

$$\delta R = -\langle \psi_R^+, \delta\mathbf{M}\phi \rangle. \quad (\text{F.33})$$

Also in this case [Salvatores, 1988] we can define sensitivity coefficients as

$$S_X = \langle \psi_R^+, \mathbf{X}\phi \rangle \quad (\text{F.34})$$

where X can be the operators \mathbf{A} , \mathbf{F} or a single element of these operators such as multi-group cross section.

F.2.3 Equivalent Generalized Perturbation Theory

This formulation of the perturbation theory [Salvatores, 1988] allows to calculate reactivity coefficients. A reactivity coefficient can be defined as a reactivity variation

$$\Delta\rho = \left(1 - \frac{1}{k_p}\right) - \left(1 - \frac{1}{k}\right) = \frac{1}{k} - \frac{1}{k_p} \quad (\text{F.35})$$

given by a perturbation of the Boltzmann operator $\delta\mathbf{M}_p$ such that

$$\begin{aligned} \mathbf{M}_p &= \mathbf{M} + \delta\mathbf{M}_p, \\ \phi_p &= \phi + \delta\phi_p, \\ k_p &= k + \delta k_p. \end{aligned} \quad (\text{F.36})$$

We define the same equations for another perturbed state that modifies the Boltzmann operator of $\delta\mathbf{M}_s$ and see the effect of this new perturbation on the reactivity coefficient [Salvatores, 1988]. Furthermore we can suppose also the two perturbation happening

consequentially giving a Boltzmann operator $\mathbf{M}_{\mathbf{PS}} = \mathbf{M} + \delta\mathbf{M}_{\mathbf{S}} + \delta\mathbf{M}_{\mathbf{P}}$. The variation of the reactivity coefficient can be written as

$$\delta(\Delta\rho) = \Delta\rho' - \Delta\rho = \left(\frac{1}{k_p} - \frac{1}{k_{ps}}\right) - \left(\frac{1}{k} - \frac{1}{k_p}\right). \quad (\text{F.37})$$

We can apply the Standard Perturbation Theory and obtain

$$\left(\frac{1}{k_p} - \frac{1}{k_{ps}}\right) = \frac{1}{I_f^p} \langle \phi_p^+, \delta\mathbf{M}_{\mathbf{S}}\phi_p \rangle, \quad (\text{F.38})$$

$$\left(\frac{1}{k} - \frac{1}{k_s}\right) = \frac{1}{I_f} \langle \phi^+, \delta\mathbf{M}_{\mathbf{S}}\phi \rangle. \quad (\text{F.39})$$

$$(\text{F.40})$$

Considering a constant perturbation we have finally

$$\delta(\Delta\rho) = \left\{ \frac{1}{I_f} \langle \phi_p^+, \phi_p \rangle - \frac{1}{I_f} \langle \phi^+, \phi \rangle \right\} \Delta\mathbf{M}_{\mathbf{S}}, \quad (\text{F.41})$$

that gives a linear expression that relates the reactivity coefficient variation to a perturbation of the transport operator. We can therefore define the sensitivity coefficient in the same way we have previously done:

$$S_X = \frac{\partial(\Delta\rho)}{\Delta\rho} \bigg/ \frac{\partial X}{X} = \left\{ \frac{1}{I_f^p} \langle \phi_p^+, X\phi_p \rangle - \frac{1}{I_f} \langle \phi^+, X\phi \rangle \right\}, \quad (\text{F.42})$$

which shows that only the direct and the adjoint problem in the reference and in the p -state are necessary.

F.3 Nuclide Concentration Applications

Thanks to the GPT we can also apply the sensitivity analysis to the evolution problem of nuclide concentrations in a nuclear reactor [Salvatores, 1988]. We can call \mathbf{A} the operator that describes the evolution of the isotopic densities, giving the following differential direct problem:

$$\frac{dn(t)}{dt} = \mathbf{A}n(t), \quad (\text{F.43})$$

with the initial condition $n(0) = n_0$.

Applying the GPT we can consider a generic functional of the density vector $n(t)$:

$$Q = \langle h^+, n(t_F) \rangle, \quad (\text{F.44})$$

where h^+ is a vector whose components are zero except one $h_i = 1$ that, multiplied by n_F , gives the density at the final time $t = t_F$. This functional as defined here allows to find the variation on a final nuclide density due to a perturbation in the evolution operator. Perturbation in the evolution operator can be induced by cross sections, decay constants, fission yields, neutron flux. We can write the adjoint equation such as

$$-\frac{dn^+(t)}{dt} = \mathbf{A}^+n^+(t), \quad (\text{F.45})$$

where \mathbf{A}^+ is the adjoint operator of \mathbf{A} . We can also define the initial condition for the adjoint differential problem (at $t = t_F$ since it is a reversed problem)

$$n^+(t_F) = h^+. \quad (\text{F.46})$$

The direct perturbed problem can be written as

$$\frac{dn'(t)}{dt} = (\mathbf{A} + \delta\mathbf{A})n'(t). \quad (\text{F.47})$$

Following a procedure close to what we did for the generalized theory in neutronic application we can multiply the Eq. F.47 by n^+ and Eq. F.45 by n' integrating over the all time domain, and then subtract both the equations:

$$\int_{t_0}^{t_F} \frac{d}{dt}(n^+ \cdot n')dt - \int_{t_0}^{t_F} (n^+ \cdot \mathbf{A}n' - \mathbf{A}^+n^+ \cdot n')dt - \int_{t_0}^{t_F} n^+ \cdot \delta\mathbf{A}n'dt = 0, \quad (\text{F.48})$$

where the second term is zero thanks to the definition of adjoint operator.

It can be shown [Salvatores, 1988] that the last equation can be reduced to the following expression:

$$n^+ \delta n|_{t=t_F} = - \int_{t_0}^{t_F} n^+ \delta\mathbf{A}n'dt. \quad (\text{F.49})$$

According to the initial condition for the adjoint problem, only $n_F^{+,i} = 1$. Therefore, considering the usual first order approximation we have

$$\delta n_F^i \cong + \int_{t_0}^{t_F} n^+ \delta\mathbf{A}n'dt. \quad (\text{F.50})$$

This procedure allows us to define the sensitivity coefficient to find the variation on the nuclide concentration at the end of the irradiation due to a perturbation of the evolution operator \mathbf{A} :

$$S_i = \frac{\delta n_F^i}{n_F^i} / \frac{\delta A}{A} = \frac{1}{n_F^i} \int_{t_0}^{t_F} n^+ \cdot \mathbf{A}n'dt. \quad (\text{F.51})$$

List of Figures

1	View of the Jules Horowitz Reactor.	5
2.1	Independent mass fission yields for several thermal fissioning systems, data from JEFF-3.1.1 library.	46
2.2	Average kinetic energy as a function of the pre-neutron mass for the thermal fission of ^{235}U [Hambach et al., 1989] and ^{239}Pu [Wagemans et al., 1984].	47
2.3	Average number of prompt neutrons emitted by a fission fragment of mass A_{pre} for the thermal neutron-induced fission of ^{239}Pu , from different experiments (Refs. [Apalin et al., 1965, Nishio et al., 1995, Tsuchiya et al., 2000, Batenkov et al., 2004]).	48
2.4	Representation of the pre-scission shape (figure reproduced from Ref. [Brosa et al., 1990]). The parameters in the figure are those used by Brosa modeling the geometrical description (see Ref. [Brosa et al., 1990] for details). ζ_1 and ζ_2 are the two centers of mass of the two lobes obtained after the compound nucleus stretching.	51
2.5	(a) Pre-neutron (from Zeynalov [Zeynalov et al., 2005]) distribution and average number of prompt neutrons emitted by a primary fragment (from Vorobyev's experiment [Vorobyev et al., 2010]) for the thermal fission of ^{235}U . (b) Post-neutron mass distribution from JEFF-3.1.1 ^{235}U evaluation.	53
2.6	Example for the prompt neutron emission which gives a post-neutron fission product of mass 140.	54
2.7	5-Gaussian representation of the primary fragment distribution for the thermal fission of ^{235}U	55
2.8	Renormalization of the Gaussian distribution to only positive values. A piece-wise integration allows us to obtain discrete probabilities.	56
2.9	Prompt neutron emission probability comparison between FIFRELIN and CONRAD for different masses in the light peak of $^{235}\text{U}(n_{th}, f)$ mass distribution.	57
2.10	Prompt neutron emission probability comparison between FIFRELIN and CONRAD for different masses in the heavy peak of $^{235}\text{U}(n_{th}, f)$ mass distribution.	58
2.11	Piece-wise $\Delta Z(A)$ function using Wahl's values for the isotopic distribution parameters.	63
2.12	Piece-wise $\sigma Z(A)$ function using Wahl's values for the isotopic distribution parameters.	63
2.13	Piece-wise $F_Z(A)$ and $F_N(A)$ functions using Wahl's values for the isotopic distribution parameters.	64

3.1	A synthetic flow-chart for the nuclear data evaluation cycle. Nuclear data improvement can be performed through statistical adjustment thanks to experimental data deriving from mock-up configurations of a particular reference facility, which leads to special-purpose nuclear data library for the specific application. Otherwise, integral experiments can be designed, which have as main goal to be clean and application-independent. These results can be included in the nuclear reaction parameter evaluation process, leading to general-purpose evaluated data.	72
3.2	Conradlib dynamical libraries structure in the CONRAD project.	77
3.3	Portion of an experimental file used as input for CONRAD to analyze independent isotopic and isomeric FY. To identify the isomer we need the charge, the mass and the isomeric state.	79
3.4	Portion of an experimental file used as input for CONRAD to analyze prompt neutron multiplicity.	80
3.5	Portion of an experimental file used as input for CONRAD to analyze total prompt neutron emission probabilities.	80
3.6	Schematic picture of what has been implemented in the theory module of conradlib.	81
3.7	Example of Decay data input for CONRAD.	83
3.8	Comparison between cumulative yields generated using the CONRAD Q-matrix and the cumulative FY given in JEFF-3.1.1, for the thermal fission of ^{235}U . No significant differences have been found for almost the whole library, except for some fission products whose parents have long characteristic decay times.	85
3.9	Overview of some fission product decays. APOLLO2 fission products have been highlighted in blue. Their decays are ignored calculating their cumulative FY for APOLLO2, since they will be already considered in the inventory calculations performed by the depletion module.	87
3.10	Ratios between the CONRAD calculated APOLLO2 FY and the CEA2005-APOLIB version based on JEFF-3.1.1 for the thermal fissions of ^{235}U and ^{239}Pu	89
4.1	Schematic flow-chart of the procedure we adopted to generate FY covariance matrices.	94
4.2	Comparison between the uncertainties derived by direct uncertainty propagation of JEFF-3.1.1 isotopic uncertainties without correlations and those used in the CONRAD adjustment phase, for the thermal fission of ^{235}U	96
4.3	Comparison between JEFF-3.1.1 and CONRAD independent mass FY for the thermal fission of ^{235}U in linear scale. FY model parameters have been adjusted using CONRAD to reproduce the JEFF-3.1.1 evaluated library and generate covariances. The convolution between the pre-neutron model based on Brosa fission modes and the saw-tooth curve allows a satisfactory representation of the available FY data.	99

4.4	Comparison between JEFF-3.1.1 and CONRAD independent mass FY for the thermal fission of ^{235}U in logarithmic scale. FY model parameters have been adjusted using CONRAD to reproduce the JEFF-3.1.1 evaluated library and generate covariances. The convolution between the pre-neutron model based on Brosa fission modes and the saw-tooth curve allows a satisfactory representation of the available FY data even in the symmetry region.	100
4.5	Light peak mass and isotopic FY for the thermal fission of ^{235}U	101
4.6	Heavy peak mass and isotopic FY for the thermal fission of ^{235}U	102
4.7	Comparison between experimental (from Vorobyev [Vorobyev et al., 2010]) and CONRAD-adjusted average number of prompt neutrons emitted as function of the pre-neutron fragment mass. Slight deviations from the experimental values allow an extraordinary representation of the evaluated FY data.	103
4.8	Comparison between experimental (from Boldeman [Boldeman and Hines, 1985]) and CONRAD-evaluated total prompt neutron emission probabilities, $P_{tot}(\nu_p)$ for the thermal fission of ^{235}U . It provides the probability that a certain number of prompt neutrons are globally emitted by the fissioning system.	104
4.9	Comparison between experimental (from Boldeman [Boldeman and Hines, 1985]) and CONRAD-evaluated total prompt neutron emission probabilities, $P_{tot}(\nu_p)$ for the thermal fission of ^{235}U . In this case the Poisson distribution was used to calculate prompt neutron emission probabilities.	104
4.10	Isotopic distribution for the independent FY for the charge $Z=53$ (Iodine). The marginalization techniques allows to reproduce JEFF-3.1.1 uncertainties for the most significant yields.	106
4.11	Independent isotopic and isomeric FY (top) with their relative uncertainties (bottom) for the thermal fission of ^{235}U , from $Z=34$ up to $Z=39$	107
4.12	Independent isotopic and isomeric FY (top) with their relative uncertainties (bottom) for the thermal fission of ^{235}U , from $Z=40$ up to $Z=42$ and from $Z=50$ up to $Z=52$	108
4.13	Independent isotopic and isomeric FY (top) with their relative uncertainties (bottom) for the thermal fission of ^{235}U , from $Z=53$ up to $Z=58$	109
4.14	Independent mass FY covariance matrix for the thermal fission of ^{235}U . . .	110
4.15	Independent isotopic FY covariance matrix for the thermal fission of ^{235}U . Fission yields are ordered in ascending charge, mass and isomeric states. In this case only FY greater than 10^{-7} have been considered.	111
4.16	Decay heat uncertainty for the elementary thermal neutron induced fission of ^{235}U . The total uncertainty is given by the propagation of JEFF-3.1.1 FY. In the figure, the most significant contributions have been emphasized with different colors.	112
4.17	Decay heat uncertainty as a function of time for the elementary thermal fission of ^{235}U . The propagation of JEFF-3.1.1 FY uncertainties on the decay heat has been compared to what we obtain from CONRAD-generated FY, with and without including correlations.	113
4.18	Cumulative FY for the thermal fission of ^{235}U	116
4.19	Decay scheme for isotopes with mass equal to 148, giving ^{148}Nd	117

4.20	Comparison between JEFF-3.1.1 and CONRAD independent mass FY for the thermal fission of ^{239}Pu in linear scale. FY model parameters have been adjusted using CONRAD to reproduce the JEFF-3.1.1 evaluated library and generate covariances. The convolution between the pre-neutron model based on Brosa fission modes and the saw-tooth curve allows a satisfactory representation of the available FY data.	119
4.21	Comparison between JEFF-3.1.1 and CONRAD independent mass FY for the thermal fission of ^{239}Pu in logarithmic scale. FY model parameters have been adjusted using CONRAD to reproduce the JEFF-3.1.1 evaluated library and generate covariances. The convolution between the pre-neutron model based on Brosa fission modes and the saw-tooth curve allows a satisfactory representation of the available FY data even in the symmetry region.	119
4.22	Comparison between experimental (from Tsuchiya [Tsuchiya et al., 2000]) and CONRAD-adjusted average number of prompt neutrons emitted as function of the pre-neutron fragment mass for the thermal fission of ^{239}Pu	120
4.23	Comparison between experimental (from Gwin [Gwin et al., 1984]) and CONRAD-evaluated total prompt neutron emission probabilities, $P_{tot}(\nu_p)$ for the thermal fission of ^{239}Pu . It provides the probability that a certain number of prompt neutrons are globally emitted by the fissioning system.	120
4.24	Average number of prompt neutron emitted by a fission fragment of mass A_{pre} for the thermal neutron-induced fission of ^{239}Pu , from different experiments (Refs. [Apalin et al., 1965, Nishio et al., 1995, Tsuchiya et al., 2000, Batenkov et al., 2004]).	121
4.25	Independent mass FY covariance matrix for the thermal fission of ^{239}Pu	122
4.26	Independent isotopic FY covariance matrix for the thermal fission of ^{239}Pu . Fission yields are ordered in ascending charge, mass and isomeric states. In this case only FY greater than 10^{-7} have been considered.	123
4.27	Decay heat uncertainty as a function of time for the elementary thermal fission of ^{239}Pu . The propagation of JEFF-3.1.1 FY uncertainties on the decay heat has been compared to what we obtain from CONRAD-generated FY, with and without including correlations.	123
4.28	Comparison between JEFF-3.1.1 and CONRAD independent mass FY for the thermal fission of ^{241}Pu in linear scale. FY model parameters have been adjusted using CONRAD to reproduce the JEFF-3.1.1 evaluated library and generate covariances. The convolution between the pre-neutron model based on Brosa fission modes and the saw-tooth curve allows a satisfactory representation of the available FY data.	126
4.29	Comparison between JEFF-3.1.1 and CONRAD independent mass FY for the thermal fission of ^{241}Pu in logarithmic scale. FY model parameters have been adjusted using CONRAD to reproduce the JEFF-3.1.1 evaluated library and generate covariances. The convolution between the pre-neutron model based on Brosa fission modes and the saw-tooth curve allows a satisfactory representation of the available FY data even in the symmetry region.	126

4.30	Comparison between prior (from Tsuchiya [Tsuchiya et al., 2000] experimental values measured for the thermal fission of ^{239}Pu) and CONRAD-adjusted average number of prompt neutrons emitted as function of the pre-neutron fragment mass, for the thermal fission of ^{241}Pu	127
4.31	Comparison between experimental (from Gwin [Gwin et al., 1984]) and CONRAD-evaluated total prompt neutron emission probabilities, $P_{tot}(\nu_p)$ for the thermal fission of ^{241}Pu . It provides the probability that a certain number of prompt neutrons are globally emitted by the fissioning system.	127
4.32	Independent mass FY covariance matrix for the thermal fission of ^{241}Pu	128
4.33	Independent isotopic FY covariance matrix for the thermal fission of ^{241}Pu . Fission yields are ordered in ascending charge, mass and isomeric states. In this case only FY greater than 10^{-7} have been considered.	129
4.34	Decay heat uncertainty as a function of time for the elementary thermal fission of ^{241}Pu . The propagation of JEFF-3.1.1 FY uncertainties on the decay heat has been compared to what we obtain from CONRAD-generated FY, with and without including correlations.	129
4.35	Comparison between JEFF-3.1.1 and CONRAD independent mass FY for the fast fission of ^{238}U in linear scale. FY model parameters have been adjusted using CONRAD to reproduce the JEFF-3.1.1 evaluated library and generate covariances. The convolution between the pre-neutron model based on Brosa fission modes and the saw-tooth curve allows a satisfactory representation of the available FY data.	132
4.36	Comparison between JEFF-3.1.1 and CONRAD independent mass FY for the fast fission of ^{238}U in logarithmic scale. FY model parameters have been adjusted using CONRAD to reproduce the JEFF-3.1.1 evaluated library and generate covariances. The convolution between the pre-neutron model based on Brosa fission modes and the saw-tooth curve allows a satisfactory representation of the available FY data even in the symmetry region.	132
4.37	Comparison between prior (from Vorobyev [Vorobyev et al., 2010] experimental values measured for $^{235}\text{U}(n_{th}, f)$ and CONRAD-adjusted average number of prompt neutrons emitted as function of the pre-neutron fragment mass, for the fast fission of ^{238}U	133
4.38	Independent mass FY covariance matrix for the fast fission of ^{238}U	133
4.39	Decay heat uncertainty as a function of time for the elementary fast fission of ^{238}U . The propagation of JEFF-3.1.1 FY uncertainties on the decay heat has been compared to what we obtain from CONRAD-generated FY, with and without including correlations.	134
5.1	Example of subdivision of the sampling domain.	149
5.2	Example of LHS sampling (reproduced from [Kinoshita et al., 2014]).	150
5.3	Sample size for different level of confidence β and probability content γ for $p = 2$ parameters.	155
5.4	Sample size for different level of confidence β and probability content γ for $p = 52$ parameters.	155
5.5	Schematic representation of the URANIE-APOLLO2-MENDEL coupling for Monte Carlo uncertainty propagation.	158
6.1	Schematic representation of the UOX and MOX pin-cells.	163

6.2	Nominal reactivity values in pcm as function of burn-up for the UOX and MOX pin-cells evolution.	164
6.3	Nominal decay heat values in W as function of time for the UOX and MOX pin-cells evolution.	164
6.4	Nominal reactivity values in pcm as function of burn-up for the JHR evolution.	166
6.5	Reactivity loss uncertainty as function of burn-up for the propagation of ^{235}U thermal neutron induced FY on a UOX-pin-cell calculation. The results obtained using the sandwich formula (Det.) applied on sensitivities which were deduced from direct perturbations are in excellent agreement with Monte Carlo estimates (MC).	168
6.6	Decay heat uncertainty as function of time for the propagation of ^{235}U thermal neutron induced FY on a UOX-pin-cell calculation. The results obtained using the sandwich formula (Det.) applied on sensitivities which were deduced from direct perturbations are in excellent agreement with Monte Carlo estimates (MC).	168
6.7	Difference correlation matrices for reactivity loss (left) and decay heat (right) for the UOX pin-cell. The two matrices have been obtained subtracting term-by-term the correlation matrices obtained using the sandwich formula and the Monte Carlo uncertainty propagation.	170
6.8	Reactivity loss uncertainty as function of burn-up for the propagation of ^{235}U thermal neutron induced FY on JHR MOC calculation. The results obtained using the sandwich formula (Det.) applied on sensitivities which were deduced from direct perturbations are in excellent agreement with Monte Carlo estimates (MC).	171
6.9	UOX-pin-cell reactivity loss uncertainty due to the yields of the thermal neutron induced fission of ^{235}U . The total uncertainty is given by the propagation of JEFF-3.1.1 FY. In the figure, the most significant contributions have been emphasized with different colors.	172
6.10	^{135}Xe JEFF-3.1.1 evaluated capture cross section. ^{135}Xe is mainly given by Tellurium and Iodine decay. ^{135}Te and ^{135}I have independent FY of respectively 3.6828E-02 and 2.5486E-02.	172
6.11	Relative reactivity loss uncertainty as a function of burn-up for a PWR-UOX pin-cell. The propagation of JEFF-3.1.1 $^{235}\text{U}(n_{th}, f)$ FY uncertainties on the reactivity loss has been compared to what we obtain from FY uncertainties generated by CONRAD, with and without including correlations.	173
6.12	UOX-pin-cell decay heat uncertainty due to the yields of the thermal neutron induced fission of ^{235}U . The total uncertainty is given by the propagation of JEFF-3.1.1 FY. In the figure, the most significant contributions have been emphasized with different colors.	175
6.13	Decay heat uncertainty as a function of time for a PWR-UOX pin-cell. The propagation of JEFF-3.1.1 $^{235}\text{U}(n_{th}, f)$ FY uncertainties on the decay heat has been compared to what we obtain from FY uncertainties generated by CONRAD, with and without including correlations.	175
6.14	Correlation matrix for the UOX-pin-cell reactivity loss obtained from JEFF-3.1.1 $^{235}\text{U}(n_{th}, f)$ FY uncertainty propagation.	176
6.15	Correlation matrix for the UOX-pin-cell reactivity loss obtained from CONRAD $^{235}\text{U}(n_{th}, f)$ FY uncertainty propagation.	176

6.16	Correlation matrix for the UOX-pin-cell decay heat obtained from JEFF-3.1.1 $^{235}\text{U}(n_{th}, f)$ FY uncertainty propagation.	177
6.17	Correlation matrix for the UOX-pin-cell decay heat obtained from CONRAD $^{235}\text{U}(n_{th}, f)$ FY uncertainty propagation.	177
6.18	JHR reactivity loss uncertainty due to the yields of the thermal neutron induced fission of ^{235}U . The total uncertainty is given by the propagation of JEFF-3.1.1 FY. In the figure, the most significant contributions have been emphasized with different colors.	178
6.19	Relative reactivity loss uncertainty as a function of burn-up for the JHR. The propagation of JEFF-3.1.1 $^{235}\text{U}(n_{th}, f)$ FY uncertainties on the reactivity loss has been compared to what we obtain from FY uncertainties generated by CONRAD, with and without including correlations.	179
6.20	Correlation matrix for the JHR reactivity loss obtained from CONRAD $^{235}\text{U}(n_{th}, f)$ FY uncertainty propagation.	179
6.21	Relative reactivity loss uncertainty as a function of burn-up for the JHR in a linear scale.	183
6.22	MOX-pin-cell reactivity loss uncertainty due to the yields of the thermal neutron induced fission of ^{239}Pu . The total uncertainty is given by the propagation of JEFF-3.1.1 FY. In the figure, the most significant contributions have been emphasized with different colors.	184
6.23	Relative reactivity loss uncertainty as a function of burn-up for a PWR-MOX pin-cell. The propagation of JEFF-3.1.1 $^{239}\text{Pu}(n_{th}, f)$ FY uncertainties on the reactivity loss has been compared to what we obtain from FY uncertainties generated by CONRAD, with and without including correlations.	185
6.24	Correlation matrix for the MOX pin-cell reactivity loss obtained from CONRAD $^{239}\text{Pu}(n_{th}, f)$ FY uncertainty propagation.	185
6.25	MOX-pin-cell decay heat uncertainty due to the yields of the thermal neutron induced fission of ^{239}Pu . The total uncertainty is given by the propagation of JEFF-3.1.1 FY. In the figure, the most significant contributions have been emphasized with different colors.	186
6.26	Decay heat uncertainty as a function of time for a PWR-MOX pin-cell. The propagation of JEFF-3.1.1 $^{239}\text{Pu}(n_{th}, f)$ FY uncertainties on the decay heat has been compared to what we obtain from FY uncertainties generated by CONRAD, with and without including correlations.	187
6.27	Correlation matrix for the MOX-pin-cell decay heat obtained from CONRAD $^{239}\text{Pu}(n_{th}, f)$ FY uncertainty propagation.	187
6.28	Relative reactivity loss uncertainty as a function of burn-up for a PWR-UOX pin-cell. The propagation of JEFF-3.1.1 $^{239}\text{Pu}(n_{th}, f)$ FY uncertainties on the reactivity loss has been compared to what we obtain from FY uncertainties generated by CONRAD, with and without including correlations.	188
6.29	Decay heat uncertainty as a function of time for a PWR-UOX pin-cell. The propagation of JEFF-3.1.1 $^{239}\text{Pu}(n_{th}, f)$ FY uncertainties on the decay heat has been compared to what we obtain from FY uncertainties generated by CONRAD, with and without including correlations.	188
6.30	Relative reactivity loss uncertainty as a function of burn-up for the JHR. The propagation of JEFF-3.1.1 $^{239}\text{Pu}(n_{th}, f)$ FY uncertainties on the reactivity loss has been compared to what we obtain from FY uncertainties generated by CONRAD, with and without including correlations.	189

6.31	Relative reactivity loss uncertainty as a function of burn-up for a PWR-MOX pin-cell. The propagation of JEFF-3.1.1 $^{241}\text{Pu}(n_{th}, f)$ FY uncertainties on the reactivity loss has been compared to what we obtain from FY uncertainties generated by CONRAD, with and without including correlations.	190
6.32	Decay heat uncertainty as a function of time for a PWR-MOX pin-cell. The propagation of JEFF-3.1.1 $^{241}\text{Pu}(n_{th}, f)$ FY uncertainties on the decay heat has been compared to what we obtain from FY uncertainties generated by CONRAD, with and without including correlations.	190
6.33	Correlation matrix for the MOX pin-cell reactivity loss obtained from CONRAD $^{241}\text{Pu}(n_{th}, f)$ FY uncertainty propagation.	191
6.34	Correlation matrix for the MOX-pin-cell decay heat obtained from CONRAD $^{241}\text{Pu}(n_{th}, f)$ FY uncertainty propagation.	191
6.35	Relative reactivity loss uncertainty as a function of time for a PWR-UOX pin-cell. The propagation of JEFF-3.1.1 U238F FY uncertainties on the reactivity loss has been compared to what we obtain from FY uncertainties generated by CONRAD, with and without including correlations.	192
6.36	Decay heat uncertainty as a function of burn-up for a PWR-UOX pin-cell. The propagation of JEFF-3.1.1 U238F FY uncertainties on the decay heat has been compared to what we obtain from FY uncertainties generated by CONRAD, with and without including correlations.	193
C.1	Integral Data Assimilation methodologies available in CONRAD.	207
D.1	Comparison between elementary fission decay heat calculations for the thermal fissioning systems U235T, Pu239T and Pu241T, using JEFF-3.1.1 and CONRAD FY values.	210
D.2	Comparison between elementary fission decay heat calculations for the fast fissioning systems U238F, Pu239F and Pu240F, using JEFF-3.1.1 and CONRAD FY values.	210
E.1	Comparison between JEFF-3.1.1 and CONRAD independent mass FY for the fast fission of ^{239}Pu in linear scale. FY model parameters have been adjusted using CONRAD to reproduce the JEFF-3.1.1 evaluated library and generate covariances. The convolution between the pre-neutron model based on Brosa fission modes and the saw-tooth curve allows a satisfactory representation of the available FY data.	213
E.2	Comparison between JEFF-3.1.1 and CONRAD independent mass FY for the fast fission of ^{239}Pu in logarithmic scale. FY model parameters have been adjusted using CONRAD to reproduce the JEFF-3.1.1 evaluated library and generate covariances. The convolution between the pre-neutron model based on Brosa fission modes and the saw-tooth curve allows a satisfactory representation of the available FY data even in the symmetry region.	213
E.3	Comparison between CONRAD and JEFF-3.1.1 independent FY of Iodine isomers for the fast fission of ^{239}Pu . In the figure averages (top) and relative uncertainties (bottom) are presented. Excellent agreement has been found for the most significant FY in average and uncertainty. However, some issues have been noticed for the error bars related to small yields which exhibit unrealistic variances.	214

E.4	Comparison between prior (from Tsuchiya [Tsuchiya et al., 2000] experimental values measured for the thermal fission of ^{239}Pu) and CONRAD-adjusted average number of prompt neutrons emitted as function of the pre-neutron fragment mass, for the fast fission of ^{239}Pu	215
E.5	Decay heat uncertainty for the elementary fast neutron induced fission of ^{239}Pu . The total uncertainty is given by the propagation of JEFF-3.1.1 FY. In the figure, the most significant contributions have been emphasized with different colors.	216
E.6	Decay heat uncertainty as a function of time for the elementary fast fission of ^{239}Pu . The propagation of JEFF-3.1.1 FY uncertainties on the decay heat has been compared to what we obtain from CONRAD-generated FY, with and without including correlations.	216
E.7	Comparison between JEFF-3.1.1 and CONRAD independent mass FY for the fast fission of ^{240}Pu in linear scale. FY model parameters have been adjusted using CONRAD to reproduce the JEFF-3.1.1 evaluated library and generate covariances. The convolution between the pre-neutron model based on Brosa fission modes and the saw-tooth curve allows a satisfactory representation of the available FY data.	218
E.8	Comparison between JEFF-3.1.1 and CONRAD independent mass FY for the fast fission of ^{240}Pu in logarithmic scale. FY model parameters have been adjusted using CONRAD to reproduce the JEFF-3.1.1 evaluated library and generate covariances. The convolution between the pre-neutron model based on Brosa fission modes and the saw-tooth curve allows a satisfactory representation of the available FY data even in the symmetry region.	219
E.9	Comparison between prior (from Tsuchiya [Tsuchiya et al., 2000] experimental values measured for the thermal fission of ^{239}Pu) and CONRAD-adjusted average number of prompt neutrons emitted as function of the pre-neutron fragment mass, for the fast fission of ^{240}Pu	219
E.10	Comparison between CONRAD and JEFF-3.1.1 independent FY of Iodine isomers for the fast fission of ^{240}Pu . In the figure averages (top) and relative uncertainties (bottom) are presented. Excellent agreement has been found for the most significant FY in average and uncertainty. However, some issues have been noticed for the error bars related to small yields which exhibit unrealistic variances.	220
E.11	Decay heat uncertainty for the elementary fast neutron induced fission of ^{240}Pu . The total uncertainty is given by the propagation of JEFF-3.1.1 FY. In the figure, the most significant contributions have been emphasized with different colors.	221
E.12	Decay heat uncertainty as a function of time for the elementary fast fission of ^{240}Pu . The propagation of JEFF-3.1.1 FY uncertainties on the decay heat has been compared to what we obtain from CONRAD-generated FY, with and without including correlations.	221

List of Tables

2.1	Isomeric ratios for different cases.	66
3.1	Decay modes considered to generate the Q-matrix used in CONRAD. Transitions to metastable states have been considered, just adding <code>subm</code> and <code>subn</code> for the first and the second metastable state respectively.	84
3.2	Comparison between two Q-matrix portions, from R.Mills (see Ref. [Mills, 2014]) (top) and CONRAD (bottom).	84
4.1	Fission mode parameters best estimates (BE) and uncertainties before (prior) and after (posterior) the analysis using CONRAD for the thermal fission of ^{235}U	98
4.2	Wahl and Madland-England parameters best estimates (BE) and uncertainties before (prior) and after (posterior) the analysis using CONRAD.	98
4.3	Prompt neutron multiplicities calculated by CONRAD for the thermal fission of ^{235}U . As experimental data we picked the JEFF-3.1.1 evaluated value for the total number of prompt neutron emitted by the fissioning system, and the measurements performed by Nishio of the prompt neutron multiplicities for heavy ($\bar{\nu}_p^H$) and light ($\bar{\nu}_p^L$) fragments [Nishio et al., 1998].	105
4.4	List of the most significant cumulative FY for applications [Serot et al., 2004a]. The yield values and uncertainties are taken from JEFF-3.1.1 and refer to the thermal fission of ^{235}U , ^{239}Pu and ^{241}Pu	113
4.5	List of the most significant cumulative FY for applications [Serot et al., 2004a]. The values are referring to the thermal fission of ^{235}U . Underestimated uncertainties have represented in blue, while in red we show the over-estimations. Average values are instead quite well reproduced.	114
4.6	Example of cumulative-independent uncertainty inconsistency in JEFF-3.1.1 FY library. The cumulative yield for ^{148}Ce is mostly due to its independent yield, which decays β^- two times. The uncertainty on ^{148}Ce independent yield of 10% does not reflect the final accuracy of 0.8% we have on the cumulative, which should be instead of the order of 9%.	116
4.7	Fission mode parameters best estimates (BE) and uncertainties before (prior) and after (posterior) the analysis using CONRAD for the thermal fission of ^{239}Pu	118
4.8	Wahl and Madland-England parameters best estimates (BE) and uncertainties before (prior) and after (posterior) the analysis using CONRAD, for the thermal fission of ^{239}Pu	118

4.9	List of the most significant cumulative FY for applications [Serot et al., 2004a]. The values are referring to the thermal fission of ^{239}Pu . Under-estimated uncertainties have represented in blue, while in red we show the over-estimations. Average values are instead quite well reproduced.	124
4.10	Fission mode parameters best estimates (BE) and uncertainties before (prior) and after (posterior) the analysis using CONRAD for the thermal fission of ^{241}Pu	124
4.11	Wahl and Madland-England parameters best estimates (BE) and uncertainties before (prior) and after (posterior) the analysis using CONRAD, for the thermal fission of ^{241}Pu	125
4.12	List of the most significant cumulative FY for applications [Serot et al., 2004a]. The values are referring to the thermal fission of ^{241}Pu . Under-estimated uncertainties have been represented in blue. Average values are instead quite well reproduced.	130
4.13	Fission mode parameters best estimates (BE) and uncertainties before (prior) and after (posterior) the analysis using CONRAD for the fast neutron induced fission of ^{238}U	130
4.14	Wahl and Madland-England parameters best estimates (BE) and uncertainties before (prior) and after (posterior) the analysis using CONRAD for the fast neutron induced fission of ^{238}U	131
6.1	Isotopic fraction for the PuO_2 contained in the MOX fuel.	163
6.2	Application of the Scheffé and Tukey formula $N = m \frac{\left(\frac{\chi_{\beta, 2m}^2}{2m} - 1\right) \sqrt{\gamma+1}}{1-\gamma}$ to PWR-pin-cells and JHR cases. The parameter values we look at are 52, 54 and 59 in the three quasi-static calculations.	169
6.3	The cumulative yield of ^{135}I is roughly given by the sum of the independent yields related to ^{135}Te , ^{135}Sb and ^{135}Sn . Performing the quadratic sum of their uncertainties, which is equivalent to propagate their uncertainty without any correlations, cannot provide the 3.4% found in JEFF-3.1.1.	183
B.1	Definition of file types (MF) in a ENDF sub-library.	202
E.1	Fission mode parameters best estimates (BE) and uncertainties before (prior) and after (posterior) the analysis using CONRAD for the fast fission of ^{239}Pu	212
E.2	Wahl and Madland-England parameters best estimates (BE) and uncertainties before (prior) and after (posterior) the analysis using CONRAD, for the fast fission of ^{239}Pu	212
E.3	Fission mode parameters best estimates (BE) and uncertainties before (prior) and after (posterior) the analysis using CONRAD for the fast fission of ^{240}Pu	217
E.4	Wahl and Madland-England parameters best estimates (BE) and uncertainties before (prior) and after (posterior) the analysis using CONRAD, for the fast fission of ^{240}Pu	217

Bibliography

- [Abdel-Khalik, 2013] Abdel-Khalik, H. S. (2013). *Overview of Hybrid Subspace Methods for Uncertainty Quantification, Sensitivity Analysis*. ANNALS OF NUCLEAR ENERGY, 52:28–46.
- [Ackermann and Abt, 1984] Ackermann, H. and Abt, K. (1984). *Designing the Sample Size for Non-Parametric, Multivariate Tolerance Regions*. BIOMETRIC JOURNAL, 26:723–734.
- [Aliberti et al., 2006] Aliberti, G., Palmiotti, G., Salvatores, M., Kim, T. K., Taiwo, T., Anitescu, M., Kodeli, I., Sartori, E., Bosq, J. C., and Tommasi, J. (2006). *Nuclear Data Sensitivity, Uncertainty and Target Accuracy Assessment for Future Nuclear Systems*. ANNALS OF NUCLEAR ENERGY, 33:700–733.
- [Amouroux, 2014] Amouroux, C. (2014). *Mesure des Rendements de Fission de l'Am-242 auprès du Spectromètre Lohengrin (réacteur ILL) et Amélioration et Validation du Code Semi-Empirique GEF*. PhD thesis, UNIVERSITÉ PARIS SUD.
- [Apalin et al., 1965] Apalin, V. F., Gritsyuk, Y. N., Kutikov, I. E., Lebedev, V. I., and Mikaelian, L. A. (1965). *Neutron Emission from ^{233}U , ^{235}U and ^{239}Pu Fission Fragments*. NUCLEAR PHYSICS, 71:553–560.
- [Archier, 2011] Archier, P. (2011). *Contribution à l'Amélioration des Données Nucléaires Neutroniques du Sodium pour le Calcul des Réacteurs de Génération IV*. PhD thesis, INSTITUT POLYTECHNIQUE DE GRENOBLE, FRANCE.
- [Archier et al., 2012] Archier, P., Buiron, L., De Saint Jean, C., and Dos Santos, N. (2012). *Nuclear Data Uncertainty Propagation for Neutronic Key Parameters of CEA's SFR V2B and CFV Sodium Fast Reactor Designs*. In INTERNATIONAL CONFERENCE ON THE PHYSICS OF REACTORS, PHYSOR2012, Knoxville. ANS.
- [Archier et al., 2013] Archier, P., De Saint Jean, C., Kopecky, S., Litaize, O., Noguère, G., Schillebeeckx, P., and Volev, K. (2013). *Recent Development in the CONRAD Code Regarding Experimental Corrections*. EPJ WEB OF CONFERENCES, 42:02004:1–6.
- [Archier et al., 2014a] Archier, P., De Saint Jean, C., Litaize, O., Noguère, G., Berge, L., Privas, E., and Tamagno, P. (2014a). *CONRAD Evaluation Code: Development Status and Perspectives*. NUCLEAR DATA SHEETS, 118:488–490.
- [Archier et al., 2014b] Archier, P., De Saint Jean, C., Noguère, G., Litaize, O., Leconte, P., and Bouret, C. (2014b). *COMAC: Nuclear Data Covariance Matrices Library for Reactor Applications*. In INTERNATIONAL CONFERENCE ON THE PHYSICS OF REACTORS, PHYSOR2014, Kyoto.
- [Arwade et al., 2010] Arwade, S., Moradi, M., and Louhghalam, A. (2010). *Variance Decomposition and Global Sensitivity for Structural Systems*. ENGINEERING STRUCTURES, 32:1–10.
- [Auffero et al., 2015] Auffero, M., Bidaud, A., Hursin, M., Leppänen, J., Palmiotti, G., Pelloni, S., and Rubiolo, P. (2015). *A Collision History-Based Approach to Sensitivity/Perturbation Calculations in the Continuous Energy Monte Carlo Code SERPENT*. ANNALS OF NUCLEAR ENERGY, 85:245–258.
- [Bail, 2009] Bail, A. (2009). *Mesures de Rendements Isobariques et Isotopiques des Produits de Fission Lourds sur le Spectromètre de Masse Lohengrin*. PhD thesis, UNIVERSITÉ DE BORDEAUX.
- [Bail et al., 2011] Bail, A., Serot, O., Mathieu, L., Litaize, O., Materna, T., Köster, U., Faust, H., Letourneau, A., and Panebianco, S. (2011). *Isotopic Yield Measurement in the Heavy Mass Region for ^{239}Pu Thermal Neutron Induced Fission*. PHYSICAL REVIEW C, 84:034605.
- [Bateman, 1910] Bateman, H. (1910). *The Solution of a System of Differential Equations Occurring in the Theory of Radioactive Transformations*. In PROCEEDINGS CAMBRIDGE PHILOSOPHICAL SOCIETY, volume 15, pages 423–427.
- [Batenkov et al., 2004] Batenkov, O. A., Boykov, G. A., Hamsch, F.-J., Hamilton, J. H., Jakovlev, V. A., Kalinin, V. A., Laptev, A. B., Sokolov, V. E., and Vorobyev, A. S. (2004). *Prompt Neutron Emission in the Neutron-Induced Fission of ^{239}Pu and ^{235}U* . In INTERNATIONAL CONFERENCE ON NUCLEAR DATA FOR SCIENCE AND TECHNOLOGY, volume 769, pages 1003–1007, Santa Fe. American Institute of Physics.

Bibliography

- [Bell and Glasstone, 1970] Bell, G. and Glasstone, S. (1970). *Nuclear Reaction Theory*. VAN NOSTRAND REINHOLD COMPANY.
- [Benoit, 2012] Benoit, J.-C. (2012). *Développement d'un Code de Propagation des Incertitudes des Données Nucléaires sur la Puissance Résiduelle dans les Réacteurs à Neutrons Rapides*. PhD thesis, UNIVERSITÉ PARIS SUD, FRANCE.
- [Berge, 2015] Berge, L. (2015). *Contribution à la Modélisation des Spectres de Neutrons Prompts de Fission. Propagation d'Incertitudes sur un Calcul de Fluence Cuve*. PhD thesis, INSTITUT POLYTECHNIQUE DE GRENOBLE, FRANCE.
- [Berge et al., 2015] Berge, L., Litaize, O., Serot, O., De Saint Jean, C., Archier, P., and Peneliau, Y. (2015). *Study on Prompt Fission Neutron Spectra and Associated Covariances for $^{235}\text{U}(n_{th}, f)$ and $^{239}\text{Pu}(n_{th}, f)$* . PHYSICS PROCEDIA, 64:55–61.
- [Bethe, 1937] Bethe, H. (1937). *Nuclear Physics B. Nuclear Dynamics, Theoretical*. REV. MOD. PHYS., 9:69–244.
- [Bignan and Estrade, 2012] Bignan, G. and Estrade, J. (2012). *The Jules Horowitz Reactor, a New High Performances European MTR (Material Testing Reactor) with Modern Experimental Capacities Toward an International Center of Excellence*. In INTERNATIONAL GROUP ON RESEARCH REACTORS, IGORR14, Prague. European Nuclear Society.
- [Boldeman and Hines, 1985] Boldeman, J. W. and Hines, M. G. (1985). *Prompt Neutron Emission Probabilities following Spontaneous and Thermal Neutron Fission*. NUCLEAR SCIENCE AND ENGINEERING, 91:114–116.
- [Borgonuovo, 2006] Borgonuovo, E. (2006). *Measuring Uncertainty Importance: Investigation and Comparison of Alternative Approaches*. RISK ANALYSIS, 26.
- [Boutoux et al., 2013] Boutoux, G. et al. (2013). *The SOFIA Experiment*. PHYSICS PROCEDIA, 47:166–171.
- [Brosa et al., 1990] Brosa, U., Grossmann, S., and Muller, U. (1990). *Nuclear Scission*. PHYSICS REPORTS, 4:167–262.
- [Brosa et al., 1999] Brosa, U., Knitter, H.-H., shuan Fan, T., min Hu, J., and lian Bao, S. (1999). *Systematics of Fission-Channel Probabilities*. PHYSICAL REVIEW C, 59:767–775.
- [Brun et al., 2015] Brun, E., Damian, F., Diop, C. M., Dumonteil, E., Hugot, F. X., Jouanne, C., Lee, Y. K., Malvagi, F., Mazzolo, A., Petit, O., Trama, J. C., Visonneau, T., and Zoia, A. (2015). *TRIPOLI-4, CEA, EDF and AREVA Reference Monte Carlo Code*. ANNALS OF NUCLEAR ENERGY, 82:151–160.
- [Cabellos et al., 2011] Cabellos, O., García Herranz, N., Diez, C. J., Alvarez Cascos, R., Sanz Gonzalo, J., Serrano, F., and Sauvan, P. (2011). *Propagation of Nuclear Data Uncertainties in Transmutation Calculations Using ACAB Code*. JOURNAL OF THE KOREAN PHYSICAL SOCIETY, 50:1268–1271.
- [Camprini, 2012] Camprini, P. C. (2012). *Power Transient Analyses for Reflector Experimental Devices During Shut-Downs in Jules Horowitz Reactor (JHR)*. Technical Report RdS/2012/1353, ENEA.
- [Camprini, 2013] Camprini, P. C. (2013). *Power Transient Analysis of Experimental Devices for Jules Horowitz Material Testing Reactor (JHR)*. PhD thesis, UNIVERSITY OF BOLOGNA, ITALY.
- [Capote and Smith, 2008] Capote, R. and Smith, D. L. (2008). *An Investigation of the Performance of the Unified Monte Carlo Method of Neutron Cross Section Data Evaluation*. NUCLEAR DATA SHEETS, 109:2768–2773.
- [Capote et al., 2010] Capote, R., Smith, D. L., and Trkov, A. (2010). *Nuclear Data Evaluation Methodology Including Estimates of Covariances*. EPJ WEB OF CONFERENCES, 8.
- [Chatillon et al., 2015] Chatillon, A. et al. (2015). *Accurate Measurements of Fission-Fragment Yields in $^{234,235,236,238}\text{U}(g,f)$ with the SOFIA Set-Up*. In WONDER-2015: FOURTH INTERNATIONAL WORKSHOP ON NUCLEAR DATA EVALUATION FOR REACTOR APPLICATIONS, Aix-en-Provence. To be published in EPJ Web Conferences.
- [Chebboubi, 2015] Chebboubi, A. (2015). *Contribution à l'Étude de la Fission Nucléaire: de LOHENGRIN à FIPPS*. PhD thesis, UNIVERSITY OF GRENOBLE, FRANCE.
- [Chiba and Smith, 1991] Chiba, S. and Smith, D. (1991). *A Suggested Procedure for Resolving an Anomaly in Least-Squares Data Analysis Known as Peelle's Pertinent Puzzle and the General Implications for Nuclear Data Evaluation*. Technical Report NDM-121, ANL.
- [Conrad, 2000] Conrad, K. (2000). *Probability distributions and maximum entropy*. University Lecture.
- [Döderlein et al., 2008] Döderlein, C., D'Aletto, C., Di Salvo, J., Gueton, O., and Sireta, P. (2008). *The 3D Neutronics Scheme for the Development of the Jules Horowitz Reactor*. In INTERNATIONAL CONFERENCE ON THE PHYSICS OF REACTORS, PHYSOR2008, Interlaken. PSI.

- [De Saint Jean et al., 2010a] De Saint Jean, C., Archier, P., Noguère, G., Bernard, D., Tommasi, J., and Blaise, P. (2010a). *Uncertainty Evaluation of Nuclear Reaction Model Parameters Using Integral and Microscopic Measurements with the CONRAD Code*. In INTERNATIONAL CONFERENCE ON NUCLEAR DATA FOR SCIENCE AND TECHNOLOGY.
- [De Saint Jean et al., 2010b] De Saint Jean, C., Habert, B., Archier, P., Noguère, G., Bernard, D., Tommasi, J., and Blaise, P. (2010b). *Uncertainty Evaluation of Nuclear Reaction Model Parameters Using Integral and Microscopic Measurements. Covariances Evaluation with CONRAD Code*. In EPJ WEB OF CONFERENCES.
- [De Saint Jean et al., 2007] De Saint Jean, C., Habert, B., Litaize, O., Noguère, G., and Suteau, C. (2007). *Status of CONRAD, a Nuclear Reaction Analysis Tool*. In INTERNATIONAL CONFERENCE ON NUCLEAR DATA FOR SCIENCE AND TECHNOLOGY, Nice.
- [De Saint Jean et al., 2009] De Saint Jean, C., Noguère, G., Habert, B., and Ioossand, B. (2009). *A Monte Carlo Approach to Nuclear Model Parameter Uncertainties Propagation*. NUCLEAR SCIENCE AND ENGINEERING, 161:363–370.
- [Dematté, 1996] Dematté, L. (1996). *Investigation of the Fission Fragments Mass and Energy Distributions of $^{236,238,240,242,244}\text{Pu}(SF)$* . PhD thesis, UNIVERSITY OF GENT, BELGIUM.
- [Diez et al., 2015] Diez, C. J., Cabellos, O., and Martínez, J. S. (2015). *Nuclear Data Uncertainty Propagation in Depletion Calculations Using Cross Section Uncertainties in One-group or Multi-group*. NUCLEAR DATA SHEETS, 123:79–89.
- [Doré et al., 2014] Doré, D., Farget, F., Lecolley, F.-R., Lehaut, G., Materna, T., Pancin, J., Panebianco, S., and Papaevangelou, T. (2014). *FALSTAFF: A New Tool for Fission Fragment Characterization*. NUCLEAR DATA SHEETS, 119:346–348.
- [Faust and Geltenbort, 1981] Faust, H. and Geltenbort, P. (1981). *Calibration and Adjustment Procedures for LOHENGRIN*. Technical Report 81FA45S, ILL.
- [Fiorito et al., 2014] Fiorito, L., Diez, C., Cabellos, O., Stankovskiy, A., Van den Eynde, G., and Labeau, P. E. (2014). *Fission yield covariance generation and uncertainty propagation through fission pulse decay heat calculation*. ANNALS OF NUCLEAR ENERGY, 69:331–343.
- [Fiorito et al., 2016] Fiorito, L., Stankovskiy, A., Van den Eynde, G., Diez, C. J., Cabellos, O., and Labeau, P. E. (2016). *Generation of Fission Yield Covariances to Correct Discrepancies in the Nuclear Data Libraries*. ANNALS OF NUCLEAR ENERGY, 88:12–23.
- [Fröhner, 1997] Fröhner, F. (1997). *Assigning Uncertainties to Scientific Data*. NUCLEAR SCIENCE AND ENGINEERING, 126:1–18.
- [Fröhner, 2000] Fröhner, F. (2000). *Evaluation and Analysis of Nuclear Resonance Data*. Technical Report JEFF Report 18, OECD-NEA.
- [Gaudier, 2010] Gaudier, F. (2010). *URANIE: The CEA/DEN Uncertainty and Sensitivity Platform*. PROCEDIA SOCIAL AND BEHAVIORAL SCIENCES, 2:7660–7661.
- [Gönnenwein, 2014] Gönnenwein, F. (2014). *Neutron-Induced Fission*. JULIOT-CURIE SUMMER SCHOOL LECTURE.
- [Glaeser et al., 1994] Glaeser, H., Hofer, E., Kloos, M., and Skorek, T. (1994). *Uncertainty and Sensitivity Analysis of a Post-Experiment Calculation in Thermal-Hydraulics*. RELIABILITY ENGINEERING AND SYSTEM SAFETY, 45:19–33.
- [Golfier et al., 2009] Golfier, H., Lenain, R., Calvin, C., Lautard, J. J., and Baudron, A. M. (2009). *APOLLO3: a Common Project of CEA, AREVA and EDF for the Development of a new Deterministic Multi-Purpose Code for Core Physics Analysis*. In INTERNATIONAL CONFERENCE ON MATHEMATICS, COMPUTATIONAL METHODS AND REACTOR PHYSICS (M&C-2009), New York, USA.
- [Goorley et al., 2015] Goorley, T. et al. (2015). *Features of MCNP6*. ANNALS OF NUCLEAR ENERGY, 87:772–783.
- [Guba et al., 2003] Guba, A., Makai, M., and Pál, L. (2003). *Statistical Aspects of Best Estimate Method*. RELIABILITY ENGINEERING AND SYSTEM SAFETY, 80:217–232.
- [Gwin et al., 1984] Gwin, R., Spencera, R. R., and Ingle, R. W. (1984). *Measurement of the Energy Dependence of Prompt Neutron Emission from ^{233}U , ^{235}U , ^{239}Pu , and ^{241}Pu for $E=0.005$ to 10 eV Relative to Emission from Spontaneous Fission of ^{252}Cf* . NUCLEAR SCIENCE AND ENGINEERING, 87:381–404.
- [Habert, 2009] Habert, B. (2009). *Estimation des Incertitudes dans l'Évaluation des Sections Efficaces de Réactions Nucléaires*. PhD thesis, PHD THESIS, UNIVERSITY OF GRENOBLE.
- [Habert et al., 2010] Habert, B., De Saint Jean, C., Noguère, G., Leal, L., and Rugama, Y. (2010). *Retroactive Generation of Covariance Matrix of Nuclear Model Parameters Using Marginalization Techniques*. NUCLEAR SCIENCE AND ENGINEERING, 166:276–287.

- [Hahn and Strassmann, 1939] Hahn, O. and Strassmann, F. (1939). *Über den Nachweis und das Verhalten der bei der Berstrahlung des Urans Mittels Neutronen Entstehenden Erdalkalimetalle*. *NATURWISSENSCHAFTEN*, 27:11.
- [Hambusch et al., 1989] Hambusch, F. J., Knitter, H. H., Budtz-Jørgensen, C., and Theobald, J. P. (1989). *Fission Mode Fluctuations in the Resonance of ^{235}U* . *NUCLEAR PHYSICS A*, 491:56–90.
- [Hébert, 2009] Hébert, A. (2009). *Applied Reactor Physics*. PRESSES INTERNATIONALES POLYTECHNIQUE.
- [Henderson and Searle, 1981] Henderson, H. and Searle, S. (1981). *On Deriving the Inverse of a Sum of Matrices*. *SIAM REVIEW*, 23:53–60.
- [Herman, 2011] Herman, M. (2011). *Covariance Data in Fast Neutron Region*. OECD-NEA WPEC-SG 24.
- [Herman et al., 2007] Herman, M., Capote, R., Carlson, B. V., Obložinský, P., Sin, M., Trkov, A., Wienke, H., and Zerkin, V. (2007). *EMPIRE: Nuclear Reaction Model Code System for Data Evaluation*. *NUCLEAR DATA SHEETS*, 108:2655–2715.
- [Hernández Solís et al., 2013] Hernández Solís, A., Demazière, C., and Ekberg, C. (2013). *Uncertainty and Sensitivity Analyses Applied to the DRAGONv4.05 Code Lattice Calculations and Based on JENDL-4 Data*. *ANNALS OF NUCLEAR ENERGY*, 57:230–245.
- [Icrane, 2006] Icrane, D. (2006). *Jules Horowitz Reactor, a New Material Testing Reactor in Europe*. *NUCLEAR ENGINEERING TECHNOLOGY*, 38:437–442.
- [Icrane et al., 2008] Icrane, D., Chaix, P., and Alamo, A. (2008). *Jules Horowitz Reactor: a High Performance Material Testing Reactor*. *C. R. PHYSIQUE*, 9:445–456.
- [Kellett and Mills, 2009] Kellett, M. A. and Mills, R. (2009). *The JEFF-3.1/-3.1.1 Radioactive Decay Data and Fission Yields Sub-Libraries*. Technical Report JEFF REPORT 20, OECD-NEA.
- [Kessedjian, 2015] Kessedjian, G. (2015). *Des Données Nucléaires Expérimentales à l'Évaluation: Contribution à l'Analyse Statistique dans la Réduction des Données et les Tests d'Hypothèses-Application à la Fission*. HDR Thesis University of Grenoble, France.
- [Kinoshita et al., 2014] Kinoshita, K., T.Endo, Yamamoto, A., Kodama, Y., Ohoka, Y., T.Ushio, and H.Nagano (2014). *Uncertainty Quantification of Neutronics Characteristics using Latin Hypercube Sampling Method*. In *PHYSOR 2014*, Kyoto.
- [Klein et al., 2009] Klein, J. C., Thiollay, N., Di Salvo, J., Bignan, G., Bosq, J. C., Sireta, P., Wieryszkov, J. P., Alexandre, P., and Garnier, D. (2009). *AMMON: an Experimental Program in the EOLE Critical Facility for the Validation of the Jules Horowitz Reactor Neutron and Photon HORUS3D Calculation Scheme*. In *INTERNATIONAL GROUP ON RESEARCH REACTORS, IGORR12*, pages 28–30, Beijing. CEA.
- [Koning et al., 2007] Koning, A., Hilaire, S., and Duijvestijn, M. (2007). *TALYS-1.0*. In *INTERNATIONAL CONFERENCE ON NUCLEAR DATA FOR SCIENCE AND TECHNOLOGY*, Nice.
- [Koning, 2015] Koning, A. J. (2015). *Bayesian Monte Carlo Method for Nuclear Data Evaluation*. *NUCLEAR DATA SHEETS*, 123:207–213.
- [Koning and Rochman, 2008] Koning, A. J. and Rochman, D. (2008). *Towards Sustainable Nuclear Energy: Putting Nuclear Physics to Work*. *ANNALS OF NUCLEAR ENERGY*, 35:2024–2030.
- [Lautard et al., 1990] Lautard, J. J., Loubiere, S., and Fedon-Magnaud, C. (1990). *CRONOS, a Modular Computational System for Neutronic Core Calculations*. In *IAEA TOPICAL MEETING*, Cadarache. CEA.
- [Lawrence, 1965] Lawrence, J. N. P. (1965). *Static Fission-Barrier Calculations of a Two-Parameter Liquid Drop*. *PHYSICAL REVIEW*, 139:1227–1231.
- [Leconte, 2009] Leconte, P. (2009). *Qualification of the APOLLO2.8 Code Package for the Calculation of the Fuel Inventory and Reactivity Loss of UOx Spent Fuels in BWRs*. *ANNALS OF NUCLEAR ENERGY*, 36:362–367.
- [Leonard and Hsu, 1999] Leonard, T. and Hsu, J. S. (1999). *Bayesian Methods, An Analysis for Statisticians and Interdisciplinary Researchers*. CAMBRIDGE UNIVERSITY PRESS.
- [Leray, 2012] Leray, O. (2012). *Détermination, maîtrise et réduction des biais et incertitudes de la réactivité du Réacteur Jules Horowitz*. PhD thesis, UNIVERSITY OF GRENOBLE, FRANCE.
- [Leray et al., 2012a] Leray, O., Hudelot, J. P., Antony, M., Doderlein, C., Santamarina, A., Bernard, D., and Vaglio-Gaudard, C. (2012a). *Neutronics Experimental Validation of the Jules Horowitz Reactor Fuel by Interpretation of the VALMONT Experimental Program - Transposition of the Uncertainty on the Reactivity of JHR with JEF-2.2 and JEFF-3.1.1*. *IEEE TRANSACTIONS ON NUCLEAR SCIENCE*, 59:1335–1343.
- [Leray et al., 2012b] Leray, O., Vaglio-Gaudard, C., Hudelot, J. P., Santamarina, A., Noguère, G., and Di Salvo, J. (2012b). *Sensitivity and Uncertainty Analysis Applied to the JHR Reactivity Prediction*. In *INTERNATIONAL CONFERENCE ON THE PHYSICS OF REACTORS, PHYSOR2012*, Knoxville. ANS.

- [Litaize et al., 2013] Litaize, O., Archier, P., Becker, B., Schillebeeckx, P., and Kopecky, S. (2013). *Validation of Capture Yield Calculations in the Resolved Resonance Energy Range with CONRAD Code*. EPJ WEB OF CONFERENCES, 42:02003:1–6.
- [Litaize and Serot, 2010] Litaize, O. and Serot, O. (2010). *Investigation of Phenomenological Models for the Monte Carlo Simulation of the Prompt Fission Neutron and γ Emission*. PHYSICAL REVIEW C, 82:054616–1–11.
- [MacFarlane et al., 2000] MacFarlane, R. E. et al. (2000). *NJOY-99.0: Code System for Producing Pointwise and Multigroup Neutron and Photon Cross Section from ENDF/B Data*. Technical Report No. PSR-480, LANL.
- [Madland and England, 1977] Madland, D. and England, T. (1977). *The Influence of Isomeric States on Independent Fission Product Yields*. NUCLEAR SCIENCE ENGINEERING, 4:859–865.
- [Martin, 2013] Martin, F. (2013). *Étude des Distributions en Masse, Charge Nucléaire et énergie cinétique des produits de fission de $l^{233}U(n_{th}, f)$ et du $^{241}Pu(n_{th}, f)$ Mesurées auprès du Spectromètre de Masse Lohengrin (ILL)*. PhD thesis, INSTITUT POLYTECHNIQUE DE GRENOBLE, FRANCE.
- [Martinez et al., 2014] Martinez, J. S., Zwermann, W., Gallner, L., Puente-Espel, F., Cabellos, O., Velkov, K., and Hannstein, V. (2014). *Propagation of Neutron Cross Section, Fission Yield, and Decay Data Uncertainties in Depletion Calculations*. NUCLEAR DATA SHEETS, 118:480–483.
- [Mattoon et al., 2012] Mattoon, C. M., Beck, B. R., Patel, N. R., Summers, N. C., and Hedstrom, G. W. (2012). *Generalized Nuclear Data: a New Structure (with Supporting Infrastructure) for Handling Nuclear Data*. NUCLEAR DATA SHEETS, 113:3145–3171.
- [Möller et al., 2009] Möller, P., Sierk, A. J., Ichikawa, T., Iwamoto, A., Bengtsson, R., Uhrenholt, H., and Aberg, S. (2009). *Heavy-Element Fission Barriers*. PHYSICAL REVIEW C, 79:064304–1–38.
- [Mills, 1995] Mills, R. (1995). *Fission Product Yields Evaluation*. PhD thesis, PHD THESIS, UNIVERSITY OF BIRMINGHAM.
- [Mills, 2012] Mills, R. (2012). *Improved Fission Product Yield Evaluation Methodologies*. WPEC SUBGROUP 37 PROPOSAL.
- [Mills, 2014] Mills, R. W. (2014). *Uncertainty Propagation of Fission Product Yield Data in Spent Fuel Inventory Calculations*. NUCLEAR DATA SHEETS, 118:484–487.
- [Moxon et al., 2010] Moxon, M. C., Ware, T. C., and Dean, C. J. (2010). *REFIT-2009: a Least Square Fitting Program for Resonance Analysis of Neutron Transmission, Capture, Fission and Scattering Data*. Technical report, UKNSF.
- [Neudecker et al., 2012] Neudecker, D., Frühwirth, R., and Leeb, H. (2012). *Peelle’s Pertinent Puzzle: A Fake Due to Improper Analysis*. NUCLEAR SCIENCE AND ENGINEERING, 170:64–60.
- [Nishio et al., 1995] Nishio, K., Nakagome, Y., and Kanno, I. (1995). *Measurement of Fragment Mass Dependent Kinetic Energy and Neutron Multiplicity for Thermal Neutron Induced Fission of Plutonium-239*. JOURNAL OF NUCLEAR SCIENCE AND TECHNOLOGY, 32:404–414.
- [Nishio et al., 1998] Nishio, K., Nakagome, Y., Yamamoto, H., and Kimura, I. (1998). *Multiplicity and Energy of Neutrons from $^{235}U(n_{th}, f)$ Fission Fragments*. NUCLEAR PHYSICS A, 632:540–558.
- [Obložinský et al., 2010] Obložinský, P. et al. (2010). *Endf-6 formats manual*. Technical report, BROOKHAVEN NATIONAL LABORATORY.
- [Otuka et al., 2014] Otuka, N. et al. (2014). *Towards a More Complete and Accurate Experimental Nuclear Reaction Data Library (EXFOR): International Collaboration Between Nuclear Reaction Data Centers (NRDC)*. NUCLEAR DATA SHEETS, 120:272–276.
- [Palmiotti et al., 2014] Palmiotti, G. et al. (2014). *Combined Use of Integral Experiments and Covariance Data*. NUCLEAR DATA SHEETS, 118:596–636.
- [Palmiotti et al., 2009] Palmiotti, G., Salvatores, M., Aliberti, G., Hiruta, H., McKnight, R., Obložinský, P., and Yang, W. S. (2009). *A Global Approach to the Physics Validation of Simulation Codes for Future Nuclear Systems*. ANNALS OF NUCLEAR ENERGY, 36:355–361.
- [Panjer, 1973] Panjer, H. H. (1973). *On the Decomposition of Moments by Conditional Moments*. THE AMERICAN STATISTICIAN, 27:170–171.
- [Papoulis, 2002] Papoulis, A. (2002). *Probability, Random Variables and Stochastic Processes*. MCGRAW-HILL.
- [Pigni et al., 2015] Pigni, M. T., Francis, M. W., and Gauld, I. C. (2015). *Investigation of Inconsistent ENDF/B-VII.1 Independent and Cumulative Fission Product Yields with Proposed Revisions*. NUCLEAR DATA SHEETS, 123:231–236.
- [Poenaru and Greiner, 1997] Poenaru, D. N. and Greiner, W. (1997). *Experimental Techniques in Nuclear Physics*. DE GRUYTER.

- [Privas, 2015] Privas, E. (2015). *Contribution à l'Évaluation des Incertitudes sur les Sections Efficaces Neutroniques pour les Réacteurs à Neutrons Rapides*. PhD thesis, INSTITUT POLYTECHNIQUE DE GRENOBLE, FRANCE.
- [Raynal, 1994] Raynal, J. (1994). *ECIS-94*. Technical Report No. CEA-N-2772, CEA-SACLAY.
- [Regnier, 2013] Regnier, D. (2013). *Contribution à l'Étude des Gammas Prompts de Fission*. PhD thesis, INSTITUT POLYTECHNIQUE DE GRENOBLE, FRANCE.
- [Reuss, 2008] Reuss, P. (2008). *Nuclear Engineering*. EDP SCIENCES.
- [Rodriguez-Tajes et al., 2014] Rodriguez-Tajes, C. et al. (2014). *Transfer Reactions in Inverse Kinematics: An Experimental Approach for Fission Investigations*. PHYSICAL REVIEW C, 89:024614–1–15.
- [Roe, 2001] Roe, B. P. (2001). *Probability and Statistics in Experimental Physics*. SPRINGER.
- [Ruggieri et al., 2006] Ruggieri, J.-M., Tommasi, J., Lebrat, J. F., Suteau, C., Plisson-Rieunier, D., De Saint Jean, C., Rimpault, G., and Sublet, J. C. (2006). *ERANOS-2.1: the International Code System for GEN-IV Fast Reactor Analysis*. In INTERNATIONAL CONGRESS ON ADVANCES IN NUCLEAR POWER PLANTS-ICAPP, Reno, Nevada.
- [Saltelli et al., 2008] Saltelli, A., Tarantola, S., Andres, T., and Ratto, M. (2008). *Global Sensitivity Analysis. The Primer*. JOHN WILEY AND SONS.
- [Saltelli et al., 2004] Saltelli, A., Tarantola, S., Campolongo, F., and Ratto, M. (2004). *Sensitivity Analysis in Practice: A Guide to Assessing Scientific Models*. JOHN WILEY AND SONS.
- [Salvatores, 1988] Salvatores, M. (1988). *Perturbation Theory and Sensitivity Analysis*. EDF BULLETIN DE LA DIRECTION DES ETUDES ET RECHERCHES, 1:33.
- [Salvatores et al., 2007] Salvatores, M., Aliberti, G., Palmiotti, G., Rochman, D., Oblozinsky, P., Hermann, M., Talou, P., Kawano, T., Leal, L., Koning, A., and Kodeli, I. (2007). *Nuclear Data Needs for Advanced Reactor Systems: a NEA Nuclear Science Committee Initiative*. In INTERNATIONAL CONFERENCE ON NUCLEAR DATA FOR SCIENCE AND TECHNOLOGY, pages 879–882, Nice. CEA.
- [Salvatores and Palmiotti, 1985] Salvatores, M. and Palmiotti, G. (1985). *LMFBR Design Parameter Uncertainties and Target Accuracies*. ANNALS OF NUCLEAR ENERGY, 12:291–306.
- [Salvatores et al., 2008] Salvatores, M., Palmiotti, G., Aliberti, G., and Yang, W. S. (2008). *Needs and Issues of Covariance Data Application*. NUCLEAR DATA SHEETS, 109:2725–2732.
- [SAMMY, 2008] SAMMY (2008). *User's Guide: Multilevel R-Matrix Fits to Neutron Data Using Bayes' Equations*.
- [Sanchez et al., 1988] Sanchez, R., Mondot, J., Stankovski, A., Cossic, A., and Zmijarevic, I. (1988). *APOLLO II: a User-Oriented, Portable, Modular, Code for Multigroup Transport Assembly Calculations*. NUCLEAR SCIENCE AND ENGINEERING, 100:352–362.
- [Schillebeeckx et al., 1992] Schillebeeckx, P., Wagemans, C., Deruytter, A., and Barthélémy, R. (1992). *Comparative Study of the Fragments Mass and Energy Characteristics in the Spontaneous Fission of Pu-238, Pu-240 and Pu-242 and in the Thermal Neutron Induced Fission of Pu-239*. NUCLEAR PHYSICS A, 545:623–645.
- [Schmidt et al., 2000] Schmidt, K.-H. et al. (2000). *Relativistic Radioactive Beams: A New Access to Nuclear-Fission Studies*. NUCLEAR PHYSICS A, 665:221–267.
- [Schmitt et al., 1966] Schmitt, H. W., Neiler, J. H., and Walter, F. J. (1966). *Fragment Energy Correlation Measurements for ^{252}Cf Spontaneous Fission and ^{235}U Thermal-Neutron Fission*. PHYSICAL REVIEW, 141:1146–1160.
- [Serot et al., 2014] Serot, O., Amouroux, C., Bidaud, A., Capellan, N., Chabod, S., Ebran, A., Faust, H., Kessedjian, G., Kœster, U., Letourneau, A., Litaize, O., Martin, F., nad L. Mathieu, T. M., Panebianco, S., Regis, J.-M., Rudigier, M., Sage, C., and Urban, W. (2014). *Recent Results from Lohengrin on Fission Yields and Related Decay Properties*. NUCLEAR DATA SHEETS, 119:320–323.
- [Serot et al., 2004a] Serot, O., Roque, B., and Santamarina, A. (2004a). *Review of the Most Reactor Relevant Cumulative Fission Product Yields*. Technical Report JEFF DOC No. 1055, OECD-NEA.
- [Serot et al., 2004b] Serot, O., Wagemans, C., and Heyse, J. (2004b). *New Results on Helium and Tritium Gas Production from Ternary Fission*. In INTERNATIONAL CONFERENCE ON NUCLEAR DATA FOR SCIENCE AND TECHNOLOGY, Santa Fe.
- [Serot et al., 2007] Serot, O., Wagemans, C., Vermote, S., Heyse, J., Soldner, T., Geltenbort, P., AlMahamid, I., Floyd, J., and Lukens, W. W. (2007). *Tritium Production from Ternary Fission*. In INTERNATIONAL CONFERENCE ON NUCLEAR DATA FOR SCIENCE AND TECHNOLOGY, Nice.
- [Shannon, 1948] Shannon, C. (1948). *A Mathematical Theory of Communication*. THE BELL SYSTEM TECHNICAL JOURNAL, 27:379–423.

- [Sheffé, 1943] Sheffé, H. (1943). *Statistical Inference in the Non-Parametric Case*. ANNALS OF MATHEMATICAL STATISTICS, 14:305–327.
- [Sheffé and Tukey, 1944] Sheffé, H. and Tukey, J. W. (1944). *A Formual for Sample Sizes for Population Tolerance Limits*. ANNALS OF MATHEMATICAL STATISTICS, 15:217.
- [Smith, 1990] Smith, D. (1990). *Probability, Statistics and Data Uncertainties in Nuclear Science and Technology*, volume 4. OECD-NEA COMMITTEE SERIES.
- [Smith, 1993] Smith, D. (1993). *A Least-Squares Computational Tool-Kit*. Technical Report NDM-128, ANL.
- [Smith, 2004] Smith, D. (2004). *Covariance Matrices for Nuclear Cross Sections Derived from Nuclear Model Calculations*. Technical Report NDM-159, ANL.
- [Smith, 2008] Smith, D. (2008). *A Unified Monte Carlo Approach to Fast Neutron Cross Section Data Evaluation*. Technical Report NDM-166, ANL.
- [Smith, 2004] Smith, D. L. (2004). *Nuclear Data Uncertainties in 2004: A Perspective*. In INTERNATIONAL CONFERENCE ON NUCLEAR DATA FOR SCIENCE AND TECHNOLOGY, volume 769, pages 320–325, Santa Fe. AIP.
- [Smith, 2014] Smith, R. (2014). *Uncertainty Quantification: Theory, Implementation and Applications*. SIAM-COMPUTATIONAL SCIENCE AND ENGINEERING.
- [Soppera et al., 2014] Soppera, N., Bossant, M., and Dupont, E. (2014). *JANIS-4.0: An Improved Version of the NEA Java-Based Nuclear Data Information System*. NUCLEAR DATA SHEETS, 120:294–298.
- [Stacey, 2007] Stacey, W. M. (2007). *Nuclear Reactor Physics*. WILEY-VCH.
- [Strutinsky, 1968] Strutinsky, V. M. (1968). *Shell Effects in Nuclear Masses and Deformation Energies*. NUCLEAR PHYSICS A, 122:1–33.
- [Sublet et al., 2014] Sublet, J.-C., Koning, A., and Rochman, D. (2014). *TENDL-2012 Processing, Verification and Validation Steps*. NUCLEAR DATA SHEETS, 118:418–421.
- [Suyama and Mochizuki, 2005] Suyama, K. and Mochizuki, H. (2005). *Effect of Neutron Induced Reactions of Neodymium-147 and 148 on Burn-up Evaluation*. JOURNAL OF NUCLEAR SCIENCE AND TECHNOLOGY, 42:661–669.
- [Tamagno, 2015] Tamagno, P. (2015). *Challenging Fission Cross Section Simulation with Long Standing Macro-Microscopic Model of Nucleus Potential Energy Surface*. PhD thesis, UNIVERSITÉ DE BORDEAUX, FRANCE.
- [Taylor, 1997] Taylor, J. (1997). *An Introduction to Error Analysis: The Study of Uncertainties in Physical Measurements*. UNIVERSITY SCIENCE BOOKS.
- [Terranova et al., 2015a] Terranova, N., Archier, P., Serot, O., Bernard, D., De Saint Jean, C., and Sumini, M. (2015a). *A Model for Fission Yield Uncertainty Propagation Based on the URANIE Platform*. In JOINT INTERNATIONAL CONFERENCE ON MATHEMATICS AND COMPUTATION (M&C), SUPERCOMPUTING IN NUCLEAR APPLICATIONS (SNA) AND THE MONTE CARLO (MC) METHODS, Nashville.
- [Terranova et al., 2015b] Terranova, N., Serot, O., Archier, P., De Saint Jean, C., and Sumini, M. (2015b). *Covariance Matrix Evaluations for Independent Mass Fission Yields*. NUCLEAR DATA SHEETS, 123:225–230.
- [Terranova et al., 2015c] Terranova, N., Serot, O., Archier, P., Vallet, V., De Saint Jean, C., and Sumini, M. (2015c). *A Covariance Generation Methodology for Fission Product Yields*. In WONDER-2015: FOURTH INTERNATIONAL WORKSHOP ON NUCLEAR DATA EVALUATION FOR REACTOR APPLICATIONS, Aix-en-Provence. To be published in EPJ Web Conferences.
- [Terrell, 1962] Terrell, J. (1962). *Neutron yields from individual fission fragments*. PHYSICAL REVIEW, 127.
- [Truchet et al., 2015] Truchet, G., Leconte, P., Santamarina, A., Brun, E., Damian, F., and Zoia, A. (2015). *Computing Adjoint-Weighted Kinetics Paramters in TRIPOLI-4 by the Iterated Fission Probability Method*. ANNALS OF NUCLEAR ENERGY, 85:17–26.
- [Tsuchiya et al., 2000] Tsuchiya, C., Nakagome, Y., Yamana, H., Moriyama, H., Nishio, K., Kanno, I., Shin, K., and Kimura, I. (2000). *Simultaneous Measurement of Prompt Neutrons and Fission Fragments for $^{239}\text{Pu}(n_{th}, f)$* . JOURNAL OF NUCLEAR SCIENCE AND TECHNOLOGY, 37:941–948.
- [Tukey, 1947] Tukey, J. W. (1947). *Non-parametric estimation II: Statistically Equivalent Blocks and Tolerance Regions-The Continuous Case*. ANNALS OF MATHEMATICAL STATISTICS, 18:529–539.
- [Vaglio-Gaudard, 2014] Vaglio-Gaudard, C. (2014). Private Communication.
- [Vaglio-Gaudard et al., 2014] Vaglio-Gaudard, C., Colombier, A. C., Hudelot, J. P., Leray, O., Lemaire, M., Sergeyeva, V., Di Salvo, J., Gruel, A., and Siréta, P. (2014). *Analysis of the AMMON Experimental Program in the EOLE Facility Supporting the Qualification of the JHR Neutron and Photon Tools*. IEEE TRANSACTIONS ON NUCLEAR SCIENCE, 61:2246–2253.

- [Vaglio-Gaudard et al., 2012] Vaglio-Gaudard, C., Leray, O., Colombier, A. C., Gueton, O., Hudelot, J. P., Valentini, M., Di Salvo, J., Gruel, A., Klein, J. C., Roche, A., Beretz, D., Geslot, B., Girard, J. M., Jammes, C., and Siréta, P. (2012). *Monte Carlo Interpretation of the AMMON/REF Experiment in EOLE for the JHR Reactor Calculations*. In INTERNATIONAL CONFERENCE ON THE PHYSICS OF REACTORS, PHYSOR2012, Knoxville. ANS.
- [Vorobyev et al., 2010] Vorobyev, A., Shcherbakov, O., Gagarski, A. M., Val'ski, G. V., and Petrov, G. A. (2010). *Investigation of the Prompt Neutron Emission Mechanism in Low Energy Fission of $^{235,233}\text{U}(n_{th}, f)$ and $^{252}\text{Cf}(sf)$* . EPJ WEB CONFERENCE, 8.
- [Žerovnik et al., 2011] Žerovnik, G., Trkov, A., and Kodeli, I. (2011). *A Correlated Sampling Method for Multivariate Normal and Log-normal Distributions*. In PROCEEDINGS 20TH INTERNATIONAL CONFERENCE OF NUCLEAR ENERGY FOR NEW EUROPE 2011, pages 409.1–7, Bovec, Slovenia.
- [Wagemans, 1991] Wagemans, C. (1991). *The Nuclear Fission Process*. CRC PRESS.
- [Wagemans et al., 1984] Wagemans, C., Allaert, E., Deruytter, A., Barthélémy, R., and Schillebeeckx, P. (1984). *Comparison of the Energy and Mass Characteristics of the $^{239}\text{Pu}(n_{th}, f)$ and the $^{240}\text{Pu}(SF)$ Fragments*. PHYSICAL REVIEW C, 30:218–223.
- [Wahl, 1988] Wahl, A. (1988). *Nuclear charge distribution and delayed neutron yields for thermal neutron induced fission of ^{235}U , ^{233}U , ^{239}Pu and for spontaneous fission of ^{252}Cf* . ATOMIC AND NUCLEAR DATA TABLES, 39:1–156.
- [Wahl, 2000] Wahl, A. (2000). *Compilation and Evaluation of Fission Yield Nuclear Data*. Technical Report TECDOC-1168, IAEA.
- [Wahl, 2002] Wahl, A. (2002). *Systematics of Fission-Product Yields*. Technical Report LA-13928, LANL.
- [Wald, 1943] Wald, A. (1943). *An Extension of Wilks' Method Setting Tolerance Limits*. ANNALS OF MATHEMATICAL STATISTICS, 14:45–55.
- [Weinberg and Wigner, 1958] Weinberg, A. and Wigner, E. (1958). *The physical theory of neutron chain reactors*. THE UNIVERSITY OF CHICAGO PRESS.
- [Wilks, 1941] Wilks, S. S. (1941). *Determination of Sample Sizes for Setting Tolerance Limits*. ANNALS OF MATHEMATICAL STATISTICS, 12:91–96.
- [Wilks, 1942] Wilks, S. S. (1942). *Statistical Prediction with Special Reference to the Problem of Tolerance Limits*. ANNALS OF MATHEMATICAL STATISTICS, 18:400–409.
- [Wilks, 1962] Wilks, S. S. (1962). *Mathematical Statistics*. JOHN WILEY & SONS.
- [Williams, 1979] Williams, M. L. (1979). *Development of Depletion Perturbation Theory for Coupled Neutron/Nuclide Fields*. NUCLEAR SCIENCE AND ENGINEERING, 70:20–36.
- [Williams et al., 2013] Williams, M. L., Ilas, G., Jessee, M. A., Rearden, B. T., Wiarda, D., Zwermann, W., Gallner, L., Klein, M., Krzykacz-Hausmann, B., and Pautz, A. (2013). *A Statistical Sampling Method for Uncertainty Analysis with SCALE and XSUSA*. NUCLEAR TECHNOLOGY, 183:515–526.
- [Zeynalov et al., 2005] Zeynalov, S., Furman, W., and Hamsch, J.-F. (2005). *Investigation of Mass-TKE Distributions of Fission Fragments from the $^{235}\text{U}(n,f)$ -Reaction in Resonances*. In 13TH INTERNATIONAL SEMINAR ON INTERACTION OF NEUTRONS WITH NUCLEI ISINN-13, Dubna.
- [Zwermann et al., 2009] Zwermann, W. et al. (2009). *Influence of Nuclear Covariance Data on Reactor Core Calculations*. In PROCEEDINGS SECOND INTERNATIONAL WORKSHOP ON NUCLEAR DATA EVALUATION FOR REACTOR APPLICATIONS (WONDER-2009), pages 99–104, Cadarache, France.